The role of PHGDH in hypoxic adaptation and metabolic reprogramming

Eduard Petrosyan

Wolfson College

Thesis submitted to the University of Oxford in accordance with the requirements for the degree of Doctor of Philosophy (DPhil)

University of Oxford

Department of Oncology

Trinity Term 2026

Acknowledgments

First of all, I would like to thank my supervisor, Prof. Ester Hammond, for all the support and great supervision she gave me throughout the entire DPhil. Especially towards the end of the degree, with the unexpected changes in the timeline and the stress that came alongside it, I cannot highlight enough how important it was to have someone like her guiding me through it all. From intense scientific discussions to occasional pep talks and messages like “Don’t crash the Dropbox again…”, none of this would be possible without your help. You pushed me to be a better scientist since the day I joined the lab. And of course, it is impossible to go through the highlights of my PhD without mentioning the day I walked into the lab to find a swarm of pigeons around my bench (I do not think anything can beat that). I hope they serve their purpose for many more years to come. Thank you once again for everything! I would also like to thank Dr Monica Olcina, my second supervisor, for all the discussions and her readiness to help with anything necessary for my project. I appreciate it very much!

Massive thanks to current and former members of the Hammond lab for always being very supportive of me. Çağla (Cags), you are the first person I met from the Hammond lab and went on to become one of my closest friends throughout my time in Oxford. Your ability to get HYPED instantly and vibe under the BB bangers (usually pre-Retreat) is what helped to get through a lot of hard days. To all the formals, night outs and the peak year of 2023. I still have the lists, so we still have some unfinished business here. Tiffany, if it wasn’t for you, I would never have known the true importance of the four letters: E-N-F-J. The fact that us being ENFJs was the first thing we bonded over, says everything about friendship. You are one of the most amazing, ambitious, friendly, extroverted, and all-around legendary friends I have. The way you worked and the amount of passion and effort you put into everything you committed to truly inspired me. From the late nights in the lab to the formals and pub sessions, you have been a crucial part of the past few years! Hala, in the list of things that motivated me and kept me going, Amr Diab’s playlist and dinner at Za’atar are very high up (VERY NICE!!! *clap*). All the chats over lunch, Big Soc nights, Strava updates, and many more, I am very happy to get to know you and have a friend like you. Thank you for all the help in the lab and all the discussions! Kat, I am glad that I got to share my PhD experience with you! To all the memes (6-7), 3 pm snack time, and other legendary moments in the lab. Also, a huge thank you to Oli, Bright, Sophie, Bozhena, and Chumin for everything.

Big thank you to Nuria (Valeee!) for always being there for me, no matter when or where. Always having great advice in any situation and providing a strategic supply of Kinder Buenos. You introduced me to the rich world of Reggaeton, for which I am also super grateful. My Spanish vocabulary became much richer during the past few years, which I hope you can

appreciate (Muchas gracias!). Jamie (Boshhh!), I am very lucky to have a friend like you! You have been one of the rare people whom I could talk to about anything from science to life. In HBAC or outside, with or without Domino's, none of this would have been as good without you as part of it. Gonzalo (Hermano!!!), saying that I have had some of the best conversations with you will be a big understatement. Learning more about Spain or having conversations about history, politics, or any other topic has been something I was always looking forward to and will still do. I am going to wait for that trip to Armenia! I also want to thank all my other friends inside and outside of the Department of Oncology: Bruno (bouldering buddy), Matt, Dominika (VERY GOOD!), Nicole, Kate, Celia, Melanie, David, Miriam, Nathalie, Kelly, Kevin, Jong, Kris, Conor, Ash, Jack, Jiyoung, Zach, Pash, Sovan, and Iain.

Last but not least, I would like to thank my parents and my amazing brother! I would not be who I am without you. Պապ ջան, Մամ ջան, անչափ շնորհակալ եմ ամենի համար, ինչ դուք արել եք ինձ համար՝ նույնիսկ մինչև Օքսֆորդ գալը: Ես չէի կարող ավելի բախտավոր լինել, որ դուք կաք ու կողքիս եք: Արտ ջան, այս ամեն ինչը շատ ավելի դժվար կլիներ, եթե ես չունենայի քեզ նման եղբայր: Հուսով եմ՝ դու կհասնես այն ամենին, ինչին ձգտում ես քո կյանքում:

I am also extremely grateful to the Clarendon Fund for their support of my studies and for making my dream of studying at Oxford a reality.

Thank you, everyone!!!

Abstract

Hypoxia is a common feature of solid tumours and is associated with poor prognosis and resistance to therapy. Attempts to therapeutically target hypoxic tumour cells have shown limited clinical success. This thesis investigates the role of phosphoglycerate dehydrogenase (PHGDH), the rate-limiting enzyme of the serine synthesis pathway (SSP), in hypoxic adaptation and response to radiotherapy. PHGDH expression is induced under severe hypoxia (<0.1% O_2). This induction is driven by combined HIF-1 and PERK-ATF4 signalling, linking oxygen sensing with cellular stress responses.

Loss of PHGDH was demonstrated to result in substantial metabolic rewiring. Increased glycolytic flux and lactate production were observed, alongside enhanced HIF-1 signalling. PHGDH-deficient cells showed improved survival and sustained proliferation under hypoxic conditions. Targeting PHGDH alone, therefore, did not impair adaptation to hypoxia. We demonstrated that the effect of PHGDH loss on radiosensitivity depends on extracellular serine availability. No radiosensitisation was observed under standard or physiological conditions. In contrast, complete serine deprivation resulted in significant radiosensitisation in both normoxia and hypoxia. Reduced glutathione (GSH) levels accompanied this effect, supporting a role for redox imbalance in radiation response. Targeting the SSP is therefore highly context-dependent and influenced by nutrient availability, which is often overlooked in experimental design. PHGDH also exhibits non-canonical behaviour in hypoxia, including nuclear localisation and a potential association with R-loop biology, although this requires further investigation.

Overall, PHGDH functions as a hypoxia-regulated metabolic enzyme with limited utility as a standalone therapeutic target. Moreover, our findings highlight the importance of metabolic context in determining the need to account for tumour microenvironmental conditions in therapeutic strategies.

Table of Contents

ACKNOWLEDGMENTS ---------- 1

ABSTRACT ---------- 3

LIST OF ABBREVIATIONS ---------- 8

LIST OF FIGURES ---------- 17

LIST OF TABLES ---------- 21

1.1 Cancer ---------- 22
- **1.1.1 What is cancer?** ---------- 22
- **1.1.2 Hallmarks of cancer** ---------- 22
- **1.1.3 The tumour microenvironment** ---------- 25

1.2 Hypoxia ---------- 27
- **1.2.1 Defining hypoxia** ---------- 27
- **1.2.2 Origins of tumour hypoxia** ---------- 28
- **1.2.3 Clinical significance of tumour hypoxia** ---------- 29
- **1.2.4 Hypoxia and therapy resistance** ---------- 30
- **1.2.4.1 Hypoxia and radioresistance** ---------- 30
- **1.2.4.2 Hypoxia and chemoresistance** ---------- 31
- **1.2.4.3 Other therapeutic modalities** ---------- 32
- **1.2.5 Measuring hypoxia** ---------- 32

1.3 Biological response to hypoxia ---------- 34
- **1.3.1 HIF-signalling** ---------- 34
- **1.3.2 Replication stress and DNA damage response** ---------- 37
- **1.3.3 Unfolded protein response** ---------- 40
- **1.3.4 Reactive Oxygen Species** ---------- 41

1.4 Metabolic adaptations to hypoxia ---------- 42
- **1.4.1 Hypoxia and Glycolysis** ---------- 42
- **1.4.2 Lipid metabolism in hypoxia** ---------- 45

1.5 The serine synthesis pathway ---------- 48
- **1.5.1 Overview of SSP** ---------- 48
- **1.5.2 Alternative sources of serine** ---------- 49
- **1.5.3 The role of SSP in 1C metabolism** ---------- 50
- **1.5.3.1 Compartmentalisation of 1C metabolism** ---------- 52
- **1.5.4 The role of the SSP in redox homeostasis** ---------- 54
- **1.5.5 Key mechanisms of SSP regulation** ---------- 57
- **1.5.5.1 Induction of SSP** ---------- 57
- **1.5.5.2 Repression of SSP** ---------- 59
- **1.5.6 The SSP and cancer** ---------- 61
- **1.5.7 Dietary restriction of serine as a therapeutic strategy** ---------- 63
- **1.5.8 Folate cycle as a target for therapeutic agents** ---------- 64

1.6 PHGDH in cancer ---------- 67
- **1.6.1 The structure of PHGDH** ---------- 67
- **1.6.2 Post-translational regulation of PHGDH** ---------- 69

1.6.3 Therapeutic strategies for targeting PHGDH ---- 70
1.6.4 Non-canonical roles of PHGDH ---- 73

1.7 Aims of this study ---- 76

CHAPTER 2: MATERIALS AND METHODS ---- 77

2.1 Cell culture ---- 77

2.2 Mycoplasma Testing ---- 77

2.3 Cryopreservation and thawing of cells ---- 78
2.3.1 Freezing cells ---- 78
2.3.2 Thawing cells ---- 78

2.4 Exposure to hypoxia ---- 78

2.5 Generation of CRISPR-Cas9 knockout clones ---- 78

2.6 PHGDH CRISPR-Cas9 knockout validation by Sanger sequencing ---- 80

2.7 Cell proliferation assay ---- 81

2.8 RNA extraction and purification ---- 81

2.9 Complementary DNA (cDNA) synthesis by reverse transcription ---- 82

2.10 Quantitative PCR (qPCR) ---- 83

2.12 Western blotting ---- 84

2.13 Cellular fractionation ---- 85

2.14 Immunofluorescence ---- 85

2.15 siRNA knockdown ---- 86

2.16 R-loop co-immunoprecipitation with S9.6 antibody ---- 86
2.16.1 Sample harvesting ---- 86

2.16.2 Conjugation of S9.6 antibody to protein A Dynabeads ---- 87
2.16.3 Chemical crosslinking of S9.6 antibody to protein A Dynabeads ---- 88
2.16.4 S9.6 Co-immunoprecipitation ---- 88
2.16.5 DNA precipitation and gel electrophoresis ---- 88

2.17 Transient transfection ---- 89

2.18 MitoSOX red staining ---- 89

2.19 MTT assay ---- 90

2.21 Real-time metabolic flux analysis (glycolytic stress test) ---- 90

2.22 Transformation of DH5α competent cells ---- 91

2.23 Dual luciferase luminescence assay ---- 92

2.24 Metabolomic analysis ---- **93**

2.25 FL-1 glutathione assay ---- **93**

2.26 Statistical analysis ---- **93**

CHAPTER 3: HYPOXIC REGULATION OF PHGDH AND THE EFFECT OF ITS LOSS ON CELL METABOLISM ---- **95**

3.1 Introduction ---- **95**

3.2 Results ---- **97**
3.2.1 PHGDH is amplified in lung cancer patients ---- 97
3.2.2 PHGDH expression is positively correlated with Buffa and Winter hypoxia signatures 98
3.2.3 PHGDH is induced both at the mRNA and protein level in hypoxia (<0.1% O_2) ---- 100
3.2.4 Hypoxia leads to an increase in nuclear PHGDH ---- 103
3.2.5 The mechanism of PHGDH induction in hypoxia ---- 104
3.2.6 PHGDH induction under physiological and serine/glycine-deprived conditions ---- 109
3.2.7 Generating and validating PHGDH CRISPR-Cas9 knockouts ---- 111
3.2.8 Characterising the metabolic changes in PHGDH KO cells ---- 114

3.3 Discussion ---- **120**

CHAPTER 4: THE EFFECT OF HYPOXIA AND SERINE AVAILABILITY ON RADIORESISTANCE IN THE ABSENCE OF PHGDH ---- **123**

4.1 Introduction ---- **123**

4.2 Results ---- **125**
4.2.1 The knockout of PHGDH does not increase radiosensitivity in DMEM ---- 125
4.2.2 Loss of PHGDH does not increase radiosensitivity in HPLM ---- 126
4.2.3 Loss of PHGDH increases radiosensitivity in MEM ---- 128
4.2.4 Loss of PHGDH does not affect the redox balance in the presence of extracellular serine 129
4.2.5 Serine deprivation drives reduced glutathione levels ---- 131
4.2.6 Exposure to hypoxia leads to improved survival in PHGDH knockout cells ---- 133
4.2.7 Loss of PHGDH does not reduce proliferation rates at <0.1% O_2 ---- 136
4.2.8 PHGDH KO cells showed elevated levels of glycolysis ---- 137
4.2.9 Enhanced HIF-signalling in PHGDH KO cells ---- 139

4.3 Discussion ---- **144**

CHAPTER 5: INVESTIGATING THE NUCLEAR FUNCTION OF PHGDH UNDER HYPOXIA ---- **146**

5.2 Results ---- **148**
5.2.1 PHGDH potentially interacts with R-loops ---- 148
5.2.2 Optimisation of R-loop co-IP protocol with S9.6 antibody ---- 150
5.2.3 LC-MS analysis revealed no detectable level of PHGDH enrichment in FLO-1 cells 154

5.3 Discussion ---- **162**

CHAPTER 6: FINAL DISCUSSION ---- **164**

6.1 Discussion ---------- 164

6.2 Concluding remarks ---------- 173

CHAPTER 7: APPENDIX ---------- 174

7.1 Papers published from this thesis ---------- 175

7.2 Conference presentations ---------- 175

CHAPTER 8: REFERENCES ---------- 176

List of Abbreviations

AARE – Amino acid response element
ABCB1 – ATP-binding cassette transporter B1 (MDR1)
ACLY – ATP-citrate lyase
ACO2 – Aconitase 2
AF9 – ALL1-fused gene from chromosome 9 protein
ALDH1L1 – Aldehyde dehydrogenase 1 family member L1
ALDH1L2 – Aldehyde dehydrogenase 1 family member L2
ALDOA – Aldolase A
AMP – Adenosine monophosphate
AMPK – AMP-activated protein kinase
ANOVA – Analysis of variance
ANT2 – Adenine nucleotide translocator 2
AP-MS – Affinity purification-mass spectrometry
APOBEC3B – Apolipoprotein B mRNA editing enzyme catalytic subunit 3B
ARCON – Accelerated radiotherapy with carbogen and nicotinamide
ARNT – Aryl hydrocarbon receptor nuclear translocator (HIF-1β)
ASC1 – Alanine-serine-cysteine transporter 1 (SLC7A10)
ASCT1 – Alanine-serine-cysteine transporter 1 (SLC1A4)
ASCT2 – Alanine-serine-cysteine transporter 2 (SLC1A5)
ASS1 – Argininosuccinate synthase 1
ATCC – American Type Culture Collection
ATF3 – Activating transcription factor 3
ATF4 – Activating transcription factor 4
ATF6 – Activating transcription factor 6
ATM – Ataxia telangiectasia mutated kinase
ATP – Adenosine triphosphate
ATR – Ataxia telangiectasia and Rad3-related kinase
ATRIP – ATR-interacting protein
AXIN – Axis inhibition protein
BCA – Bicinchoninic acid (assay)
BiP – Binding immunoglobulin protein (GRP78)
53BP1 – P53-binding protein 1
BSA – Bovine serum albumin
CAFs – Cancer-associated fibroblasts
CAIX – Carbonic anhydrase IX
CAR-T – Chimeric antigen receptor T cell
CBP – CREB-binding protein

CD11b – Cluster of differentiation 11b
CD8 – Cluster of differentiation 8
CD80 – Cluster of differentiation 80
CD86 – Cluster of differentiation 86
CDC5L – Cell division cycle 5-like protein
cDNA – Complementary DNA
CDP – Cytidine diphosphate
ChIP – Chromatin immunoprecipitation
CHK1 – Checkpoint kinase 1
CHK2 – Checkpoint kinase 2
CHX – Cycloheximide
CoA – Coenzyme A
CPT – Camptothecin
CRISPR – Clustered regularly interspaced short palindromic repeats
CTAD – C-terminal transactivation domain
CUL3 – Cullin 3
CXCL5 – C-X-C motif chemokine ligand 5
CXCR2 – C-X-C motif chemokine receptor 2
DAMPs – Damage-associated molecular patterns
DAPI – 4',6-Diamidino-2-phenylindole
DCFDA – 2',7'-Dichlorofluorescein diacetate
DDB1 – Damage-specific DNA binding protein 1
DDR – DNA damage response
DDX17 – DEAD-box helicase 17
DDX18 – DEAD-box helicase 18
DDX3X – DEAD-box helicase 3, X-linked
DDX5 – DEAD-box helicase 5
DEAD-box – Asp-Glu-Ala-Asp RNA helicases
DEAH-box – Asp-Glu-Ala-His RNA helicases
DEPC – Diethyl pyrocarbonate
DHFR – Dihydrofolate reductase
DHX15 – DEAH-box helicase 15
DHX9 – DEAH-box helicase 9
DMEM – Dulbecco's Modified Eagle Medium
DMP – Dimethyl pimelimidate
DMSO – Dimethyl sulfoxide
DNA – Deoxyribonucleic acid
dNTP – Deoxyribonucleotide triphosphate
DRIP – DNA:RNA immunoprecipitation
DSB – DNA double-strand break

dsDNA – Double-stranded DNA
dTMP – Deoxythymidine monophosphate
DTT – Dithiothreitol
dUMP – Deoxyuridine monophosphate
ECAR – Extracellular acidification rate
ECM – Extracellular matrix
EDTA – Ethylenediaminetetraacetic acid
EF5 – 2-(2-Nitro-1H-imidazol-1-yl)-N-(2,2,3,3,3-pentafluoropropyl)acetamide
EHMT2 – Euchromatic histone lysine methyltransferase 2 (G9A)
eIF2α – Eukaryotic initiation factor 2 alpha
eIF4A – Eukaryotic initiation factor 4A
eIF4F – Eukaryotic initiation factor 4F complex
eIF4G – Eukaryotic initiation factor 4G
EMT – Epithelial-mesenchymal transition
ENO1 – Enolase 1
EPAS1 – Endothelial PAS domain protein 1 (HIF-2α)
ER – Endoplasmic reticulum
ERAD – Endoplasmic reticulum-associated degradation
ETC – Electron transport chain
FABP3 – Fatty acid binding protein 3
FAZA – [18F]-Fluoroazomycin arabinoside
FBS – Foetal bovine serum
FBXW7β – F-box and WD repeat domain-containing 7 beta
FC – Fold change
FDR – False discovery rate
FH – Fumarate hydratase
FIH – Factor inhibiting HIF
FL-1 – Fluorescent thiol-responsive probe FL-1
FLuc – Firefly luciferase
FMISO – Fluoromisonidazole
FOXM1 – Forkhead box protein M1
fTHF – Formyl-tetrahydrofolate
5-FU – 5-Fluorouracil
G9A – G9a histone methyltransferase (EHMT2)
GBM – Glioblastoma multiforme
GCLC – Glutamate-cysteine ligase catalytic subunit
GCLM – Glutamate-cysteine ligase modifier subunit
gDNA – Genomic DNA
GLOBOCAN – Global Cancer Observatory
GLS – Glutaminase

GLUT1 – Glucose transporter 1
GMP – Guanosine monophosphate
GO – Gene ontology
GPx – Glutathione peroxidases
GPX4 – Glutathione peroxidase 4
GR – Glutathione reductase
gRNA – Guide RNA
GRP78 – Glucose-regulated protein 78 (BiP)
GS – Glutathione synthetase
GSH – Glutathione (reduced form)
GSK-3β – Glycogen synthase kinase-3 beta
GSSG – Glutathione (oxidised form)
γH2AX – Gamma-H2AX (phosphorylated histone H2AX)
H3K9me1 – Histone H3 lysine 9 monomethylation
H3K9me3 – Histone H3 lysine 9 trimethylation
HAPs – Hypoxia-activated prodrugs
HCys – Homocysteine
HEPES – 4-(2-Hydroxyethyl)-1-piperazineethanesulfonic acid
HIF – Hypoxia-inducible factor
HIF-1 – Hypoxia-inducible factor 1
HIF-1α – Hypoxia-inducible factor 1 alpha
HIF-1β – Hypoxia-inducible factor 1 beta
HIF-2α – Hypoxia-inducible factor 2 alpha
HIF-3α – Hypoxia-inducible factor 3 alpha
HIPK2 – Homeodomain-interacting protein kinase 2
HK2 – Hexokinase 2
HMOX1 – Heme oxygenase 1
HNRNPM – Heterogeneous nuclear ribonucleoprotein M
HNSCC – Head and neck squamous cell carcinoma
HPLM – Human plasma-like medium
HRE – Hypoxia response element
HSP90AB1 – Heat shock protein 90 alpha family class B member 1
HX4 – [18F]-Flortanidazole (hypoxia PET tracer)
IARC – International Agency for Research on Cancer
IC50 – Half-maximal inhibitory concentration
ICE – Inference of CRISPR Edits (analysis tool)
IDH1 – Isocitrate dehydrogenase 1
IDH2 – Isocitrate dehydrogenase 2
IGF2BP3 – Insulin-like growth factor 2 mRNA-binding protein 3
IgG – Immunoglobulin G

ILF3 – Interleukin enhancer-binding factor 3
IMP – Inosine monophosphate
IP – Immunoprecipitation
IR – Ionising radiation
IRE1α – Inositol-requiring enzyme 1 alpha
ITGA2 – Integrin subunit alpha 2
JASPAR – Open-access database of transcription factor binding profiles
JOSD2 – Josephin domain-containing protein 2
KCl – Potassium chloride
KDM4C – Lysine demethylase 4C
KDM6A – Lysine demethylase 6A
KEAP1 – Kelch-like ECH-associated protein 1
KEGG – Kyoto Encyclopedia of Genes and Genomes
αKG – Alpha-ketoglutarate
KO – Knockout
KRAS – Kirsten rat sarcoma viral proto-oncogene
LARP7 – La-related protein 7
LAT1 – L-type amino acid transporter 1 (SLC7A5)
LAT2 – L-type amino acid transporter 2 (SLC7A8)
LC-MS – Liquid chromatography-mass spectrometry
LDHA – Lactate dehydrogenase A
LDHC – Lactate dehydrogenase C
LDS – Lithium dodecyl sulphate (sample buffer)
LET – Linear energy transfer
LFQ – Label-free quantification
LUAD – Lung adenocarcinoma
LUSC – Lung squamous cell carcinoma
MAPK – Mitogen-activated protein kinase
MATR3 – Matrin 3
MC – Methionine cycle
MCT4 – Monocarboxylate transporter 4
MDR1 – Multidrug resistance protein 1 (ABCB1)
MDSCs – Myeloid-derived suppressor cells
MEM – Minimum essential medium
METTL3 – Methyltransferase-like 3
MFI – Median fluorescence intensity
miRNA – MicroRNA
MitoSOX – Mitochondrial superoxide indicator (MitoSOX Red)
MMPs – Matrix metalloproteinases
MRI – Magnetic resonance imaging

mRNA – Messenger RNA
MS – Methionine synthase
mtDNA – Mitochondrial DNA
mtEFG2 – Mitochondrial elongation factor G2
mTHF – 5,10-methylene-tetrahydrofolate
MTHFD – Methylenetetrahydrofolate dehydrogenase
MTHFD1 – Methylenetetrahydrofolate dehydrogenase 1 (cytosolic)
MTHFD2 – Methylenetetrahydrofolate dehydrogenase 2 (mitochondrial)
MTT – 3-(4,5-Dimethylthiazol-2-yl)-2,5-diphenyltetrazolium bromide
MYBBP1A – MYB-binding protein 1a
MYC – Myelocytomatosis oncogene
NaCl – Sodium chloride
NAD – Nicotinamide adenine dinucleotide
NADH – Reduced nicotinamide adenine dinucleotide
NaDOC – Sodium deoxycholate
NADP – Nicotinamide adenine dinucleotide phosphate
NADPH – Reduced nicotinamide adenine dinucleotide phosphate
NAT10 – N-acetyltransferase 10
NBD – Nucleotide-binding domain
NCL – Nucleolin
NEM – N-ethylmaleimide
NIMRAD – Nicotinamide with accelerated radiotherapy
NK – Natural killer (cells)
NOP58 – NOP58 ribonucleoprotein
NOX4 – NADPH oxidase 4
NPC – Nuclear pore complex
NPM1 – Nucleophosmin 1
NQO1 – NAD(P)H:quinone oxidoreductase 1
NRF2 – Nuclear factor erythroid 2-related factor 2
NSCLC – Non-small cell lung cancer
NTAD – N-terminal transactivation domain
OCR – Oxygen consumption rate
ODDD – Oxygen-dependent degradation domain
OE – Overexpression
OE-MRI – Oxygen-enhanced MRI
OER – Oxygen enhancement ratio
OXPHOS – Oxidative phosphorylation
p300 – E1A-binding protein p300
PABPC1 – Poly(A)-binding protein cytoplasmic 1
PARP1 – Poly(ADP-ribose) polymerase 1

PBMCs – Peripheral blood mononuclear cells
PBS – Phosphate-buffered saline
PCA – Principal component analysis
PCBP1 – Poly(RC) binding protein 1
PCBP2 – Poly(RC) binding protein 2
PCR – Polymerase chain reaction
PD-1 – Programmed death-1
PD-L1 – Programmed death-ligand 1
PDAC – Pancreatic ductal adenocarcinoma
PDCD11 – Programmed cell death 11
PDH – Pyruvate dehydrogenase
PDI – Protein disulphide isomerase
PDK1 – Pyruvate dehydrogenase kinase 1
PERK – Protein kinase R-like ER kinase
PET – Positron emission tomography
PFA – Paraformaldehyde
PFK – Phosphofructokinase
PFK1 – Phosphofructokinase-1
PFKFB3 – 6-Phosphofructo-2-kinase/fructose-2,6-bisphosphatase 3
3-PG – 3-Phosphoglycerate
PHD – Prolyl hydroxylase domain
PHGDH – Phosphoglycerate dehydrogenase
3-PHP – 3-Phosphohydroxypyruvate
PIPES – Piperazine-N,N'-bis(2-ethanesulfonic acid)
PKCζ – Protein kinase C isoform zeta
PKM – Pyruvate kinase M
PKM2 – Pyruvate kinase M2
PLAUR – Plasminogen activator urokinase receptor
PPAR – Peroxisome proliferator-activated receptor
PPP – Pentose phosphate pathway
PRDX3 – Peroxiredoxin 3
PRMT1 – Protein arginine methyltransferase 1
PRPF8 – pre-mRNA processing factor 8
PSAT1 – Phosphoserine aminotransferase 1
PSPH – Phosphoserine phosphatase
PTBP1 – Polypyrimidine tract-binding protein 1
PTM – post-translational modification
PUFAs – Polyunsaturated fatty acids
RBX1 – RING-box protein 1
rDNA – Ribosomal DNA

RFWD3 – RING finger and WD repeat domain 3 (E3 ubiquitin ligase)
RLuc – Renilla luciferase
RNA – Ribonucleic acid
RNF5 – Ring finger protein 5 (E3 ubiquitin ligase)
RNH1 – Ribonuclease/angiogenin inhibitor 1
RNP – Ribonucleoprotein
RNR – Ribonucleotide reductase
ROS – Reactive oxygen species
RPA – Replication protein A
RPMI – Roswell Park Memorial Institute medium
RSB – Resuspension buffer
RT – Room temperature
RT-qPCR – Reverse transcription quantitative PCR
SAH – S-Adenosylhomocysteine
SAM – S-Adenosylmethionine
SASP – Senescence-associated secretory phenotype
SBD – Substrate-binding domain
SDH – Succinate dehydrogenase
SDS – Sodium dodecyl sulphate
SEM – Standard error of the mean
SETX – Senataxin
SFXN1 – Sideroflexin 1
sgRNA – Single guide RNA
SHMT1 – Serine hydroxymethyltransferase 1
SHMT2 – Serine hydroxymethyltransferase 2
siRNA – Small interfering RNA
SIRT2 – Sirtuin 2
SLC12A4 – Solute carrier family 12 member 4
SLC1A4 – Solute carrier family 1 member 4 (ASCT1)
SLC1A5 – Solute carrier family 1 member 5 (ASCT2)
SLC25A15 – Solute carrier family 25 member 15
SLC6A14 – Solute carrier family 6 member 14
SLC7A11 – Solute carrier family 7 member 11
SLC7A5 – Solute carrier family 7 member 5 (LAT1)
SLC7A8 – Solute carrier family 7 member 8 (LAT2)
SLS – Sodium lauroyl sarcosinate
SNAT1 – Sodium-coupled neutral amino acid transporter 1 (SLC38A1)
SNAT2 – Sodium-coupled neutral amino acid transporter 2 (SLC38A2)
SNAT4 – Sodium-coupled neutral amino acid transporter 4 (SLC38A4)
ssDNA – Single-stranded DNA

SSP – Serine synthesis pathway
SSRI – Selective serotonin reuptake inhibitor
STAT3 – Signal transducer and activator of transcription 3
SUMOylation – Small ubiquitin-like modifier modification
SYBR – SYBR Green (fluorescent DNA intercalating dye)
SYVN1 – Synoviolin 1 (E3 ubiquitin ligase)
TAMs – Tumour-associated macrophages
TBL3 – Transducin beta-like 3
TBS – Tris-buffered saline
TCA – Tricarboxylic acid (cycle)
TCGA – The Cancer Genome Atlas
THF – Tetrahydrofolate
TIGAR – TP53-induced glycolysis and apoptosis regulator
TME – Tumour microenvironment
TP53 – Tumour protein p53
TRCs – Transcription-replication conflicts
Tregs – Regulatory T cells
Tris-HCl – Tris-hydrochloric acid buffer
Trx – Thioredoxin
TrxR – Thioredoxin reductase
TSS – Transcription start site
UCHL3 – Ubiquitin carboxyl-terminal hydrolase L3
UDP – Uridine diphosphate
UPR – Unfolded protein response
UTB – Urea Tris ß-mercaptoethanol lysis buffer
UTP14A – UTP14 small subunit processome component A
UV – Ultraviolet
VEGF – Vascular endothelial growth factor
VHL – Von Hippel-Lindau tumour suppressor
WB – Western blot
WCL – Whole cell lysate
WDR3 – WD repeat domain 3
WT – Wild-type
XBP1 – X-box binding protein 1
XBP1s – Spliced X-box binding protein 1
XRN2 – 5'-3' Exoribonuclease 2
YY2 – Yin Yang 2

List of Figures

Figure 1.1: Hallmarks of cancer: new dimensions ---------- 23

Figure 1.2: Multidimensional framework of cancer ---------- 24

Figure 1.3: Cellular and stromal interactions driving tumour progression within the microenvironment ---------- 26

Figure 1.4: Spatial gradients of oxygenation within solid tumours ---------- 28

Figure 1.5: Regulation of HIF signalling under normoxic and hypoxic conditions ---------- 35

Figure 1.6: Unfolded protein response (UPR) signalling pathways ---------- 40

Figure 1.7: HIF-1-mediated metabolic reprogramming under hypoxia ---------- 44

Figure 1.8: Metabolic pathways sustaining fatty acid synthesis under hypoxia ---------- 46

Figure 1.9: Serine metabolism: *de novo* biosynthesis and other mechanisms ---------- 48

Figure 1.10: Integration of serine metabolism with 1C, nucleotide, and methylation pathways ---------- 51

Figure 1.11: Coupling of serine-driven 1C metabolism to NADPH production and glutathione-dependent redox control ---------- 53

Figure 1.12: Serine-glycine metabolism and glutathione (GSH) synthesis ---------- 54

Figure 1.13: Epigenetic and transcriptional regulation of the SSP ---------- 57

Figure 1.14: Transcriptional and post-transcriptional repression of the SSP ---------- 60

Figure 1.15: The role of SSP in increased cancer cell proliferation and metastasis formation ---------- 62

Figure 1.16: Evolutionary variation in PHGDH domain architecture ---------- 67

Figure 1.17: Post-translational modification (PTM) landscape of PHGDH across functional domains ---------- 69

Figure 1.18: Serine-independent functions of PHGDH in tumorigenesis and metabolic reprogramming ---------- 74

Figure 3.1: Expression of SSP genes in normal versus tumour tissues of TCGA lung cancer patients ---------- 97

Figure 3.2: Correlation of PHGDH, PSAT1, and PSPH expression with the Buffa hypoxia metagene signature ---------- 98

Figure 3.3: Correlation of PHGDH, PSAT1, and PSPH expression with the Winter hypoxia metagene signature ---------- 99

Figure 3.4: Alteration frequency of the *PHGDH* gene in TCGA cancer types ---------- 100

Figure 3.5: The effect of hypoxia (<0.1% O_2) exposure on PHGDH mRNA expression levels ---------- 101

Figure 3.6: The effect of hypoxia (<0.1% O_2) exposure on PHGDH protein levels ---------- 102

Figure 3.7: The effect of 2% O_2 exposure on PHGDH protein and mRNA levels ---------- 103

Figure 3.8: Hypoxia leads to an increase in nuclear PHGDH ---------- 104

Figure 3.9: HIF-1α-dependent transcriptional regulation of PHGDH in response to hypoxia ---------- 105

Figure 3.10: HIF-1β-dependent transcriptional regulation of PHGDH in response to hypoxia ---------- 106

Figure 3.11: Assessment of UPR-dependent regulation of PHGDH expression in hypoxia ---------- 107

Figure 3.12: Predicted transcription factor binding sites ---------- 108

Figure 3.13: The effect of extracellular serine on PHGDH induction ---------- 109

Figure 3.14: Validation of PHGDH KO clones using Sanger sequencing ---------- 111

Figure 3.15: The effect of PHGDH on cell proliferation ---------- 112

Figure 3.16: Effects of PHGDH knockout on cell proliferation across different culture media ---------- 113

Figure 3.17: Statistical summary IC-MS analysis on PHGH Con and KO cells ---------- 114

Figure 3.18: Metabolomic analysis of parental control and PHGDH KO cells ---------- 115

Figure 3.19: Metabolic changes resulting from the knockout of PHGDH ---------- 116

Figure 3.20: The effect of PHGDH KO on purine metabolism ---------- 118

Figure 3.21: The effect of PHGDH KO on pyrimidine synthesis ---------- 119

Figure 4.1: The effect of culture media on radiosensitivity ---------- 125

Figure 4.2: The effect of PHGDH KO on radiosensitivity in normoxia and hypoxia, in DMEM ----------

Figure 4.3: The effect of PHGDH KO on radiosensitivity in normoxia and hypoxia, in HPLM ----------

Figure 4.4: The effect of PHGDH KO on radiosensitivity in normoxia and hypoxia, in MEM ----------

Figure 4.5: The effect of PHGDH loss on intracellular ROS levels ---------- 130

Figure 4.6: Loss of PHGDH leads to reduced GSH levels in the absence of extracellular serine ----------

Figure 4.7: PHGDH KO cells survive better under hypoxia compared to Con cells --------- 133

Figure 4.8: PHGDH KO cells survive better under hypoxia compared to Con cells in HPLM but not in MEM ---------- 134

Figure 4.9: PHGDH rescue optimisation in KO cells ---------- 135

Figure 4.10: The effect of PHGDH overexpression in PHGDH KO cells in hypoxia --------- 135

Figure 4.11: The effect of PHGDH KO on cell proliferation in hypoxia ---------- 136

Figure 4.12: Intracellular pyruvate and lactate levels based on IC-MS metabolite analysis in PHGDH KO and parental control cells ---------- 137

Figure 4.13: The effect of PHGDH KO on extracellular lactate and glycolysis levels ------- 138

Figure 4.14: HIF-1α induction in parental and PHGDH KO cells ---------- 139

Figure 4.15: Schematic representation of HRE-Firefly luciferase (FLuc) reporter assay -- 140

Figure 4.16: PHGDH loss induces HIF-signalling ---------- 140

Figure 4.17: PHGDH KO leads to stronger induction of HIF-target genes ---------- 141

Figure 4.18: Macrophage polarisation following hypoxia exposure (<0.1% O_2) ---------- 142

Figure 4.19: Macrophage polarisation following exposure to media conditioned with parental and PHGDH KO cells at 21% and <0.1% O_2 ---------- 143

Figure 5.1: PHGDH was identified in three out of four published interactomes ---------- 149

Figure 5.2: Schematic representation of S9.6 co-IP experimental workflow ---------- 150

Figure 5.3: Optimisation of S9.6/R-loop co-IP method ---------- 151

Figure 5.4: S9.6 heavy and light chains detected in S9.6 co-IP western blots ---------- 152

Figure 5.5: S9.6 heavy and light chains detected ---------- 153

Figure 5.6: Validation of S9.6 co-IP samples for LC-MS analysis ---------- 154

Figure 5.7: PCA of LC-MS results ---------- 155

Figure 5.8: Overlapping S9.6 co-IP interactome with available R-loop interactomes -------- 156

Figure 5.9: Overlap of proteins identified across all 5 interactomes ---------- 157

Figure 5.10: Overlap between normoxic and hypoxic R-loop interactomes ---------- 159

Figure 5.11: Pathway enrichment analysis of hypoxia-specific R-loop interactome --------- 159

Figure 5.12: Hierarchical clustering of differentially enriched proteins in S9.6 pulldown samples ---------- 161

List of tables

Table 1.1: Small molecule inhibitors of PHGDH classified by mechanism of action ---------- 71

Table 2.1: Cell lines used in the study ---------- 77

Table 2.2: gRNA sequences used for the generation of PHGDH knockout clones ---------- 79

Table 2.3: Primer sequences (5'-3') used for PCR amplification of the human PHGDH exon 2 targeted by CRISPR-Cas9 ribonucleoprotein complex (RNP) ---------- 80

Table 2.4: PCR master mix ---------- 80

Table 2.5: Thermal cycler settings for PCR amplification ---------- 81

Table 2.6: Reagents used for cDNA synthesis ---------- 82

Table 2.7: Reagents for qPCR reaction mix ---------- 83

Table 2.8: Primer sequences and concentrations used for RT-qPCR ---------- 83

Table 2.9: List of primary antibodies used for western blotting, immunofluorescence and immunoprecipitation experiments ---------- 84

Table 2.10: List of secondary antibodies used for Western blotting and immunofluorescence ---------- 85

Table 2.11: Seahorse cartridge port layout and compound concentration ---------- 91

Table 5.1: List of targets identified in all R-loop interactomes ---------- 158

Table 5.2: Gene ontology analysis of proteins common in all interactomes ---------- 158

Table 7.1: Media composition. All media components, including those added prior to use, are shown ---------- 174

Chapter 1: Introduction

1.1 Cancer

1.1.1 What is cancer?

Cancer is a term encompassing more than 200 different diseases that share fundamental characteristics: uncontrolled cellular proliferation, evasion of normal growth constraints, and the capacity to invade and disseminate to distant sites through metastasis. The global burden of cancer is substantial and increasing. According to the most recent GLOBOCAN estimates published by the International Agency for Research on Cancer (IARC), around 20 million new cancer cases and approximately 9.7 million deaths were estimated worldwide in 2022. Approximately 1 in 5 individuals will develop cancer over the course of their lifetime (Bray et al., 2024). Demographic projections suggest this burden will rise sharply, reaching an estimated 35 million annual new cases by 2050. Despite advances in early detection and targeted therapeutics, cancer remains the second leading cause of death globally after cardiovascular disease (World Health Organisation, 2024), underlining the urgency of fundamental research into its biology.

1.1.2 Hallmarks of cancer

The conceptual framework for understanding how normal cells undergo malignant transformation owes much to the landmark paper by Hanahan and Weinberg, published in 2000. It was proposed that the acquisition of six biological capabilities was sufficient to induce a tumourigenic phenotype: self-sufficiency in growth signals, insensitivity to anti-growth signals, evasion of apoptosis, limitless replicative potential, sustained angiogenesis, and tissue invasion and metastasis (Hanahan & Weinberg, 2000). Importantly, the framework suggested that cancer develops through a stepwise process, whereby cells progressively acquire these capabilities through somatic mutation and clonal selection.

In 2011, Hanahan and Weinberg published a major revision of this model, adding two further hallmark capabilities: the reprogramming of cellular energy metabolism and immune evasion

(Hanahan & Weinberg, 2011). Crucially, this update also included two enabling characteristics: genome instability and mutation, and tumour-promoting inflammation, which underpin the acquisition of hallmark capabilities rather than constituting hallmarks themselves. Alongside this, the 2011 revision introduced the role of tumour microenvironment (TME), recognising the importance of recruited stromal and immune cells in tumourigenesis.

The concept of hallmarks was further refined in 2022, when Hanahan published 'Hallmarks of Cancer: New Dimensions', adding four emerging features (**Figure 1.1**) (Hanahan, 2022).

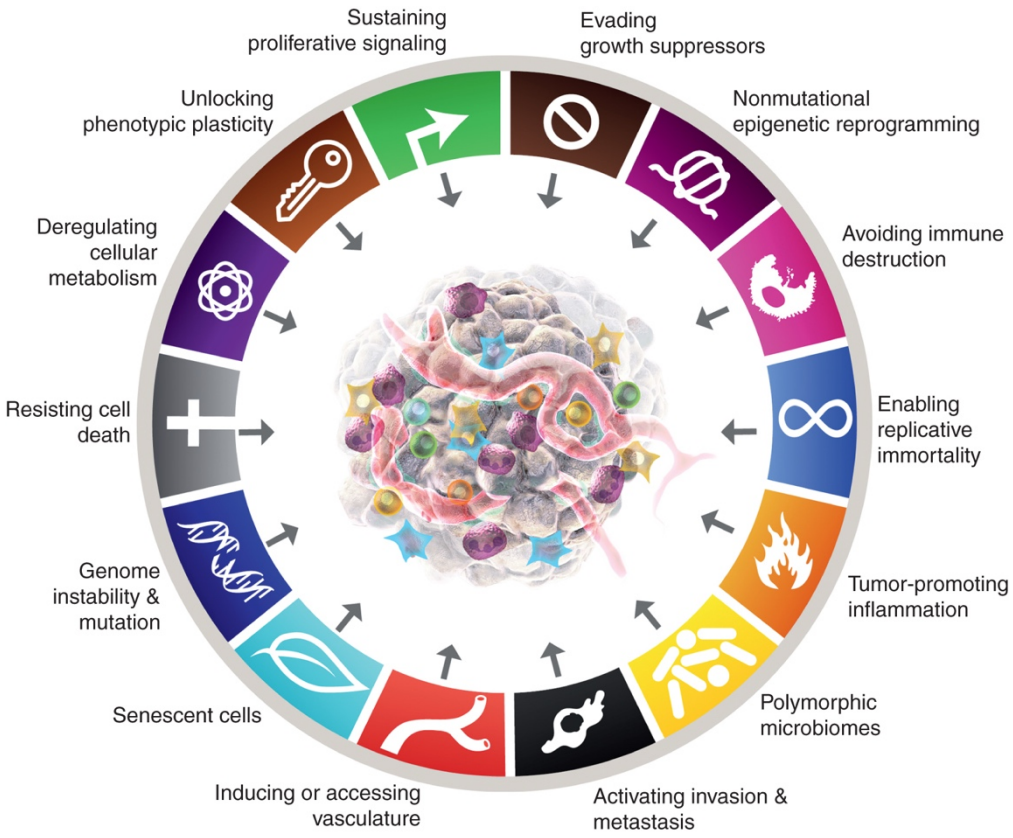

Figure 1.1 Hallmarks of cancer: new dimensions. The figure depicts the expanded framework of cancer hallmarks. Genome instability and tumour-promoting inflammation were defined as enabling characteristics in 2011 (Hanahan & Weinberg, 2011). The 2022 update further introduced unlocking phenotypic plasticity and senescent cells as additional enabling characteristics. Non-mutational epigenetic reprogramming and polymorphic microbiomes were recognised as emerging hallmarks. The remaining traits constitute the established core hallmarks of cancer. Reproduced from Hannah D.A., Hallmarks of Cancer: New Dimensions. Cancer Discovery. 2022;12(1):31-46. © 2022 American Association for Cancer Research. License number: 6225851065821. Reprinted with permission.

One new hallmark capability was proposed: the ability to unlock phenotypic plasticity and disrupted differentiation, whereby cancer cells de-differentiate to acquire stem-like, therapy-resistant states. Two new enabling characteristics were also introduced: non-mutational epigenetic reprogramming and polymorphic microbiomes. Finally, senescent cells were added to the group of functionally important cell types within the TME (Hanahan, 2022).

Most recently, Hanahan published a comprehensive update that represents the most current iteration of this framework (Hanahan, 2026). Rather than simply adding new hallmarks, this update reframes cancer biology as a multidimensional ecosystem, organised into four distinct but interconnected conceptual dimensions. (**Figure 1.2**).

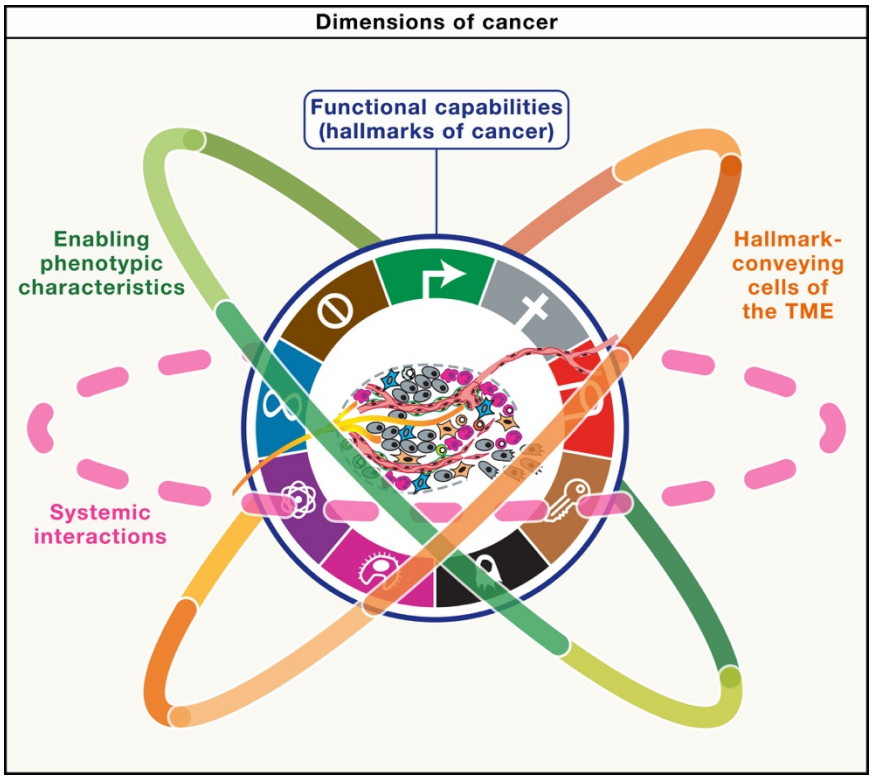

Figure 1.2 Multidimensional framework of cancer. Conceptual model illustrating the four interacting dimensions of cancer: acquired hallmark capabilities, enabling phenotypic characteristics, hallmark-conveying cells of the tumour microenvironment, and systemic host interactions. Adapted from Hanahan, 2026 and distributed under the Creative Commons Attribution 4.0 International License (CC BY 4.0) (http://creativecommons.org/licenses/by/4.0/).

The hallmarks defined originally in earlier versions remain central but are now positioned as one of the dimensions within a broader architecture. These hallmarks are supported by

enabling phenotypic characteristics that facilitate their emergence and persistence. The framework also emphasises host cells within the TME, including cancer-associated fibroblasts (CAFs), endothelial cells, pericytes, innate and adaptive immune cells, adipocytes, and neurons. In addition, systemic factors, particularly ageing and obesity, were recognised as shaping tumour behaviour and progression. Together, these dimensions portray cancer as a dynamic biological system rather than a purely cell-autonomous process (Hanahan, 2026).

1.1.3 The tumour microenvironment

It has long been recognised that a tumour, rather than being an isolated group of cancer cells, is a complex tissue interacting with a variety of non-cancerous cellular and non-cellular components, collectively referred to as the TME (Anderson & Simon, 2020). One of the earliest documented observations of this principle dates back to 1863, when Rudolf Virchow first noted leukocyte infiltration as a characteristic feature of solid tumours, suggesting a link between inflammation and cancer (Maman & Witz, 2018; Virchow, 1863). Later, Paget's influential 'seed and soil' hypothesis established that metastatic colonisation depends on the properties of the host tissue (Paget, 1889). The modern understanding of the TME is significantly more detailed, encompassing a range of cellular populations and physical parameters that together influence tumour behaviour, therapy response, and metastasis.

The cellular compartment of the TME includes CAFs, which remodel the extracellular matrix (ECM), secrete growth-promoting cytokines including TGF-β, and can exert both tumour-suppressive and tumour-promoting functions depending on context (Calon et al., 2012; Orimo et al., 2005; Valkenburg et al., 2018). Endothelial cells form the tumour vasculature, characterised by leaky and chaotic vessel architecture, creating heterogeneous gradients of oxygen, nutrients, and pH throughout the tumour mass. Immune cells constitute a particularly complex and context-dependent TME component: tumour-associated macrophages (TAMs), myeloid-derived suppressor cells (MDSCs), and regulatory T cells (Tregs) are frequently polarised towards immunosuppressive phenotypes that facilitate immune evasion. Cytotoxic

CD8+ T cells and natural killer (NK) cells, however, retain tumouricidal potential, the efficacy of which is determined by the TME (Anderson & Simon, 2020; Tumeh et al., 2014). The balance between these populations determines whether a tumour is immunologically ‘hot’ or ‘cold’, with profound implications for the response to immunotherapy (Galon et al., 2006). The non-cellular TME encompasses the ECM, a dynamic scaffold that can be remodelled, promoting tumour invasion (Levental et al., 2009). Secreted soluble factors such as cytokines, chemokines, and growth factors further mediate signalling between cellular TME populations, leading to maintained tumour growth and immune evasion (Orimo et al., 2005) (**Figure 1.3**).

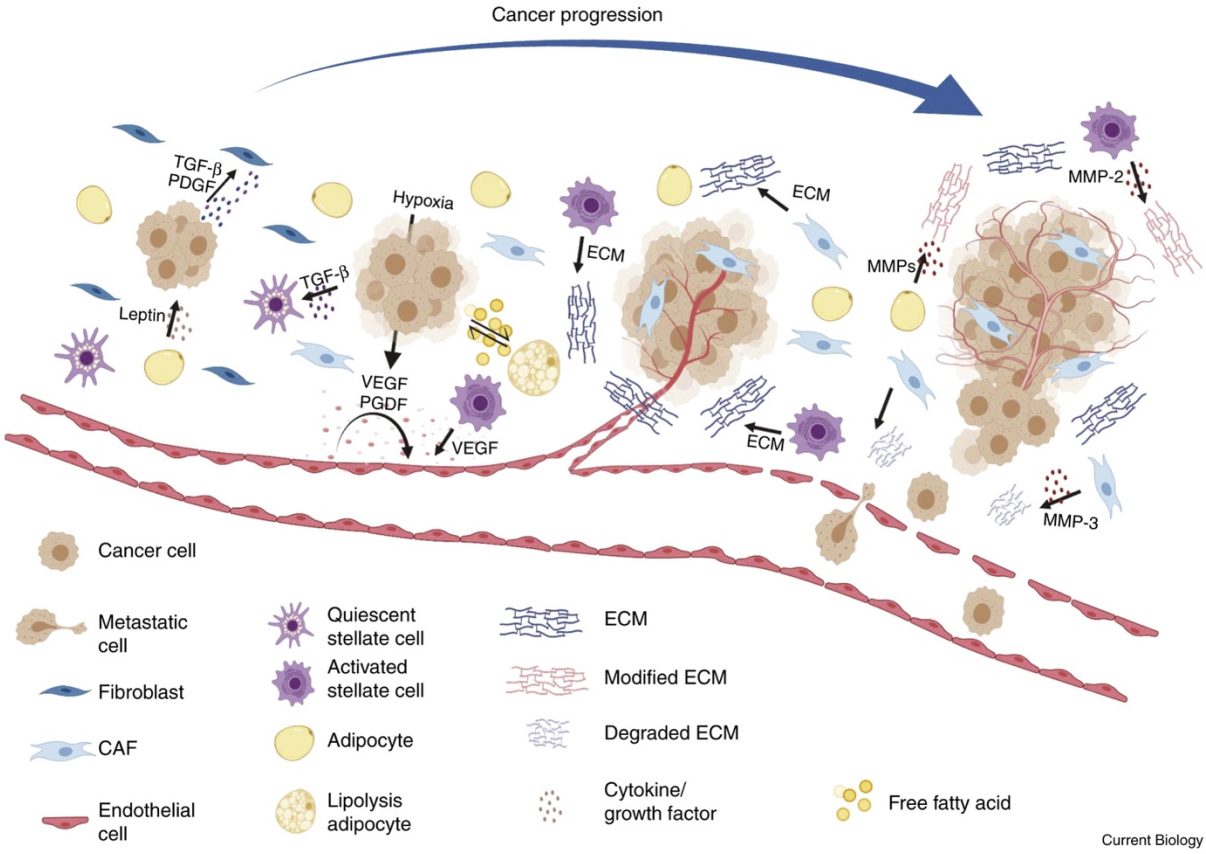

Figure 1.3 Cellular and stromal interactions driving tumour progression within the microenvironment. Schematic representation of tumour progression highlighting reciprocal interactions between cancer cells and components of the tumour microenvironment. Hypoxia promotes angiogenesis and metabolic reprogramming, while activated fibroblasts, stellate cells, adipocytes, and endothelial cells contribute to matrix modification and protease-mediated ECM degradation via matrix metalloproteinases (MMPs). These coordinated interactions facilitate invasion, vascularisation, and metastatic dissemination. Reproduced from Anderson N.M. and Simon M.C., The Tumor Microenvironment. Current Biology. 2020;30(16). © 2020 Elsevier. License number: 6225940379422. Reprinted with permission.

Two emerging TME constituents have received growing attention in recent years. Intratumoral microbial communities (i.e. the microbiome) have been shown to modulate immune activation and influence chemotherapy metabolism. For example, *Fusobacterium nucleatum* enrichment in colorectal tumours promotes chemoresistance and immune evasion through direct interaction with cancer cells (Rubinstein et al., 2013; T. Yu et al., 2017). Separately, senescent cells were shown to accumulate within the TME. Through their pro-inflammatory senescence-associated secretory phenotype (SASP), these cells can promote tumour invasion and metastasis despite being proliferatively arrested (Coppé et al., 2008).

Particularly relevant to this thesis is the physical microenvironment generated by aberrant vasculature and elevated metabolic demand. Elevated interstitial pressure, acidic pH, and most importantly hypoxia, a state of insufficient oxygen, arise in almost all solid tumours. Hypoxia has been recognised as a negative prognostic factor since the 1950s and is now established as a potent driver of therapeutic resistance, genomic instability, and immune evasion (Gray et al., 1953; Thomlinson & Gray, 1955).

1.2 Hypoxia

1.2.1 Defining hypoxia

Hypoxia is described as a state of insufficient tissue oxygenation, arising in both normal physiological contexts and in pathologies including tumours (Hammond et al., 2014). Different terms are used in the field to describe distinct oxygenation states. Normoxia refers to the atmospheric oxygen concentration of 21% O_2 used as the standard condition in experimental design *in vitro*. Physoxia denotes the tissue-specific oxygen concentration in healthy tissue, which varies considerably by organ: approximately 4.6% O_2 in the brain versus 8.0% O_2 in the intestine (Carreau et al., 2011; Dings et al., 1998). Consequently, what is considered hypoxic is relative to the tissue of interest.

Hypoxia broadly describes oxygen concentrations sufficient to stabilise the transcription factor hypoxia-inducible factor (HIF), the master regulator of the cellular response to low oxygen (G. L. Wang et al., 1995). Radiobiological hypoxia is a term defining oxygen concentrations below

0.13% O_2, at which maximal radioresistance is observed (Hall & Giaccia, 2006). Hypoxia can be classified into mild (0.5–3% O_2) or severe (<0.1% O_2) categories, where each activates unique stress responses as well as common adaptive pathways (M. Olcina et al., 2010). Anoxia (0% O_2) is defined as the complete absence of oxygen, associated with the necrotic cores within the tumour regions, largely lacking any vascularisation (Vaupel et al., 1989).

1.2.2 Origins of tumour hypoxia

Hypoxia is a near-universal feature of solid tumours and occurs through two mechanistically distinct processes. The first is diffusion-limited or chronic hypoxia, arising when rapidly proliferating tumour cells outgrow their oxygen supply. Molecular oxygen diffuses from functional capillaries but is progressively consumed by metabolically active cells before reaching distances beyond ~150-180 μm. Cells at this threshold become progressively hypoxic and, at greater distances, anoxic (Thomlinson & Gray, 1955) (**Figure 1.4**).

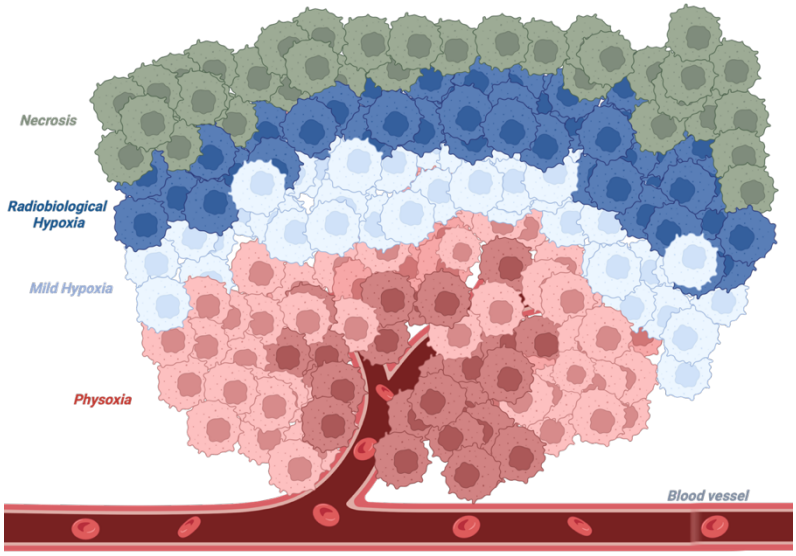

Figure 1.4 Spatial gradients of oxygenation within solid tumours. Schematic illustrating the formation of oxygen gradients within tumour tissue as the distance from the blood vessel increases. Cells located near functional vasculature experience physiological oxygen levels (physoxia). With increasing distance from the vessel, oxygen availability progressively decreases, producing regions of hypoxia. At the greatest distance from the oxygen supply, sustained oxygen deprivation results in necrotic cell death. These gradients generate heterogeneous microenvironments that influence tumour cell metabolism, gene expression, and therapeutic response. Created in https://BioRender.com.

Secondly, perfusion-limited or acute hypoxia results from the transient collapse or blockage of structurally abnormal tumour blood vessels (Chaplin et al., 1987). Tumour vasculature, formed under the influence of HIF-driven pro-angiogenic signalling, is chaotically organised, with blind-ended vessels, arterio-venous shunts and incomplete endothelial coverage (Baluk et al., 2005). These structural defects transiently deprive the tumour cells of oxygen (Dewhirst et al., 1998).

A third subtype, cycling hypoxia, can be described as regular oscillations between severe oxygen deprivation and reoxygenation (Cárdenas-Navia et al., 2008; Lanzen et al., 2006). Reoxygenation generates bursts of reactive oxygen species (ROS) through mitochondrial electron transport chain dysfunction, causing oxidative DNA damage and promoting replication catastrophe (Bader et al., 2021; Chouchani et al., 2014). The vascular dysfunction driving these hypoxic subtypes is itself sustained by a HIF-mediated feed-forward loop: HIF-induced VEGF promotes new vessel formation, but the resulting chaotic vasculature perpetuates rather than resolves tumour hypoxia (Baluk et al., 2005).

1.2.3 Clinical significance of tumour hypoxia

Direct measurements of intratumoral pO_2 using polarographic electrodes established that hypoxic tumours are associated with significantly worse clinical outcomes independently of stage and treatment (Nordsmark et al., 1994). In head and neck squamous cell carcinoma (HNSCC), a tumour pO_2 below 10 mmHg (~1.4% O_2) was associated with a 3-year locoregional control rate of 28% vs 71% in tumours with higher oxygenation levels (Nordsmark & Overgaard, 2000). This prognostic effect has been confirmed across cervical, prostate, breast, soft tissue sarcoma and lung cancers (McKeown, 2014; Walsh et al., 2014). Additionally, hypoxia selectively pressures tumour evolution. p53 mutations arise preferentially in severely hypoxic regions due to p53-dependent apoptosis being the fate of hypoxic cells in a wild-type setting. This means p53 loss provides a survival advantage under oxygen deprivation (Graeber et al., 1996). Hypoxic tumours also exhibit significantly elevated rates of distant metastasis. In soft tissue sarcoma, tumour median pO_2 was 7.5 mmHg (~1% O_2) in

patients who developed metastases versus 20 mmHg (~2.6% O_2) in those who did not (Brizel et al., 1996).

1.2.4 Hypoxia and therapy resistance

1.2.4.1 Hypoxia and radioresistance

Radiotherapy is indicated for approximately 50% of all cancer patients, spanning curative, combined modality and palliative settings (H. Zhu et al., 2024). Ionising radiation generates hydroxyl radicals from water molecules, which react with DNA to produce strand breaks. The predominant lethal lesion is the DNA double-strand break (DSB). Under aerobic conditions, molecular oxygen reacts with radiation-induced DNA radicals to form stable, irreversible DNA peroxyl radicals. In hypoxia, endogenous thiols reduce these radicals to their original state before fixation can occur, chemically reversing the damage (Hall & Giaccia, 2018). This is known as the oxygen fixation hypothesis (Gray et al., 1953).

The oxygen enhancement ratio (OER) measures this effect. A dose 2-3.5 times higher is needed at <0.13% O_2 to produce the same cell death levels compared to normoxic conditions, with the OER decreasing sharply as pO_2 exceeds ~3 mmHg (~0.4% O_2) (Gray et al., 1953; Wouters & Brown, 1997). Both acutely and chronically hypoxic cells exhibit similar radioresistance at equivalent pO_2, indicating that even transiently hypoxic cells form a clinically relevant radioresistant subgroup (Higgins & Hammond, 2022; Wadsworth et al., 2022).

Strategies to overcome hypoxic radioresistance have faced a challenging clinical history. Oxygen delivery methods, including hyperbaric oxygen (usually pO_2 ~3 atm) and ARCON (accelerated radiotherapy plus carbogen inhalation and nicotinamide), have failed to show consistent benefits outside limited subgroups (Horsman & Overgaard, 2016; Janssens et al., 2012). An alternative approach for targeting hypoxic tumours is to reduce tumour oxygen consumption. Atovaquone, a mitochondrial complex III inhibitor, significantly decreased the hypoxic fraction in non-small cell lung carcinoma (NSCLC) patients in the phase II ATOM trial (Skwarski et al., 2021). Nimorazole mimics oxygen by fixing radiation-induced radical damage and remains the only hypoxia-targeting radiosensitiser in routine clinical use, administered

with primary radiotherapy for HNSCC in Denmark (Overgaard, 2011; Overgaard et al., 1998). However, the UK-based phase III NIMRAD trial tested nimorazole with biomarker-selected HNSCC patients but failed to demonstrate a significant benefit (Thomson et al., 2024). Together, these highlight a major challenge in translating hypoxia-targeting strategies to the clinic.

Hypoxia-activated prodrugs (HAPs) were designed with a dual rationale: selective cytotoxicity under hypoxia and potential radiosensitisation by targeting hypoxic tumour cells that are otherwise protected from radiation (Mistry et al., 2017). Despite this, HAPs have consistently failed phase III trials owing to inadequate patient stratification by hypoxic fraction and variable tumour reductase expression (Spiegelberg et al., 2019). The failure of oxygen delivery approaches and HAPs to consistently deliver clinical benefit may in part reflect limitations in the potency, selectivity, or tumour penetration of the compounds tested. It also suggests that, potentially, restoring tumour oxygenation alone may be insufficient to resolve hypoxic radioresistance.

1.2.4.2 Hypoxia and chemoresistance

Chemotherapy resistance in hypoxic tumours reflects both impaired drug delivery and hypoxia-induced cellular adaptation. Structurally abnormal and poorly perfused vasculature restricts the penetration of agents such as doxorubicin and 5-fluorouracil (5-FU), limiting diffusion beyond approximately 100 μm from functional vessels (Tannock, 1998). Hypoxia-associated reductions in proliferation further impair the activity of cell cycle-dependent chemotherapeutics, including antimetabolites and taxanes (Kyle et al., 2007; Tannock, 1968). At the molecular level, HIF-1α promotes resistance through transcriptional induction of multidrug transporters, including MDR1/ABCB1, alongside activation of pro-survival and anti-apoptotic signalling pathways (Jing et al., 2019; Q. Zhao et al., 2015). Hypoxia also enhances autophagy, contributing to drug sequestration and reduced cytotoxic efficacy (Bellot et al., 2009). Efforts to therapeutically target HIF-1α have been hindered by limited selectivity and systemic toxicity, and no HIF-1α-directed agents are currently clinically approved (McAleese

et al., 2021; Semenza, 2012; Q. Zhao et al., 2015). Belzutifan (Welireg), a selective inhibitor for HIF-2α, is the only clinically approved, HIF-directed therapeutic agent used to treat VHL-mutant clear cell renal cell carcinoma (Jonasch et al., 2021).

1.2.4.3 Other therapeutic modalities

Hypoxia was shown to undermine surgery by increasing rates of locoregional recurrence and distant metastasis. In cervical carcinoma, hypoxic tumours showed significantly more extensive parametrial infiltration at resection (Hockel et al., 1996). Similarly, response to immunotherapy was also suggested to be compromised. HIF-1α promotes immune evasion by recruiting immunosuppressive myeloid and regulatory cell populations that suppress cytotoxic T cell infiltration, while also directly upregulating PD-L1 on tumour cells, thereby contributing to T cell exclusion (Abou Khouzam et al., 2022; Graham & Unger, 2018). Recently, it has been demonstrated that tumour hypoxia contributes directly to acquired resistance to anti-PD-1/PD-L1 checkpoint blockade in lung cancer. In murine models, selective targeting of hypoxic tumour regions using HAPs delayed the emergence of immunotherapy resistance and prolonged treatment response (Robles-Oteíza et al., 2025). Another study demonstrated that hypoxia reduces antigen presentation via MHC-I by inducing autophagy, which leads to reduced infiltration of cytotoxic T-cells and immune evasion. Inhibiting autophagy or alleviating tumour hypoxia restored antigen presentation and resulted in increased T-cell recognition, opening new therapeutic avenues to target hypoxic cancer cells (Estephan et al., 2025).

1.2.5 Measuring hypoxia

Robust measurement of tumour oxygenation is critical for patient stratification in hypoxia-targeted trials and for validating preclinical models. The historical gold standard is the polarographic oxygen electrode, which provides direct pO_2 readings within tumour tissue and was used in the landmark studies linking hypoxia to clinical prognosis (Brizel et al., 1996).

However, electrode measurements are invasive, spatially limited, and cannot distinguish viable from necrotic tissue, restricting their current clinical use (Vaupel et al., 1989).

In laboratory and clinical biopsy settings, exogenous hypoxia markers offer an immunohistochemical alternative. Pimonidazole and EF5 are 2-nitroimidazole-based compounds that undergo enzymatic bio-reduction in cells at pO_2 below ~10 mmHg (<1% O_2), covalently adducting to intracellular thiol-containing proteins and enabling detection with specific antibodies (Kaanders et al., 2002; Koch, 2002; Varia et al., 1998). Endogenous markers such as CAIX and GLUT-1 are directly transcribed by HIF-1α and provide proxy readouts of hypoxia from biopsy material without exogenous compound administration. However, these reflect HIF signalling activation rather than direct pO_2 levels (Airley et al., 2003).

For non-invasive clinical imaging, positron emission tomography (PET) with nitroimidazole radiotracers is the current gold standard. [^{18}F]-fluoromisonidazole (FMISO) and [^{18}F]-FAZA undergo selective reduction and intracellular retention in hypoxic viable cells. Moreover, the [^{18}F]-HX4 and copper-complexed dithiosemicarbazone (Cu-ATSM) derivatives represent newer alternatives with improved pharmacokinetics (Dubois et al., 2011; Y. Huang et al., 2021; Z. Xu et al., 2017). PET enables three-dimensional spatial mapping of tumour oxygenation and has informed dose-painting radiotherapy strategies. MRI-based methods are emerging as radiation-free alternatives. Oxygen-enhanced MRI (OE-MRI), which exploits the paramagnetic properties of dissolved O_2 to generate contrast, was recently demonstrated to be clinically feasible and well-tolerated in HNSCC patients, generating hypoxic fraction estimates within ten minutes in a standard clinical workflow (McCabe et al., 2024).

Hypoxia gene expression signatures are an alternative, indirect approach to measuring tumour hypoxia. Each signature consists of a set of genes whose transcription is modulated under hypoxic conditions and can be used to generate a hypoxia score from bulk tumour RNA (Buffa et al., 2010; Chi et al., 2006; Winter et al., 2007). The rationale behind this approach is the induction of transcriptional programmes under low oxygen conditions, including upregulation of HIF-1 targets, glycolytic enzymes, and angiogenic factors. The resulting mRNA

profile can therefore serve as a surrogate measure of the hypoxic phenotype. Signatures have been derived through two broad approaches: identifying genes differentially expressed in hypoxic versus normoxic cells, or selecting genes whose expression correlates with direct hypoxia measurements such as electrode-measured pO_2 or pimonidazole binding in tumour samples (Harris et al., 2015; L. Yang & West, 2018). Among those most widely used are the signatures of Buffa et al., Winter et al., Ragnum et al. and others. Over 30 such gene sets have now been published, with considerable heterogeneity in their derivation and performance across tumour types (Di Giovannantonio et al., 2025; Harris et al., 2015).

1.3 Biological response to hypoxia

1.3.1 HIF-signalling

Prolyl hydroxylase domain proteins (PHD1/2/3) belong to the Fe(II)/α-ketoglutarate-dependent dioxygenase superfamily. These enzymes exert their catalytic function by consuming one atom of molecular oxygen and simultaneously decarboxylating α-KG to succinate and CO_2 (Epstein et al., 2001; Kaelin & Ratcliffe, 2008). The need for these two substrates, combined with relatively high Km values, makes PHDs extremely sensitive to small changes in oxygen level. PHD2 is the dominant isoform responsible for HIF-1α suppression under normoxia. This was demonstrated in mice with PHD2 loss, where constitutive HIF-1α activity resulted in cardiomyopathy (Takeda et al., 2006).

Under normoxia, PHDs hydroxylate HIF-1α at proline 402 and 564 residues within the oxygen-dependent degradation domain (ODDD). This gives rise to a binding interface for the von Hippel-Lindau (VHL) tumour suppressor protein, which operates within an E3 ubiquitin ligase complex comprised of elongin B and C, Cullin 2, and RBX1 (Ivan et al., 2001; Kamura, Conrad, et al., 1999; Kamura, Koepp, et al., 1999). VHL-mediated polyubiquitination targets HIF-1α to the 26S proteasome, maintaining its half-life at approximately five minutes in normoxia (Lonergan et al., 1998). Factor inhibiting HIF (FIH) provides a second, independent regulatory layer. FIH hydroxylates the asparagine 803 residue within the C-terminal transactivation

domain (CTAD), physically obstructing the binding of p300/CBP coactivator even when HIF-1α avoids proteasomal degradation (Lando et al., 2002; Mahon et al., 2001). Because FIH has a lower Km for oxygen than PHDs, it retains its activity partially under milder hypoxia, making its activity oxygen-dependent (Koivunen et al., 2007).

Lack or reduced oxygen levels inhibit PHD and FIH activity, enabling HIF-1α stability, accumulation and heterodimerisation with the constitutively expressed ARNT/HIF-1β subunit (**Figure 1.5**). The heterodimer recruits p300/CBP via its N-terminal transactivation domain (NTAD) and, simultaneously, via the CTAD when FIH is inhibited (Arany et al., 1996). The assembled transactivation complex binds to R-CGTG motif-containing hypoxia response elements (HREs), acting as a transcription factor.

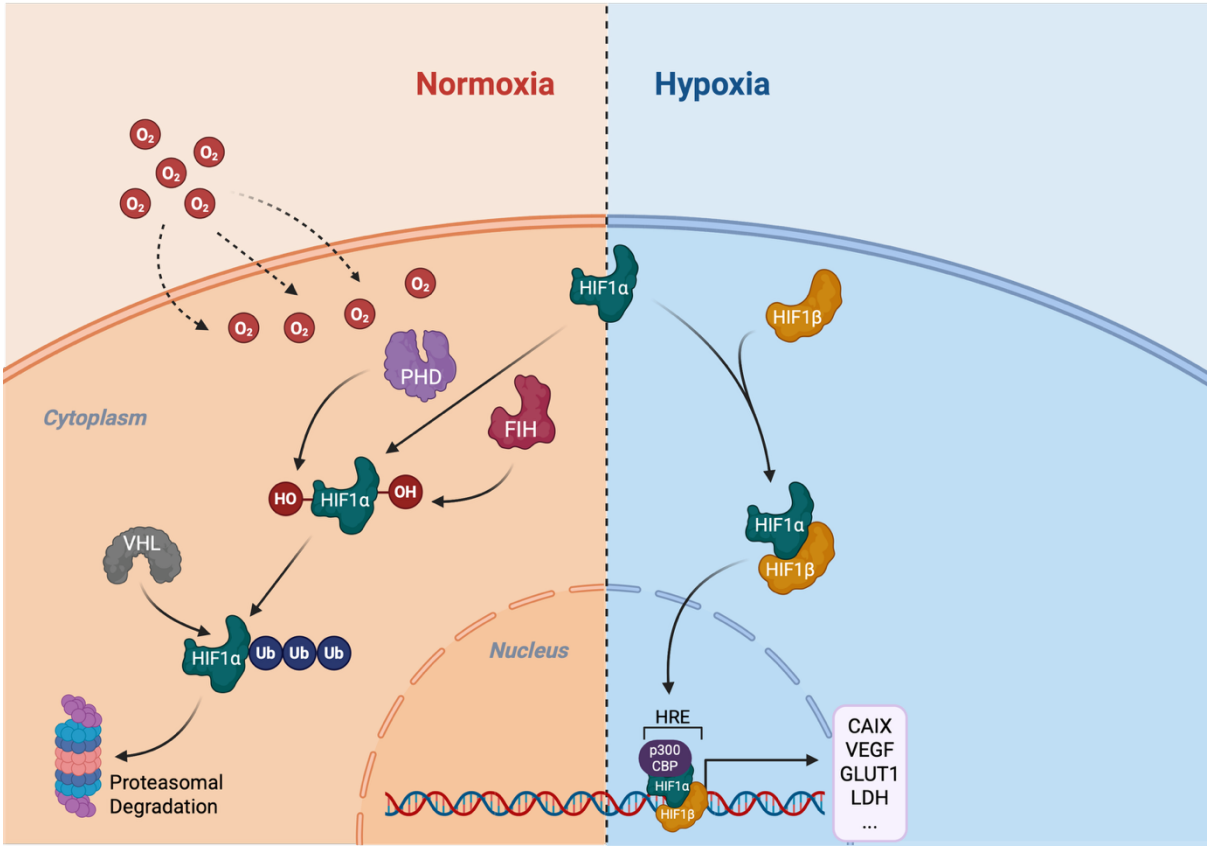

Figure 1.5 Regulation of HIF signalling under normoxic and hypoxic conditions. Schematic illustrating oxygen-dependent regulation of HIF. Under normoxia, oxygen-dependent PHDs and FIH hydroxylate HIF-1α, enabling recognition by the VHL ubiquitin ligase complex and subsequent proteasomal degradation. Under hypoxia, hydroxylation is inhibited, allowing HIF1α to stabilise and dimerise with HIF-1β. The HIF complex translocates to the nucleus, binds HREs, and activates transcription of genes involved in angiogenesis, metabolism, and pH regulation. Created in https://BioRender.com.

This interaction results in the induction of target genes encoding proteins for angiogenesis, glycolysis, pH regulation, and survival, including VEGF, GLUT1, LDHA, PDK1, and CAIX (Semenza, 2012; Wenger et al., 1998).

Three HIF-α isoforms occupy distinct biological niches. HIF-1α broadly controls the glycolytic and angiogenic transcriptional programme. HIF-2α (EPAS1) was shown to selectively induce the pluripotency transcription factors such as OCT4, coupling hypoxia to cancer stem cell maintenance and resistance to cytotoxic therapy (Covello et al., 2006). Additionally, HIF-2α promotes cell proliferation by upregulating c-myc pathway signalling (Gordan et al., 2007). HIF-3α lacks a functional CTAD and acts as a dominant-negative regulator by competing with HIF-1α and HIF-2α for ARNT dimerisation. Moreover, HIF-3α transcription is HIF-1α-dependent, forming a negative feedback loop that limits the magnitude of the hypoxic response (Maynard et al., 2005).

In addition to oxygen depletion, HIF-1α is stabilised under normoxia by oncometabolites that competitively inhibit PHD catalytic activity. Succinate and fumarate accumulation in succinate dehydrogenase- and fumarate hydratase-deficient tumours, respectively, each displaces the required cofactor α-KG from the PHD active site, leading to HIF-1α stabilisation. Together, these states are termed pseudo-hypoxia (Isaacs et al., 2005; Selak et al., 2005). More recently, serine deprivation was also shown to stabilise HIF-1α under normoxia in an AMPK-dependent manner (Yun et al., 2023). Together, these mechanisms show that the oxygen-sensing system also responds to metabolic cues. Loss of VHL, occurring in approximately 90% of clear cell renal cell carcinoma, represents a genetic form of pseudo-hypoxia. Lack of this tumour suppressor leads to reduced recognition and degradation of hydroxylated HIF-1α or HIF-2α, which results in increased transcriptional activity of HIF (Gnarra et al., 1994; Maxwell et al., 1999).

The immunological consequences of HIF-1α activation extend beyond pro-tumourigenic transcriptional reprogramming. HIF-1α directly transactivates PD-L1 (CD274) via a canonical HRE within its promoter, enabling hypoxic tumour cells to engage PD-1 on infiltrating cytotoxic T-lymphocytes and suppress anti-tumour immunity within the hypoxic niche (Noman et al.,

2014). This mechanistic connection between oxygen-sensing machinery and immune checkpoint expression has major implications for the design of combined radiotherapy and immunotherapy strategies in hypoxic tumours.

Recently, a non-canonical role of HIF-1α has been described in the nucleolus. Here, it was reported to engage with RNA polymerase I (RNA Pol I) machinery at ribosomal DNA (rDNA) and lead to increased ribosomal RNA transcription and ribosome biogenesis under hypoxic (1% O_2) stress (Elhamamsy et al., 2025).

1.3.2 Replication stress and DNA damage response

Severe hypoxia, (<0.1% O_2), results in replication stress and activates the DNA damage response (DDR) without direct genotoxic insult, through depletion of deoxyribonucleotide triphosphate (dNTP) pools (Hammond et al., 2002; Olcina et al., 2010). Ribonucleotide reductase (RNR) is the rate-limiting enzyme for dNTP synthesis. Its catalytic mechanism requires a tyrosyl radical maintained by a di-iron-oxo centre in the RRM2 small subunit, a step strictly dependent on molecular oxygen (Foskolou et al., 2017; Nordlund & Reichard, 2006; Zou & Elledge, 2003). Under <0.1% O_2 conditions, RNR function is disrupted, leading to the reduction of the dNTP pool. Such reduced nucleotide availability underpins the induction of replication stress in hypoxia (Pires et al., 2010).

ATR is the primary response enzyme to replication stress (Zeman & Cimprich, 2014). Stress signals, such as reduced nucleotide pool and replication-transcription conflict, can stall the progression of the replication fork and act as factors initiating the ATR response. A stalled replication fork is coated by RPA, which stabilises the exposed ssDNA and prevents its cleavage by endonucleases (Michel et al., 2018; Zou & Elledge, 2003). The RPA-ssDNA complex is then recognised by ATRIP, which subsequently recruits ATR to the lesion site. Following TopBP1-dependent activation, ATR phosphorylates downstream targets such as CHK1, which leads to activation of nucleotide synthesis pathways, reduced origin firing, and reduced G2 phase entry (Achuthankutty et al., 2019; Saxena & Zou, 2022). ATR also phosphorylates RPA at Ser-33 to limit further ssDNA accumulation under stress (Vassin et al.,

2009). Downstream of ATR, p53 is phosphorylated at Ser-15 and accumulates specifically in S-phase cells undergoing replication stress. ATR inhibition substantially reduces both p53 Ser-15 phosphorylation and protein accumulation, establishing p53 as a downstream effector of the hypoxic replication arrest (Hammond et al., 2002).

Critically, in hypoxia the DDR is induced without detectable DSBs. γH2AX and 53BP1 foci are absent under severe hypoxia, mechanistically distinguishing it from radiation-induced damage (Bencokova et al., 2009). ATM is additionally activated through a DSB-independent mechanism driven by replication stress and altered chromatin context rather than strand break recognition (Olcina et al., 2013).

Replication stress induced under radiobiological hypoxia (<0.1% O_2) is associated with R-loop accumulation (Hamperl et al., 2017; Ramachandran et al., 2021). R-loops are three-stranded co-transcriptional structures comprised of an RNA:DNA hybrid and a displaced non-template ssDNA strand, first characterised by Thomas, White and Davis in 1976 (Thomas et al., 1976). Their formation is promoted by G-rich non-template sequences, negative supercoiling behind the transcription complex, and template strand discontinuities (Aguilera & García-Muse, 2012). Physiologically, R-loops regulate transcription termination via SETX and XRN2, immunoglobulin class switch recombination, and other functions (Skourti-Stathaki et al., 2011; Wagschal et al., 2012; K. Yu et al., 2003).

At severe hypoxia below 0.1% O_2, consistent with the threshold for DDR and UPR activation, R-loops accumulate at rDNA repeats, stalling RNA Pol I (T. S. Ma et al., 2023). ROS generated in hypoxia promote R-loop accumulation, likely through oxidative modification of chromatin-associated proteins or the RNA strand itself. SETX, an R-loop-resolving helicase, is induced in hypoxia via the PERK-ATF4 axis, directly coupling UPR signalling to genome stability through R-loop resolution. SETX depletion amplifies R-loop burden, accelerates fork collapse, and generates widespread DNA damage under hypoxic replication stress (T. S. Ma et al., 2023; Ramachandran et al., 2021).

Persistent R-loops are a primary source of transcription-replication conflicts (TRCs). Specifically, head-on collisions between the replisome and the transcription machinery are

more genotoxic than co-directional encounters, as they promote fork stalling and collapse. This stress primarily activates the ATR-CHK1 signalling pathway, while subsequent double-strand breaks (DSBs) at collapsed forks secondarily trigger the ATM-CHK2 DNA damage response (Hamperl et al., 2017; M. M. Olcina et al., 2013). The displaced ssDNA within R-loops serves as a substrate for APOBEC3B, a cytidine deaminase that facilitates C to T transitions. In the peritumoural vasculature, cycling hypoxia induces APOBEC3B through replication catastrophe, resulting in the localised kataegis-pattern hypermutation often observed in hypoxic tumour regions (Bader et al., 2021). This mechanistic chain, from intermittent hypoxia, through replication stress driven by R-loops, to increased mutational burden, directly links the hypoxic microenvironment to the genomic instability underpinning therapeutic resistance.

1.3.3 Unfolded protein response

Like the DDR, the UPR is robustly activated only under severe hypoxia, with O_2 levels below 0.1% (Koritzinsky et al., 2013). The mechanistic trigger is the oxygen dependency of disulphide bond formation in the ER lumen. Protein disulphide isomerase (PDI) catalyses oxidative protein folding through its active-site CXXC motifs. This is coupled to the Ero1 flavooxidase, which uses oxygen as its terminal electron acceptor to re-oxidise PDI. Under severe hypoxia, Ero1 function is impaired, leading to reduced PDI oxidative capacity and misfolded protein accumulation (Frand & Kaiser, 1998; Mezghrani et al., 2001). PERK, IRE1α, and ATF6 are three ER sensors, kept inactive by BiP/GRP78 association under homeostasis and released upon accumulation of misloaded proteins (A. S. Lee, 2005) (**Figure 1.6**).

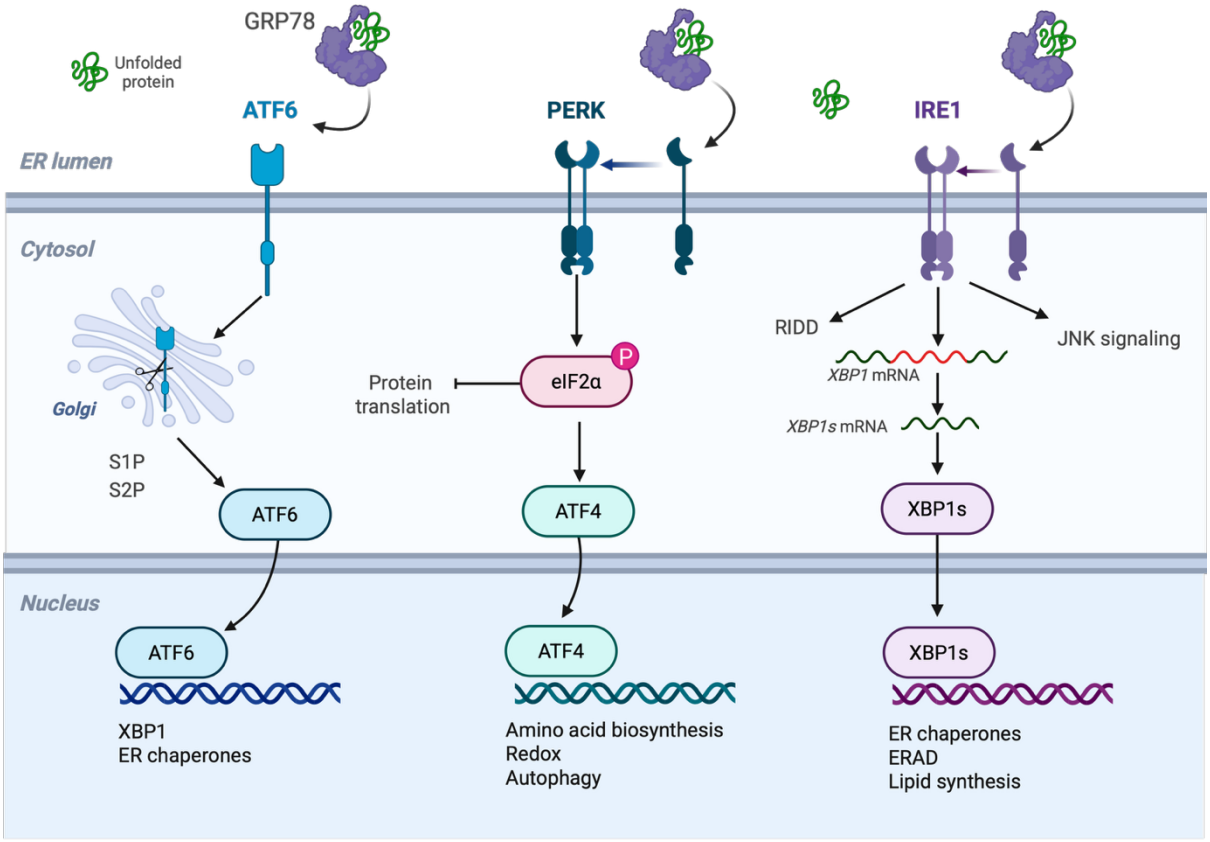

Figure 1.6 Unfolded protein response (UPR) signalling pathways. Schematic illustrating the three principal branches of the UPR activated during ER stress. ATF6 is transported to the Golgi, where proteolytic cleavage generates an active transcription factor that induces ER chaperones and XBP1 expression. PERK phosphorylates eIF2α, attenuating global protein translation while promoting selective translation of ATF4, which regulates genes involved in amino acid metabolism, redox homeostasis, and autophagy. IRE1 mediates unconventional splicing of XBP1 mRNA to produce the active transcription factor XBP1s, which induces ER chaperones, ER-associated degradation components, and lipid synthesis genes. Together, these pathways coordinate adaptive responses that restore ER proteostasis. Created in https://BioRender.com.

Following trans-autophosphorylation, PERK phosphorylates eIF2α at Ser-51, globally suppressing cap-dependent translation while enabling ATF4 synthesis (Harding et al., 2000). Emerging data implicate chronic ATF4 signalling under hypoxia in $CD8^+$ T cell exhaustion, positioning the PERK-eIF2α-ATF4 axis as a mediator of immune evasion in addition to its cell-intrinsic role (Pauneto et al., 2025). This finding places UPR alongside HIF-1α/PD-L1 as a convergent mechanism of hypoxia-driven immune suppression.

IRE1α splices XBP1 mRNA to generate XBP1s, a transcription factor that induces genes involved in ER-associated degradation (ERAD) and ER expansion. Under prolonged ER stress, IRE1α also promotes the degradation of ER-localised mRNAs through regulated IRE1-dependent decay (RIDD) (Hollien & Weissman, 2006). In parallel, ATF6 translocates to the Golgi apparatus, where sequential cleavage by site-1 and site-2 proteases releases the active ATF6 fragment (ATF6f), which induces ER chaperones including BiP/GRP78, GRP94 and calreticulin (Haze et al., 1999). Collectively, the three UPR arms convert localised ER folding stress into a coordinated programme of translational reprogramming and expanded folding capacity.

1.3.4 Reactive Oxygen Species

Reactive oxygen species (ROS) are generated principally at complexes I and III of the mitochondrial electron transport chain through univalent oxygen reduction, yielding superoxide ($O_2^{-}\bullet$) and hydrogen peroxide (H_2O_2) (Murphy, 2009). Although the mechanism by which hypoxia influences cellular ROS is still highly contested, it is suggested that the exposure to 1-3% O_2 leads to an increase in ROS (Bell et al., 2007; Chandel et al., 2000; Sen et al., 2024; Twigger et al., 2024).

Under limited oxygen availability, reduced electron flux through complex III increases semiquinone residence time at the Qo site, elevating univalent superoxide generation into the intermembrane space. Resulting H_2O_2 then oxidises the PHD2 Fe^{2+} cofactor to inactive Fe^{3+}, amplifying HIF-1α stabilisation in a feedforward loop (Chandel et al., 2000; Schroedl et al.,

2002). This requires intact mitochondrial function: ρ^0 cells, lacking mtDNA, fail to exhibit hypoxic ROS elevation, confirming the ETC as the primary source and the crucial need for proper mitochondrial function (Brunelle et al., 2005; Guzy et al., 2005). HIF-1α induces NOX4, providing a constitutively active non-mitochondrial H_2O_2 source that sustains this feedforward signal (Diebold et al., 2010)

ROS accumulation in hypoxia activates the KEAP1-NRF2 antioxidant axis (Bae et al., 2024). Oxidation of reactive cysteine residues on KEAP1 disrupts CUL3-mediated NRF2 degradation, enabling NRF2 to transactivate genes encoding GCLC/GCLM, NQO1, HMOX1, and the mitochondria-localised peroxiredoxin PRDX3 (Itoh et al., 1997; Reczek & Chandel, 2017). GSH, one of the two main thiol-based redox buffers, is significantly upregulated in hypoxia, whereas Thioredoxin (TRX) activity remains relatively stable under the same hypoxic conditions (Twigger et al., 2024). When these systems become overwhelmed, peroxidation of polyunsaturated fatty acids (PUFAs) drives ferroptosis, a process normally suppressed by the phospholipid hydroperoxide reductase GPX4 in a GSH-dependent manner (Bersuker et al., 2019).

1.4 Metabolic adaptations to hypoxia

1.4.1 Hypoxia and Glycolysis

Deregulation of cellular metabolism is one of the hallmarks of cancer (Hanahan, 2022). A defining feature of this reprogramming is the Warburg effect, characterised by a shift towards glycolysis-based glucose metabolism even in the presence of sufficient oxygen (Warburg, 1925, 1956). While this metabolic configuration is further amplified under hypoxic conditions through the stabilisation of HIF-1α, the constitutive preference for aerobic glycolysis allows cancer cells to prioritise biomass production and redox balance to support tumour growth. The cellular response to acute hypoxia is two-staged, with a rapid metabolic phase preceding transcriptional reprogramming. As oxidative phosphorylation declines and ATP levels fall, allosteric inhibition of phosphofructokinase-1 (PFK1) and pyruvate kinase is relieved, leading to an immediate increase in glycolytic flux (Marsin et al., 2002; Mor et al., 2011). This rapid

metabolic adjustment sustains ATP production before gene expression changes occur. Over subsequent hours, HIF-1α-dependent transcriptional reprogramming reinforces and stabilises this glycolytic phenotype.

Another way cancer cells maintain high levels of glycolysis in hypoxia is by increasing glucose uptake. This enhanced import of glucose is mainly mediated by a HIF-1-dependent increase in glucose transporter GLUT1 (Behrooz & Ismail-Beigi, 1997; Ebert et al., 1995; Hayashi et al., 2004; Wood et al., 1998). While less efficient in terms of ATP yield per molecule of glucose, this metabolic configuration supports rapid ATP generation and facilitates the diversion of glycolytic intermediates into biosynthetic pathways required for proliferation (Eales et al., 2016).

In addition to GLUT1, HIF-1α induces hexokinase 2 (HK2), which phosphorylates glucose to glucose-6-phosphate at the entry point of glycolysis. The HK2 promoter contains functional hypoxia response elements that are directly bound by HIF-1α (Mathupala et al., 2001; Riddle et al., 2000). HIF-1α further enhances glycolytic flux by upregulating PFKFB3, a bifunctional enzyme with a markedly higher kinase-to-phosphatase activity ratio. This promotes accumulation of fructose-2,6-bisphosphate, a potent allosteric activator of PFK1 (Minchenko et al., 2002; Obach et al., 2004). The expression of other glycolytic enzymes, including aldolase A (ALDA), enolase 1 (ENO1), phosphoglycerate kinase 1 (PGK1), pyruvate kinase M (PKM), lactate dehydrogenase A (LDHA), lactate dehydrogenase C (LDHC), and lactate dehydrogenase 5 (LDH-5), was also upregulated through HIF-1 signalling via HREs in their respective promoters (Z. Chen et al., 2023; Firth et al., 1994; Koukourakis et al., 2003; Semenza et al., 1994, 1996). To facilitate lactate efflux and prevent intracellular acidification, HIF-1α also induces monocarboxylate transporter 4 (MCT4), enabling the export of lactate produced by enhanced glycolysis and sustaining continued glycolytic flux (Ullah et al., 2006) (**Figure 1.7**).

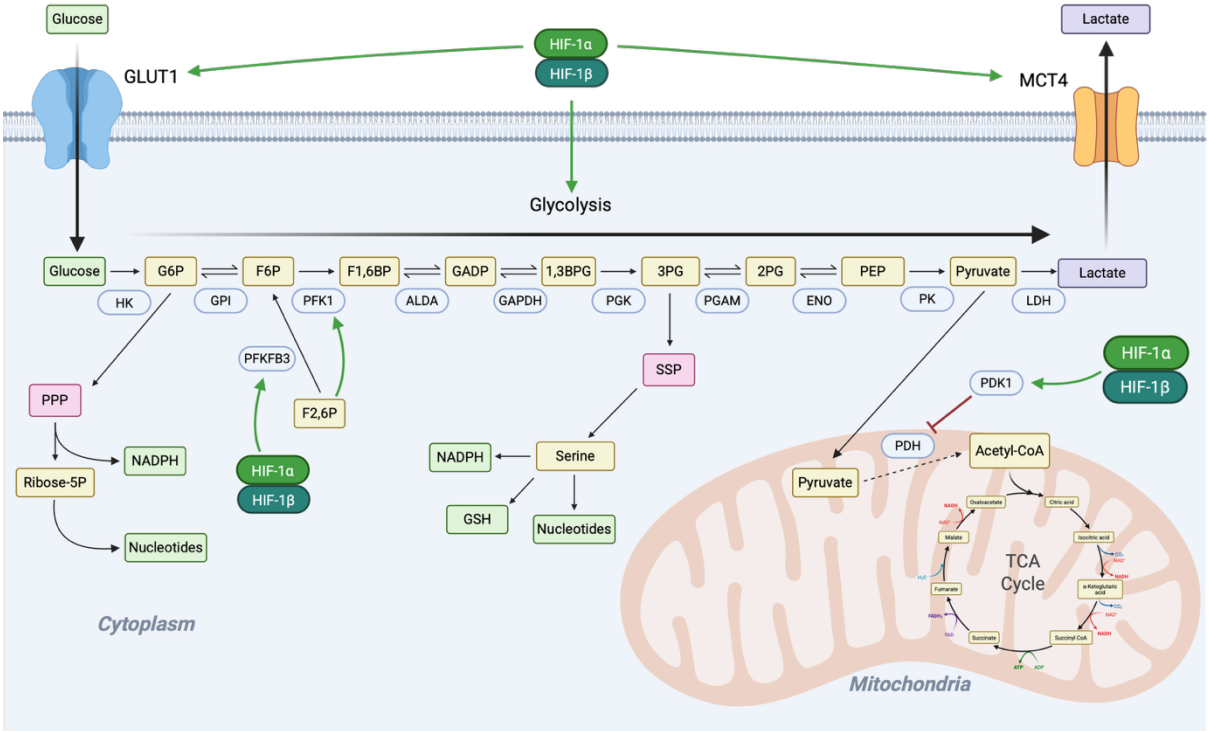

Figure 1.7 HIF-1-mediated metabolic reprogramming under hypoxia. Under hypoxic conditions, HIF-1α enhances glucose uptake and upregulates glycolytic enzymes, promoting increased conversion of glucose to lactate. Glycolytic intermediates are diverted into the pentose phosphate pathway (PPP) to generate NADPH and ribose-5-phosphate for nucleotide synthesis. 3-phosphoglycerate is redirected into the serine synthesis pathway (SSP), supporting serine, glutathione (GSH), and nucleotide production. HIF-1α induces PDK1, which inhibits pyruvate dehydrogenase (PDH), limiting mitochondrial acetyl-CoA generation and TCA cycle flux. Green arrows indicate HIF-1-dependent upregulation, whereas red bars denote HIF-1-mediated inhibition. Created in https://BioRender.com.

Together, these mechanisms demonstrate how HIF-1α coordinates metabolic shift towards glycolysis, essential for cancer cell survival and proliferation within the hypoxic TME.

In hypoxia, stabilised HIF-1α leads to the induction of pyruvate dehydrogenase kinase 1 (PDK1), which subsequently leads to the inhibition of pyruvate dehydrogenase (PDH). PDH catalyses the irreversible conversion of pyruvate into acetyl-CoA, linking glycolysis with the tricarboxylic acid (TCA) cycle (Dupuy et al., 2015; Kim et al., 2006). By inhibiting TCA initiation and increasing glycolysis, levels of lactate increase, and production of ROS from oxidative phosphorylation decreases. Cumulatively, these lead to reduced levels of hypoxia-induced apoptosis in cells (Papandreou et al., 2006).

Additionally, the HIF-1α-driven glycolytic programme is counterbalanced by the tumour suppressor p53, which induces expression of TIGAR (TP53-induced glycolysis and apoptosis

regulator). TIGAR functions as a fructose-2,6-bisphosphatase, lowering intracellular fructose-2,6-bisphosphate levels and thereby attenuating PFK1 activity and glycolytic flux (Bensaad et al., 2006). Through this mechanism, p53 shifts metabolism away from rapid glycolysis and toward pathways that favour redox homeostasis. Consequently, loss of p53 function, which is common in malignancies, removes an important constraint on HIF-1α-mediated metabolic reprogramming. In other words, loss of p53 removes an important metabolic checkpoint, permitting greater glycolytic flux in response to hypoxic signalling. These opposing regulatory influences highlight that glycolysis in cancer is dynamically controlled, and that tumour progression reflects disruption of this metabolic balance rather than simple constitutive activation.

One of the consequences of reduced flux through the TCA is the redirection of glucose-derived carbons into alternative biosynthetic pathways. Glucose can be shunted into the pentose phosphate pathway (PPP) to generate NADPH and ribose-5-phosphate for reductive biosynthesis and nucleotide production (Anastasiou et al., 2011; L. Gao et al., 2004; Gumaa et al., 1969; Racker, 1954). 3-phosphoglycerate (3-PG) can be diverted into the serine biosynthesis pathway via PHGDH, fuelling one-carbon (1C) metabolism (serine-glycine-1C pathway) that supplies one-carbon units for nucleotide synthesis, methylation reactions and NADPH production (Locasale et al., 2011a). Under hypoxic conditions, when oxidative metabolism is constrained, cells further compensate through glutamine-dependent anaplerosis and reductive carboxylation of α-ketoglutarate to generate citrate for lipid biosynthesis (DeBerardinis et al., 2007; Wise et al., 2011). Together, these metabolic changes enable proliferating cancer cells to meet anabolic demands (nucleotides, amino acids, lipids) and to maintain redox homeostasis under oxygen-restricted conditions.

1.4.2 Lipid metabolism in hypoxia

Under normoxic conditions, acetyl-CoA generated from glycolysis-derived pyruvate serves as the principal carbon source for *de novo* fatty acid synthesis. In hypoxia, however, pyruvate entry into the TCA cycle is suppressed, limiting mitochondrial acetyl-CoA production and

consequently reducing lipid biosynthesis (Papandreou et al., 2006). To compensate, hypoxic cells reprogram their metabolism to utilise alternative carbon sources, such as glutamine or acetate, to sustain acetyl-CoA pools and maintain lipid synthesis (Kamphorst et al., 2014; Wise et al., 2011).

Cancer cells rely on acetate as a crucial nutrient to maintain cell growth, especially under metabolic stress. Hypoxic conditions promote increased acetate uptake across several tumour types, including breast, cervical, colon, lung, and prostate cancers (Kamphorst et al., 2014; Munir et al., 2019; Schug et al., 2015; Yoshii et al., 2009). Alternatively, the removal of acetyl groups from histones by histone deacetylases acts as an alternative source of acetate (Inoue & Fujimoto, 1969) (**Figure 1.8**).

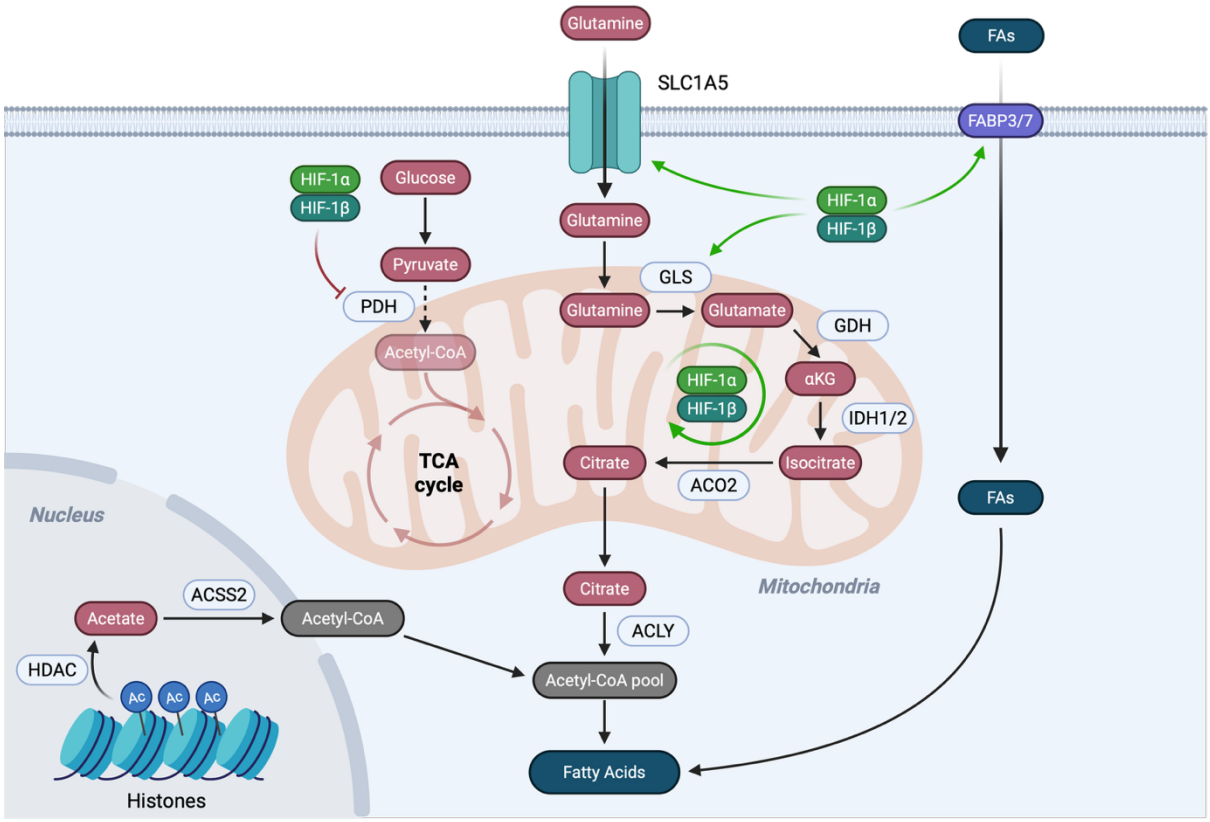

Figure 1.8 Metabolic pathways sustaining fatty acid synthesis under hypoxia. Under hypoxic conditions, HIF-1α suppresses pyruvate dehydrogenase (PDH), limiting glucose-derived acetyl-CoA entry into the TCA cycle. Glutamine uptake is enhanced and metabolised via glutaminase (GLS) to glutamate and subsequently to α-ketoglutarate (αKG). Through reductive carboxylation mediated by IDH1/2 and ACO2, αKG is converted to citrate, which is exported to the cytosol and cleaved by ATP-citrate lyase (ACLY) to generate acetyl-CoA for fatty acid synthesis. Acetate provides an additional carbon source via ACSS2-dependent conversion to acetyl-CoA, including acetate released through histone deacetylation. HIF-1 also promotes fatty acid uptake through upregulation of FABP3/7. Green arrows indicate HIF-1-dependent upregulation, whereas red bars denote inhibition. Created in https://BioRender.com

Moreover, fatty acids can be directly imported. To compensate for reduced levels of fatty acid synthesis from glucose-derived acetyl-CoA, hypoxic cancer cells upregulate the exogenous uptake. Specifically, breast and ovarian cancer cells, as well as glioblastomas, have shown HIF-1α-dependent increase in fatty acid binding proteins (FABP3 and FABP7), which are responsible for the uptake and the intracellular trafficking of these macromolecules (Bensaad et al., 2014).

Beyond acetate utilisation and lipid scavenging, glutamine represents a predominant alternative carbon source in hypoxia, to which many cancer cells become metabolically dependent. Under low oxygen conditions, glutamine supports lipid synthesis via reductive carboxylation of glutamine-derived α-ketoglutarate to generate citrate (Metallo et al., 2012; Mullen et al., 2012). In this pathway, glutamine is converted to glutamate and subsequently to α-ketoglutarate, which undergoes reductive carboxylation by isocitrate dehydrogenase (IDH1/IDH2) operating in the reverse direction, producing isocitrate and then citrate. The resulting citrate is exported to the cytosol and cleaved by ATP-citrate lyase (ACLY) to regenerate acetyl-CoA for fatty acid and cholesterol synthesis (Metallo et al., 2012). Isotopic tracing studies using ^{13}C-labelled glutamine have demonstrated that, under hypoxic conditions, glutamine becomes a dominant lipogenic carbon source, contributing more substantially to the acetyl-CoA pool than acetate (Kamphorst et al., 2014; Metallo et al., 2012). This metabolic shift is driven in part by HIF-1α, which suppresses pyruvate dehydrogenase activity through upregulation of PDK1, thereby diverting carbon flux away from glucose oxidation and toward glutamine-dependent reductive metabolism (Kim et al., 2006; Papandreou et al., 2006). Consequently, glutamine deprivation or inhibition of glutaminase markedly impairs lipid synthesis and proliferation in hypoxic cancer cells, underscoring their dependence on glutamine as a lipogenic substrate (Wise et al., 2011).

1.5 The serine synthesis pathway

1.5.1 Overview of SSP

Amino acids are essential building blocks necessary for maintaining the normal physiological function of the cell. Serine is a non-essential amino acid playing a central role in several metabolic pathways. Given its importance, cells have evolved multiple mechanisms to ensure sufficient serine availability to support cell homeostasis. The *de novo* serine synthesis pathway (SSP) is central in maintaining this homeostasis. In healthy, fasting adults, around 73% of intracellular serine is produced via the SSP (Gregory et al., 2000; Kalhan et al., 2003). Similar contributions have also been reported in other animal models, such as rats, in which approximately 69% of the serine is newly synthesised (Kalhan et al., 2011). The SSP was first characterised in the 1950s by radiobiological tracer experiments, which demonstrated the conversion of glycolytic intermediate 3-phosphoglycerate (3-PG) into serine via O-phosphoserine (i.e. phosphorylation pathway) (Ichihara & Greenberg, 1955). The SSP comprises of 3 reaction steps, all of which take place in the cytoplasm of the cell (**Figure 1.9**).

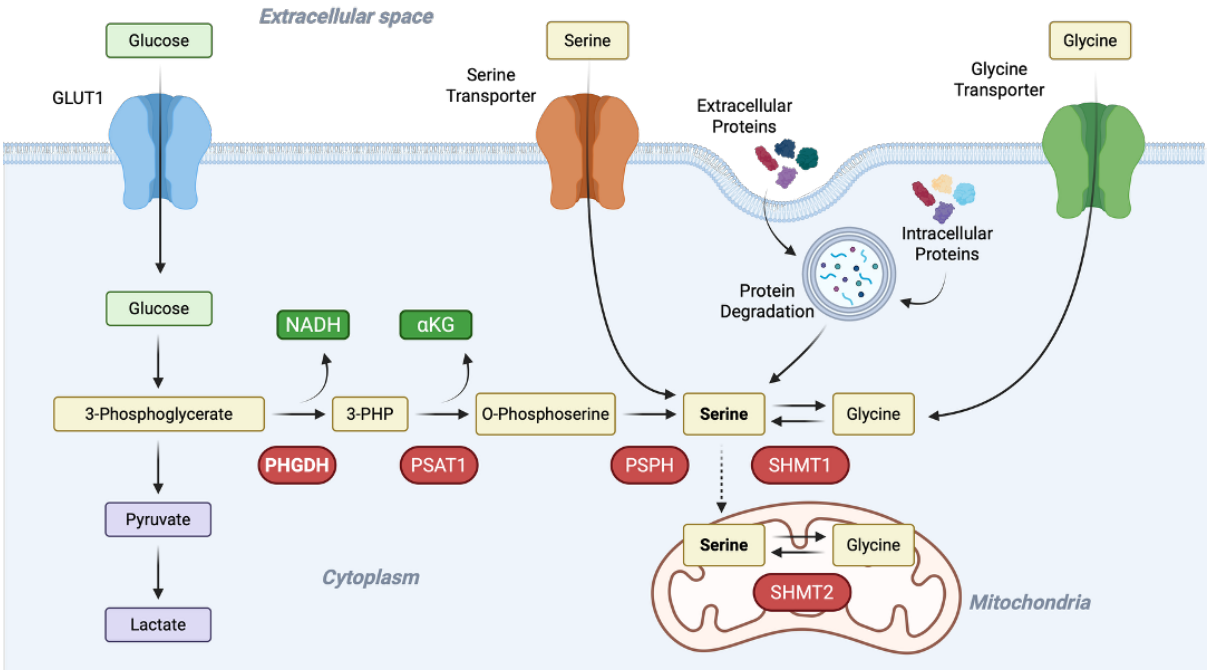

Figure 1.9 Serine metabolism: *de novo* biosynthesis and other mechanisms. Serine is derived from glucose via the serine synthesis pathway (PHGDH, PSAT1, PSPH), imported from the extracellular space, or generated through protein degradation. Serine and glycine interconversion occurs in the cytosol (SHMT1) and mitochondria (SHMT2). Created in https://BioRender.com

First, 3-PG is oxidised, giving rise to 3-phosphohydroxypyruvate (3-PHP). The first reaction of the pathway is the rate-limiting step catalysed by 3-phosphoglycerate dehydrogenase (PHGDH). PHGDH requires nicotinamide adenine dinucleotide (NAD+), which it converts into reduced nicotinamide adenine dinucleotide (NADH) following the 3-PG oxidation. Next, 3-PHP undergoes transamination with glutamate, mediated by phosphoserine aminotransferase 1 (PSAT1), generating O-phosphoserine. Phosphoserine, as a direct intermediate of the phosphorylated SSP, has been identified in metabolomic studies as a reliable surrogate marker of *de novo* pathway activity (Locasale et al., 2011a; Possemato et al., 2011). As a result of this reaction, glutamate is converted into alpha-ketoglutarate (αKG). Lastly, O-phosphoserine is dephosphorylated by phosphoserine phosphatase (PSPH) to generate L-serine. This newly produced serine can then be used to reversibly make glycine, which is catalysed by serine hydroxymethyl transferase 1/2 (SHMT1/2) (Geeraerts et al., 2021; Locasale & Cantley, 2011). The difference between SHMT1 and SHMT2 is their subcellular localisation. SHMT1 is predominantly found in the cytoplasm, whereas SHMT2 is mitochondrial. The *de novo* SSP utilises approximately 10% of 3-PG generated during glycolysis (Locasale et al., 2011a).

1.5.2 Alternative sources of serine

Due to high serine demand, cells can acquire this amino acid via mechanisms beyond the SSP. Major SSP-independent sources of serine include import from the extracellular environment, protein catabolism, and glycine. Alanine serine cysteine threonine transporter 1/2 (ASCT1/2), sodium coupled neutral amino acid transporter 1/2/4 (SNAT1/2/4), and L-type amino acid transporter 1/2 (LAT1/2) have been shown to transport extracellular serine into the cell (Arriza et al., 1993; Bröer, 2022; Kanai et al., 1998; Mackenzie et al., 2003; Oppedisano et al., 2004; Segawa et al., 1999). Lastly, ASC1 (SLC7A10) has been identified as the principal serine transporter in the central nervous system, illustrating potential cell-type-specificity in serine demand and transport (Ehmsen et al., 2016; Fukasawa et al., 2000; Rosenberg et al., 2013). ASC1, ASCT1/2 and SNAT1/2/4 are sodium-dependent transporters, whereas LAT1/2

and SFXN1 are sodium-independent. ASCT2 (SLC1A5), although primarily a glutamine transporter, was recently found to be the main serine importer in breast and many other cancer cell lines (Conger et al., 2023). A recent study identified SLC6A14 and SLC25A15 as major serine transporters in the cytoplasm and mitochondria, respectively, dual targeting of which leads to reduced proliferation in colorectal cancer (Papalazarou et al., 2023). The same study found SLC12A4, an ion cotransporter, to also facilitate serine uptake by replenishing Cl^- levels necessary for the proper SLC6A14 function. Additionally, sideroxflexin 1 (SFXN1) was also found to contribute to the mitochondrial transport of serine, while not affecting the overall cellular import (Kory et al., 2018).

Other sources of serine include the degradation of both intra- and extracellular proteins. Endogenous proteins can serve as a source of serine following autophagic degradation under nutrient stress; however, this route was determined insufficient for maintaining cell proliferation (Galluzzi et al., 2015). Extracellular proteins were suggested as a more reliable source of serine (Q. Wu et al., 2020). Specifically, pancreatic ductal carcinoma cells (PDAC) can import proteins via micropinocytosis, which are subsequently degraded, providing serine to meet cellular demand for the amino acid (Kamphorst et al., 2015). Other cancer types can scavenge albumin, which is rich in serine residues, and replenish its levels (Finicle et al., 2018). Moreover, in conditions of limited availability, serine can also be synthesised from glycine mediated by its interconversion via the SHMT1 and SHMT2 enzymes (Ye et al., 2014).

Once synthesised or acquired through other means, serine feeds into multiple pathways that are central to cell survival and proliferation. These pathways are involved in redox homeostasis, one-carbon (1C) metabolism, synthesis of sphingolipids and phospholipids (Mattaini et al., 2016).

1.5.3 The role of SSP in 1C metabolism

The interconversion of serine into glycine is the primary source of 1C units necessary for the folate and methionine cycles. Although other pathways exist that supply these groups, cancer cells have a bias towards serine-derived 1C units (T. W. M. Fan et al., 2019).

1C metabolism is especially crucial for the synthesis of purines and pyrimidines, which are key to cell growth and proliferation. In a reaction catalysed by SHMT1/2 enzymes, serine donates a 1C unit to tetrahydrofolate (THF), generating glycine and 5,10-methylene-THF (5,10-mTHF) (**Figure 1.10**). 5,10-mTHF mediates the conversion of deoxyuridine monophosphate (dUMP) to deoxythymidine monophosphate (dTMP), a pyrimidine nucleotide (Labuschagne et al., 2014). Additionally, 5,10-mTHF acts as a precursor for inosine monophosphate (IMP), which is then converted into adenosine monophosphate (AMP) and guanosine monophosphate (GMP). This *de novo* purine synthesis is mediated through the oxidation of 5,10-mTHF into 10-formyl-THF (10-fTHF).

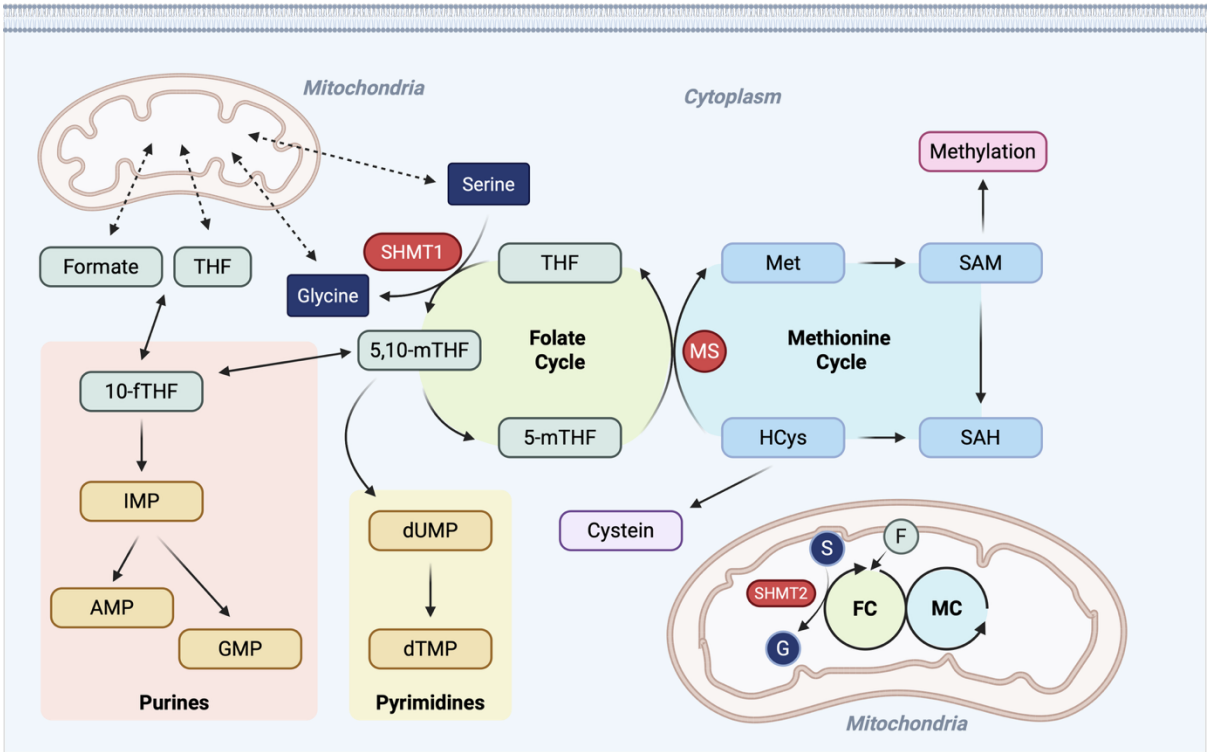

Figure 1.10 Integration of serine metabolism with 1C, nucleotide, and methylation pathways. Serine is converted to glycine by SHMT1 in the cytoplasm and SHMT2 in the mitochondria, donating one-carbon units to tetrahydrofolate (THF) and generating 5,10-methylene-THF (5,10-mTHF). Folate cycle intermediates support *de novo* purine (IMP, AMP, GMP) and thymidylate (dTMP) synthesis. One-carbon units are also transferred to the methionine cycle via methionine synthase (MS), enabling production of methionine (Met) and S-adenosylmethionine (SAM) for cellular methylation reactions. S-adenosylhomocysteine (SAH) is recycled to homocysteine (HCys). In mitochondria, serine catabolism contributes to formate production, which fuels cytosolic one-carbon metabolism. FC, folate cycle; MC, methionine cycle. Created in https://BioRender.com

In addition to oxidation into 10-fTHF, 5,10-mTHF can also be reduced into 5-methyl-THF (5-mTHF). The methyl group from 5-mTHF is then transferred to homocysteine (re-methylation), giving rise to methionine, another important cellular building block. Generation of methionine, catalysed by methionine synthase (MS), requires a vitamin B12 cofactor and acts as the step linking the folate cycle with the methionine cycle. As a result of this reaction, THF is generated, restarting the folate cycle. Methionine is then adenylated, yielding S-adenosylmethionine (SAM). This reaction is crucial because SAM affects epigenetic regulation, biosynthesis of creatine and polyamine, sulphur metabolism and others (Mentch et al., 2015). SAM is then demethylated into S-adenosylhomocysteine (SAH). The ratio between SAM and SAH is crucial for the synthesis of pro-inflammatory cytokines such as IL-1β, broadening the influence of 1C metabolism and serine (Maddocks et al., 2016). As the last step of the methionine cycle, SAH is deadenylated back to homocysteine. Homocysteine is a precursor for another amino acid residue, cysteine (Quéré et al., 1999). Overall, SSP is indispensable for maintaining the physiological levels of crucial biomolecules, including amino acids, nucleotides and others.

1.5.3.1 Compartmentalisation of 1C metabolism

Another important consideration when discussing 1C metabolites is the subcellular localisation. Studies initially conducted in *Saccharomyces cerevisiae* suggested that the 1C metabolic pathways described above occur simultaneously in the cytoplasm and mitochondria (Appling, 1991; Barlowe & Appling, 1988), 1991; Barlowe & Appling, 1988). Serine interconversion into glycine is the key difference between these compartments. SHMT1 is the enzyme catalysing the reaction in the cytoplasm, whereas in mitochondria it is mediated by SHMT2. Clinical studies showed that SHMT2 specifically is overexpressed in various tumour vs normal tissues, indicating a bias towards the mitochondrial arm of the pathway in cancer cells (M. Jin et al., 2021; Y. Jin et al., 2022; Yin, 2015). These two compartments, however, do not act in isolation and in fact are highly interconnected. THF cofactor derivatives, such as 5,10-mTHF and 10-fTHF, cannot cross the mitochondrial membrane; however, following the

cleavage of the fTHF, free formate and THF are generated, which can enter the mitochondria without any need for transporters (Ducker et al., 2016). Serine and glycine can also translocate into the mitochondria, acting as 1C donors to the formate cycle there (Cybulski & Fisher, 1976, 1977) (**Figure 1.11**).

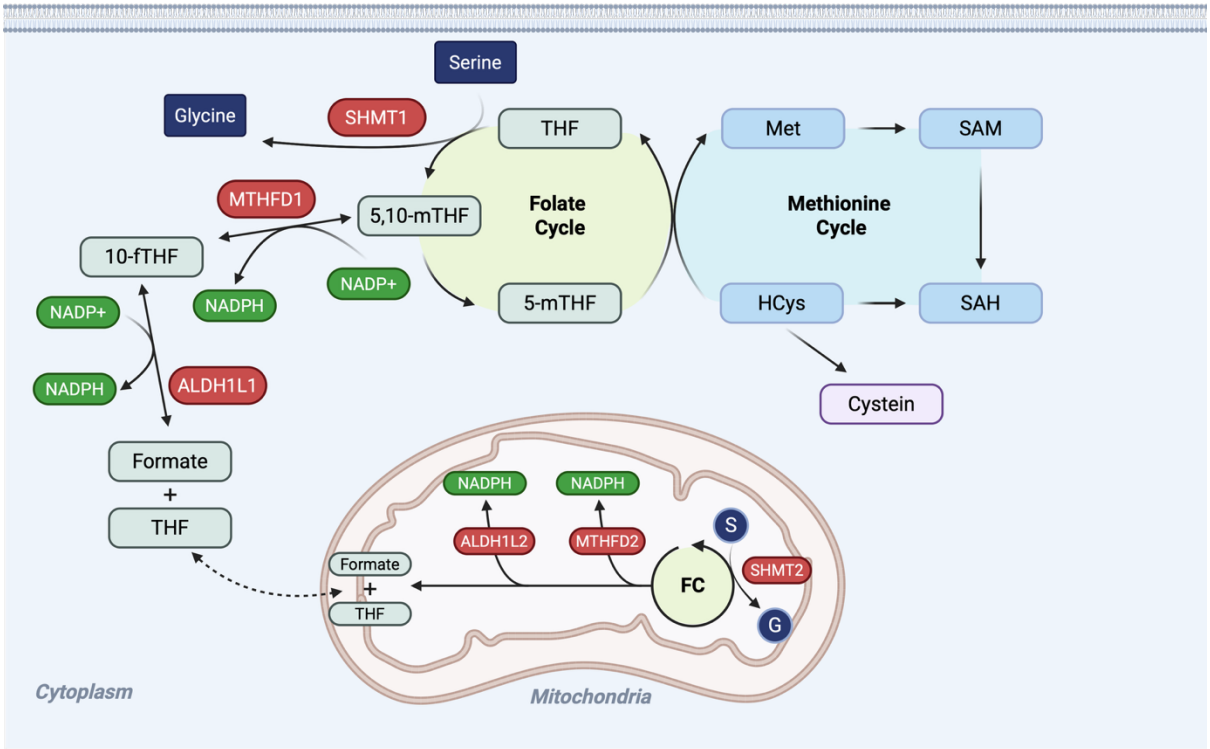

Figure 1.11 Coupling of serine-driven 1C metabolism to NADPH production and glutathione-dependent redox control. In the cytoplasm, SHMT1 converts serine to glycine, generating 5,10-mTHF that enters the folate cycle. MTHFD1 and ALDH1L1 contribute to NADPH production and formate generation, linking 1C flux to redox balance. One-carbon units support the methionine cycle, enabling S-adenosylmethionine synthesis and homocysteine recycling. Homocysteine can enter the trans-sulfuration pathway to produce cysteine, a precursor for glutathione (GSH) synthesis. In mitochondria, SHMT2-driven serine catabolism and MTHFD2/ALDH1L2 activity generate NADPH and formate, which is exported to the cytosol. FC, folate cycle; Met, methionine; SAM, S-adenosylmethionine; SAH, S-adenosylhomocysteine. Created in https://BioRender.com

Although serine and glycine are interconvertible, it is serine and not glycine that is the functionally dominant 1C donor in cancer cells. It was suggested that exogenous glycine cannot substitute for serine in supporting cancer cell proliferation (Labuschagne et al., 2014). Instead, serine is selectively consumed and converted to intracellular glycine and 1C units for nucleotide synthesis. This selectivity highlights the importance of maintaining serine production through the SSP, as disruption of this pathway compromises 1C-dependent biosynthesis and impairs cell growth.

1.5.4 The role of the SSP in redox homeostasis

Serine and glycine metabolism is important for maintaining physiological redox homeostasis. Fine-tuning the levels of intracellular ROS is key to proper cell function. A major mechanism through which serine and glycine metabolism supports redox balance is by sustaining the synthesis of glutathione (GSH), the principal antioxidant defence system in cells (Maddocks et al., 2013).

GSH, a tripeptide antioxidant composed of glutamate, cysteine and glycine, plays a central role in buffering cellular redox stress by scavenging ROS. GSH is synthesised in two steps: γ-glutamylcysteine ligase (GCL) first joins glutamate and cysteine to form γ-glutamylcysteine, and glutathione synthetase (GS) then adds glycine to produce GSH (**Figure 1.12**).

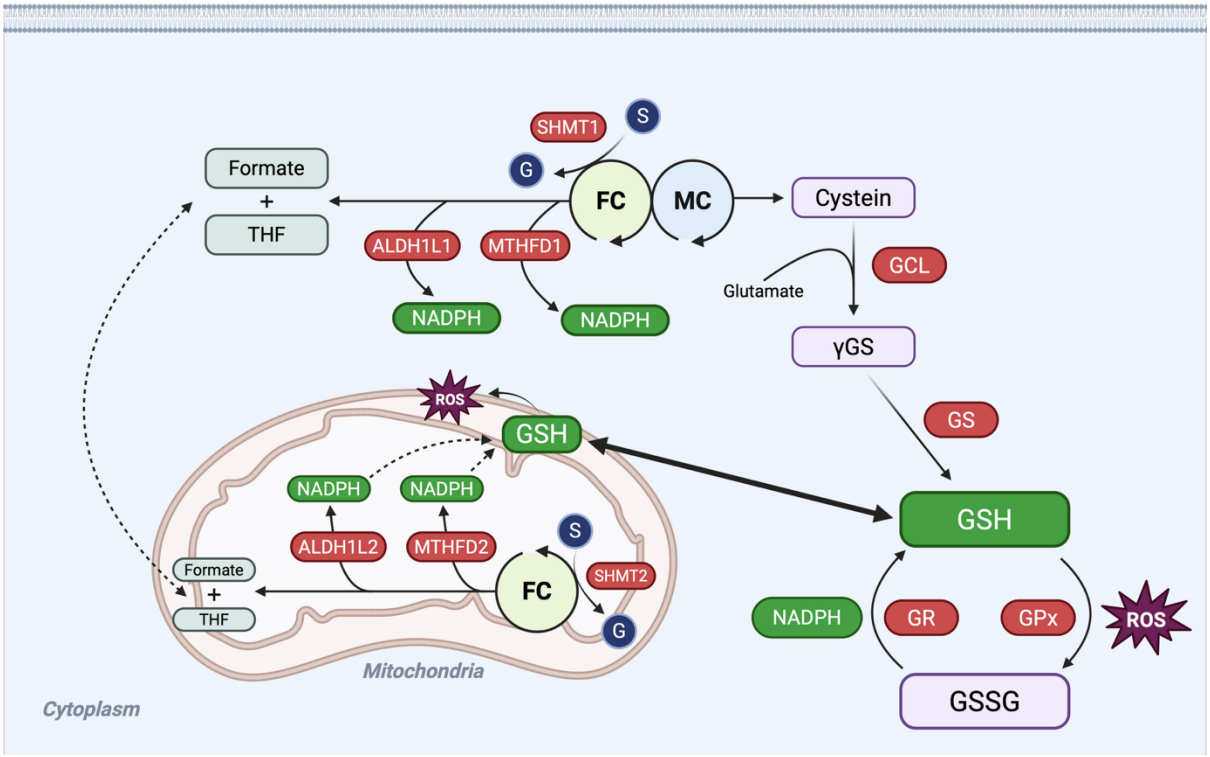

Figure 1.12 Serine-glycine metabolism and glutathione (GSH) synthesis. Serine metabolism through the folate cycle (FC) and methionine cycle (MC) contributes to cellular redox homeostasis by supporting GSH production. Serine is converted to glycine by SHMT1/2, providing a key precursor for GSH synthesis together with cysteine and glutamate via γ-glutamylcysteine synthetase (GCL) and glutathione synthetase (GS). 1C metabolism enzymes (MTHFD1/2 and ALDH1L1/2) generate NADPH, which maintains GSH in its reduced form through glutathione reductase (GR). Reduced GSH detoxifies ROS via glutathione peroxidases (GPx), forming oxidised glutathione (GSSG), thereby linking serine metabolism to antioxidant defence and redox balance.

Although GSH is synthesised exclusively in the cytoplasm, it is distributed to other cellular compartments, including the mitochondria and endoplasmic reticulum (Marí et al., 2009). The majority of cellular GSH (approximately 80-85%) resides in the cytosol, whereas around 10-15% is localised within mitochondria (Meredith & Reed, 1982; Yuan & Kaplowitz, 2009). Serine is a key contributor to the GSH precursor pool. As discussed, glycine can be generated via direct uptake or conversion from serine and cysteine via the trans-sulfuration pathway linked to 1C metabolism. Upon neutralisation of ROS, reduced GSH is oxidised into glutathione disulfide (GSSG) in a reaction catalysed by glutathione peroxidase enzymes (GPXs). GSSG can be reduced back into GSH by glutathione reductase (GR), in an NADPH-dependent manner (Franklin et al., 2009; Mills, 1957; Racker, 1955; Thompson & Meister, 1976).

NADPH is an important cofactor that ensures the maintenance of the reduced GSH pool, ensuring redox homeostasis. Through its integration with 1C metabolism and glutathione biosynthesis, the SSP plays a central role in sustaining cellular NADPH levels. The conversion of 5,10-mTHF into 10-fTHF, as part of the folate cycle, requires cofactor NADP+ and generates NADPH as a result. This reaction takes place in the cytoplasm and mitochondria, catalysed by methylenetetrahydrofolate dehydrogenase, cyclohydrolase and formyltetrahydrofolate synthetase (MTHFD) 1 and 2, respectively. Although most of the NADPH in this reaction is generated in the mitochondria (via MTHFD2), MTHFD1-mediated cytosolic NADPH production has also been described (Lewis et al., 2014). Another pathway generating NADPH is the oxidation of 10-fTHF, which produces formate and THF. This reaction is catalysed by aldehyde dehydrogenase 1 family member L1 (ALDH1L1) in the cytosol and ALDH1L2 in the mitochondria (Ducker et al., 2016; Krupenko et al., 2020).

Mitochondrial serine catabolism becomes particularly important under hypoxic conditions, where SHMT2 is induced in a HIF-1α-dependent manner, especially in MYC-amplified cancers. In this setting, cooperation between HIF-1α signalling and elevated MYC activity enhances mitochondrial 1C flux and NADPH production, thereby limiting ROS accumulation and promoting tumour cell survival under hypoxic stress (Ye et al., 2014).

Importantly, ROS also appear to regulate PHGDH directly, as redox-sensitive cysteine residues can undergo oxidative modification and alter enzyme oligomerisation and activity. PHGDH C281 and C18/C19 residues were found to be susceptible to oxidative modification, with C281 located near the catalytic H293 residue, suggesting potential effects on enzyme function (Grueso et al., 2019). Oxidative modification of C116, a residue critical for structural integrity, can promote disulfide bond formation and disrupt PHGDH oligomerisation, leading to reduced enzymatic activity (Spillier et al., 2019). This link between ROS and PHGDH suggests the presence of a reciprocal feedback loop. Specifically, ROS can modulate PHGDH activity, while PHGDH-driven SSP in turn supports redox homeostasis.

1.5.5 Key mechanisms of SSP regulation

1.5.5.1 Induction of SSP

Due to its important metabolic and physiological role, the SSP is tightly regulated at transcriptional, post-transcriptional and post-translational levels.

At the epigenetic level, histone H3 methyltransferase G9A, also known as Euchromatic Histone Lysine Methyltransferase 2 (EHMT2), is required to sustain the SSP gene expression by H3K9 monomethylation (H3K9me1) (**Figure 1.13A**).

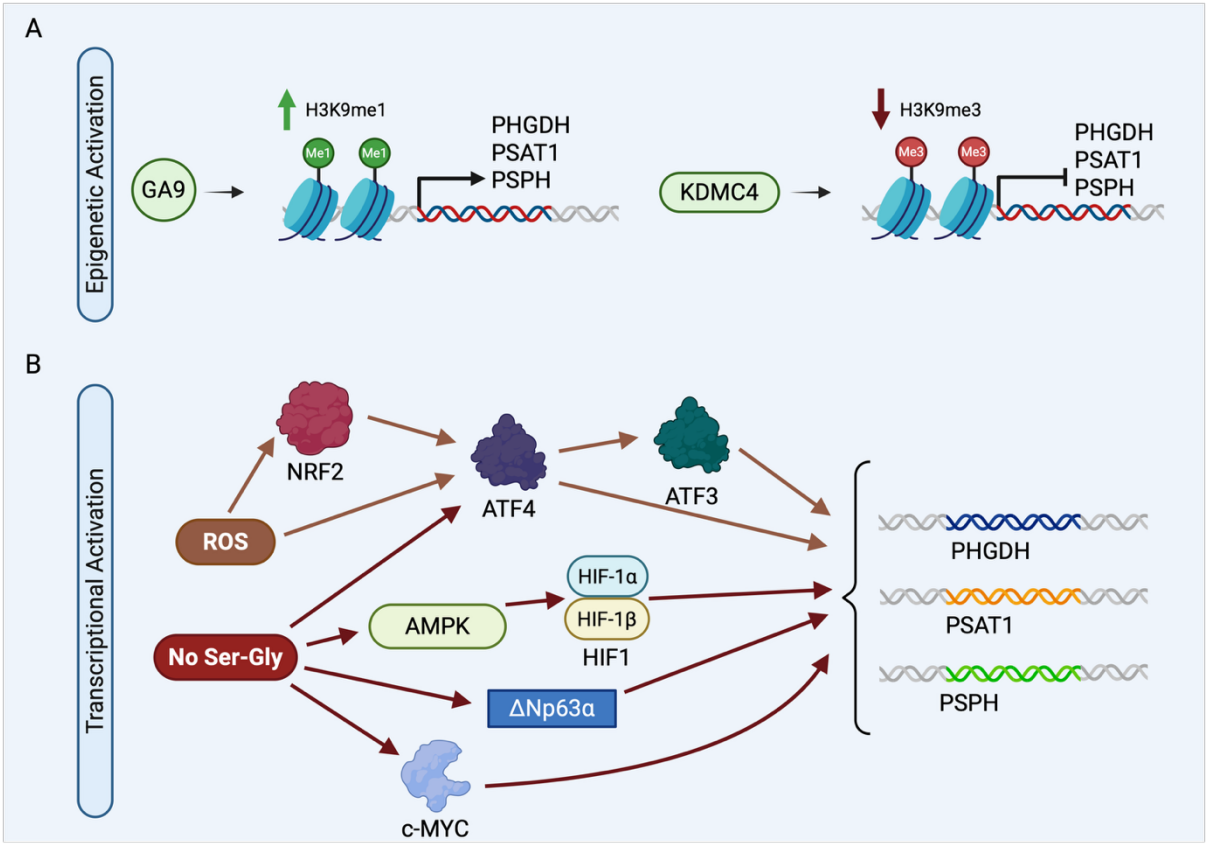

Figure 1.13 Epigenetic and transcriptional regulation of the SSP. A. The expression of the SSP enzymes (PHGDH, PSAT1, PSPH) is controlled at both epigenetic and transcriptional levels. Epigenetically, G9A-mediated H3K9 monomethylation promotes transcriptional activation, whereas KDMC4 removes repressive H3K9 trimethylation to facilitate gene expression. **B.** Transcriptionally, ROS and serine-glycine deprivation activate NRF2 and ATF4 signalling, with ATF3 enhancing ATF4 stability and target gene induction. AMPK-dependent stabilisation of HIF-1α, c-MYC, and ΔNp63α further contributes to SSP gene upregulation. Together, these regulatory networks coordinate metabolic adaptation by inducing PHGDH, PSAT1, and PSPH expression under stress conditions. Created in https://BioRender.com

An increase in this epigenetic mark was also found to induce expression of SSP genes under serine and glycine deprivation (J. Ding et al., 2013). Lysine demethylase 4C (KDMC4), another

histone modifier, epigenetically activates the SSP gene expression through the removal of repressive H3K9 trimethylation (H3K9me3). Increased levels of these mono- and tri-methylation marks were shown to promote cell survival and proliferation regardless of serine and glycine availability (E. Zhao et al., 2016).

Multiple transcription factors have been suggested to regulate the expression of SSP genes directly. ATF4, part of the UPR signalling pathway, has been described as a key regulator of the SSP (M. Yang & Vousden, 2016). Multiple studies, in different cancer models, have described ATF4 to interact with the amino acid response elements (AARE) within the promoter regions of PHGDH, PSAT1 and PSPH genes (R. Xu et al., 2020; Ye et al., 2012). In NSCLC under increased oxidative stress, nuclear factor erythroid 2-related factor 2 (NRF2), a key regulator of redox homeostasis, promotes the expression of SSP genes by transcriptionally activating ATF4 (DeNicola et al., 2015). Upon serine deprivation, Activating Transcription Factor 3 (ATF3) is induced in an ATF4-dependent manner, which then binds and increases the stability of ATF4, leading to the induction of SSP genes. Additionally, ATF3 is also capable of inducing the SSP, independently of ATF4 (X. Li et al., 2021). Together, these studies indicate the importance, and the central role played by ATF3/4 in regulating serine synthesis (**Figure 1.13B**).

A recent study in glioblastoma cells has also linked the SSP regulation with HIF-signalling. Specifically, under serine-glycine deprivation, increased ROS levels lead to the stabilisation of HIF-1α in an AMP-activated protein kinase (AMPK)-dependent manner. Activated HIF-1α signalling was shown to lead to increased expression of all three SSP genes. CHIP-qPCR analysis identified hypoxia response elements (HREs) in the promoter regions of PHGDH, PSAT1 and PSPH. This HIF-dependent induction of SSP was shown to increase antioxidant levels and maintain cell survival (Yun et al., 2023).

Moreover, chromatin immunoprecipitation (CHIP)-based analysis in Hep3B cells identified direct c-Myc binding to the E-box sequences close to the transcription start sites (TSS) of all SSP genes. When deprived of glucose and glutamine, SSP enzymes were induced in a c-

Myc-dependent manner. The c-Myc-mediated activation of SSP leads to improved cell survival and enhanced proliferation (Sun et al., 2015).

The most recently described transcriptional regulator of SSP genes is the lung squamous cell carcinoma (TCGA-LUSC) lineage-specific oncogene ΔNp63α. This transcriptional regulator was suggested to directly transactivate the expression of not only all SSP genes but also serine transporter ASCT1 (SLC1A4). This ΔNp63α-dependent induction in SSP was shown to improve redox balance and increase nucleotide synthesis, leading to better repair of carboplatin-mediated DNA damage and therapy resistance (Deng et al., 2026).

1.5.5.2 Repression of SSP

There is also a set of regulators that repress the expression of SSP genes. Studies in the malignant melanoma cell line A375 demonstrated that p53 directly represses the transcription of PHGDH, thereby suppressing *de novo* serine synthesis. Upon exposure to serine-deprived conditions, these p53 wild-type cells underwent pronounced growth arrest and, if the nutrient stress persisted, p53-mediated apoptosis (Ou et al., 2015). This growth arrest reflects a metabolic prioritisation strategy, whereby cells redirect the remaining available serine away from nucleotide synthesis and towards glutathione production, to buffer rising ROS levels. When this antioxidant response proves insufficient to resolve the metabolic stress, p53 signalling escalates towards apoptosis (Maddocks et al., 2013). Additionally, breast cancer cells harbouring p53 missense mutations showed elevated expression of SSP genes and increased serine import under nutrient-deprived conditions. This metabolic adaptation supports sustained cell growth and proliferation (Tombari et al., 2023). A tumour suppressor Yin Yang 2 (YY2) was found to directly bind to the promoter region of PHGDH in HCT116 colorectal cancer, repressing SSP and resulting in elevated ROS levels. Importantly, YY2 can also enhance the expression of p53, further enhancing its suppressive effect on the SSP (J. Li et al., 2023; L. Li et al., 2020) (**Figure 1.14A**).

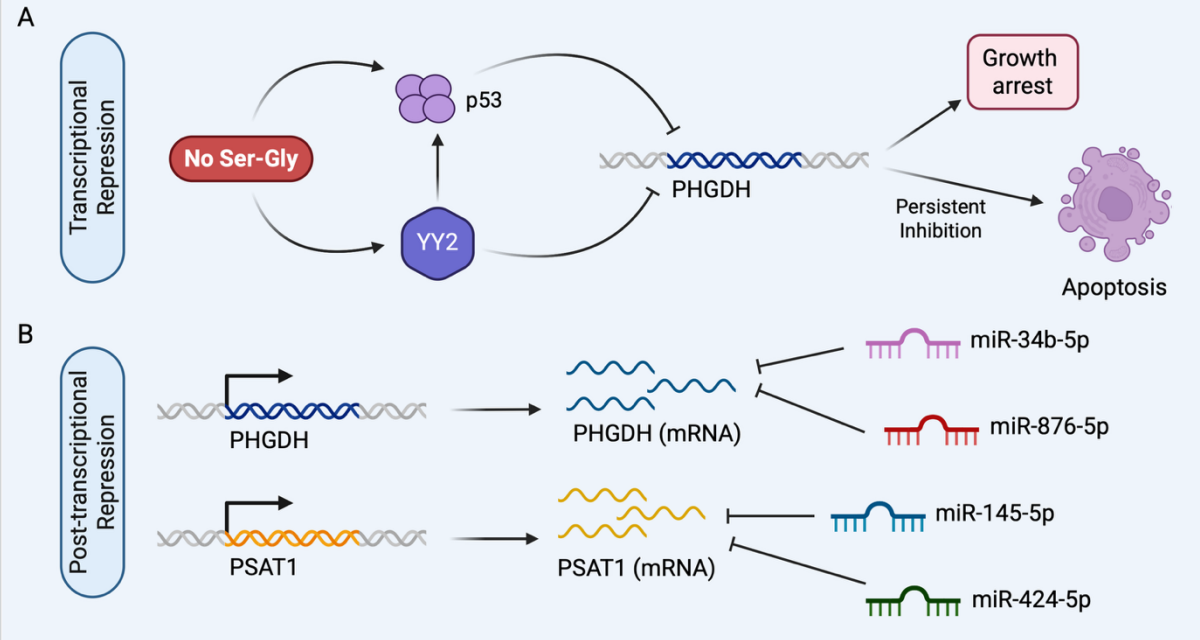

1.14 Transcriptional and post-transcriptional repression of the SSP. A. Serine-glycine deprivation activates tumour suppressor pathways that repress SSP gene expression. p53 suppresses PHGDH transcription, promoting apoptosis under metabolic stress. The transcription factor YY2 further inhibits PHGDH expression and can enhance p53 activity, reinforcing transcriptional repression. **B.** At the post-transcriptional level, specific microRNAs directly target SSP transcripts. miR-34b-5p and miR-876-5p bind PHGDH mRNA, whereas miR-145-5p and miR-424-5p target PSAT1 mRNA, reducing mRNA stability and translation. Together, these mechanisms limit SSP activity and sensitise cells to stress-induced cell death. Created in https://BioRender.com

Serine synthesis is also highly regulated post-transcriptionally. In hepatocellular carcinoma models, PHGDH, PSAT1 and PSPH mRNA were found to carry m6A modification added by methyltransferase-like 3 (METTL3). This modification subsequently leads to the recruitment of m6A-reader insulin-like growth factor 2 mRNA-binding protein 3 (IGF2BP3), increasing mRNA stability and translational efficiency (Chan et al., 2024). As in previous cases, these factors lead to increased antioxidant levels and enhanced cell survival. In contrast to m^{6}A-mediated stabilisation, serine synthesis can also be negatively regulated by microRNAs (miRNAs). In endocrine-resistant ER$^+$ breast cancer cells, downregulation of miR-145-5p, miR-424-5p, miR-34b-5p, and miR-876-5p, which directly target the 3′UTRs of PHGDH and PSAT1, relieves post-transcriptional repression and leads to increased SSP expression. Restoration of these miRNAs suppresses SSP gene expression and re-sensitises cells to endocrine therapy, highlighting miRNA-mediated control as a key regulatory mechanism of serine metabolism (Petri et al., 2023) (**Figure 1.14B**).

Different feedback loops within the SSP and glycolysis fine-tune the activation level of the pathway. Serine is an activator of the M2 isoform of pyruvate kinase (PKM2), which catalyses the final step of glycolysis. When serine levels are low, PKM2 activity is inhibited. Lower glycolytic rates result in increased availability of 3-PG, which is then fed into the SSP, increasing the rates of serine synthesis. Similarly, elevated intracellular serine levels can trigger a negative feedback mechanism that suppresses *de novo* serine synthesis, redirecting metabolic flux toward glycolysis (Chaneton et al., 2012; M. Yang & Vousden, 2016; Ye et al., 2012). Additionally, another glycolytic metabolite, 2-phosphoglycerate (2-PG), which is directly downstream of 3-PG, was suggested to act as an activator of PHGDH. Accumulation of 2-PG, which also occurs in the case of PKM2 inhibition, can lead to the diversion of 3-PG from glycolysis into the SSP (Hitosugi et al., 2012).

1.5.6 The SSP and cancer

The SSP plays a key role in maintaining cancer cell growth and proliferation. Patients with PHGDH overexpression in lung cancer cells, compared to healthy tissue, showed poorer survival and an increased risk of developing metastasis (J. Zhu et al., 2016). Amplifications and higher expression of other SSP genes were also observed in the head and neck, ovarian cancers, sarcomas and glioblastomas (Feng et al., 2022; D. Huang et al., 2025; J. Wang et al., 2019). Conversely, a recent study demonstrated that low PHGDH expression in breast cancer cells increases cancer cell dissemination and metastasis formation (Rossi et al., 2022). Similarly, recent evidence in pancreatic cancer indicates that low PHGDH expression in metastatic cells hijacks serine from neighbouring hepatocytes via the CXCL5/CXCR2 axis, thereby facilitating liver colonisation and poorer patient outcomes (**Figure 1.15**) (L. Shen et al., 2022).

Collectively, these studies highlight the complex role of serine synthesis in tumour progression and its impact on patient survival. In bladder cancer, PHGDH was found to interact with an RNA-binding protein, poly(RC) Binding Protein 2 (PCBP2), leading to decreased degradation of PHGDH and upregulation of SLC7A11. Higher levels of SLC7A11 lead to ferroptosis

inhibition, subsequently promoting malignant tumour progression (L. Shen et al., 2022). Another study showed elevated serine levels in hepatocellular carcinoma, which is caused by hyperactivation of PHGDH with no induction in its expression levels. The increase in PHGDH activity is mediated through its methylation by protein arginine methyltransferase 1 (PRMT1) at Arg-236 residue. Overall, the intracellular accumulation of serine is suggested to be predictive of poor patient prognosis (K. Wang et al., 2023).

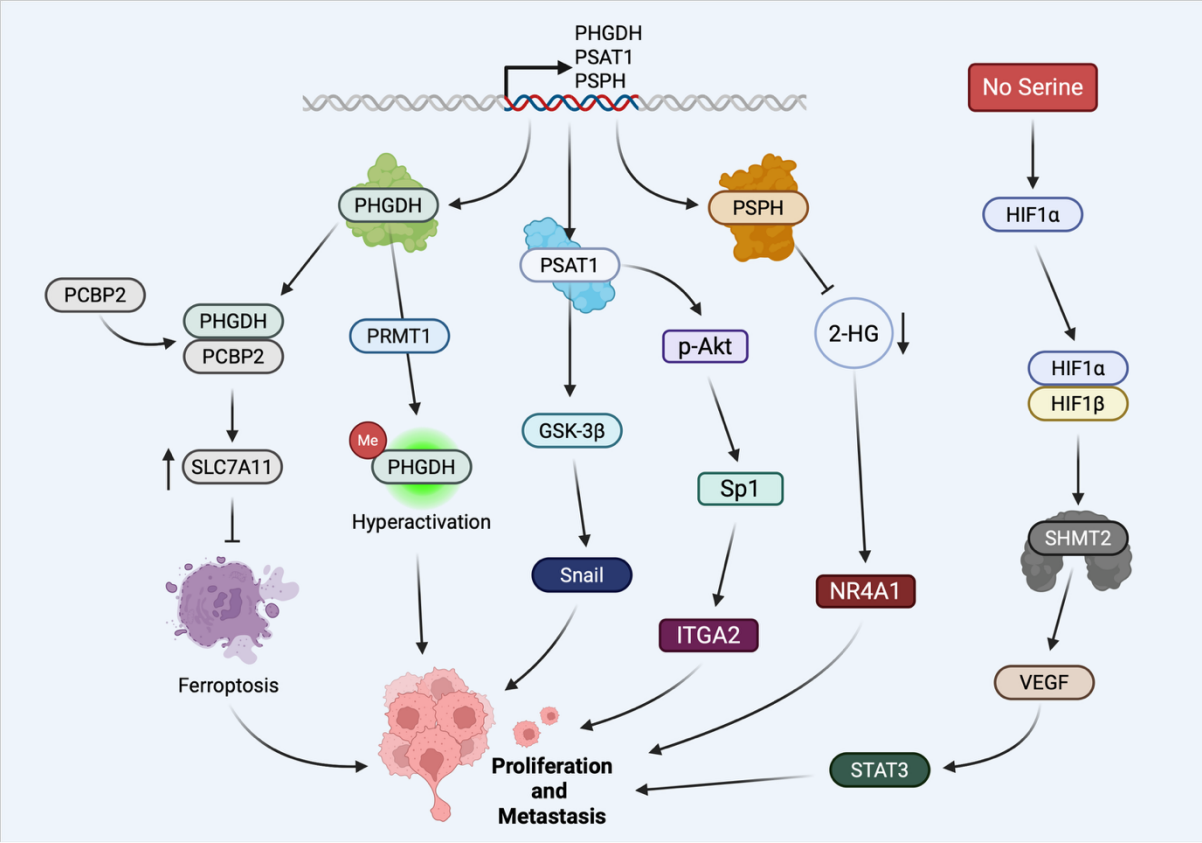

Figure 1.15 The role of SSP in increased cancer cell proliferation and metastasis formation. Beyond their metabolic roles, serine synthesis pathway (SSP) enzymes contribute to tumour growth and metastasis through signalling interactions. PHGDH activity is enhanced by PRMT1-mediated methylation, promoting tumour cell proliferation. PHGDH can also interact with PCBP2 to increase SLC7A11 expression, suppressing ferroptosis. PSAT1 activates the GSK-3β/Snail and p-Akt/Sp1 pathways, leading to ITGA2 induction and enhanced invasive capacity. PSPH has been linked to reduced 2-hydroxyglutarate (2-HG) levels and activation of NR4A1, supporting tumour progression. Under serine deprivation, HIF-1α stabilisation induces SHMT2 expression and downstream VEGF-STAT3 signalling, promoting angiogenesis and metastatic potential. Collectively, these findings highlight signalling roles of SSP enzymes that extend beyond one-carbon metabolism and contribute to aggressive tumour phenotypes. Created in https://BioRender.com

In oesophageal cancer cells, increased PSAT1 expression was suggested to enhance tumorigenesis and metastasis formation. The mechanism behind the poorer patient prognosis

was the induction of glycogen synthase kinase-3β (GSK-3β) and Snail signalling by PSAT1 (B. Liu et al., 2016). In oestrogen receptor-negative (ER-) breast cancer cells, PSAT1 was associated with increased risk of cell dissemination and metastasis. PSAT1 was shown to induce nuclear translocation of special protein 1 (Sp1) via p-Akt signalling induction. Nuclear Sp1 then facilitates the expression of integrin subunit alpha 2 (ITGA2), resulting in enhanced cell migration and invasion (X. Zhang et al., 2024).

In NSCLC, elevated levels of PSPH showed increased induction in mitogen-associated protein kinase (MAPK) signalling cascade, ultimately leading to increased cancer cell proliferation and invasion capacity (Liao et al., 2019). Additionally, elevated PSPH levels were also documented in melanoma patients. PSPH expression was suggested to reduce 2-hydroxyglutarate (2-HG) levels, leading to increased activity of nuclear receptor subfamily 4, group A, member 1 (NR4A1). This signalling activation is responsible for increased cell proliferation and epithelial-mesenchymal transition (EMT) (Rawat et al., 2021) (**Figure 1.15**).

Importantly for hypoxic tumours, SHMT2, which catalyses the serine to glycine interconversion, enhances HIF-1α stability in gastric cancer cells. Downstream HIF-1 signalling was then shown to result in increased activation of the VEGF-STAT3 axis. These ultimately lead to increased angiogenesis and metastasis (W. Wang et al., 2023).

1.5.7 Dietary restriction of serine as a therapeutic strategy

Metabolic enzymes have gained significant attention as drug targets, driven by an improved understanding of disease-associated metabolic dependencies. Among these, serine has repeatedly been identified as a central metabolite. The most recent example is the use of dietary restriction of serine in mouse models to overcome therapy resistance in glioblastoma (GBM). Tumours, like GBM, which rely on serine uptake rather than *de novo* glucose-derived synthesis, allow excess glucose to be redirected toward pathways that promote therapy resistance (Scott et al., 2025). Specifically, glucose-derived carbons are diverted into nucleotide biosynthesis via the PPP instead of entering the SSP. Concurrently, imported serine

fuels 1C metabolism, further supporting nucleotide production. Together, sustained or elevated nucleotide pools promote invasive growth and enhance resistance to radiotherapy and chemotherapy. Consequently, restricting extracellular serine availability forces increased reliance on solely glucose-derived serine synthesis, thereby reducing nucleotide production, limiting cell growth, and enhancing sensitivity to therapies (Scott et al., 2025). Importantly, depletion of environmental serine and other nonessential amino acids is clinically achievable through specialised non-essential amino acid restriction (NEAAR) diets (ClinicalTrials.gov ID: NCT05078775). Another study also suggested restriction of extracellular serine and glycine to improve GBM patient response to radiotherapy (Falcone et al., 2022). Additionally, dietary restriction of serine in tandem with PHGDH inhibition was shown to lead to accumulation of deoxysphingolipids in colorectal, breast and lung cancer cells, resulting in lower growth rate (Muthusamy et al., 2020).

1.5.8 Folate cycle as a target for therapeutic agents

Tumours characterised by elevated serine and glycine synthesis were suggested to exhibit increased sensitivity to clinically approved antifolate agents that target the folate cycle (see 1C metabolism in section 1.1.2). In this context, inhibitors of dihydrofolate reductase (DHFR), such as methotrexate and pemetrexed, disrupt THF regeneration required for 1C metabolism and have also been shown to inhibit SHMT activity, contributing to improved therapeutic responses (Daidone et al., 2011; Vazquez et al., 2013). Other approved drugs that similarly target the purine and pyrimidine synthesis are pralatrexate and 5-fluorouracil (5-FU) (Amelio et al., 2014; Spears et al., 1982; P. Su et al., 2026). Sertraline, a selective serotonin reuptake inhibitor (SSRI), has been shown to inhibit SHMT2, the enzyme responsible for catalysing the interconversion of serine and glycine. By disrupting this key step of serine metabolism, sertraline depletes glycine availability for GSH synthesis, thereby compromising cellular redox homeostasis and elevating ROS. The increased oxidative stress burden was shown to impair DNA damage repair capacity, ultimately enhancing radiotherapy sensitivity in NSCLC (Sánchez-Castillo et al., 2024).

Importantly, the SSP promotes tumour adaptation to radiotherapy by sustaining nucleotide production and antioxidant defence (Falcone et al., 2022). Serine-derived 1C units generated by SHMT1/2 are required for nucleotide synthesis. Reduced serine availability, specifically, has been shown to reduce the supply of 1C units into the folate cycle, impairing *de novo* purine synthesis. A smaller nucleotide pool results in replication arrest and an inability to efficiently repair DNA damage. Overall, serine-driven nucleotide depletion represents a complementary mechanism of radiosensitisation, acting alongside disrupted redox homeostasis to overwhelm tumour DNA repair capacity (Falcone et al., 2022; Labuschagne et al., 2014).

Mitochondrial SHMT2-mediated serine catabolism was shown to result in NADPH production and limit ROS accumulation under stress, promoting cell survival (Ye et al., 2014). This compartmentalised folate metabolism contributes directly to cellular NADPH pools, reinforcing redox buffering capacity (Ducker et al., 2016; J. Fan et al., 2014). In head and neck squamous cell carcinoma (HNSCC), radioresistance is driven, in part, by NRF2-mediated upregulation of the SSP, which diverts glycolytic flux to enhance DNA repair and redox buffering (DeNicola et al., 2015; Mims et al., 2015). Furthermore, 1C-dependent SAM synthesis couples serine availability to histone methylation dynamics, providing a mechanism for epigenetic adaptation during stress (Mentch et al., 2015). Together, these studies support a model in which SSP activity promotes radioresistance by coordinating nucleotide biosynthesis, NADPH generation, GSH levels, and methylation-dependent chromatin regulation.

Moreover, the SSP is an important determinant of immunotherapy response, acting as a metabolic regulator that shapes the tumour microenvironment (TME). Hyperactivation of the rate-limiting enzyme PHGDH drives enhanced serine flux and promotes tumour-associated macrophage (TAMs) polarisation toward an immunosuppressive, M2-like phenotype that limits T-cell recruitment and activation (Ouyang et al., 2023). In parallel, PHGDH upregulation in tumour endothelial cells drives aberrant vessel sprouting and intratumoral hypoxia, establishing an immune-hostile vascular microenvironment. Such T cell-exclusionary niche was shown to confer GBM resistance to CAR-T cell immunotherapy (D. Zhang et al., 2023). Overall, pharmacological targeting of the SSP is emerging as a promising strategy to reverse

macrophage-mediated immune suppression and sensitise tumours to immunomodulatory therapies (Cai et al., 2024; D. Huang et al., 2025; Mullarky et al., 2016).

1.6 PHGDH in cancer

1.6.1 The structure of PHGDH

Due to its crucial, rate-limiting role in the SSP, PHGDH is conserved across organisms ranging from bacteria to mammals. However, three different isoforms of the protein exist. Type I PHGDH is expressed in mammals, plants and some bacteria (**Figure 1.16**). Type I PHGDH has the most complex structure, comprised of two substrate-binding domains (SBDs) flanking a nucleotide-binding (NBD) domain. SBDs are responsible for engaging with 3-PG, and NBDs bind to NAD+ co-factors. Two additional domains, allosteric binding domain (ASB) and aspartate kinase-chorismate mutase-tyrosinase A prephenate dehydrogenase domain (ACT), are also present in Type I PHGDH.

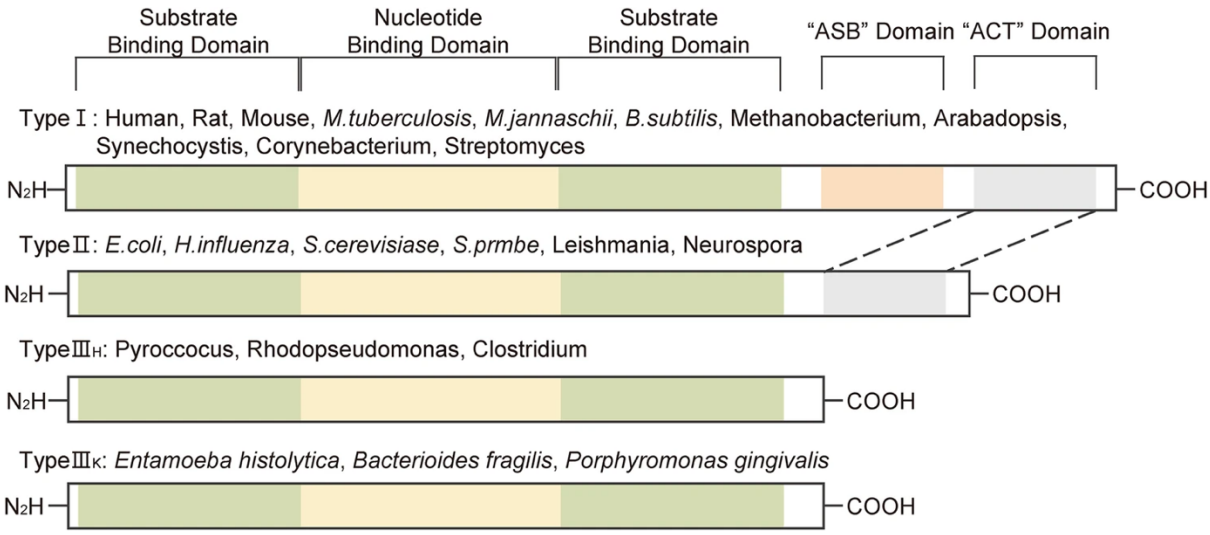

Figure 1.16 Evolutionary variation in PHGDH domain architecture. Comparative schematic of PHGDH protein organisation across species. Type I PHGDH, present in mammals, plants and several bacteria, contains conserved substrate-binding and nucleotide-binding domains followed by C-terminal regulatory regions, including ASB and ACT domains. Type II enzymes, identified in organisms such as *E. coli* and yeast species, maintain the catalytic core but exhibit truncated or altered regulatory segments. Type III enzymes, subdivided into Type IIIH and Type IIIK, largely consist of the catalytic core with minimal or absent C-terminal regulatory extensions. The N- and C-termini are indicated to highlight structural differences between groups. Adapted from Lee et al., 2024 and distributed under the Creative Commons Attribution 4.0 International License (CC BY 4.0) (http://creativecommons.org/licenses/by/4.0/)

The ASB domain functions as an allosteric binding site for the substrate 3-PG, allowing the enzyme to sense substrate availability at a site distinct from the catalytic active site, thereby

providing an additional layer of regulation over enzymatic activity (Dey et al., 2005; Grant et al., 2004; C. M. Lee et al., 2024). The ACT domain, which is exclusive to Type I PHGDH, serves as the primary feedback regulatory module, binding L-serine to suppress enzyme activity when serine levels are sufficient within the cell (Grant, 2006; Mullarky et al., 2016). The functional importance of both domains extends beyond their individual regulatory roles. The physical interaction between these domains across the dimer-dimer interface is the structural basis for the homotetrameric assembly of Type I PHGDH, coupling quaternary structure directly to allosteric regulation in a manner absent from the simpler Type II and Type III isoforms (Dey et al., 2005; Mullarky et al., 2016).

The functional unit of Type I PHGDH is a homotetramer, assembled as a dimer of dimers, in which two catalytic dimers associate through their C-terminal regulatory domains (ASB and ACT domains) (Dey et al., 2005). This tetrameric architecture is not merely structural; it is required for allosteric regulation, as the conformational changes required for feedback inhibition can only be transmitted within the context of the full tetrameric assembly (Mullarky et al., 2016). Within this tetramer, the ASB and ACT domains occupy the core of the dimer-dimer interface, where they make extensive contacts with their counterparts from the opposing dimer (Dey et al., 2005). The ASB domain contributes to the structural integrity of the tetramer while simultaneously relaying information about substrate availability across subunits. The ACT domain binds L-serine at a site formed cooperatively between opposing subunits, meaning that serine binding is only geometrically possible when the tetramer is intact (Grant, 2006). This architecture effectively locks catalytic output, substrate sensing, and feedback inhibition into a single integrated quaternary unit, a level of regulatory sophistication that is progressively lost in Type II, which retains ASB but lacks ACT, and absent in Type III isoforms, which exist as simpler homodimers (Dey et al., 2005; C. M. Lee et al., 2024) (**Figure 1.16**).

1.6.2 Post-translational regulation of PHGDH

Beyond transcriptional control, PHGDH activity is further regulated at the post-translational level through covalent modifications that influence its function (**Figure 1.17**).

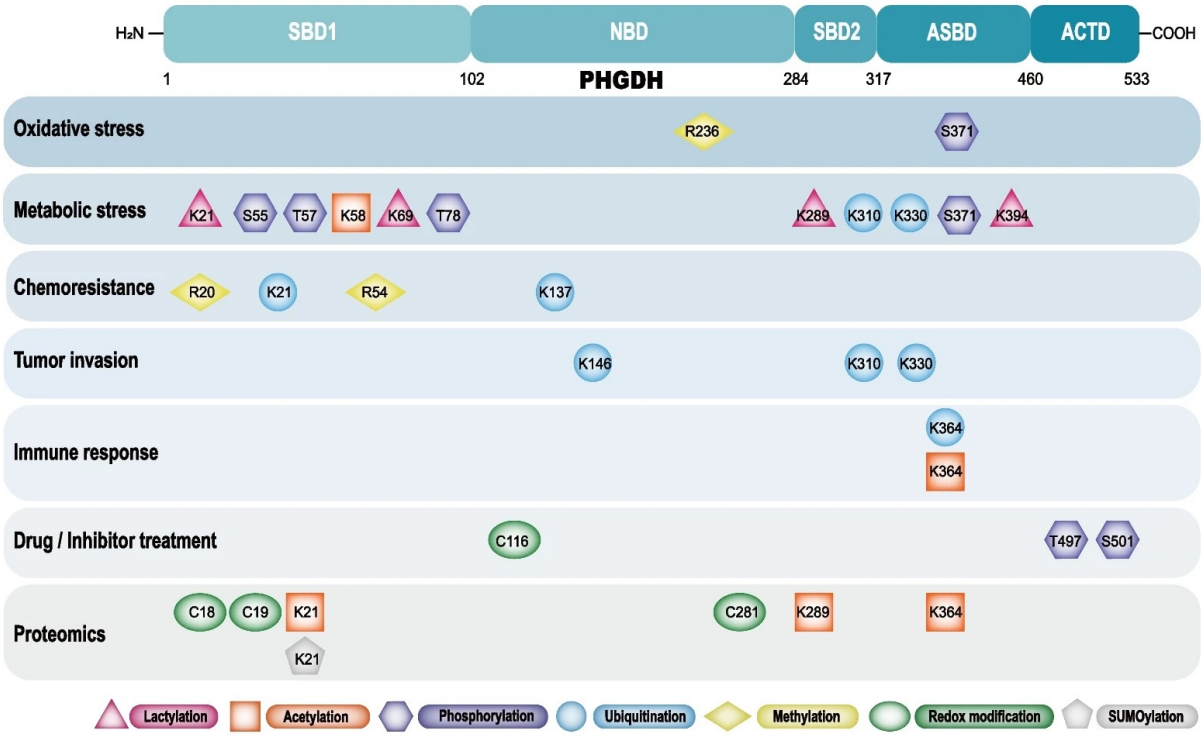

Figure 1.17 Post-translational modification (PTM) landscape of PHGDH across functional domains. Schematic overview of PHGDH domain organisation and mapped PTM sites. Residue-specific modifications are categorised according to biological contexts, including oxidative stress, metabolic stress, chemoresistance, tumour invasion, immune response, drug or inhibitor treatment, and proteomic analyses. Identified PTMs include lactylation, acetylation, phosphorylation, ubiquitination, methylation, redox modification, and SUMOylation, illustrating the multi-layered regulation of PHGDH under physiological and pathological conditions. Reproduced from (M. Shu et al., 2025), licensed under the Creative Commons Attribution 4.0 International License (CC BY 4.0) (http://creativecommons.org/licenses/by/4.0/)

Ubiquitination represents an additional layer of PHGDH regulation, primarily controlling protein stability. Several E3 ligases have been shown to promote PHGDH degradation, thereby reducing SSP activity and serine biosynthesis (Dalton, 2020; C. Wang et al., 2020; W. Zhang et al., 2025). Conversely, deubiquitinating enzymes such as UCHL3 and JOSD2 enhance PHGDH stability and sustain serine production (Y. Wang et al., 2023; N. Zhao et al., 2024). Moreover, PHGDH can undergo lysine lactylation, a modification derived from intracellular lactate that increases under conditions of elevated glycolytic flux (D. Zhang et al., 2019). Disruption of glyoxalase 2 (Glo2) results in lactyl-glutathione accumulation, promoting non-

enzymatic lactylation of PHGDH at residues K21, K69, K289, and K394. This modification suppresses PHGDH catalytic activity, limiting the conversion of 3-PG to serine and reducing intracellular serine biosynthesis (Trujillo et al., 2025).

Additional PHGDH can be acetylated, leading to enhanced protein activity. Proteins such as Tip60 can reversibly acetylate PHGDH (K58), leading to increased protein stability by blocking RNF5-mediated ubiquitination in response to glucose starvation (C. Wang et al., 2020). Other PTMs for PHGDH include methylation, SUMOylation, deamidation, and S-palmitoylation (M. Shu et al., 2025).

1.6.3 Therapeutic strategies for targeting PHGDH

The important role of PHGDH as a metabolic driver in cancers stimulated significant interest in drug discovery. A structurally diverse collection of inhibitors has been reported, spanning allosteric compounds, cofactor-competitive agents, targeted protein degraders, and others (Arlt et al., 2021; Z. Huang et al., 2024; Mullarky et al., 2016; Pacold et al., 2016; Q. Wang et al., 2017; J.-Y. Zhao et al., 2021). Despite this progress, none have advanced to clinical trial, reflecting challenges in achieving sufficient potency while minimising unwanted off-target effects.

The earliest pharmacological validation of PHGDH involved first-generation compounds identified through high-throughput screening. CBR-5884 was identified as a weak and selective inhibitor that disrupts the active tetrameric state in favour of an inactive dimeric conformation by binding at the ASB-ACT interface (**Table 1.1**). This provided the first chemical evidence that PHGDH quaternary structure fluctuation is pharmacologically exploitable, though the compound proved unstable in mouse plasma (Mullarky et al., 2016). Similarly, NCT-503 was found to reduce glucose-derived serine production and suppress growth in melanoma and breast cancer cells with amplified PHGDH expression (Pacold et al., 2016).

Table 1.1: Small molecule inhibitors of PHGDH classified by mechanism of action

Inhibitor	Class	Mechanism	IC_{50}	Reference
NCT-503	Non-competitive and allosteric	Binding pocket unresolved	2.5 μM	(Pacold et al., 2016)
CBR-5884	Non-competitive and allosteric	Likely binding to ASB-ACT interface	33 μM	(Mullarky et al., 2016)
PKUMDL-WQ-2101	Non-competitive and allosteric	Binds SBD Site I (R134, K57, T59)	34.8 μM	(Q. Wang et al., 2017)
PKUMDL-WQ-2201	Non-competitive and allosteric	Binds SBD Site II (T56, K57, T59)	35.7 μM	(Q. Wang et al., 2017)
α-Ketothioamides	Non-competitive and allosteric	Binding pocket unresolved	~8.7 μM	(Ravez et al., 2017)
Piperazine-1-thioureas	Non-competitive and allosteric	Binding pocket unresolved	~1-5 μM	(Rohde et al., 2018)
Pyrazole-5-carboxamides	Non-competitive and allosteric	Binding pocket unresolved	sub-μM	(J.-Y. Zhao et al., 2021)
BI-4916 / BI-4924	Co-factor competitive	Binding NBD cofactor pocket	3 nm	(Weinstabl et al., 2019)
Indole amides	Co-factor competitive	Binding NBD cofactor pocket	~1-10 μM	(Mullarky et al., 2019)
D8	Co-factor competitive	Binding NBD cofactor pocket (D175)	2.8 μM	(D. Gao et al., 2023)
Disulfiram	Covalent agent	Tetramer to inactive disulfide-linked dimer (Cys116)	n/a	(Spillier et al., 2019)
B12	Covalent agent	Disturbed tetramer assembly and allosteric sensing (Cys421)	~0.29 μM	(Cao et al., 2024)
Withangulatin A	Natural product	Perturbs substrate binding (Cys295)	0.29 μM	(C. Chen et al., 2022)
Oridonin	Natural product	Perturbs substrate binding (Cys18)	0.5 μM	(Tan et al., 2022)
Ixocarpalactone A	Natural product	Binding pocket unresolved	~9.8 μM	(M. Zheng et al., 2019)
Azacoccone E	Natural product	Binding pocket unresolved	1.66 μM	(J. Guo et al., 2019)
LXH-3-71	Targeted protein degrader	E3-ligase mediated proteasomal degradation	n/a	(Z. Huang et al., 2024)

However, recent studies suggested NCT-503 reduces glucose-derived citrate synthesis independently of PHGDH expression, suggesting an off-target effect on central carbon metabolism. The precise mechanism underlying this off-target effect remains unclear,

representing a significant limitation in the use of NCT-503 for metabolic studies (Arlt et al., 2021).

Structure-based virtual screening has also identified two novel allosteric sites within the PHGDH substrate-binding domain. Compounds PKUMDL-WQ-2101 and PKUMDL-WQ-2201 target these sites specifically, demonstrating dose-dependent suppression of PHGDH-amplified breast cancer cell lines. Unlike cofactor-competitive agents, these inhibitors avoid the challenges of high intracellular NAD+ concentrations by binding to regulatory regions. Metabolomic profiling and CRISPR-knockout models have validated their specificity, showing that dual-site targeting by these two drugs can synergistically inhibit enzyme activity and suppress *in vivo* tumour growth (Q. Wang et al., 2017).

Perhaps the most promising therapeutic strategy involves cofactor-competitive inhibition, which has yielded the most potent PHGDH inhibitors to date. By targeting the NAD+/NADH binding pocket of the NBD directly, indole amide compounds like BI-4924 achieve single-digit nanomolar IC_{50} values. Because of the high cytosolic NAD+ levels, a prodrug strategy using BI-4916 was implemented to achieve the necessary intracellular enrichment of the active drug (Weinstabl et al., 2019). Compared to the direct administration of the active inhibitor (BI-4924), utilising the ethyl ester prodrug (BI-4916) facilitated a 140-fold increase in cytosolic enrichment of the drug (J.-Y. Zhao et al., 2021).

The covalent modification of surface cysteine residues has recently emerged as an alternative strategy for the irreversible inhibition of PHGDH. Disulfiram, a treatment for chronic alcoholism, was also found to be a covalent allosteric inhibitor of PHGDH. This small molecule targets and oxidises the Cys116 residue, abrogating the polymerisation of PHGDH. Specifically, it prevents the tetramerisation of PHGDH and results in the formation of inactive dimers or monomers of PHGDH (Spillier et al., 2019). Another inhibitor that was suggested to act in a similar mechanism was B12 (benzo[b]thiophene-1,1-dioxide series). B12 forms a covalent bond with the Cys421 residue of PHGDH, preventing its polymerisation and allosteric substrate sensing (Cao et al., 2024).

Similarly, various natural products act through covalent modification at unique residues to induce enzyme inactivation. Withangulatin A, isolated from the plant *Physalis angulata*, modifies Cys295 to block the substrate-binding domain and elevate intracellular reactive oxygen species (C. Chen et al., 2022). Oridonin, derived from *Rabdosia rubescens*, targets Cys18 to dislocate the substrate-interacting residue R54 and reduce enzyme affinity (Tan et al., 2022). Other plant-derived molecules, such as Ixocarpalactone A from *Physalis ixocarpa* and the fungal derivative Azacoccone E, have shown inhibitory activity in xenograft models (J. Guo et al., 2019; M. Zheng et al., 2019). However, a major limitation of this class remains the broad cysteine reactivity common to many covalent natural products. This lack of specificity raises significant concerns regarding their therapeutic index and potential for off-target effects in humans.

The most conceptually novel approach to PHGDH inhibition uses "molecular glues" to induce protein degradation. In colorectal cancer models, the compound LXH-3-71 covalently binds to the C281 residue of PHGDH to facilitate the recruitment of the E3 ligase DDB1 . This interaction induces the selective polyubiquitination and proteasomal degradation of the enzyme, effectively reducing cancer cell stemness and tumour growth (Z. Huang et al., 2024). By eliminating the protein, this PTM-based non-catalytic strategy offers a novel way to overcome the limitations of conventional active-site inhibition of PHGDH.

1.6.4 Non-canonical roles of PHGDH

The majority of identified PHGDH mutations were found to diminish its enzymatic activity, which appears inconsistent with the dependence of some cancers on SSP amplification (Possemato et al., 2011; C. Wang et al., 2025). This paradox may reflect a reliance of certain tumours on non-metabolic functions of PHGDH that contribute to progression and metastasis. An example of a non-catalytic function of PHGDH is its phosphorylation and subsequent nuclear translocation under glucose starvation. Following glucose deprivation in pancreatic cancer cells, the S371 (serine-371) residue of PHGDH was found to be phosphorylated in a p38-dependent manner, leading to its nuclear translocation. Subsequent phosphorylation of

the S55 by AMPK enhances the NADH production by PHGDH and depletes the nuclear pool of NAD+. Reduced NAD+ levels lower PARP1 activity and c-Jun transcriptional activity, thereby increasing cancer cell proliferation (C. Ma et al., 2021) (**Figure 1.18**).

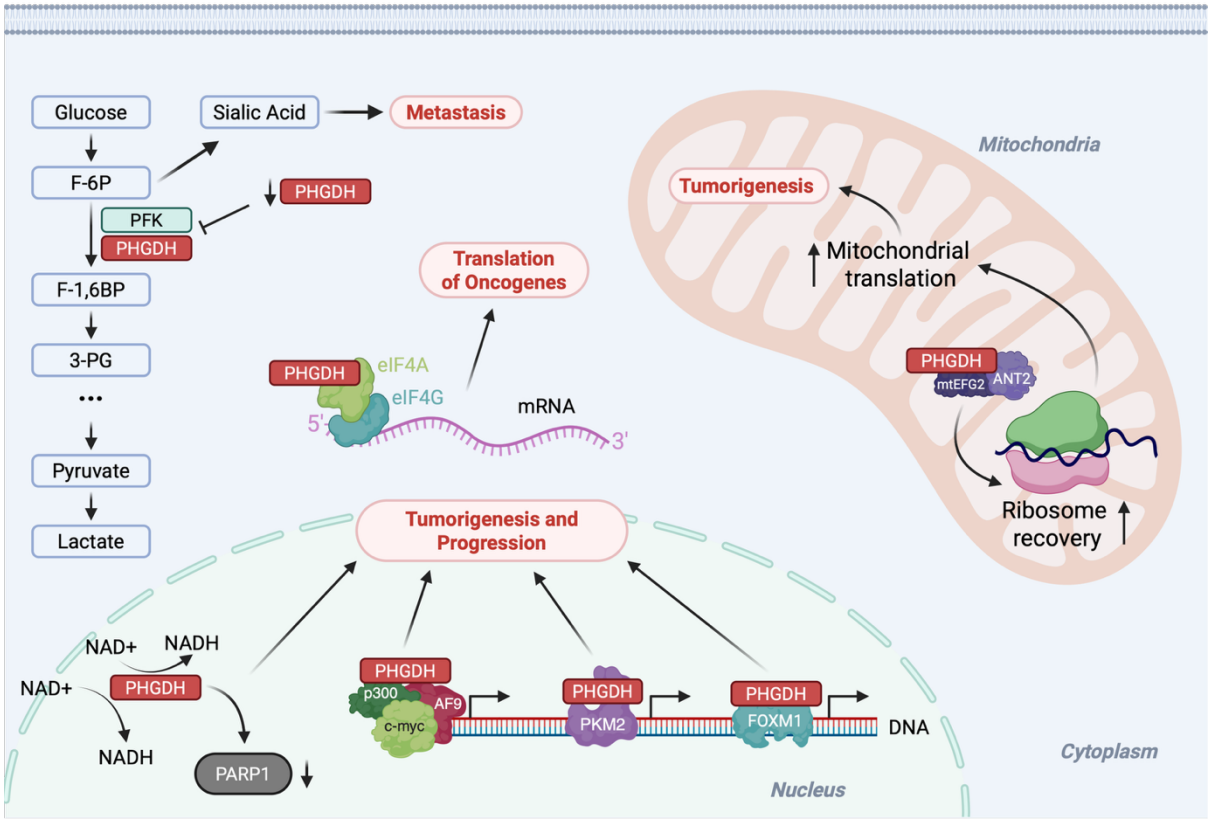

Figure 1.18 Serine-independent functions of PHGDH in tumorigenesis and metabolic reprogramming. Schematic overview of PHGDH functions beyond its canonical role in serine biosynthesis. In the cytoplasm, PHGDH interacts with translation initiation factors (eIF4A and eIF4G) to enhance oncogene translation. Within mitochondria, PHGDH associates with proteins such as mtEFG2 and ANT2 to support mitochondrial translation and ribosome recovery, contributing to tumorigenesis. In the nucleus, PHGDH interacts with transcriptional regulators to modulate gene expression programs that drive tumour progression. Additionally, PHGDH influences NAD+/NADH balance and PARP1 activity, linking metabolic state to DNA-associated processes. Collectively, these interactions illustrate the multifaceted role of PHGDH in cancer progression beyond its enzymatic activity in the serine synthesis pathway. Created in https://BioRender.com. Schematic representation based on information from C. Wang et al., 2025.

Low PHGDH expression has been associated with poorer outcomes in breast cancer patients. This is driven by a non-catalytic function of PHGDH in which reduced interaction with phosphofructokinase (PFK) redirects glycolytic flux toward the hexosamine-sialic acid pathway. Notably, in circulating tumour cells and early metastatic lesions, PHGDH-low expression increases sialic acid production, enhancing surface glycosylation and promoting migration and invasion independent of its enzymatic activity (Rossi et al., 2022).

In the cytoplasm, PHGDH stabilises the eukaryotic initiation factor 4F (eIF4F) complex by directly binding its subunits A and G (eIF4A and eIF4G). eIF4F bound to PHGDH then interacts with the 5'-end of the mRNA, promoting oncogene expression (X. Ma et al., 2019).

Low 3-PG levels were also shown to result in PHGDH interaction with scaffold protein AXIN, in tandem with HIPK2 kinase. This trimer then forms a complex with p53, leading to its phosphorylation (Ser46) and induction of apoptosis (Y.-Q. Wu et al., 2023). PHGDH interactions with other proteins are not restricted to the cytoplasm. In hepatocellular carcinoma cells, PHGDH localises to the inner mitochondrial membrane, where it interacts with adenine nucleotide translocase 2 (ANT2) and recruits mitochondrial elongation factor G2 (mtEFG2) to enhance mitochondrial ribosome recovery and mtDNA-encoded protein expression. Through these protein-protein interactions, mitochondrial PHGDH promotes tumorigenesis by supporting mitochondrial translation and bioenergetic function (Y. Shu et al., 2022). In the nucleus, PHGDH interacts with p300 (transcriptional co-activator). The PHGDH-p300 complex then promotes the activation of PKM2, which induces the expression of oncogenes and genes related to glycolysis mainly through histone-phosphorylation (Y. Wu et al., 2023). It is important to note that PKM2 is also a downstream target of HIF1α, suggesting a potential convergence between hypoxia- and PHGDH-mediated coactivation of gene expression (J. Wang et al., 2021). The PHGDH-p300 complex also interacts with c-myc, leading to increased neutrophil recruitment, chemokine production, and tumour-associated macrophage (TAM). This results in cancer progression and is regulated by the PHGDH/p300/c-myc/AF9 axis (H. Zhu et al., 2023). Forkhead box protein 1 (FOXM1) is a crucial transcription factor for oncogene expression. The N-terminal region of FOXM1 leads to its degradation. PHGDH binds to the N-terminal end of the protein, leading to increased stability and induction of pro-cancer gene expression (J. Liu et al., 2013; C. Wang et al., 2025).

1.7 Aims of this study

- Characterise how PHGDH expression is regulated under hypoxia.
- Investigate the impact of PHGDH loss on radiosensitivity under normoxic and hypoxic conditions across varying extracellular serine levels.
- Investigate non-canonical roles for PHGDH in hypoxia

Chapter 2: Materials and Methods

2.1 Cell culture

Unless otherwise indicated, cells were grown in Dulbecco's Modified Eagle Medium (DMEM) supplemented with 10% (v/v) foetal bovine serum (FBS) and 1% penicillin-streptomycin antibiotic solution (**Table 2.1**). All cell lines were cultured at 37˚C and 5% CO_2, in humidified incubators. Upon reaching 70-80% confluence, cells were passaged using 0.25% Trypsin-EDTA (ThermoFisher Scientific).

Table 2.1: Cell lines used in the study.

Name	Cancer type	Media	Source
A549	Non-small cell lung cancer	DMEM	ATCC
H460	Large cell lung cancer	DMEM	ATCC
RKO	Colorectal adenocarcinoma	DMEM	ATCC
FLO-1	Oesophageal adenocarcinoma	DMEM	Prof. Katherine Vallis (University of Oxford)

2.2 Mycoplasma Testing

All cell lines used in this study were routinely tested for Mycoplasma contamination using MycoAlert Mycoplasma Detection Kit (Lonza), in accordance with the manufacturer's instructions. In brief, 2 ml of culture media was spun down at 200 x *g* for 5 min and 100 μl of supernatant was transferred into a flat-bottomed, white-walled, 96-well plastic plate. Sterile phosphate-buffered saline (PBS) was used as a negative control. A positive control was provided by the manufacturer. MycoAlert reagent (100 μl) was added to the samples and incubated for 5 min at room temperature. Luminescence was measured using a POLARstar Omega microplate reader. After the measurement, 100 μl of MycoAlert substrate was added to the sample-containing wells and incubated for 10 min at room temperature. A second luminescence measurement was taken following the incubation, and the ratio of both readings was recorded. A ratio value of less than 0.9 was considered a negative reading for Mycoplasma.

2.3 Cryopreservation and thawing of cells

2.3.1 Freezing cells

Once confluent, cells were harvested and centrifuged at 300 x *g* in complete media (containing FBS). Following centrifugation, the supernatant was removed, and the pellet was resuspended in a freezing medium (90% FBS and 10% dimethyl sulfoxide (DMSO)) and transferred into cryovials at an approximate concentration of $2x10^6$ cells/ml. Vials were stored at -70˚C for up to one week, followed by transfer to liquid nitrogen for long-term cryopreservation.

2.3.2 Thawing cells

Cryovials, containing frozen cells, retrieved from liquid nitrogen, were thawed quickly in a 37˚C water bath. Cells were transferred into complete media and spun down at 300 x *g* for 5 min. Following centrifugation, the supernatant containing DMSO was removed, and the cell pellet was resuspended in complete media. Cells were then transferred into small flasks/dishes and incubated in a humidified incubator at 37˚C and 5% CO_2.

2.4 Exposure to hypoxia

For hypoxia exposure, cells plated in glass dishes, were incubated in Whitley H35 Hypoxystation (Don Whitley Scientific) set to 0.5-2% O_2. Radiobiological hypoxia was reached by incubating cells in a BACTRON II anaerobic chamber (Shel Labs) and Whitley A35 Workstation (Don Whitley Scientific). The oxygen concentration in the hypoxia chambers was regularly verified using anaerobic indicator strips (Fisher Scientific). To avoid the introduction of excess oxygen into hypoxic chambers, cells were cultured in glass dishes for all hypoxic experiments, except clonogenic survival assays, for which 6-well plastic plates were used.

2.5 Generation of CRISPR-Cas9 knockout clones

Tubes containing Synthego guide RNA (gRNA) were briefly centrifuged and rehydrated in 1X TE buffer to generate a 100 μM solution. Following reconstitution, 3 μM gRNA stocks were made by diluting the oligos in Opti-MEM I reduced serum media (Gibco). Two reaction mixes

per gRNA were prepared. The guide mix containing 25 μl Opti-MEM I Reduced Serum Media, 1.3 μl sgRNA pool (3 μM stock), 1.0 μl Cas9 (3 μM stock) and 1.0 μl Cas9 PLUS Reagent (Invitrogen). Second reaction mix contained 25 μl Opti-MEM I Reduced Serum Media and 1.5 μl Lipofectamine CRISPRMAX transfection reagent (Invitrogen). Both mixes were incubated for 10 min at room temperature (RT), following which they were combined and incubated for an additional 10 min. During the incubation period, a suspension of 100000 cells in 500 μl of complete growth media was prepared. Cells were then resuspended in the reaction mix containing the gRNAs (**Table 2.2**). The cell suspension was then transferred to a 24-well plate (250 μl per well). Following 24 h incubation, the media was replaced with complete growth media. Cells were then allowed to grow for 7 days. The knockout status of this pooled population was validated using western blotting.

Table 2.2: gRNA sequences used for the generation of PHGDH knockout clones.

Guide #	Sequence	Exon
1	U*U*U*CUGCUUCAGGACUGUGA + Synthego modified EZ scaffold	2
2	A*G*C*UGCGUUGAUGACAUCAG + Synthego modified EZ scaffold	2
3	A*G*G*UGUGGACAAUGUGGAUC + Synthego modified EZ scaffold	2

N*N*N* indicate 2'-O-methyl analogues and 3'-phosphorothioate internucleotide linkages

For clonal selection, a cell suspension of 50 cells in 10 ml complete growth media was prepared and aliquoted into a flat-bottomed 96-well plate and incubated in a humidified incubator (37˚C, 5% CO_2) for up to 14 days to allow colony formation. Western blotting was performed using lysates derived from single-cell clones, and the those lacking PHGDH expression were selected for further validation by Sanger sequencing.

2.6 PHGDH CRISPR-Cas9 knockout validation by Sanger sequencing

Genomic DNA (gDNA) was extracted from parental and knockout clones using the Quick-DNATM Miniprep kit (Zymo Research) in accordance with the manufacturer's instructions. To amplify the genomic region containing PHGDH, PCR primers were designed using the Primer3 tool on Benchling online software to generate 800-1000 bp long amplicons (**Table 2.3**).

Table 2.3: Primer sequences (5'-3') used for PCR amplification of the human PHGDH exon 2 targeted by CRISPR-Cas9 ribonucleoprotein complex (RNP).

Primer	Sequence	Length	%GC	Tm	Amplicon (bp)
Fwd	GAACCCAGGCCTGACCAATGGC	22	63.6%	62.0˚C	982
Rvs	AGAGGTGCAAGCAACTGCGCAT	22	54.5%	62.0˚C	

Q5 High-Fidelity DNA polymerase kit (New England Biolabs) was used to perform the PCR amplification of the CRISPR-targeted genomic region. Detailed concentrations and amounts of reagents used for the PCR master mix are shown (**Table 2.4**). 100 ng of total gDNA was diluted in 25 μl of master mix, following which they were briefly centrifuged and amplified using a T100 thermal cycler (BioRad). The annealing temperature was calculated using the New England Biolabs online Tm calculator tool (https://tmcalculator.neb.com/#!/main). The details of the PCR protocol are shown (**Table 2.5**).

Table 2.4: PCR master mix

Reagent	Volume (μl)	Concentration
5x Q5 reaction buffer	5	1x
10 mM dNTPs (Thermo Fisher Scientific)	0.5	200 μM
10 μM forward primer	1.25	500 nM
10 μM reverse primer	1.25	500 nM
Q5 High-Fidelity DNA Polymerase	0.25	0.02 U/μl
Sample DNA	Varying	100 ng
Nuclease-free water	25 μl total	

Table 2.5: Thermal cycler settings for PCR amplification

Step	Temperature	Time (sec)	Number of Cycles
Initial denaturation	98˚C	60	1X
Denaturation	98˚C	10	35X
Annealing	72˚C	10	
Extension	72˚C	30	
Final extension	72˚C	120	1X

The amplified PCR product was then purified using the QIAquick PCR Purification Kit (Qiagen) in accordance with the vendor's instructions. The DNA content was quantified NanoDrop™ spectrophotometer (ThermoFisher Scientific). Samples were sent to Genewiz (Azenta Life Sciences, Abingdon, United Kingdom) for Sanger sequencing. Upon receipt, sequencing results were analysed and visualised using the Inference of CRISPR Edits (ICE) tool from Synthego.

2.7 Cell proliferation assay

Cells were counted using a Neubauer Pattern Haematocytometer (Hawksley AC1000), and 4000 cells were seeded in a flat-bottomed 24-well plate in sets of technical triplicates (total number of wells = number of days x 3). For the daily count, cells were treated with 200 μl Trypsin-EDTA solution, which was then quenched with 200 μl media following cell detachment. The cell suspension was thoroughly mixed and counted using a Haematocytometer.

2.8 RNA extraction and purification

RNA extraction was performed by cell lysis with TRI-Reagent (Sigma-Aldrich T9424). Cells were washed with 1 ml of PBS twice and harvested in 1 ml of TRI-Reagent. To extract the RNA, 200 μl of 100% chloroform was added to the suspension, vortexed for 15 sec, and incubated at room temperature for 3 min. Samples were then spun down 15000 x *g* for 15 min at 4˚C. The top clear layer, containing the RNA, was carefully separated, without disrupting the rest of the sample, and transferred into fresh Eppendorf tubes. the isolated RNA fraction was mixed with 100% isopropanol and centrifuged for at 15000 x *g* for 10 min at 4˚C. The

supernatant was discarded, and the pellet washed in 70% (v/v) ethanol and spun down again at 7500 x *g* for 5 min at 4˚C. The supernatant was discarded, and the pellet dried at room temperature for 20 min (until completely dry). The dried pellet was then resuspended in 30 μl ultrapure, DEPC-treated water (ThermoFisher Scientific). RNA concentration was determined using a NanoDrop™ spectrophotometer, with absorbance measured at 260 nm (ThermoFisher Scientific). The RNA purity was confirmed with A260/A280 ratios of around 2.0.

2.9 Complementary DNA (cDNA) synthesis by reverse transcription

cDNA was synthesised using the Verso cDNA synthesis kit (ThermoFisher Scientific). 500 ng of RNA was mixed with cDNA synthesis buffer, dNTP mix, RT enhancer, RNA primer, Verso enzyme (ThermoFisher Scientific) and DEPC-treated water (ThermoFisher Scientific) in proportions shown (**Table 2.6**). The PCR reaction was run at 42˚C for 60 min, 95˚C for 2 min and kept at 4˚C. Samples were stored at -20˚C.

Table 2.6: Reagents used for cDNA synthesis

Reagent	Volume (μl)
RNA	5
cDNA synthesis buffer	2
dNTP mix	1
RNA primer	0.5
RT enhancer	0.5
Verso enzyme	0.5
DEPC water	0.5

2.10 Quantitative PCR (qPCR)

For the qPCR SYBR Green PCR master mix (Applied Biosystems) and 7500 FAST Real-Time PCR machine (Applied Biosystems) were used. cDNA samples were mixed with forward and reverse primers for target genes, SYBR Green PCR master mix, and DEPC-treated water as shown in **Table 2.7** in 96-well microplates. The run protocol was as follows: preparation at 50°C for 20 seconds and 95°C for 15 minutes; 40 cycles at 95°C for 15 seconds, 60°C for 30 seconds and 72°C for 30 seconds; melting curve at 95°C for 15 seconds, 60°C for 1 minute, 95°C for 30 seconds and 60°C for 15 seconds. 18S was used as a reference housekeeping gene, and the ΔΔCt method was used to determine relative mRNA fold change. Working concentrations and sequences for the used primers are shown in **Table 2.8**.

Table 2.7: Reagents for qPCR reaction mix

Regent	Volume/Well (μl)
cDNA	5
SYBR Green	12.5
Forward primer	2.5
Reverse primer	2.5
DEPC water	2.5

Table 2.8: Primers sequences and concentrations used for RT-qPCR

Gene	Conc.	Forward Primer	Reverse Primer
18S	10 μM	GCCCGAAGCGTTTACTTTGA	TCCATTATTCCTAGCTGCGGTATC
PHGDH	1 μM	CTGCGGAAAGTGCTCATCAGT	TGGCAGAGCGAACAATAAGGC
CAIX	1 μM	CTTGGAAGAAATCGCTGAGG	TGGAAGTAGCGGCTGAAGTC
ATF4	1 μM	TGACCTGGAAACCATGCCAG	AATGATCTGGAGTGGAGGAC
GLUT1	1 μM	TTGCAGGCTTCTCCAACTGGAC	CAGAACCAGGAGCACAGTGAAG
VEGF	1 μM	ATCTTCAAGCCATCCTGTGTGC	CAAGGCCCACAGGGATTTTC
LDHA	1 μM	AGGCTACACATCCTGGGCTAT	CCCAAAATGCAAGGAACACTA

2.11 Cell lysis for western blotting

For each experimental condition, 10^6 cells were seeded into 10 cm glass dishes and incubated overnight in humidified incubators (37˚C, 5% CO_2). For protein harvesting, cells were lysed in fresh UTB lysis buffer consisting of 75 mM Tris, 9 M urea and 0.1% (v/v) 2-mercaptoethanol (pH 7.5).

2.12 Western blotting

Lysed samples were mixed with 2X Laemmli Buffer, with 2-Mercaptoethanol (150 mM), and boiled at 100˚C for 10 min. Afterwards, samples were loaded into 4-20% Mini-PROTEAN TGX pre-cast gels (Bio-Rad 4561095) and run at 120 V and 3.0 A in Tris-Glycine-SDS running buffer (1X). Semi-dry transfer onto nitrocellulose membranes was conducted using the Trans-Blot Turbo transfer system (Bio-Rad 1704150). The membrane was blocked using a 1:1 mix of Tris Buffer Saline (TBS) and Intercept Blocking Buffer (LI-COR 927-70001) for one hour at room temperature on an orbital shaker. Primary antibodies (**Table 2.9**), diluted in blocking buffer, were incubated on the membrane overnight at 4˚C. After primary antibody incubation, samples were incubated with secondary antibodies (**Table 2.10**) diluted in a blocking buffer for 1 hour at room temperature. Following both primary and secondary antibody incubations, three cycles of 5 min washes were completed using 0.1% (v/v) TBS-Tween solution.

Table 2.9: List of primary antibodies used for western blotting, immunofluorescence and immunoprecipitation experiments

Protein	Species	Dilution	Application	Vendor	Ref No
HIF-1α	Mouse	1:1000	WB	BD Biosciences	NB100-105
PHGDH	Mouse	1:1000	WB	Novus Biologicals	NBP1-87311
RNase H1	Mouse	1:1000	WB	Santa Cruz	sc-365267
DHX9	Rabbit	1:1000	WB	Bethyl Laboratories	A300-854A
PARP1	Rabbit	1:1000	WB	Cell Signalling Tech	9542
S9.6	Mouse	5 µg	IP	Kerafast	Kf-Ab01137-23.0
V5	Mouse	1:500	IF	Invitrogen	46-0705
β-Actin	Mouse	1:2000	WB	Santa Cruz	sc-69879

Table 2.10: List of secondary antibodies used for western blotting and immunofluorescence

Name	Host	Reactivity	Dilution	Application	Vendor	Ref No
IRDye 800CW	Donkey	Mouse	1:7500	WB	LI-COR	926-32212
IRDye 680RD	Goat	Mouse	1:7500	WB	LI-COR	926-68070
IRDye 800CW	Donkey	Rabbit	1:7500	WB	LI-COR	926-32213
IRDye 680RD	Goat	Rabbit	1:7500	WB	LI-COR	926-68071

2.13 Cellular fractionation

Cells were gently scraped in 1 ml of ice-cold PBS and centrifuged for 5 min at 500 x *g*, 4°C. The supernatant was discarded, and another round of ice-cold PBS wash was performed. The cell pellet was then resuspended in cellular fractionation buffer consisting of 10 mM HEPES, 10 mM KCl, 340 mM sucrose, and 10% (w/v) glycerol supplemented with 10% Triton X-100. The volume of the cellular fractionation buffer was determined based on the pellet size (i.e. approximately twice the volume of the cellular pellet). Samples were incubated on ice for 5 min and spun down for 5 min, at 500 x *g*, 4°C. The supernatant (cytoplasmic fraction) was collected and stored in fresh Eppendorf tubes. The pellet (nuclear fraction) was lysed in UTB buffer (see western blotting). The amount of protein was measured using Pierce BCA assay (ThermoFIsher Scientific) in accordance with the manufacturer's instructions. For fractionation western blots, 50 µg of protein was loaded for the cytoplasmic fraction and 100 µg for the nuclear fraction (including the respective whole cell lysate controls).

2.14 Immunofluorescence

Cells were fixed with 4% (w/v) paraformaldehyde (PFA) solution and permeabilised with 1% (v/v) Triton X-100 (Sigma-Aldrich) in PBS. Samples were then blocked for 1 hour at room temperature using a blocking buffer consisting of 2% (w/v) bovine serum albumin (BSA) in 0.1% PBS-Tween 20 solution (ThermoFisher Scientific). Primary antibody incubation was performed overnight at 4˚C. Afterwards, samples were incubated with secondary antibodies for 1 hour at room temperature. Both, primary and secondary antibodies were diluted in 2% (w/v) BSA, 0.1% PBS-Tween 20 blocking buffer. Lastly, coverslips were mounted using Prolong Gold antifade mountant containing DAPI nuclear stain (ThermoFisher Scientific) and

dried overnight at room temperature. Image acquisition was conducted using the 63x plan-apochromat DIC M27 oil immersion objective (NA=1.4) on LSM710 or LSM780 confocal microscope systems (Carl Zeiss Microscopy).

2.15 siRNA knockdown

For transfection, cells were plated at a density of 400,000 cells/ml (per well) using an antibiotic-free complete culture medium (i.e. supplemented with 10% FBS [v/v]). To generate transfection complexes, a mix of 0.2 µl/well DharmaFECT transfection reagent (Horizon Discovery) and 0.25 µM siRNA was incubated at room temperature for 20 min. The complex formation was done in serum-free culture media. Complexes were further diluted 1:2.5 in an antibiotic-free complete medium to make up the transfection medium (final volume: 1 ml). The transfection medium was then added to a 6-well plate, mixed with an equal volume of cell mix (1 ml = 400000 cells), and incubated for 16 hours at 37˚C and 5% CO_2.

2.16 R-loop co-immunoprecipitation with S9.6 antibody

2.16.1 Sample harvesting

Samples for immunoprecipitation (IP) were harvested in ice-cold PBS and centrifuged for 5 min, at 500 x *g,* at 4˚C. After carefully discarding the supernatant, the pellet was resuspended in a lysis buffer containing 85 mM potassium chloride (KCl), 5 mM PIPES (pH 8.0), 0.5% (w/v) NP-40 (ThermoFisher Scientific), supplemented with EDTA-free protease inhibitors cocktail (Roche Diagnostics). The suspension was incubated on ice for 10 min and spun down for 5 min at 4˚C, 500 x *g*. Input samples were lysed in fresh UTB buffer with 150 mM 2-Mercaptoethanol.

The resulting pellet, containing the nuclear fraction, was resuspended in protease inhibitor cocktail (Roche Diagnostics) supplemented IP lysis buffer containing 10 mM Tris-HCl (pH 7.5), 200 mM sodium chloride (NaCl), 2.5 mM magnesium chloride ($MgCl_2$), 0.2% (w/v) sodium deoxycholate (NaDOC), 0.1% sodium dodecyl sulphate (SDS), 0.05% sodium lauroyl sarcosinate (SLS), and 0.5% (v/v) Triton X-100. To lyse the nuclei and shear the DNA to

approximately 500-700 bp size, samples were incubated on ice for 10 min in IP lysis buffer and sonicated for 120 seconds (30-second ON and 90-second OFF intervals) using Bioruptor PLUS (Diagenode). Double-stranded DNA (dsDNA) concentration was determined using NanoDrop One/OneC Microvolume UV-Vis Spectrophotometer, with absorbance measured at 260 nm (ThermoFisher Scientific). Following sonication, the nuclear fraction was supplemented 1:1 (v/v) with IP buffer containing 10 mM Tris-HCl (pH 7.5), 200 mM NaCl, 2.5 mM $MgCl_2$, 0.05% (w/v) NaDOC, 0.025% SDS, 0.0125% SLS, and 0.5% (v/v) Triton X-100 supplemented with protease inhibitor cocktail (Roche Diagnostics). To measure the protein concentration in the IP samples, Pierce bicinchoninic acid assay (BCA) kit was used according to the manufacturer's instructions (ThermoFisher Scientific). Around 5-10% of the samples were saved to be used as IP input.

2.16.2 Conjugation of S9.6 antibody to protein A Dynabeads

Prior to conjugation, 40 μl of protein A Dynabeads were aliquoted into fresh 1.5 ml tubes and engaged on a stationary magnetic rack. After removing the supernatant, beads were washed three times in resuspension buffer with Triton (RSB-T) containing 10 mM Tris-HCl (pH 7.5), 200 mM NaCl, 2.5 mM $MgCl_2$ and 0.5% (v/v) Triton X-100. The washes were performed by adding the RSB-T buffer to the beads immobilised on a magnetic rack, following which tubes containing the beads were disengaged from the magnet, gently mixed by inverting and re-engaged on the magnetic rack. Following the wash steps, protein A Dynabeads were resuspended in 1 ml of IP buffer. To conjugate S9.6 and IgG isotope control antibodies with protein A Dynabeads, 5 μg of S9.6 (Kerafast) and IgG (Abcam) antibodies were added to the magnetic beads in IP buffer and incubated for 3 hours on a rotating wheel. Following the conjugation, the antibody-bead complex was washed three times in RSB-T buffer. Magnetic bead-bound proteins were eluted using 0.1 M dithiothreitol (DTT) diluted in Laemmli-b (LDS). The eluent was split equally and loaded into 2 to 3 PROTEAN TGX 4-20% gels (Bio-Rad, 4561093) and used for western blotting and silver staining. For silver stain, the ProteoSilver Kit (Merck, SLCL6363) was used according to the manufacturer's instructions.

2.16.3 Chemical crosslinking of S9.6 antibody to protein A Dynabeads

Following the conjugation of S9.6 antibody with protein A Dynabeads, the antibody-bead complexes was washed with 0.2 M triethanolamine solution (crosslinking buffer, pH=8.2) for 1 min and placed on a magnetic rack. After the wash, conjugates were incubated in crosslinking buffer supplemented with 25 mM dimethyl pimelimidate (DMP, ThermoFisher Scientific) at room temperature for 45 min with gentle agitation. Crosslinked beads were washed and incubated in 0.1 M ethanolamine solution (pH 8.2) for 30 min at room temperature, with gentle agitation. Three PBS washes were performed, following which antibody-bead complexes were washed with 0.1 M glycine-HCl (pH 2.5) to remove any non-crosslinked antibodies. Lastly, three PBS washes were performed.

2.16.4 S9.6 Co-immunoprecipitation

Following the washes, antibody-bead complexes were immobilised on a magnetic rack and the supernatant was removed. 130 μg of IP samples was added to the tubes containing the antibody-bead complexes and topped up to 400 μl with IP buffer. The mixture was incubated overnight at 4˚C on a rotating wheel. Samples were then engaged on a magnetic rack, and the supernatant was carefully removed. Samples bound to the antibody-bead complexes were washed three times for 5 min in RSB-T buffer and once in RSB buffer (RSB-T buffer without Triton X-100).

2.16.5 DNA precipitation and gel electrophoresis

To identify the fragment size generated after sonication, nuclear extracts were first treated with proteinase K (New England Biolabs) for 3 hours (fresh enzyme was added after every hour). Following protein digestion, samples were mixed with 1 M potassium acetate and spun down for 15 min, at 13000 x *g*, 4˚C. The supernatant was transferred into a fresh Eppendorf tube and mixed with 50% isopropanol to precipitate the DNA. Samples were then centrifuged for

15 min, at 13000 x *g*, 4˚C and the pellet was washed with 75% ethanol and air dried. The resulting DNA was resuspended in ultrapure, DEPC-treated water, and the concentration was measured using a NanoDrop One/OneC Microvolume UV-Vis Spectrophotometer. 5 µg of DNA was loaded into a 1.5% agarose gel, which was ran for 90 minutes at 150 V. Gels were imaged using ChemiDoc XRS+ Imaging Systems (Bio-Rad).

2.17 Transient transfection

$2x10^6$ cells were seeded in 10 cm dishes and left overnight to attach. Upon reaching 80-90% confluence cells were transfected with 16 µg of plasmid. The plasmid and 40 µl of Lipofectamine 2000 transfection reagent (Invitrogen) was mixed in 1 ml of Opti-MEM reduced serum media (Gibco), vortexed for 10 sec, spun down and incubated for 5 min at room temperature. Following incubation, two solutions containing the plasmid, and the transfection reagent were mixed, vortexed for 10 seconds, spun down and incubated for another 20 min at room temperature. Lastly, the mixture was added dropwise to the cells, gently mixed by rocking and incubated for 16-24 h.

2.18 MitoSOX red staining

Live cells were treated with MitoSOX Red (5 µM) reagent (Invitrogen) for 10 min at room temperature. Following staining, cells were fixed with 4% (v/v) PFA for 10 min and washed three times with PBS for 1 min. Coverslips were mounted with Prolong Gold antifade mountant containing DAPI nuclear stain (ThermoFisher Scientific) and dried overnight at room temperature.

2.19 MTT assay

For each treatment condition, 8000 cells were seeded in a flat-bottom 96-well plastic plate in triplicates. Following the end of the treatment period, 3-(4,5-dimethylthiazol-2-yl)-2,5-diphenyltetrazolium bromide (MTT, 0.5 mg/ml) reagent was added to the cells and incubated for 3 h at 37°C, shielded from light. After the incubation, once the formation of purple (formazan) crystals was observed, the MTT-containing media was removed. Formazan crystals were then solubilised by adding 100 μl of DMSO for 15 min at 37°C, protected from light. The absorbance was measured using a POLARstar Omega microplate reader (BMG Labtech) at 570 nm. The assay for hypoxic samples was carried out in hypoxic chambers. Viability data for both normoxic and hypoxic samples were calculated as percentage viability normalised to the normoxic and hypoxic vehicle controls, respectively.

2.20 Colony formation assay

Following trypsinisation into a homogenous single-cell suspension, cells were counted using a haematocytometer. Depending on the plating efficiency of the cell line or treatment type, 250-1000 cells were added into 6-well plastic plates in triplicates. Cells were left in 37°C incubators for up to 6 h to adhere before treatment. Following the treatment, plates were carefully transferred into 37°C and 5% CO_2 incubators and left to form colonies for up to 14 days (depending on the cell line used). Following the formation, colonies were stained by carefully removing the media and adding a crystal violet solution (0.5% w/v) with 20% ethanol and 50% methanol. After staining, colonies were counted using GelCount software (Oxford Optronix, Animalab). Only colonies containing at least 50 cells were counted and used for the analysis.

2.21 Real-time metabolic flux analysis (glycolytic stress test)

Real-time analysis of glycolytic stress was performed using the Agilent Seahorse XF analyser in accordance with the manufacturer's instructions. The day before the measurement, 8000

A549 cells were seeded into the Seahorse XF microplate in DMEM supplemented with 10% FBS and incubated overnight. Additionally, the sensor cartridge was hydrated in Seahorse XF calibrant overnight in 37°C, non-CO_2 incubator.

On the day of the measurement, the assay medium was prepared, consisting of Seahorse XF base medium supplemented with 2 mM Glutamine (GlutaMAX supplement, ThermoFisher Scientific). Additionally, the compounds for the glycolytic stress test were prepared (**Table 2.11**).

Table 2.11: Seahorse cartridge port layout and compound concentration

Port	Compound	Final Concentration	Port Concentration	Port Volume
A	Glucose	10 mM	80 mM	25 µl
B	Oligomycin	1 µM	9 µM	25 µl
C	2-Deoxyglucose	50 mM	500 mM	25 µl

Following dilution, compounds were loaded into the respective ports. The growth medium was then replaced with 175 µl of supplemented assay medium and incubated at 37°C, non-CO_2 incubator for 1 h. While incubating cells in assay media, the utility plate with the loaded sensor cartridge was placed into the Seahorse XF analyser and a calibration protocol was performed. After the calibration was completed, the Seahorse XF microplate was placed into the analyser, and 3 measurement cycles were recorded following the addition of each compound (3 min mix and 3 min measure). Extracellular acidification rate (ECAR) and oxygen consumption rate (OCR) were recorded. The readings were normalised to cell number. Cells were counted following the ECAR and OCR measurements using the brightfield channel on the Nexcelom Celigo imaging cytometer.

2.22 Transformation of DH5α competent cells

The competent *E. coli* DH5α cells were first thawed on ice and mixed with 5 µl plasmid DNA. Afterwards, the cells were incubated on ice for 30 min and heath shocked for 30-45 sec. Once cooled on ice, 500 µl of super optimal broth with catabolite repression (SOC) medium was

added to the cell suspension and incubated for 1 h, at 37°C on a mixing block (Eppendorf Thermomixer). The transformed cells were then transferred onto Luria broth (LB) agar plates supplemented with antibiotics for plasmid selection and incubated overnight at 37°C.

The following day, single colonies were picked and inoculated into a 10 ml LB media supplemented with 1% (v/v) antibiotics and grown overnight while shaking at 37°C. Transfer the bacteria suspension into a conical flask containing 200 ml of LB medium supplemented with 1% (v/v) antibiotics and continue growing for another day while shaking at 37°C. Finally, the suspension was then aliquoted into 50 ml falcon centrifuge tubes.

2.23 Dual luciferase luminescence assay

To measure HIF-induced luciferase activity, 8000 cells (A549) were seeded in a white-walled 96-well plate for luminescence measurement using the Dual-Glo luciferase assay system (Promega). Cells were co-transfected with 5xHRE-luciferase (Firefly) and Renilla luciferase reporter plasmids at a ratio of 9:1 (i.e., 90 ng Firefly to 9 ng Renilla) using Lipofectamine 2000 transfection reagent (ThermoFisher Scientific) (Shibata et al., 2000). For each time point, separate 96-well plates were used. Following overnight incubation, the transfection media was replaced with 75 µl of complete cell culture media and cells were exposed to hypoxia.

Inside the hypoxia chamber, 75 µl of Dual-Glo luciferase reagent, consisting of Dual-Glo luciferase buffer and Dual-Glo luciferase substrate, was added to the cells. Plates were incubated inside the chamber for 20 min, after which luminescence readings were taken using the POLARstar Omega microplate reader. To measure the Renilla luciferase luminescence, 75 µl of Dual-Glo Stop & Glo reagent, comprising of Dual-Glo Stop & Glo Substrate diluted in Dual-Glo Stop & Glow buffer 1:100 (v/v), was added to the cells. After incubating for 20 min at RT, luminescence measurements were taken. The ratio of Firefly to Renilla luciferase luminescence values was calculated across all conditions.

2.24 Metabolomic analysis

Cells were seeded in 10 cm plastic dishes and left to grow until reaching 90% confluency. The cell culture media was removed, and cells were washed with 5 ml of ice-cold PBS. Cells were then fixed in 500 µl ice-cold methanol for 5 min, scraped with a cell scraper, and collected in 1.5 ml Eppendorf microtubes. Cells were then spun down at 17000 x *g* for 30 min. The DNA content of the supernatant was measured using a NanoDrop™ spectrophotometer (ThermoFisher Scientific). The DNA concentration was normalised to the samples with the lowest concentration (expected range: 50-100 ng/µl, expected variation across samples: 20%). To remove the soluble proteins from the samples, 500 µl of the suspension was passed through a 10 kD molecular weight cut-off filter (Amicon Ultra, Millipore). Before filtering, the filters were washed with MiliQ water by centrifugation for 30 min at max speed. Lastly, the normalised and filtered samples were transferred into Waters Total Recovery autosampler vials with pre-slit PTFE caps, in which samples were stored at -80°C until the analysis by LC-MS. Moreover, before freezing, a quality control (QC) sample was also prepared by mixing equal volumes from all samples (10-20 µl).

2.25 FL-1 glutathione assay

Cells were seeded (8000/well) in clear, flat-bottomed 96-well plates (white-walled), with a final volume of 100 µL per well and allowed to adhere overnight. Each treatment condition was performed in triplicate. N-Acetylcysteine (NAC, 2 mM) and *N*-Ethylmaleimide (NEM; 200 µM) were used as controls and incubated with the cells for 6 h. 1 h before hypoxia treatment was complete, FL-1 (10 µM) was added to each well, and the contents of the well were mixed (Twigger et al., 2024). Following the incubation, the fluorescence was measured (excitation 485 nm, emission 520 nm) (POLARstar plate reader, BMG LabTech).

2.26 Statistical analysis

All statistical analysis in this thesis was performed with GraphPad Prism 10 software (version 10.6.1, GraphPad Software Inc.). The type of statistical test implemented is highlighted in the

legend of each figure. Statistical significance was assigned to comparisons with p values of less than 0.05 (*$p < 0.05$; **$p < 0.01$; ***$p < 0.001$; ****$p < 0.0001$). Unless indicated otherwise, error bars in result figures represent mean of three biological replicates ± standard error of the mean (SEM).

Chapter 3: Hypoxic regulation of PHGDH and the effect of its loss on cell metabolism

3.1 Introduction

Lung cancer remains the leading cause of global cancer-related mortality, responsible for approximately 1.8 million deaths in 2022 (J. Zhou et al., 2024). As for most solid tumours, hypoxia is a common characteristic of lung cancers. The hypoxic nature of lung cancer TME has been linked to therapy resistance (Falk et al., 1992; McKeown, 2014). Specifically, hypoxic lung tumours were shown to have enhanced resistance to radiotherapy, chemotherapeutic agents such as cisplatin, and EGFR tyrosine kinase inhibitors, including gefitinib (Y. Liu et al., 2010; Minakata et al., 2012; Wohlkoenig et al., 2011).

To assess the prevalence and transcriptional consequences of hypoxia in patient cohorts, several gene expression-based hypoxia signatures have been developed and validated across tumour types. These include the Winter metagene (99 genes), the Buffa metagene (51 genes), the Ragnum signature (32 genes), and the West classifier (26 genes). The West 26-gene signature was taken forward for patient stratification in the NIMRAD trial, indicating the clinical potential of these metagenes (Buffa et al., 2010; Eustace et al., 2013; Salberg et al., 2022; Thomson et al., 2024; Winter et al., 2007).

Limited oxygen availability in the TME is also known to drive changes in the cellular metabolic landscape. Hypoxic cancer cells shift from oxidative phosphorylation to glycolysis and reprogram carbon metabolism, including increased reliance on glutamine for citrate synthesis, to support growth and survival (Warburg, 1925; Wise et al., 2011). These metabolic changes are primarily driven by HIF-1 signalling. In addition to HIF-signalling, exposure to radiobiological hypoxia (<0.1% O_2) leads to the activation of the UPR pathway (Koumenis et al., 2002; Ramachandran et al., 2021; Rzymski et al., 2010). Notably, ATF4, a key transcriptional regulator of the UPR, has been shown to regulate the SSP under cadmium-induced autophagy conditions (E. Zhao et al., 2016).

Although HIF-1 signalling coordinates the broader metabolic response to hypoxia, its direct regulation of PHGDH remains poorly defined. Nonetheless, indirect evidence points to a potential link, as HIF-1α has been shown to induce SHMT2, the mitochondrial enzyme responsible for serine-to-glycine interconversion, under hypoxic conditions (Ye et al., 2014). Also, HIF-1 stabilisation under serine deprivation has been reported to upregulate SSP gene expression in glioblastoma cells, with HREs identified in the promoters of PHGDH, PSAT1, and PSPH (Yun et al., 2023). Whether hypoxia directly drives PHGDH induction in lung cancer cells, and through which mechanism, has not been established.

Serine synthesis has been studied extensively and was found to play a critical role in 1C metabolism, redox homeostasis and others (Labuschagne et al., 2014). Alongside SSP, extracellular serine availability is another regulatory factor that must be considered. Extracellular serine is a known regulator of PHGDH expression through PKM2-mediated feedback on 3-PG flux (Chaneton et al., 2012).

This chapter investigates the regulation of PHGDH under hypoxia and the metabolic consequences of its loss. Specifically, different oxygen levels and HIF-1-deficient models were used to examine the mechanisms underlying PHGDH induction. Additionally, knockout cell lines were generated to investigate the effect of PHGDH on metabolic rewiring.

Specific aims:

- Study the mechanism of PHGDH induction in hypoxia.
- Investigate the oxygen dependency of PHGDH expression.
- Determine the effect of extracellular serine levels on PHGDH expression.
- Generate and validate PHGDH CRISPR Cas9 knockout cell lines.
- Characterise the metabolic changes following loss of PHGDH.

3.2 Results

3.2.1 PHGDH is amplified in lung cancer patients

To investigate the potential relationship between the expression of the SSP and hypoxia in lung cancer, we begin by examining the expression of PHGDH, PSAT1, and PSPH in normal tissue versus in tumours. Based on available TCGA data, in lung squamous cell carcinoma (LUSC) patients, all three SSP genes showed significantly higher expression in tumour versus normal tissue, whilst in lung adenocarcinoma (LUAD) patients, only PSAT1 was significantly different (**Figure 3.1A, B**).

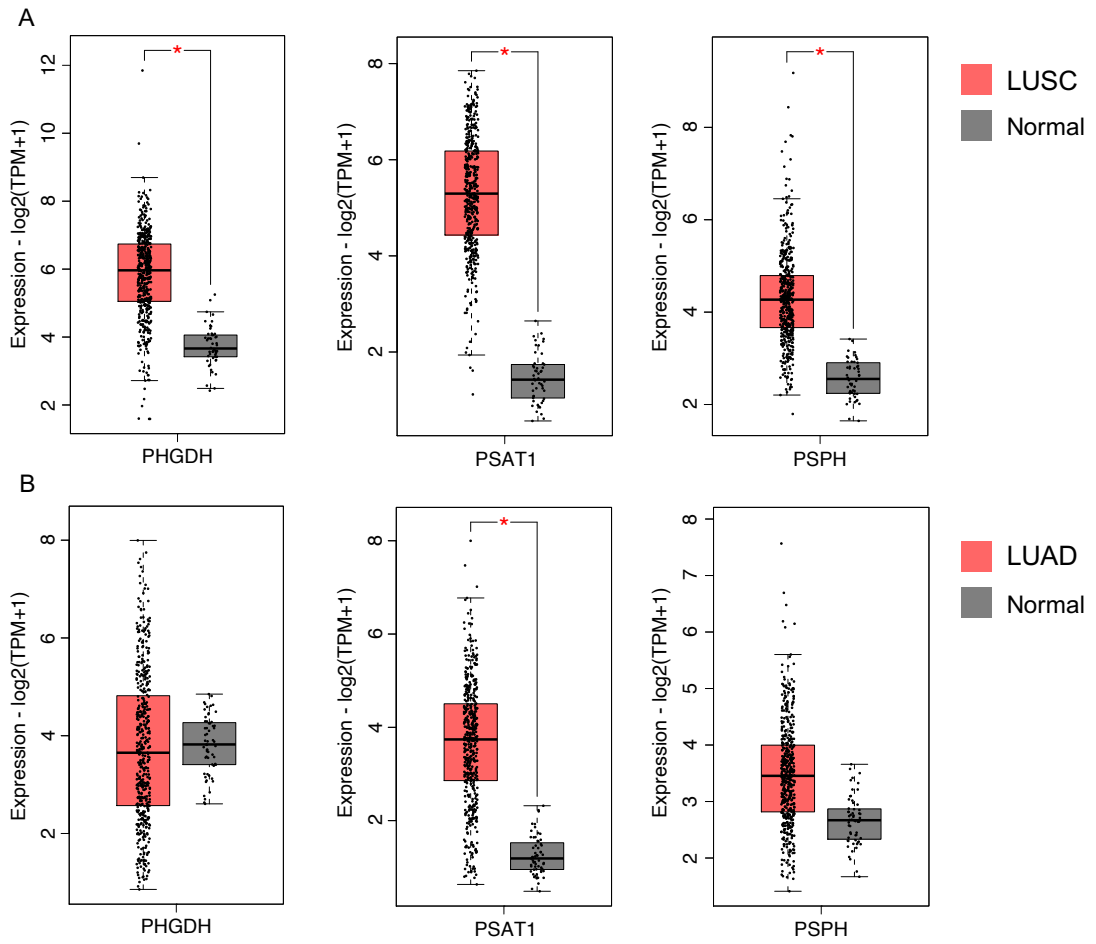

Figure 3.1 Expression of SSP genes in normal versus tumour tissues of TCGA lung cancer patients. A. Expression levels of PHGDH, PSAT1, and PSPH in TCGA LUSC patient tumour (n=486) and normal (n=50) tissue samples. **B.** Expression levels of PHGDH, PSAT1, and PSPH in TCGA LUAD patient tumour (n=483) and normal (n=59) tissue samples. The Gepia2 expression analysis tool was used to generate A and B. *$p<0.01$

3.2.2 PHGDH expression is positively correlated with Buffa and Winter hypoxia signatures

Next, we investigated the correlation between the mRNA levels of SSP genes and two validated hypoxia signatures in the lung using TCGA patient datasets (Buffa et al., 2010; 'Comprehensive Genomic Characterisation of Squamous Cell Lung Cancers', 2012; 'Comprehensive Molecular Profiling of Lung Adenocarcinoma', 2014; Winter et al., 2007). Using both Buffa and Winter signatures, all three SSP genes positively correlated in LUAD and LUSC patients (**Figures 3.2 and 3.3**).

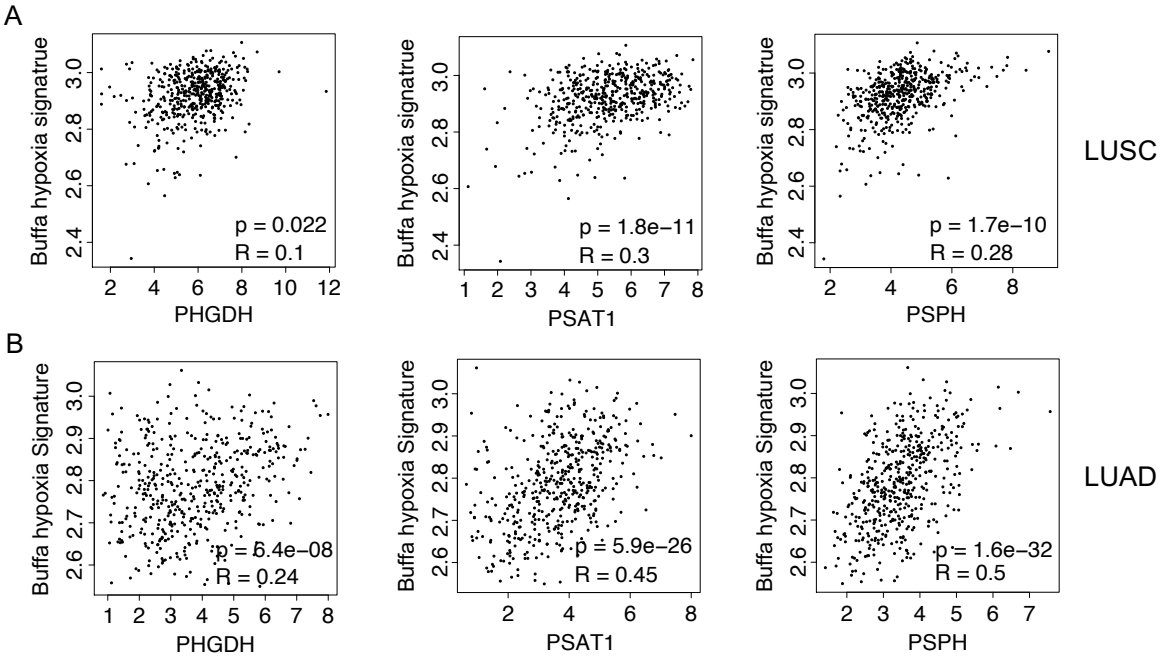

Figure 3.2 Correlation of PHGDH, PSAT1, and PSPH expression with the Buffa hypoxia metagene signature. Correlation analysis was performed using the correlation analysis tool in GPIA2 software, based on data retrieved from the TCGA LUSC (n = 486) (**A**) and LUAD (n = 483) (**B**) cancer cohorts. Pearson's rho correlation coefficient (R) was calculated.

This suggests potential hypoxia-inducibility of the SSP in patients with lung cancer. The druggable nature of PHGDH and its role as the rate-limiting step of the SSP made it the target of choice for this study. Pearson correlation analysis revealed that PHGDH mRNA expression was more strongly associated with both the Buffa (R = 0.24) and Winter (R = 0.34) hypoxia signatures in LUAD compared to LUSC (R = 0.10 and R = 0.13, respectively). As a result, LUAD was selected as the primary tumour model for subsequent analyses. Stronger

correlation in adenocarcinoma patient data indicates that hypoxia-driven regulation of PHGDH may be more prominent in LUAD than in LUSC.

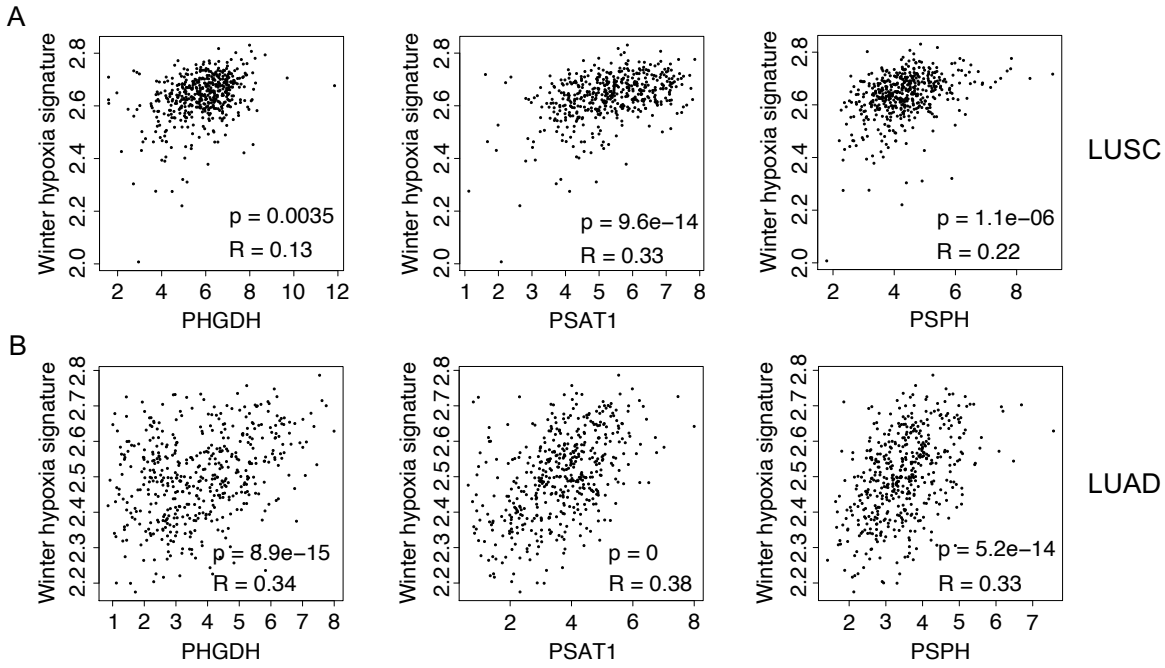

Figure 3.3 Correlation of PHGDH, PSAT1, and PSPH expression with the Winter hypoxia metagene signature. Correlation analysis was performed using the correlation analysis tool in GPIA2 software, based on data retrieved from the TCGA LUSC (n = 486) (**A**) and LUAD (n = 483) (**B**) cancer cohorts. Pearson's rho correlation coefficient (R) was calculated.

Based on TCGA data, PHGDH was also found to be altered in approximately 10% of non-small cell lung cancer (NSCLC) patients, indicating its significance in this cancer type compared with other cancers (**Figure 3.4**). For perspective, KRAS is the third most frequently mutated gene in NSCLC patients, with an alteration rate of 14.5% (C. Liu et al., 2023). Based on these findings, the A549 lung adenocarcinoma cell line was selected as the primary model for subsequent investigations of PHGDH.

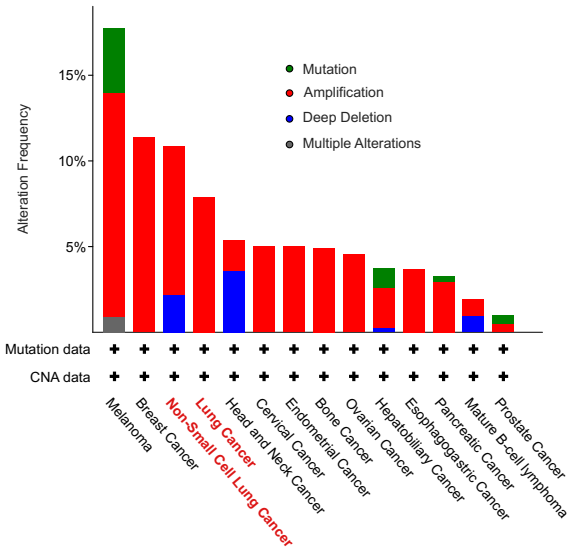

Figure 3.4 Alteration frequency of the *PHGDH* gene in TCGA cancer types. TCGA samples containing mutations and CNA (2683 samples, 2565 patients) were used for the analysis. The figure was generated using the cBioPortal software (Aaltonen et al., 2020; Cerami et al., 2012; de Bruijn et al., 2023; J. Gao et al., 2013).

3.2.3 PHGDH is induced both at the mRNA and protein level in hypoxia (<0.1% O_2)

To study the impact of hypoxic conditions on PHGDH expression *in vitro*, PHGDH mRNA levels were quantified following exposure to <0.1% O_2, using RT-qPCR. A significant increase of approximately 2 to 3-fold in PHGDH mRNA was observed following 16 h of hypoxia exposure (**Figure 3.5A**). Hypoxic conditions were validated by measuring CAIX mRNA levels alongside PHGDH. As expected, CAIX showed a significant increase in expression throughout the time course (**Figure 3.5B**). H460, a large cell lung carcinoma, was used as a second cell line to confirm the observations. In H460, PHGDH levels were increased compared to normoxia (**Figure 3.5C**). However, the kinetics of induction appeared to be different. In contrast to significant induction in mRNA only at 16 h of hypoxia induction in A549, H460 cells had approximately a 5-fold increase in PHGDH mRNA levels after 4 h of hypoxia. Hypoxic conditions were again validated for H460 by measuring the mRNA levels of CAIX. Similar to A549, CAIX levels were elevated in H460 cells alongside PHGDH (**Figure 3.5D**). Overall, these results show PHGDH to be hypoxia-inducible at the mRNA level in both cell lines.

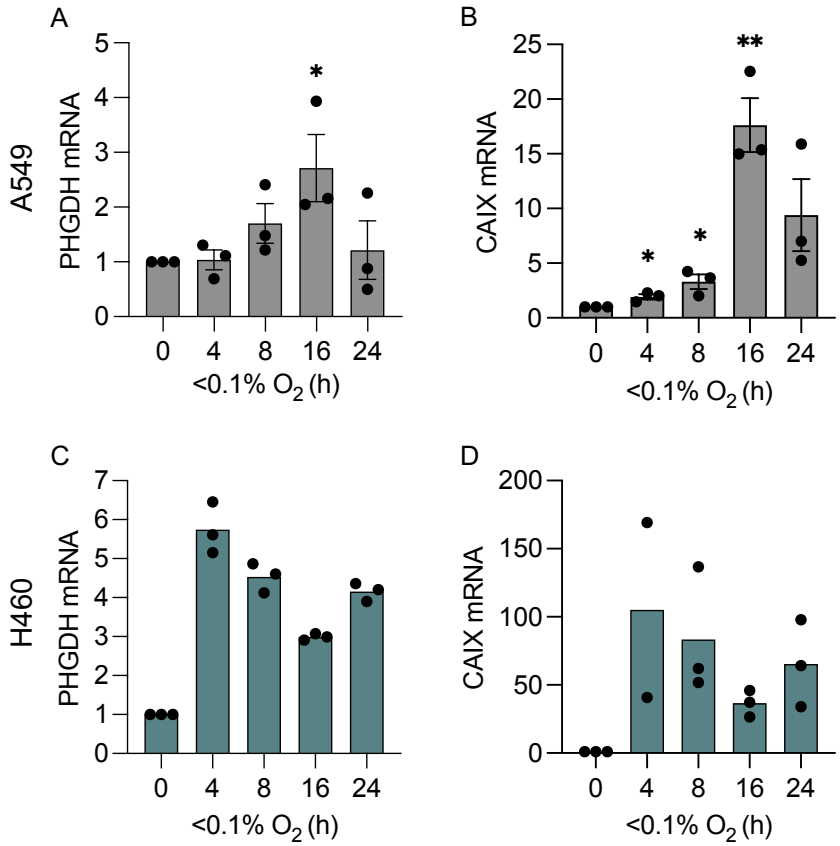

Figure 3.5 The effect of hypoxia (<0.1% O_2) exposure on PHGDH mRNA expression levels. A549 cells were exposed to <0.1% O_2 for 0-24 h, as stated. PHGDH (**A**) and CAIX (**B**) mRNA levels were measured using RT-qPCR. H460 cells were exposed to <0.1% O_2 for 0-24 h, as stated. PHGDH (**C.**) and CAIX (**D**) mRNA levels were measured using RT-qPCR. Error bars combined with individual dots represent mean ± SEM (n = 3). Absence of error bars illustrates results from one biological replicate (n=1). For statistical analysis, a two-tailed Student's *t-test* was used. **p<0.05, **p<0.01*. Absence of statistical testing represents a non-significant difference.

Next, we investigated the effect of <0.1% O_2 on PHGDH using western blotting. Consistent with the mRNA changes observed previously, PHGDH showed a significant increase in protein levels in A549 cells (**Figure 3.6A, B**). Interestingly, PHGDH protein and mRNA levels showed distinct induction kinetics in A549 cells under hypoxia. While mRNA upregulation was only significant after 16 h, protein levels were already significantly elevated at 4 h, suggesting that PHGDH protein accumulation precedes transcriptional induction. Additionally, a western blot for PHGDH was performed in H460 cells, where no significant increase in protein levels was observed after 24 h of hypoxia (**Figure 3.6C, D**). However, baseline PHGDH protein levels

were higher in H460 cells than in A549 cells, suggesting that the hypoxia inducibility of PHGDH may depend on baseline expression levels.

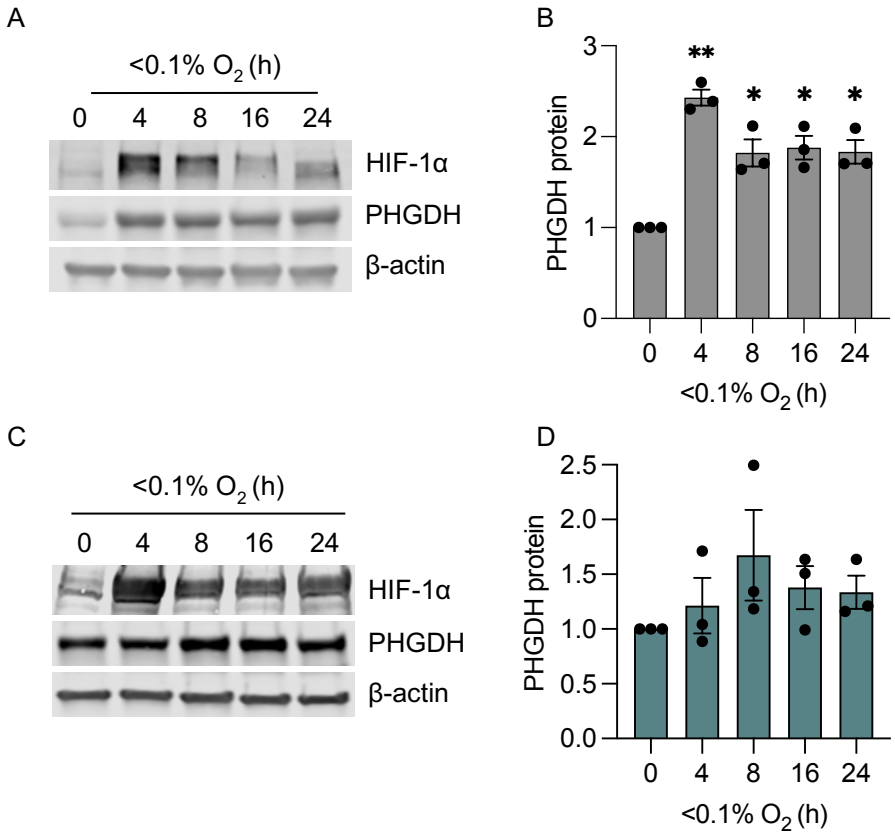

Figure 3.6 The effect of hypoxia (<0.1% O_2) exposure on PHGDH protein levels. A549 (**A, B**) and H460 (**C, D**) cells were exposed to <0.1% O_2 for 0-24 h, as indicated, followed by western blotting for PHGDH, HIF-1α and β-actin as a loading control. Quantification of changes in PHGDH are shown. Band intensities were normalised to the β-actin loading control. Error bars represent mean ± SEM, and individual dots represent independent biological replicates (n = 3). For statistical analysis, a two-tailed Student's *t-test* was used. **p<0.05, **p<0.01*. Absence of stars represents a non-significant difference.

To further understand the induction mechanism of PHGDH, the effect of milder hypoxia (2% O_2) exposure was also explored. Initially, the effect on protein levels was investigated at 2% O_2. Similarly to <0.1% O_2 conditions, exposure to 2% O_2 led to a significant, 2-fold increase in PHGDH protein levels after 4 h of exposure (**Figure 3.7A, B**). However, when measuring the mRNA levels under 2% O_2, no statistically significant induction of PHGDH mRNA expression was observed (**Figure 3.7C**). This contrasts with the significant induction previously observed at <0.1% O_2. Together, these results suggest an unusual, oxygen-dependent mechanism of induction for PHGDH gene expression.

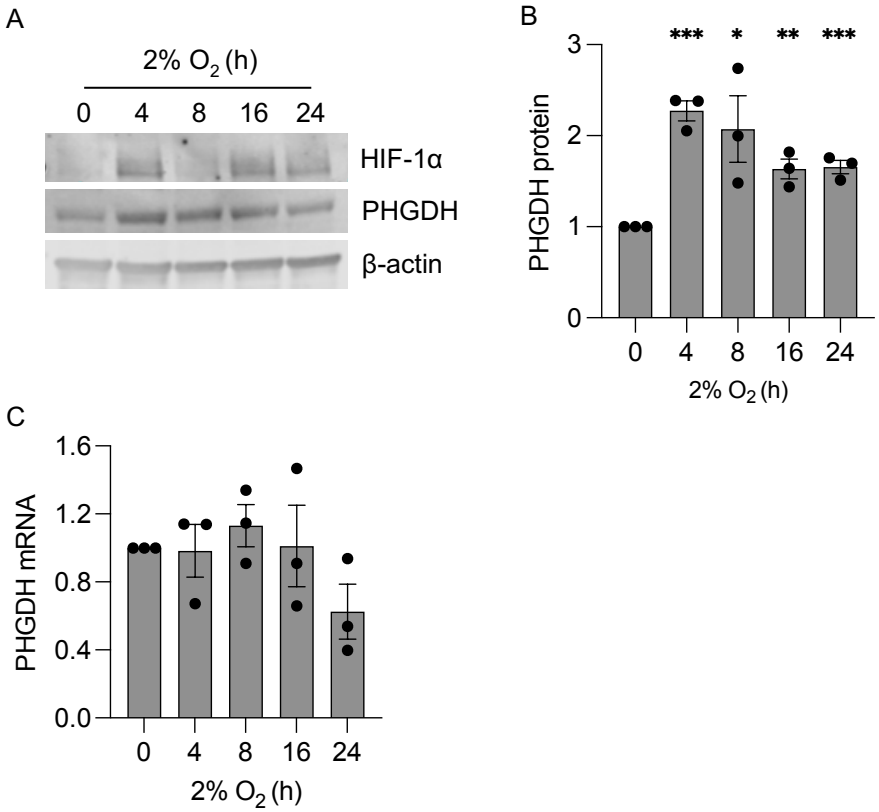

Figure 3.7 The effect of 2% O_2 exposure on PHGDH protein and mRNA levels. A. A549 cells were exposed to 2% O_2 for 0-24 h, as indicated, followed by western blotting for PHGDH, HIF-1α and β-actin as a loading control. **B.** Quantification of changes in PHGDH from western blots done on A549 cells. Band intensities were normalised to β-actin loading control. **C.** A549 cells were exposed to 2% O_2 for 0-24 h, as shown. PHGDH mRNA levels were measured using RT-qPCR. Error bars represent mean ± SEM, and individual dots represent independent biological replicates (n = 3). For statistical analysis, a two-tailed Student's *t-test* was used. **p<0.05, **p<0.01, ***p<0.001*. Absence of stars represents a non-significant difference.

3.2.4 Hypoxia leads to an increase in nuclear PHGDH

Although predominantly a cytoplasmic enzyme, PHGDH has recently been identified to perform a non-canonical role in the nucleus. Specifically, in glucose-starved cells, PHGDH was shown to translocate into the nucleus, where it acts as an indirect inhibitor of PARP1 by competing for NAD+ (C. Ma et al., 2021). We investigated the possibility of hypoxia (<0.1% O_2) acting similarly to the absence of glucose. To this end, we performed a cellular fractionation experiment, separating the nuclear and cytosolic fractions. Based on the earlier observations showing high baseline PHGDH expression in H460 cells, this cell line was selected as the experimental model to ensure the detectability of nuclear PHGDH by western blotting. Both

short (8 h) and prolonged (24 h) hypoxia timepoints were used in the experimental design. Although no significant changes in nuclear PHGDH were observed at 8 h in hypoxia, after 24 h of exposure to <0.1% O_2, PHGDH levels in the nucleus increased around 6-fold (**Figure 3.8**). Glucose deprivation (24 h) was used as a positive control and increased nuclear PHGDH levels comparable to those observed under hypoxic conditions. As expected, PHGDH was mainly detected in the cytoplasmic fraction. The nuclear accumulation of PHGDH under hypoxia raises the possibility of a nuclear function for this enzyme.

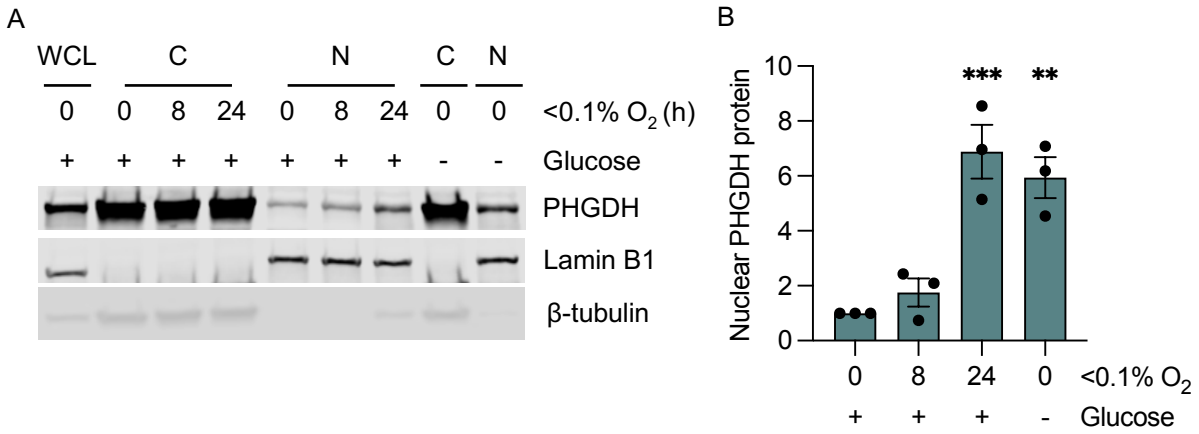

Figure 3.8 Hypoxia leads to an increase in nuclear PHGDH. A. Cellular fractionation of H460 cells in hypoxia (<0.1% O_2, timepoints indicated) and glucose-deprived media (24 h) was performed. A whole cell lysate (WCL) control was included. Lamin B1 and β-tubulin were used as loading controls for nuclear (N) and cytoplasmic (C) fractions, respectively. **B.** Quantification of changes in PHGDH from the nuclear fractionation western blot. Band intensities were normalised to β-actin loading control. Error bars represent mean ± SEM, and individual dots represent independent biological replicates (n = 3). For statistical analysis, a two-tailed Student's *t-test* was used. **p<0.05, **p<0.01, ***p<0.001*. Absence of stars represents a non-significant difference.

3.2.5 The mechanism of PHGDH induction in hypoxia

To further investigate the unexpected induction pattern of PHGDH under hypoxia, we first examined the role of HIF-1 signalling. First, we measured PHGDH mRNA levels in HIF-1α wild-type and knockout RKO colorectal carcinoma cells. Both WT and KO cells were exposed to 0.1% and 2% O_2 conditions (16 h). This time point was selected because, in radiobiological hypoxia, a significant increase in PHGDH mRNA levels was observed at 16 h of exposure. In HIF-1α WT cells, the induction of PHGDH mRNA was observed at <0.1% but not at 2% O_2 (**Figure 3.9A**). The induction levels in RKO cells were comparable to the increase observed

in A549 cells. The loss of HIF-1α led to a significant decrease in PHGDH expression at <0.1% O_2. However, PHGDH mRNA levels were still significantly higher compared to the normoxic HIF-1α KO cells. In contrast, CAIX showed significant induction under both <0.1% and 2% O_2 in RKO WT cells (**Figure 3.9B**), and unlike PHGDH, the hypoxia-mediated induction was completely abrogated in KO cells under both oxygen levels.

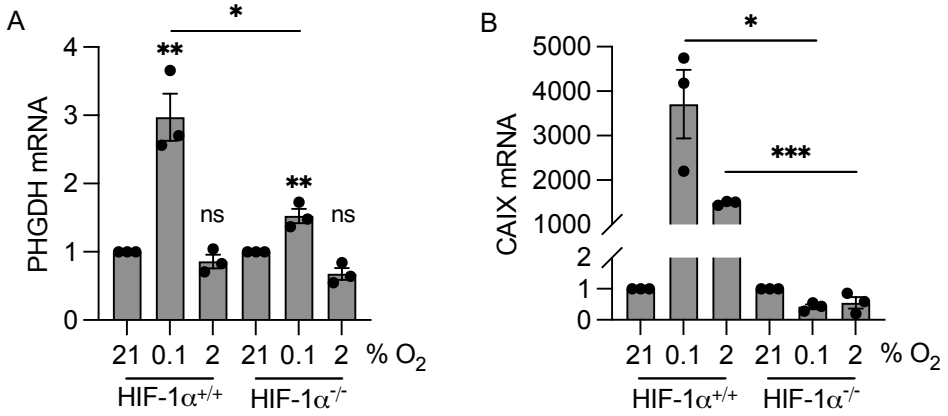

Figure 3.9 HIF-1α-dependent transcriptional regulation of PHGDH in response to hypoxia. HIF-1α wild-type and knock-out RKO cells were exposed to 21, 2, or <0.1% O_2 for 16 h and PHGDH (**A**) and CAIX (**B**) expression levels were determined using RT-qPCR. Error bars represent mean ± SEM, and individual dots represent independent biological replicates (n = 3). For statistical analysis, a two-tailed Student's *t-test* was used. **p<0.05, **p<0.01, ***p<0.001*. Absence of stars represents a non-significant difference.

Due to the availability of cDNA samples, PHGDH mRNA levels were determined in MDA-MB-231 breast cancer cell lines with transiently knocked down HIF-1β. Depletion of HIF-1β effectively reduces both HIF-1 and HIF-2-mediated signalling. In MDA-MB-231 cells, PHGDH levels were increased after 16 h of exposure to <0.1% O_2 (**Figure 3.10A**). However, no induction in 2% O_2 was observed in scramble control cells. The knockdown of HIF-1β reduced PHGDH mRNA to baseline, normoxic levels. Similar to A549 cells, in MDA-MB-231 cells, CAIX was induced under <0.1% and 2% O_2, as expected of a HIF-1 target gene (**Figure 3.10B**). Together, these data show that PHGDH expression, although HIF-1-dependent, does not follow a classical induction pattern observed in other HIF-1-regulated genes.

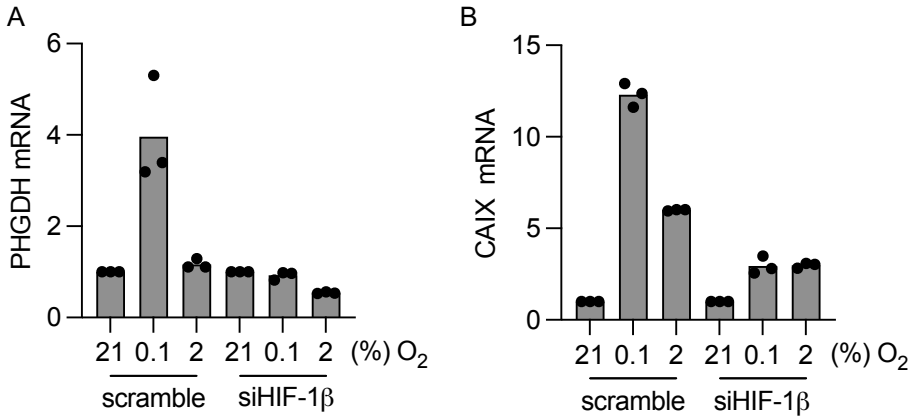

Figure 3.10 HIF-1β-dependent transcriptional regulation of PHGDH in response to hypoxia. Scramble and HIF-1β siRNA knockdown MDA-MB-231 cells were exposed to 21, 2, or <0.1% O_2 for 16 h and PHGDH (**A**) and CAIX (**B**) expression levels were determined using RT-qPCR. Bars represent median fold change. Absence of error bars illustrates results from one biological replicate (n=1). The siRNA knockdown experiment was performed by Dr Chumin Zhou.

The UPR is a well-characterised pathway induced following exposure to <0.1% O_2 but not in milder levels of hypoxia (Ramachandran et al., 2021). Based on this, the residual expression of PHGDH in HIF-1α KO cells under <0.1% O_2 could be attributed to regulation by UPR in addition to HIF. This hypothesis is supported by a recent study that demonstrated that PHGDH was induced by the PERK-ATF4 arm of the UPR pathway (Y. Yang et al., 2024). However, this link between the UPR and SSP was established in the context of Cadmium (Cd)-induced autophagy rather than hypoxia. Subsequently, we explored the role of UPR in PHGDH expression regulation under hypoxia using the AMG PERK 44 inhibitor (Smith et al., 2015). Cells were exposed to 16 h of <0.1% and 2% O_2, and fold change in PHGDH mRNA levels was determined. Due to the UPR being induced solely at <0.1% O_2, milder hypoxic (2% O_2) samples were not treated with the inhibitor. Like previous observations, PHGDH mRNA was again induced under <0.1% O_2 exposure but not 2%. This induction was completely reversed in the cells treated with the PERK inhibitor in hypoxia (<0.1% O_2) (**Figure 3.11A**). This PERK-dependent induction suggests PHGDH could be regulated by ATF4 in hypoxia (<0.1% O_2). To support these observations, the expression levels of ATF4 and CAIX were measured under the same experimental conditions. This pattern of PHGDH induction was similar to the ATF4 expression (**Figure 3.11B**). However, as expected CAIX showed increased mRNA levels at

<0.1% as well as 2% O_2, and the hypoxia-mediated induction was not affected by the treatment with PERK inhibitor (**Figure 3.11C**).

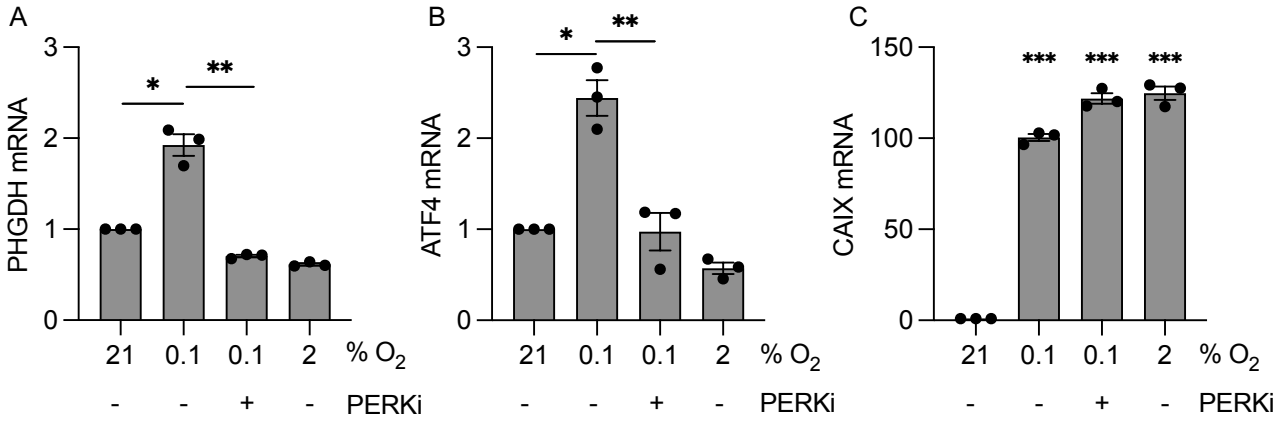

Figure 3.11 Assessment of UPR-dependent regulation of PHGDH expression in hypoxia. A549 cells were exposed to 21, 2 or <0.1% O_2 for 16 h with or without AMG PERK 44 (20 μM). RT-qPCR for PHGDH (**A**), ATF4 (**B**) and CAIX (**C**) was performed**.** Error bars represent mean ± SEM, and individual dots represent biological replicates (n = 3). For statistical analysis, a two-tailed Student's *t-test* was used. **p<0.05, **p<0.01, ***p<0.001*. Absence of stars represents a non-significant difference.

To be regulated by either HIF-1 or PERK-ATF4 signalling, transcription factor (TF) binding sites at the promoter/enhancer regions of PHGDH are required. To look for potential hypoxia-responsive elements (HREs) and ATF4 binding sites, the eukaryotic promoter and JASPAR CORE databases were used. These resources provide curated TF binding profiles, which enable prediction of HREs and ATF4-binding motifs (Dreos et al., 2017). Both HIF and ATF4-binding sequences were found 800 to 1200 bp upstream of the PHDGH transcription start site (TSS) (**Figure 3.12**). These, although being out of the promoter region, can qualify as enhancer-specific transcription factors. Together, these data show that PHGDH is regulated by PERK/ATF4 and HIF-1 in hypoxia (<0.1% O_2). HIF-1-regulation, however, is oxygen-sensitive and is not evident at milder hypoxia (2% O_2). CHIP-Seq for ATF4 and HIF-1α would be necessary to confirm the binding of these TFs to the promoter/enhancer region of PHGDH.

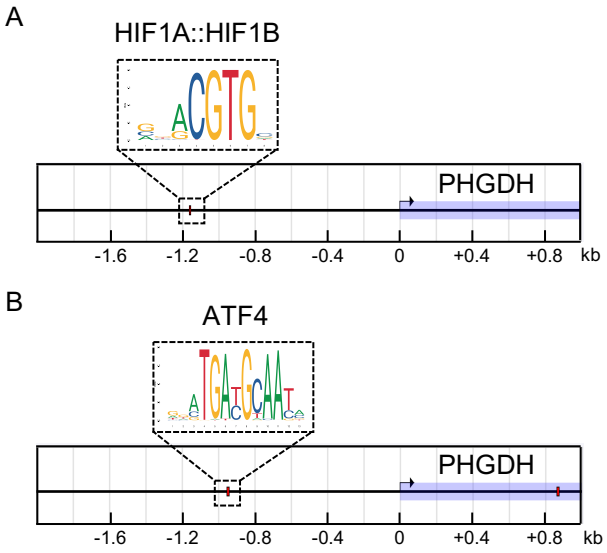

Figure 3.12 Predicted transcription factor binding sites. A, B. The positions of hypoxia-responsive elements (HRE) (**A**) and ATF4-binding domains (**B**) were determined using the Eukaryotic Promoter Database (p-value cutoff, 0.0001). The illustrated transcription factor binding motifs are from the JASPAR CORE database (Dreos et al., 2017).

3.2.6 PHGDH induction under physiological and serine/glycine-deprived conditions

In addition to *de novo* synthesis, serine can be imported into the cell via the alanine-serine-cysteine transporters 2 and 1 (ASCT2/1) (Arriza et al., 1993; Utsunomiya-Tate et al., 1996). As part of our investigation into factors and mechanisms influencing PHGDH expression, we investigated the role of extracellular serine levels on the expression of PHGDH. To this end, western blot analysis was conducted following exposure of A549 cells to media containing physiological serine levels (HPLM) or no serine (MEM) (**Figure 3.13A, Table 7.1**). When cells were cultured in HPLM, PHGDH protein levels increased significantly 1.5 to 2 times after 24 h (**Figure 3.13B, C**).

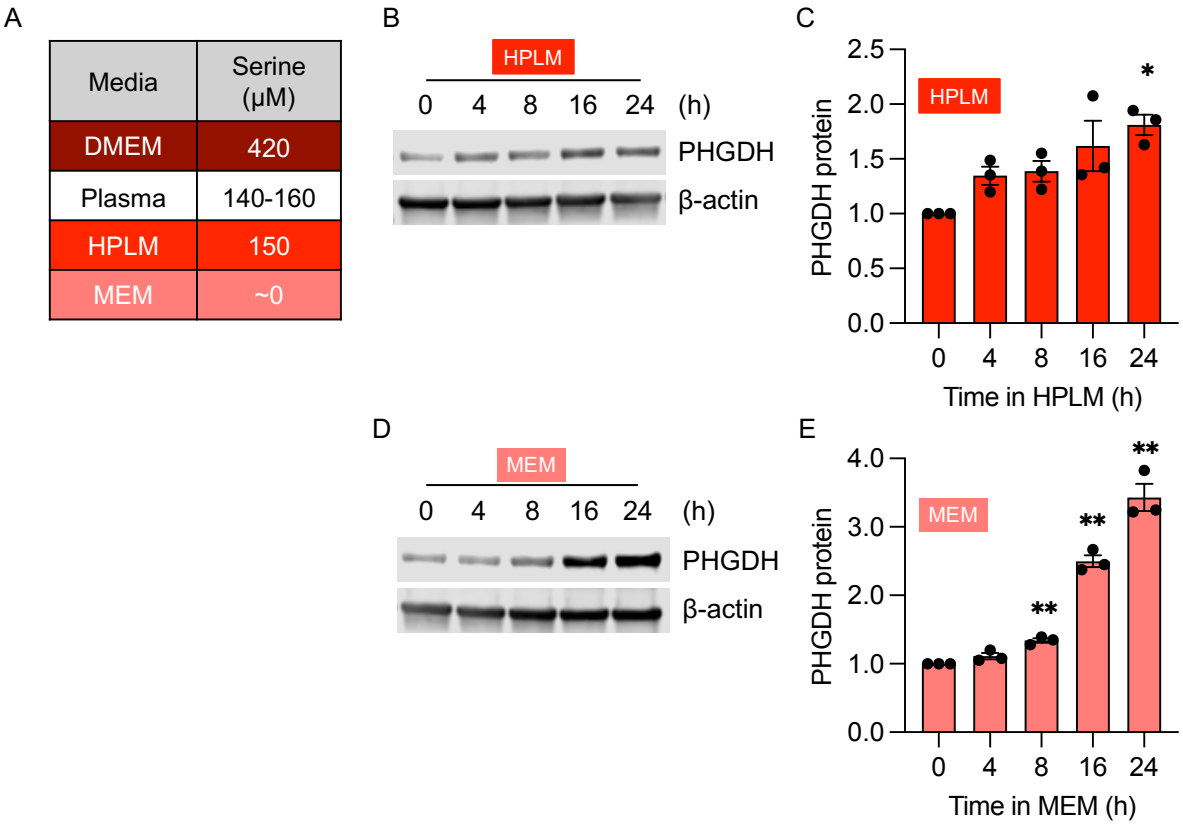

Figure 3.13 The effect of extracellular serine on PHGDH induction. A. The levels of serine (μM) in each of the media used compared to normal plasma (Wishart et al., 2012). **B.** A549 cells were exposed to HPLM for 0-24 h, as indicated, followed by western blotting for PHGDH and β-actin as a loading control. **C.** Quantification of changes in PHGDH from western blots done in HPLM. Band intensities were normalised to β-actin loading control. **D.** A549 cells were exposed to MEM for 0-24 h, as indicated, followed by western blotting for PHGDH and β-actin as a loading control. **E.** Quantification of changes in PHGDH from western blots done in MEM. Band intensities were normalised to β-actin loading control. Error bars represent mean ± SEM, and individual dots represent independent biological replicates (n = 3). For statistical analysis, a two-tailed Student's *t-test* was used. **p<0.05, **p<0.01, ***p<0.001*. Absence of stars represents a non-significant difference.

When completely deprived of extracellular serine, PHGDH increased significantly after 8 h and was 3 times higher after 24 h (**Figure 3.13D, E**). Overall, these findings show PHGDH levels to be sensitive to extracellular serine levels in addition to hypoxia, indicating elevated SSP activity in response to the limited availability of the amino acid.

3.2.7 Generating and validating PHGDH CRISPR-Cas9 knockouts

To understand the role of PHGDH in regulating cellular function and metabolism, PHGDH was knocked out from A549 cells using CRISPR-Cas9. Following knockout, three clones were selected based on the confirmed absence of the PHGDH protein using western blotting (**Figure 3.14A**). The knockout status of all selected clones was further confirmed using Sanger sequencing. The amplification of the genetic region around exon 2 of the PHGDH gene, which was targeted by the gRNA, showed 100% knockout efficiency in all three clones (**Figure 3.14 B-D**).

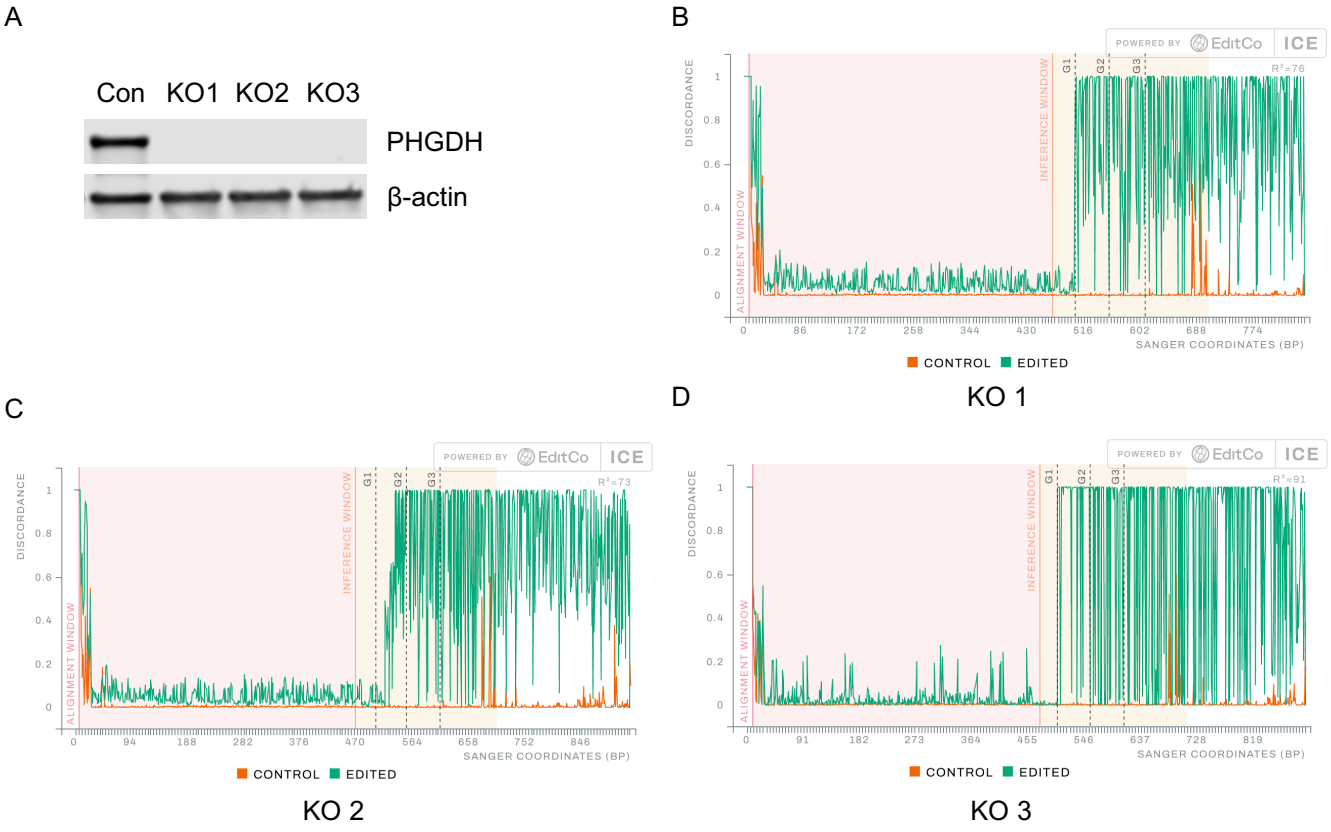

Figure 3.14 Validation of PHGDH KO clones using Sanger sequencing. A. Loss of PHGDH in A549 cells was confirmed by western blotting using lysates from parental and 3 PHGDH KO clones. β-actin was used as a loading control. **B-D.** ICE (interference of CRISPR edits) analysis of CRISPR-Cas9 edited A549 cells. Discordance between Sanger sequencing traces from an unedited parental control (orange) and the CRISPR-edited (green) cells plotted across the amplicon. The alignment and interference windows are indicated. The ICE regression score (R^2) is shown.

Following validation of the KO clones, the effect of PHGDH absence on cell proliferation was examined. Parental control and PHGDH KO cells were cultured in media with different serine

levels, and cell numbers were measured daily. When cultured in DMEM, i.e. excess extracellular serine, no significant differences in proliferation rates were observed between parental and PHGDH KO clones over 7 days (**Figure 3.15A**). Similarly, culturing cells in HPLM did not influence the proliferation rate of the PHGDH KO cells compared to the parental controls (**Figure 3.15B**). However, when exposing cells to serine/glycine-free conditions (MEM), PHGDH KO cells showed a significant reduction in proliferation rates (**Figure 3.15C**). In conclusion, three PHGDH-null clones were generated and validated, with impaired cell proliferation observed only under extracellular serine and glycine deprivation.

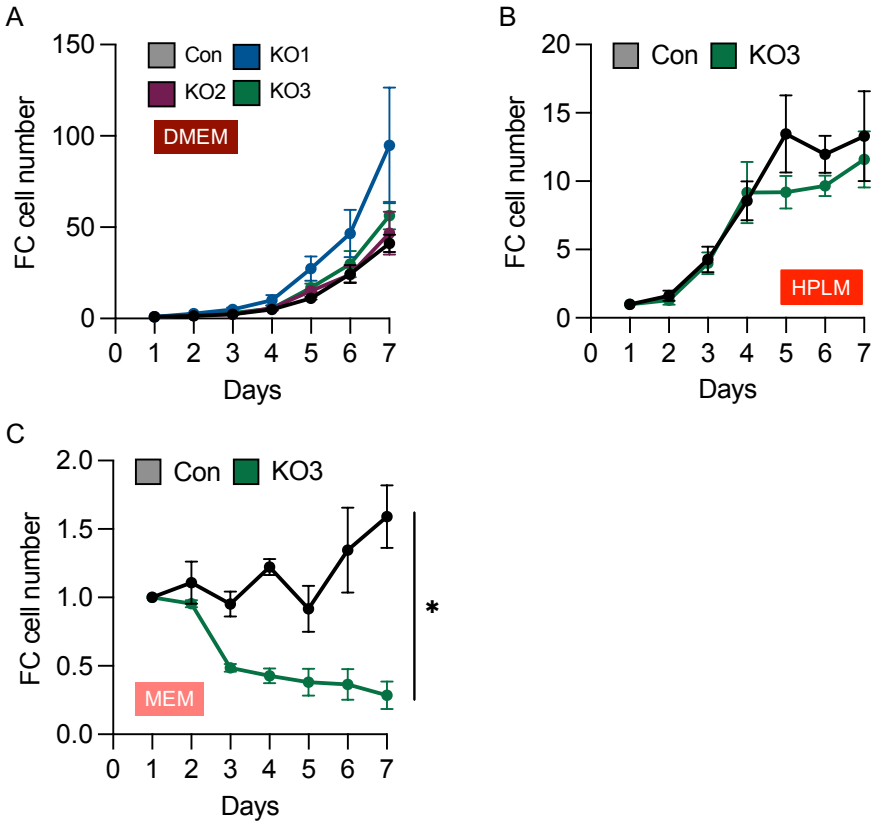

Figure 3.15 The effect of PHGDH on cell proliferation. A. Proliferation of parental and PHGDH KO cells was measured over 7 days of growth in DMEM at 21% O_2. Fold change relative to the first day post-seeding was calculated. **B.** Proliferation of parental and PHGDH KO cells was measured over 7 days of growth in HPLM. Fold change relative to the first day post-seeding was calculated. **C.** Proliferation of parental and PHGDH KO cells was measured over 7 days of growth in MEM. Fold change (FC) relative to the first day post-seeding was calculated. Error bars represent mean ± SEM, and individual dots represent independent biological replicates (n = 3). For statistical analysis, a two-tailed paired Student t-test was used. *$p<0.05$

To separate PHGDH-dependent effects from broader metabolic influences, proliferation was assessed across different media conditions in both parental control and PHGDH KO cells. In Con cells, growth varied markedly with media composition, with the highest proliferation observed in DMEM. Despite cells showing similar growth rates in HPLM until day 5, the growth plateaued afterwards. The proliferation rate of cells grown in MEM was significantly lower than in the other two media (**Figure 3.16A**). A similar overall pattern was observed in PHGDH KO cells, indicating that media composition alone strongly influences proliferation independent of PHGDH status (**Figure 3.16B**).

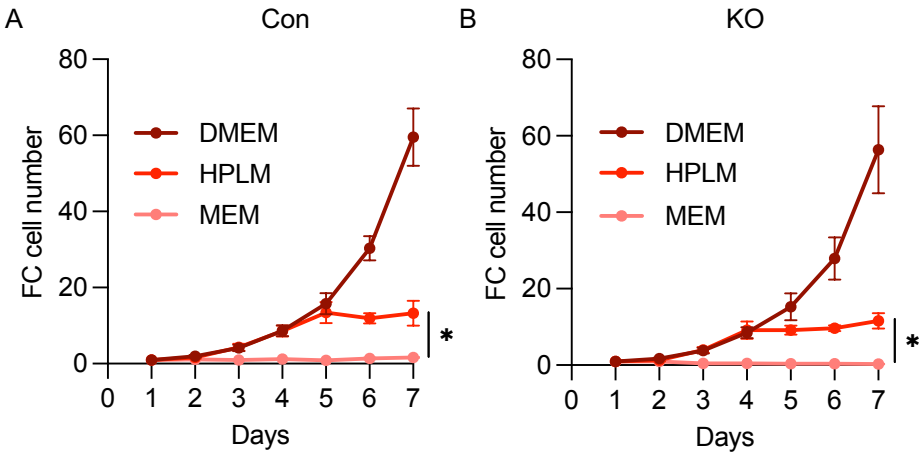

Figure 3.16 Effects of PHGDH knockout on cell proliferation across different culture media. A, B. Parental control (Con) (**A**) and PHGDH knockout (KO) (**B**) cells were cultured over 7 days in three media conditions: DMEM, HPLM, and MEM. Cell proliferation was assessed by quantifying FC cell number at the indicated time points. Fold change (FC) relative to the first day post-seeding was calculated. Error bars represent mean ± SEM, and individual dots represent independent biological replicates (n = 3). For statistical analysis, a two-tailed paired Student t-test was used. *$p<0.05$

3.2.8 Characterising the metabolic changes in PHGDH KO cells

PHGDH functions as a central enzyme in the SSP, and its loss is expected to induce broad changes in cellular metabolism. To capture these alterations, we conducted an untargeted metabolomic analysis of PHGDH KO and wild-type cells. The initial statistical analysis of the IC-MS study showed a clear, distinct metabolic phenotype in Con and KO cells. Hierarchical clustering analysis demonstrated that samples cluster according to the genotype, with control and PHDGH KO samples forming distinct branches (**Figure 3.17A**). Moreover, principal component analysis (PCA) also showed a clear segregation between parental control and PHGDH KO samples along the principal component 1 (PC1). The latter accounted for 37.5% of the total variance (**Figure 3.17B**). All replicates within each group clustered tightly together, suggesting good reproducibility and distinct metabolic changes following the knockout of PHGDH.

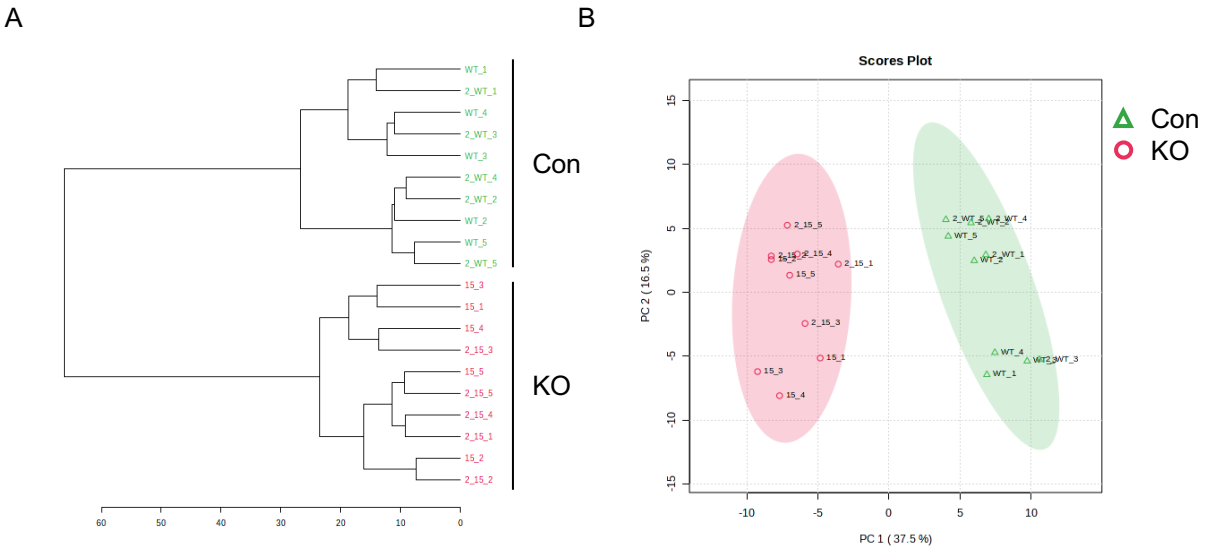

Figure 3.17 Statistical summary IC-MS analysis on PHGH Con and KO cells. A. hierarchical clustering dendrogram based on all compound features for parental control (Con) and PHDGH KO cells. **B.** Unsupervised PCA scores plot (median-centred, log-transformed, Pareto-scaled data) based on all compound features. PCA ellipses represent the 95% confidence interval for each group, and consistent clustering is observed across biological replicates in both analyses.

Detailed analysis of the clustered metabolic data revealed that a substantial proportion of intracellular metabolites were present at lower relative abundance in PHGDH KO samples compared to parental controls. However, a distinct subset of metabolites was also identified that showed increased relative abundance in PHGDH KO cells (**Figure 3.18**). These differences were again consistent across the experimental replicates, with metabolites exhibiting a coordinated pattern of either reduction or accumulation in control and KO groups. Such bidirectional changes indicate a clear shift in the global metabolic landscape following the loss of PHGDH.

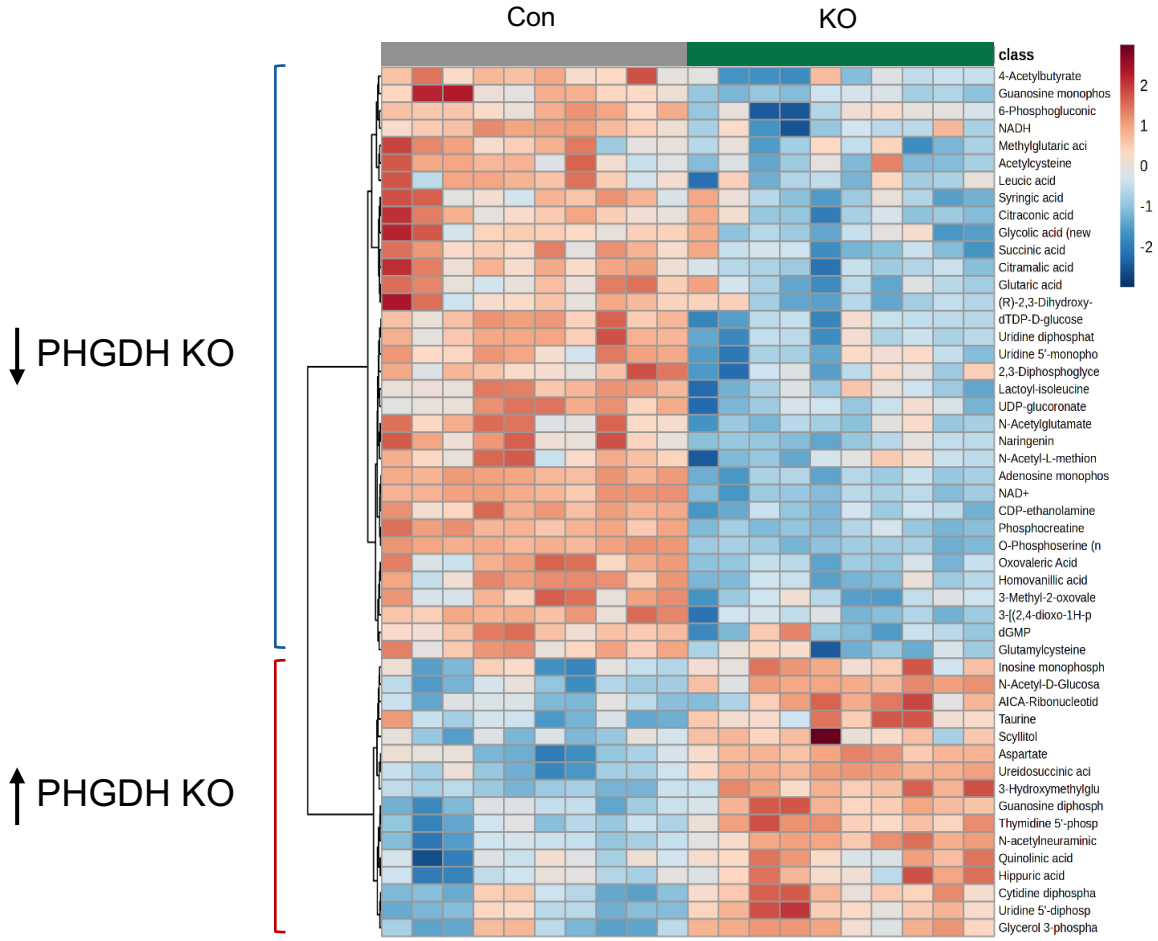

Figure 3.18 Metabolomic analysis of parental control and PHGDH KO cells. IC-MS metabolomics heatmap showing z-scored relative metabolite abundances in parental control (Con) and PHGDH KO A549 cells grown in normoxia (21% O_2), with metabolites hierarchically clustered and samples grouped by condition. Clusters with down- and upregulated metabolites in PHGDH KO cells are highlighted.

Glycolysis serves as the main source of carbon for the SSP (**Figure 3.19A**); in fact, around 15% of the carbon flux generated from glycolysis passes through the SSP (W. Zhang et al., 2017). In this context, glycolytic intermediates such as pyruvate and lactate were among the significantly upregulated metabolites in PHGDH KO cells, indicating elevated glycolysis (**Figure 3.19B**).

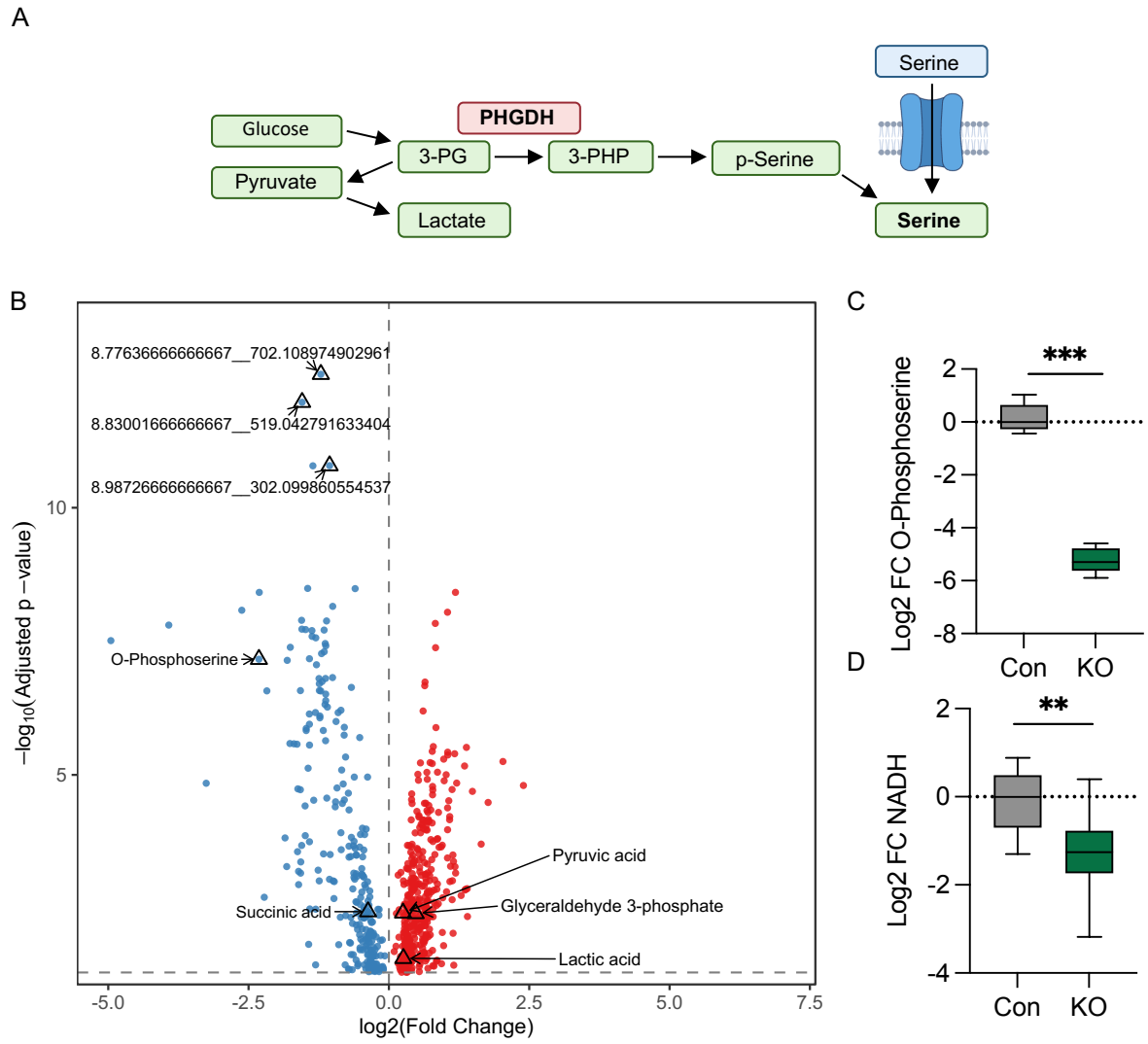

Figure 3.19 Metabolic changes resulting from the knockout of PHGDH. A. Schematic representation of glycolysis and SSP. Imported serine is highlighted in blue. **B.** Volcano plot of detected metabolites that significantly changed in PHGDH KO cells. Log_2 fold change is plotted against $-log_{10}$ adjusted p-value. Horizontal dashed line indicates significance thresholds (adjusted p-value <0.05). Significantly increased (red) and decreased (blue) metabolites are shown, with selected metabolites annotated. **C, D.** Comparisons of the levels of O-Phosphoserine (**C**), NADH (**D**) between parental control and PHGDH KO cells under normoxia (21% O_2). ****p<0.001, **p<0.01*

Total serine levels detected by the IC-MS analysis cannot be used as an indicator for the SSP due to the import of serine from the media. Instead, O-phosphoserine (SSP intermediate) levels are used to evaluate the effect of PHGDH KO on SSP. As expected, O-phosphoserine was among the most markedly downregulated metabolites in PHGDH KO cells (**Figure 3.19C**). This confirms the disruption of the SSP in our PHGDH CRISPR-Cas9 KO cells. As an additional validation of disrupted SSP function, levels of NADH were investigated. NADH is the reduced form of the PHGDH co-factor NAD+, which as expected, was significantly lower in the KO cells (**Figure 3.19D**).

SSP plays a crucial role in providing substrates for 1C metabolism and facilitating nucleotide synthesis (Locasale et al., 2011b). Consistent with this, our findings revealed alterations in nucleotide-related metabolites in PHGDH KO cells. Following functional enrichment analysis using the KEGG pathway database, the purine synthesis was identified as the most significantly enriched pathway (**Figure 3.20A**). A more detailed look into specific metabolite levels showed both adenosine (AMP) and guanosine monophosphate (GMP) levels to be lower in PHGDH KO cells (**Figure 3.20B, C**). Additionally, uric acid levels, an indicator of purine catabolism, were significantly elevated in PHGDH knockout cells compared to the parental control, indicating increased purine turnover and a shift toward purine breakdown relative to *de novo* synthesis (**Figure 3.20D**).

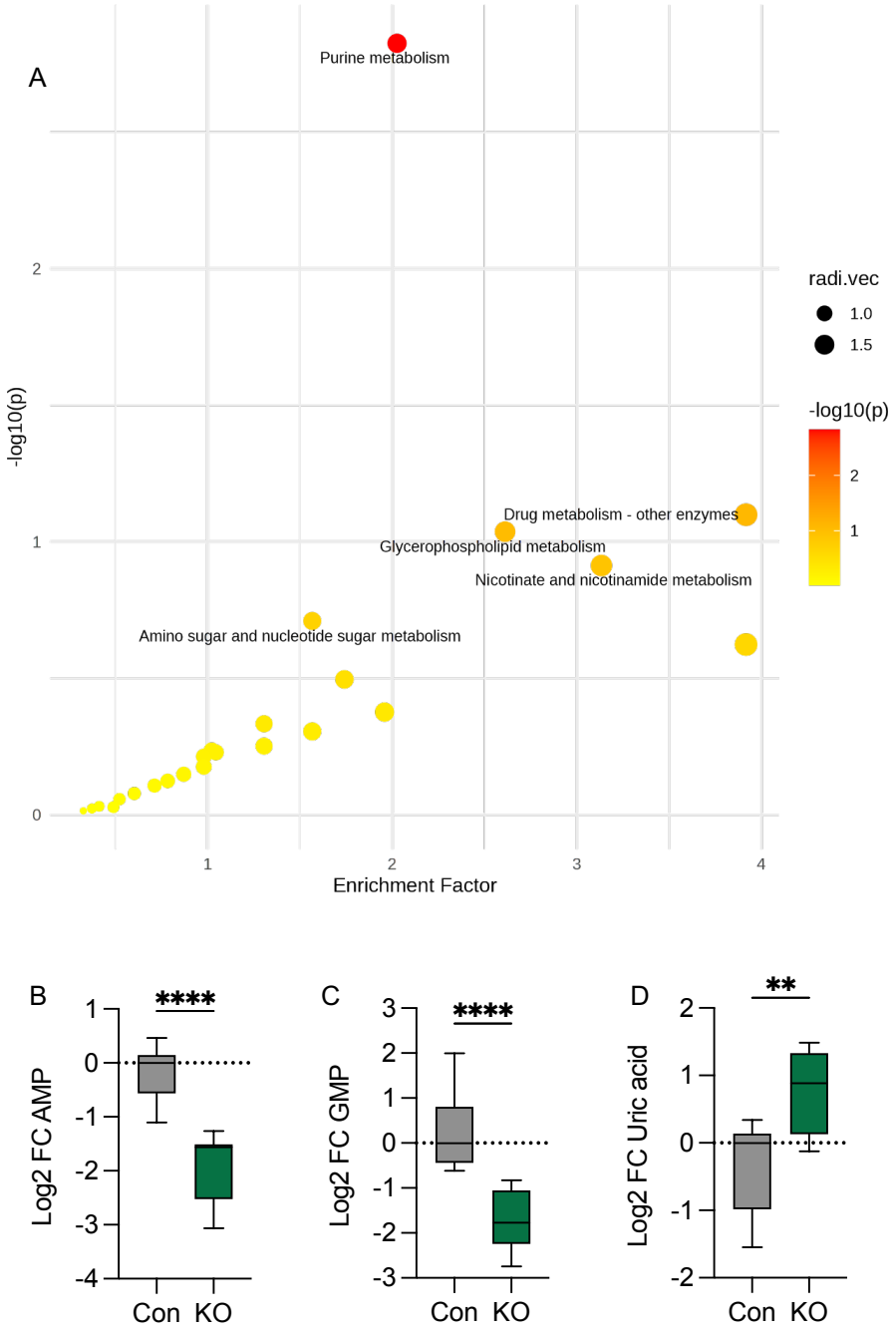

Figure 3.20 The effect of PHGDH KO on purine metabolism. A. Ungated pathway analysis for parental and PHGDH KO A549 cells based on the KEGG Pathway Database. **B, C, D.** Comparisons of the levels of adenosine monophosphate (AMP, **B**), guanosine monophosphate (GMP, **C**), and uric acid (**D**) between A549 and PHGDH KO cells under normoxia (21% O_2). ***p < 0.01 **** p < 0.0001*

Interestingly, the opposite effect was observed in pyrimidine synthesis, which was increased, unlike purines. Levels of thymidine 5'-phosphate (TMP), cytidine diphosphate (CDP) and uridine 5'-diphosphate (UDP) were significantly upregulated in PHGDH KO cells compared to A549 parental control cells (**Figure 3.21**). Overall, these data confirm that loss of PHGDH results in significant changes in the metabolic landscape of lung cancer cells, including pathways such as glycolysis and nucleotide synthesis.

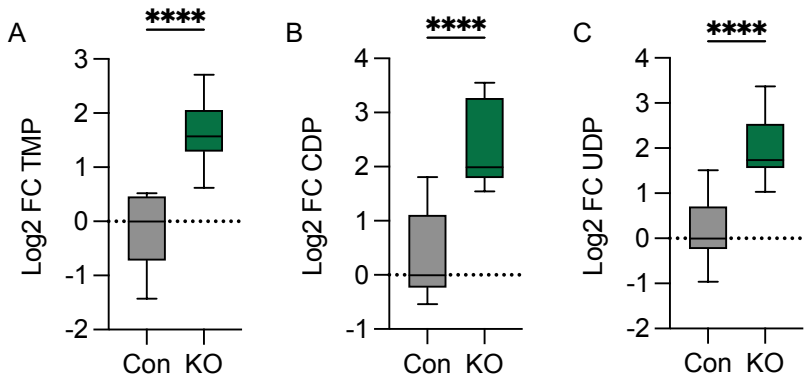

Figure 3.21 The effect of PHGDH KO on pyrimidine synthesis. A, B, C. Comparisons of the levels of thymidine 5'-phosphate (TMP, **A**), cytidine diphosphate (CDP, **B**), and uridine 5'-diphosphate (UDP, **C**) between A549 and PHGDH KO cells under normoxia (21% O_2). **** *p < 0.0001*

3.3 Discussion

Here, we investigated the relationship between the *de novo* SSP and hypoxia in the context of lung cancer. Particular emphasis was placed on the rate-limiting enzyme PHGDH.

The initial analysis of TCGA datasets showed amplification and overexpression of PHGDH in lung cancer patients. Additionally, PHGDH mRNA levels positively correlated with established hypoxia signatures. We demonstrated that PHGDH is hypoxia-inducible both at the mRNA and protein level. However, PHGDH protein levels were induced before any changes were observed in mRNA. There can be few biological explanations behind this observation. First, reduced degradation rates of PHGDH can lead to an increase in protein levels at <0.1% and 2% O_2. E3 ubiquitin ligase RNF5 was discovered to be essential in PHGDH degradation. The acetylation of PHGDH at K58 residue was found to disrupt the interaction between RNF5 and PHGDH, preventing its degradation and leading to protein accumulation. Proteins Tip60 and SIRT2 mediate the reversible acetylation and subsequent increase in PHGDH (C. Wang et al., 2020). Lower acetylation rates of PHGDH in hypoxia could potentially lead to reduced protein degradation. This hypothesis could be tested by measuring changes in PHGDH stabilisation (half-life) in normoxia and hypoxia using cycloheximide (CHX). Another possibility for earlier increase in PHGDH protein levels can be enhanced translation of pre-existing PHGDH mRNA. Although hypoxia is associated with reduced rates of protein synthesis, a subset of mRNAs are selectively translated (Young et al., 2008). Additionally, in H460 cells, unlike A549, no significant increase was observed in protein levels, despite mRNA appearing to be elevated in <0.1% O_2. Other well-characterised hypoxia-regulated proteins, such as VEGF, also showed such baseline-dependent inducibility patterns. Specifically, in breast cancer cell lines with the highest basal levels of VEGF, the hypoxic induction was moderate. This was not the case for the lines with the lowest initial levels of VEGF, which showed the strongest induction (Blancher et al., 2015).

PHGDH expression was significantly lower in HIF-1α KO cells, indicating the HIF-1-dependency at <0.1% O_2. At the same level of hypoxia, PHGDH mRNA levels were

significantly reduced in the presence of PERK inhibitor. These data suggest that PHGDH is co-regulated by the PERK-ATF4 arm of the UPR in addition to HIF at <0.1% O_2.

Interestingly, although data suggest that PHGDH is a HIF-1 target, its expression was not induced at 2% O_2. A potential model to explain this expression pattern involves the oxygen-dependency of the hydroxylation pathways, which play key roles in HIF-1α stabilisation and activity. Specifically, inhibition of the prolyl hydroxylases (PHDs) occurs at relatively higher oxygen levels, allowing HIF-1α stabilisation, while Factor Inhibiting HIF (FIH) remains active, restricting recruitment of p300/CBP and limiting transcription (Tarhonskaya et al., 2015). As oxygen levels decrease further, FIH activity is progressively lost, permitting full HIF transcriptional activity and maximal expression of a subset of FIH-sensitive target genes. Example of such FIH-sensitive, HIF-regulated genes include p21, PPARγ and PLAUR (Dayan et al., 2006). Furthermore, certain chromatin remodelling proteins, such as KDM6A, are direct oxygen sensors and can change chromatin accessibility and affect HIF binding to the HREs in an oxygen-dependent manner (A. A. Chakraborty et al., 2019).

Although HIF-1-dependent induction of PHGDH was only observed under severe hypoxia (<0.1% O_2), its overlap with ATF4 activation does not make HIF redundant. Instead, PHGDH expression may be regulated by both HIF-1 and ATF4, with full induction occurring when both transcription factors are active. The co-regulation of PHGDH by both HIF-1 and ATF4 suggests that *de novo* serine synthesis is prioritised specifically under severe hypoxia, when both pathways converge. Additionally, neutral amino acid transporters such as SLC1A5, capable of extracellular serine import, were shown to be regulated by ATF4 (Z. Zhou et al., 2025). Importantly, the same transporter was also shown to be induced in hypoxia, although regulated by HIF-2 signalling rather than HIF-1 (H. C. Yoo et al., 2020). Together, this suggests that hypoxic cells coordinate serine availability through parallel transcriptional mechanisms. While *de novo* synthesis is driven by HIF-1 and ATF4 acting on PHGDH, extracellular serine import appears governed by a distinct HIF-2-dependent pathway. This is consistent with the observation that low extracellular serine availability induces PHGDH expression, suggesting

a positive feedback loop in which the nutrient-restricted hypoxic TME further drives *de novo* serine synthesis.

In summary, we aimed to characterise the regulation of PHGDH under hypoxia and the metabolic consequences of its loss. PHGDH was confirmed to be hypoxia-inducible at both mRNA and protein levels, with transcriptional induction restricted to severe hypoxia (<0.1% O_2). This was consistent with co-regulation by HIF-1 and PERK-ATF4, with predicted binding sites identified in the PHGDH enhancer region. PHGDH expression was also shown to increase under extracellular serine restriction. Three validated CRISPR-Cas9 knockout clones were generated, and metabolomic profiling revealed disruption of the SSP, elevated glycolysis, impaired purine synthesis, and a compensatory increase in pyrimidine metabolism.

Chapter 4: The effect of hypoxia and serine availability on radioresistance in the absence of PHGDH

4.1 Introduction

Radiobiological hypoxia (<0.1% O_2) confers marked resistance to ionising radiation, quantified by the oxygen enhancement ratio (OER). The OER is defined as the ratio of radiation dose required in hypoxia versus normoxia to achieve equivalent cell kill, with values of 2-3.5 characteristic of radiobiological hypoxia. The SSP and PHGDH specifically have emerged as promising targets to improve response to therapy due to their roles in key metabolic pathways. We demonstrated that PHGDH is induced in hypoxia. Given the link between hypoxia and radioresistance, we asked how targeting PHGDH could reduce radioresistance under hypoxia. Although few studies have examined this question, the impact of PHGDH loss or inhibition on radiation response, particularly under hypoxic conditions, remains unknown.

The primary mechanism by which targeting the SSP has been proposed to influence radiosensitivity is through perturbation of intracellular redox balance (Falcone et al., 2022; X. Liu et al., 2025; Sánchez-Castillo et al., 2024; Van de Gucht et al., 2022). However, most of these studies either did not investigate the effect of hypoxia or did not consider the impact of extracellular serine/glycine availability. This is particularly important because commonly used culture media, such as DMEM or RPMI, contain supraphysiological concentrations of serine, which cells can import and thereby mask the effects of SSP inhibition (Hennequart et al., 2021).

To address these limitations, we utilised PHGDH knockout cells and examined the impact of PHGDH loss on radiosensitivity in both normoxia and hypoxia (<0.1% O_2). These experiments were conducted in three different media: DMEM (high serine), HPLM (physiological serine), and MEM (no serine).

Specific aims:

- Investigate the effect of PHGDH KO on radiosensitivity in normoxia and hypoxia.
- Examine the effect of extracellular serine on radiosensitivity in parental control and PHDGH KO cells.
- Investigate the changes in GSH levels under varying extracellular serine conditions in cells without PHGDH.

4.2 Results

4.2.1 The knockout of PHGDH does not increase radiosensitivity in DMEM

Before investigating the role of PHGDH on radiosensitivity, we examined the effect of extracellular serine and glycine levels on radiosensitivity in A549 cells. To accomplish this, cells were exposed to increasing doses of radiation (0-8 Gy) in the three different media, and a colony survival assay was carried out. No significant differences were observed in radiosensitivity between DMEM and HPLM conditions. However, irradiation in the complete absence of extracellular serine and glycine (MEM) led to a significant radiosensitisation effect compared to DMEM or HPLM (**Figure 4.1**).

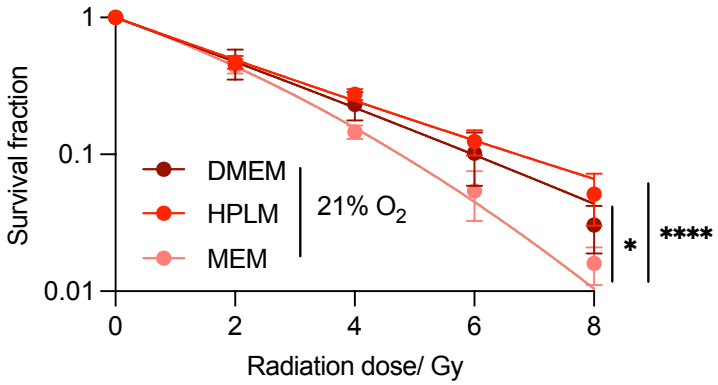

Figure 4.1 The effect of culture media on radiosensitivity. A549 cells were irradiated (0-8 Gy) in normoxia (21% O_2), followed by a colony formation assay. Before and during irradiation, cells were grown in DMEM, HPLM or MEM. Twenty-four hours after irradiation, all media were replaced with fresh DMEM. For statistical analysis, survival curves were fitted using a linear–quadratic model and compared by an extra-sum-of-squares F test. * *p<0.05, ****p<0.0001*.

Next, we investigated the effect of PHGDH on radiosensitivity. First, radiosensitivity changes in DMEM were investigated. Before analysing the effect of PHGDH KO in DMEM, the radioresistance effect due to exposure to hypoxia (<0.1% O_2) for 16 h was confirmed using parental control cells. In DMEM, cells irradiated in hypoxia were significantly more radioresistant compared to their normoxic counterparts. Moreover, the OER was 2.1, which confirmed hypoxia (<0.1% O_2) at the moment of irradiation (**Figure 4.2A**). Once the methodology was validated, the effect of PHGDH KO was analysed. When irradiated under normoxia, no significant difference was observed between parental control and PHGDH KO

cells (**Figure 4.2B**). In hypoxia, both control and KO cells showed increased radioresistance compared to normoxic cells; however, there was no PHGDH-dependent difference (**Figure 4.2C**).

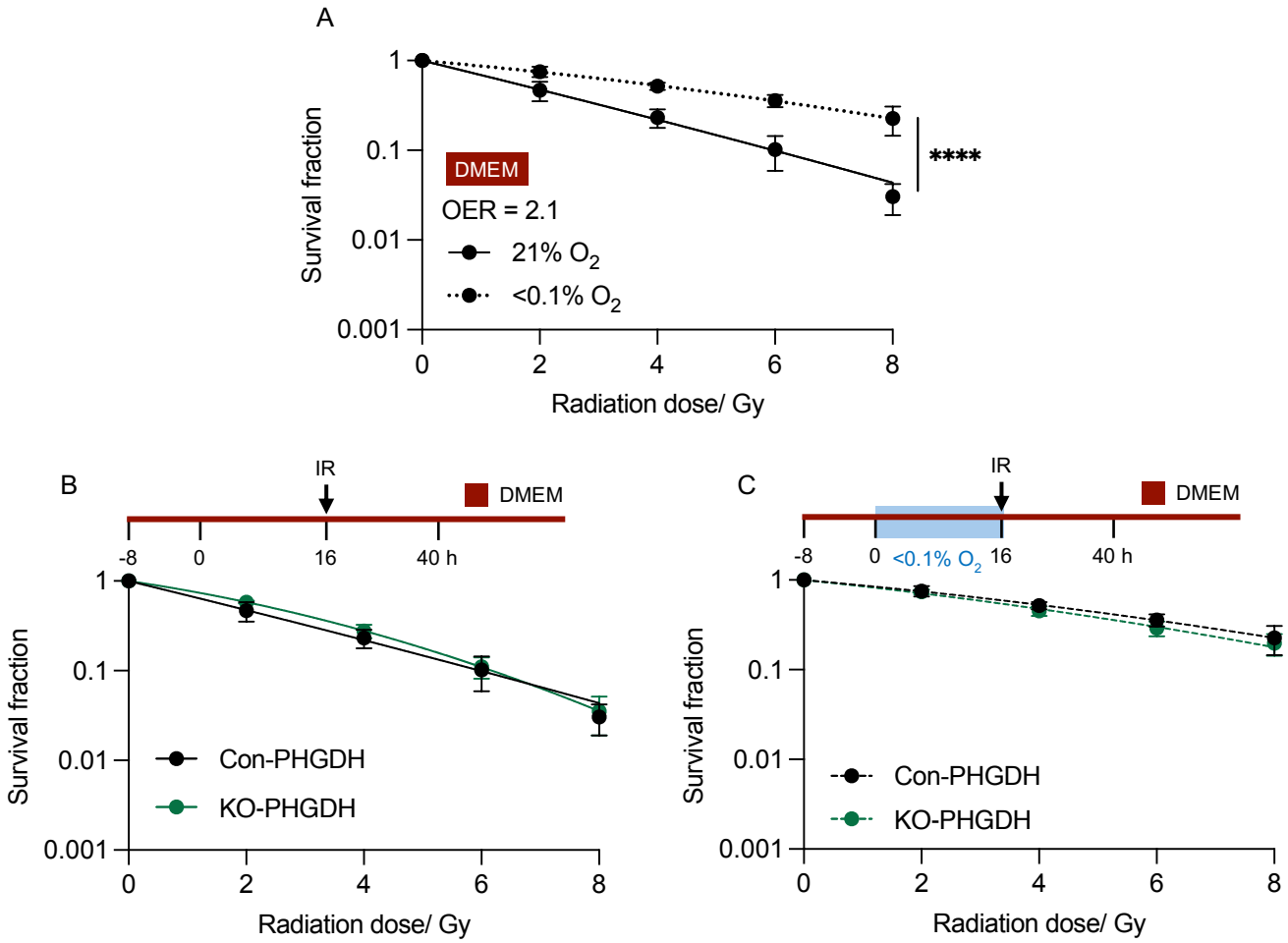

Figure 4.2 The effect of PHGDH KO on radiosensitivity in normoxia and hypoxia, in DMEM. A. A549 (parental) cells were grown in DMEM and exposed to radiation (0-8 Gy) in either normoxia (21% O_2) or hypoxia (<0.1% O_2), and radiosensitivity was determined by colony survival assay. **B, C.** A549 parental and PHGDH KO cells were irradiated (0-8 Gy) in normoxia (21% O_2, **B**) and hypoxia (<0.1% O_2, **C**), followed by a colony survival assay. A schematic of the experimental setup is indicated. The parental control (Con) data in A is the same as B and C. For statistical analysis, survival curves were fitted using a linear–quadratic model and compared by an extra-sum-of-squares F test. ****$p<0.0001$. Absence of stars represents a non-significant difference.

4.2.2 Loss of PHGDH does not increase radiosensitivity in HPLM

Here, cells were incubated in HPLM for 24 h before irradiation and kept in the same media for an additional 24 h post-irradiation. For the hypoxic condition, cells were exposed to <0.1% O_2 8 h post-seeding. Following 16 h of hypoxia exposure and irradiation, cells were kept in HPLM

for another 24 h. Following a total of 48 h incubation in HPLM, cells were swapped back into DMEM to allow colonies to form.

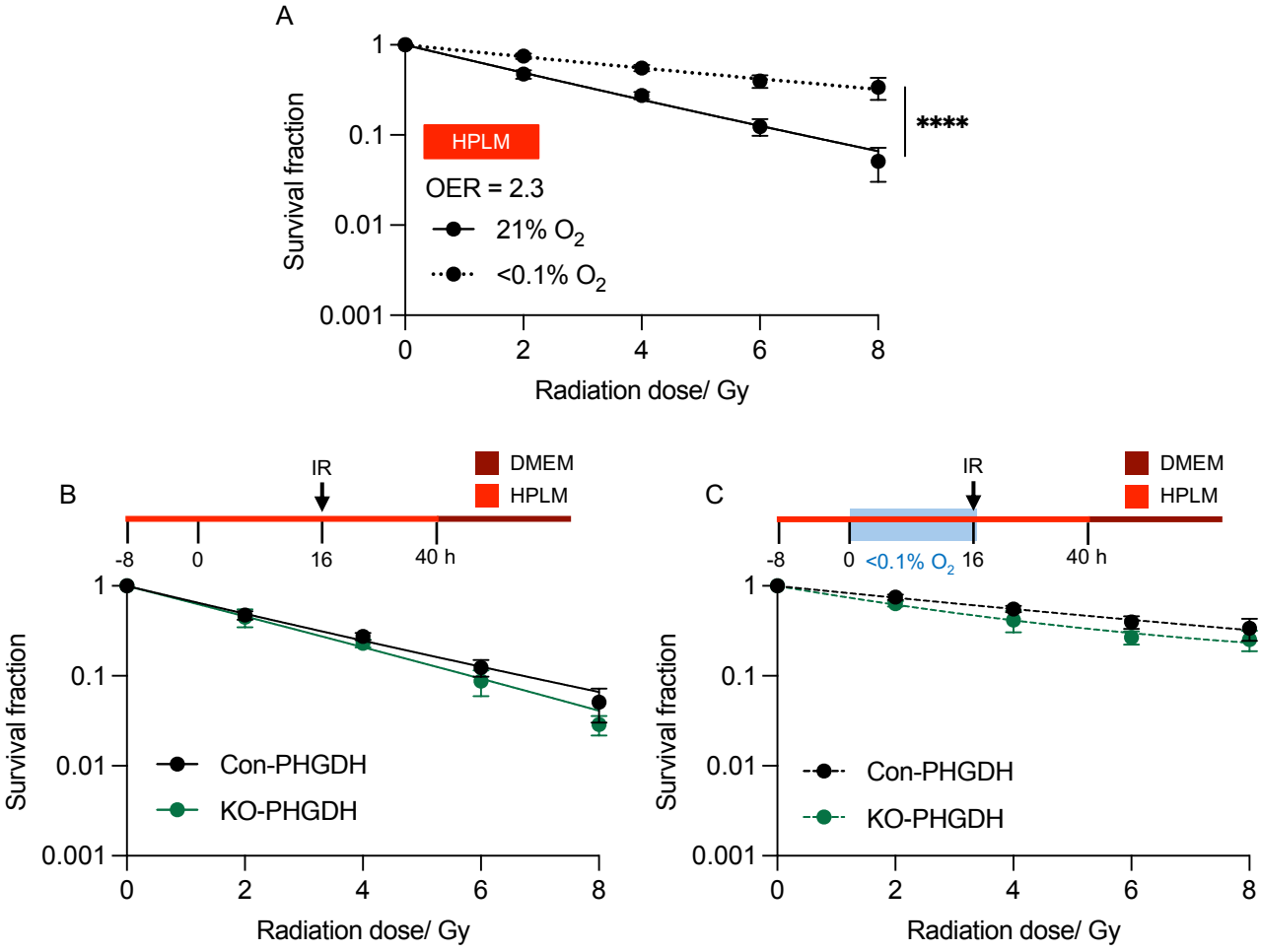

Figure 4.3 The effect of PHGDH KO on radiosensitivity in normoxia and hypoxia, in HPLM. A. A549 (parental) cells were grown in HPLM and exposed to radiation (0-8 Gy) in either normoxia (21% O_2) or hypoxia (<0.1% O_2), and radiosensitivity was determined by colony survival assay. **B, C.** A549 parental and PHGDH KO cells were irradiated (0-8 Gy) in normoxia (21% O_2, **B**) and hypoxia (<0.1% O_2, **C**), followed by a colony survival assay. 24 h before and during irradiation, cells were grown in HPLM. Twenty-four hours after irradiation, all media were replaced with fresh DMEM. A schematic of the experimental setup is indicated. The parental control (Con) data in A is the same as in B and C. For statistical analysis, survival curves were fitted using a linear–quadratic model and compared by an extra-sum-of-squares F test. ****$p<0.0001$. Absence of stars represents a non-significant difference.

Like the DMEM, hypoxia was again confirmed by calculating the $OER_{37\%}$. The OER for HPLM was 2.3, which again validated the significantly increased radioresistance expected in hypoxic conditions (**Figure 4.3A**). Under normoxia, at physiological serine and glycine levels, loss of PHGDH did not lead to any significant changes in radiosensitivity (**Figure 4.3B**). In hypoxia,

no significant changes in radiosensitivity were observed between the two lines (**Figure 4.3C**). These findings demonstrate that when grown in DMEM or HPLM, there is no PHGDH-dependent effect on radiosensitivity.

4.2.3 Loss of PHGDH increases radiosensitivity in MEM

To fully understand whether PHGDH can impact radiosensitivity, a colony survival assay was performed in MEM. As previously, cells were incubated in MEM for 48 hours, irradiated for 24 h in the absence of serine. Hypoxic samples were exposed to 16 h of <0.1% O_2 while in MEM. Like DMEM and HPLM, irradiation under hypoxia was confirmed in MEM by calculating the OER value, which was 3.4 (**Figure 4.4A**).

In contrast to media containing serine, PHGDH KO cells irradiated in MEM showed a significant increase in radiosensitivity under normoxia (**Figure 4.4B**). Although to a lesser magnitude, significant radiosensitisation was also observed in PHDGH KO cells compared to parental controls at <0.1% O_2 (**Figure 4.4C**). Together, these data indicate that significant radiosensitisation in cells without PHGDH only occurs when extracellular serine is completely removed.

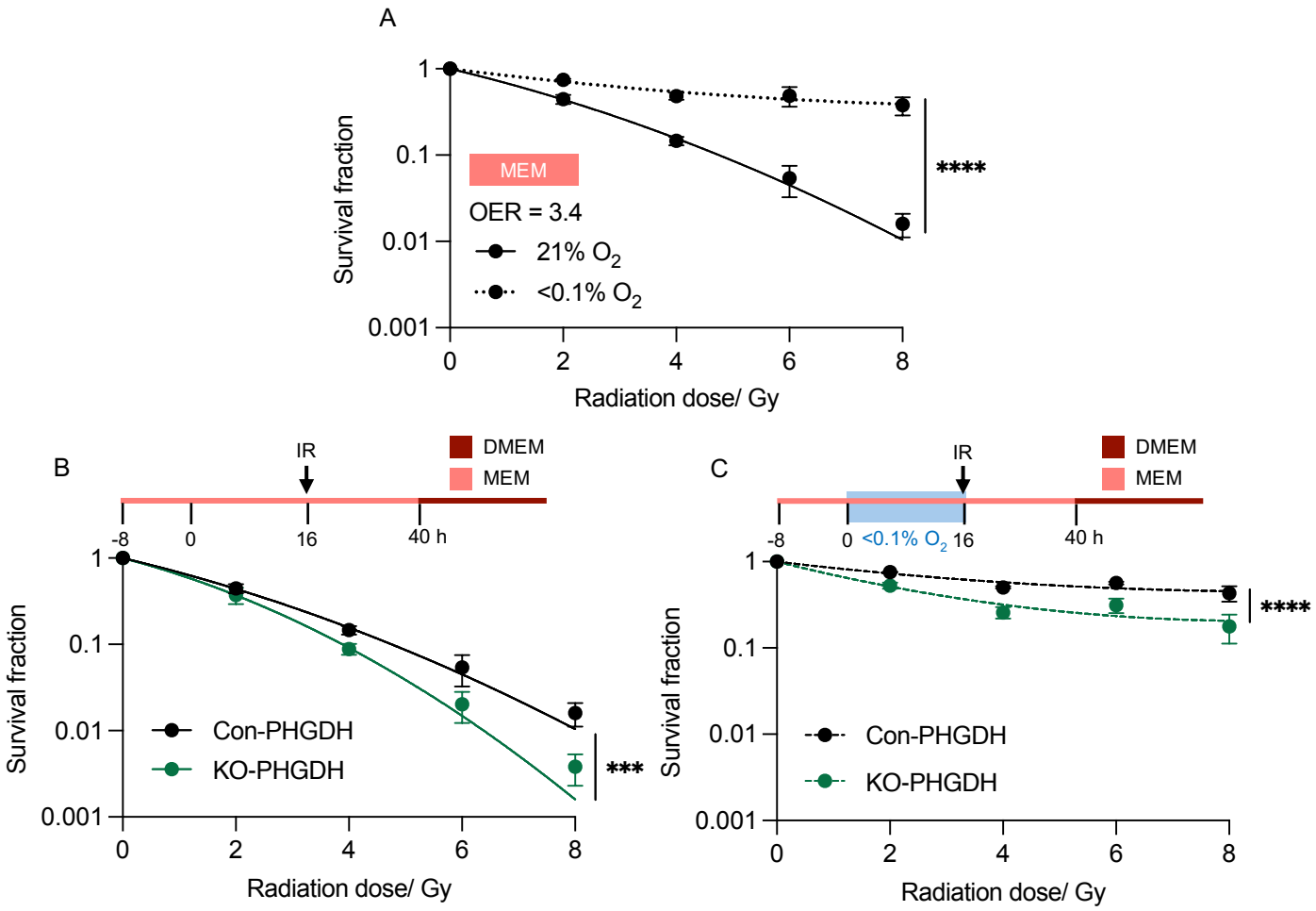

Figure 4.4 The effect of PHGDH KO on radiosensitivity in normoxia and hypoxia, in MEM. A. A549 (parental) cells were grown in MEM and exposed to radiation (0-8 Gy) in either normoxia (21% O_2) or hypoxia (<0.1% O_2), and radiosensitivity was determined by colony survival assay. **B, C.** A549 parental and PHGDH KO cells were irradiated (0-8 Gy) in normoxia (21% O_2, **B**) and hypoxia (<0.1% O_2, **C**), followed by a colony survival assay. 24 h before and during irradiation, cells were grown in MEM. Twenty-four hours after irradiation, all media were replaced with fresh DMEM. A schematic of the experimental setup is indicated. The data in A is the same as in B and C. For statistical analysis, survival curves were fitted using a linear–quadratic model and compared by an extra-sum-of-squares F test. *****p<0.0001*.

4.2.4 Loss of PHGDH does not affect the redox balance in the presence of extracellular serine

A potential mechanism by which inhibition of the serine-glycine synthesis pathway has been linked to an increase in radiosensitivity is disrupted redox homeostasis. To determine whether PHGDH loss alone was sufficient to alter the redox balance of the cell, ROS measurements were conducted in the presence of excess extracellular serine (DMEM). First, intracellular ROS levels were measured using MitoSOX Red indicator, specifically targeting the

mitochondrial superoxide. Measurements were conducted in three PHGDH KO clones alongside the parental control to eliminate the possibility of clonal differences. No significant change was observed in baseline ROS levels in PHGDH KO cells (**Figure 4.5A**).

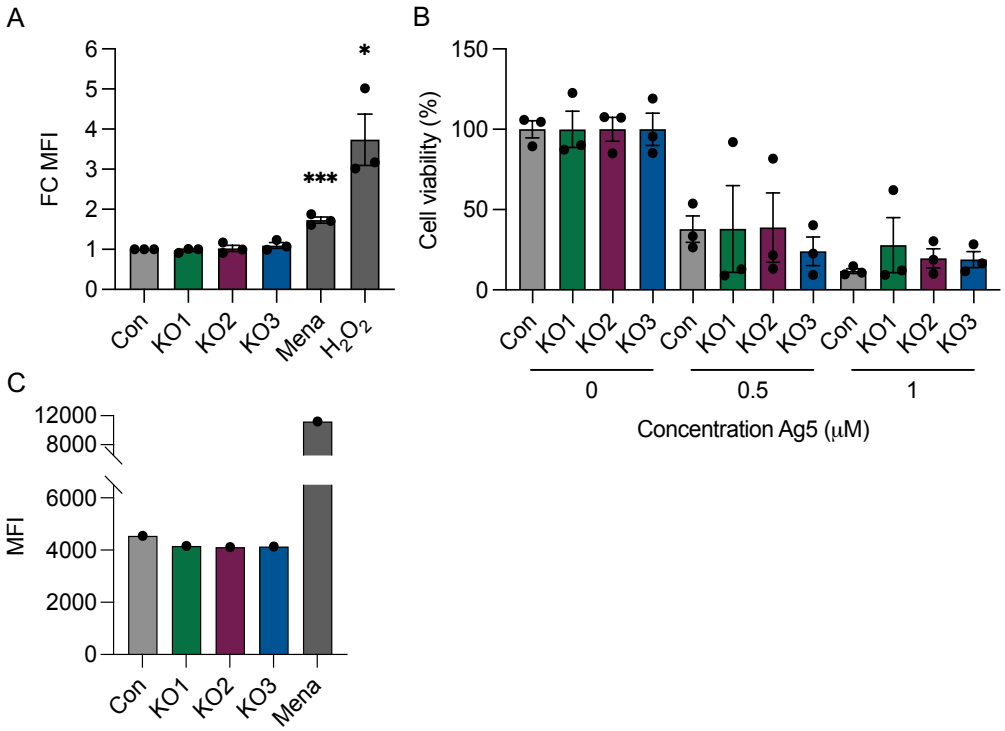

Figure 4.5 The effect of PHGDH loss on intracellular ROS levels. A. Mitochondrial superoxide was quantified using the MitoSOX Red indicator in parental control (Con) and three PHGDH KO clones (KO1–KO3). Fluorescence was measured by flow cytometry and expressed as fold change (FC) in median fluorescence intensity (MFI) relative to the parental control. Menadione (Mena; 100 μM, 6 h) and H_2O_2 (25 μM, 3 h) were used as positive controls. **B.** Cell viability was assessed by MTT assay in parental control (Con) and three PHGDH KO clones (KO1–KO3) following treatment with increasing concentrations of Ag5 (0, 0.5, and 1 μM). Absorbance values were normalised to the corresponding untreated condition and expressed as percentage viability. **C.** Total intracellular reactive oxygen species (ROS) were quantified using the DCFDA fluorescent probe in parental control (Con) and PHGDH knockout clones (KO1–KO3) (n = 1). Fluorescence was measured by flow cytometry and reported as median fluorescence intensity (MFI). Menadione (Mena) was included as a positive control to induce oxidative stress. Bars represent mean ± SEM, and individual dots represent independent biological replicates (n = 3). For statistical analysis of the MitoSOX experiment two-tailed Student's *t-test* was used. **p<0.05, ***p<0.001*. For the Ag5 MTT, one-way ANOVA was performed. Absence of stars represents a non-significant difference.

To confirm these results, alternative methods were employed to measure changes in ROS. Cell viability was assessed following Ag5 treatment, a compound reported to preferentially reduce viability in cells with elevated ROS levels (Twigger et al., 2024). No significant differences were observed in cell viability between the parental control and the PHGDH KO cells, indicating unchanged levels of intracellular ROS (**Figure 4.5B**). Lastly, total ROS levels

were measured using the DCFDA probe, which also showed no significant change in PHGDH KO cells compared to controls (**Figure 4.5C**). Although preliminary these data support a model where PHGDH-dependent radiosensitisation only occurs where redox is also changed, which does not occur in the presence of exogeneous serine.

4.2.5 Serine deprivation drives reduced glutathione levels

We measured GSH to determine whether it reflects the observed changes in radiosensitivity under varying levels of extracellular serine, both in normoxia and hypoxia. To determine the GSH levels, a thiol-responsive fluorescent probe (FL-1) was used (Twigger et al., 2024). Before the measurements, cells were incubated in the respective media for 16 h. Hypoxic samples were exposed to <0.1% O_2 for 16 h.

GSH levels in hypoxia increased significantly in parental control and PHGDH KO cells in DMEM (p_{Con} = *0.0137*; p_{KO} = *0.0142*), HPLM (p_{Con} = *0.0058*; p_{KO} < *0.00001*), and MEM (p_{Con} = *0.0006*; p_{KO} = *0.0008*) (**Figure 4.6**).

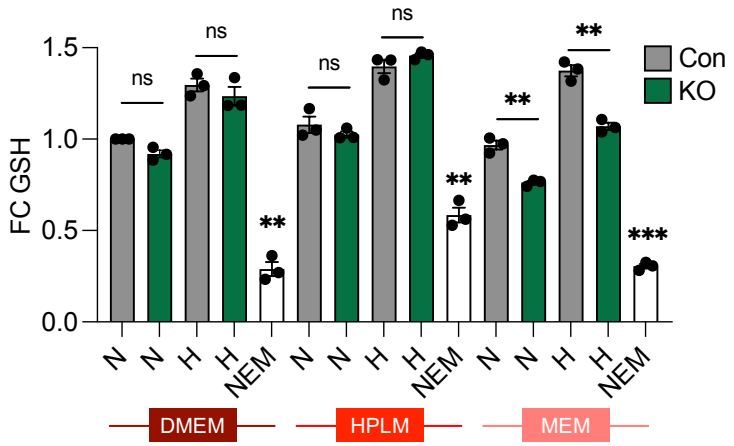

Figure 4.6 Loss of PHGDH leads to reduced GSH levels in the absence of extracellular serine. Parental control and PHGDH KO A549 cells were grown in DMEM, HPLM and MEM for 16 h, under normoxia (N, 21% O_2) or hypoxia (H, <0.1% O_2, 16 h). Fold change (FC) in GSH levels was calculated in relation to baseline levels in cells cultured in DMEM under normoxia. N-ethylmaleimide (200 µM) was used as a negative control. For statistical analysis, a two-tailed Student *t-test* was performed. **p<0.05, **p<0.01, ***p<0.001. ns* = statistically non-significant difference.

When looking at the PHGDH-dependent changes in GSH levels, no changes in cells cultured in DMEM were observed in normoxia and hypoxia (**Figure 4.6**). This result is consistent with

the ROS measurements shown before. Similarly, when grown in HPLM, GSH levels stayed unchanged in PHGDH KO cells compared to parental controls at different oxygen levels. However, in the complete lack of extracellular serine (MEM), GSH levels in PHGDH KO cells significantly decreased compared to parental control cells. A similar decrease was also observed in hypoxic samples cultured in MEM. These findings are fully consistent with the radiosensitivity pattern observed, which makes the lower GSH levels in MEM a potential explanation behind radiosensitisation in PHGDH KO cells in normoxia and hypoxia.

4.2.6 Exposure to hypoxia leads to improved survival in PHGDH knockout cells

Analysis of the unirradiated (0 Gy) controls, from colony survival assays (section 4.2.1), revealed an unexpected oxygen-dependent effect on clonogenic survival. In DMEM and HPLM, PHGDH KO cells seemed to survive better compared to the parental control cells. To investigate this further, another colony survival assay was performed, where PHGDH WT and KO cells were cultured in DMEM and exposed to normoxia and varying levels of hypoxia (2% and <0.1% O_2). The survival of cells lacking PHGDH was not affected by the hypoxia, whereas control cells showed a significant reduction in cell survival at 2% and <0.1% O_2 (**Figure 4.7**). Interestingly, these results suggest that the absence of PHGDH and, subsequently, the *de novo* SSP, leads to better adaptation of these cells to hypoxia.

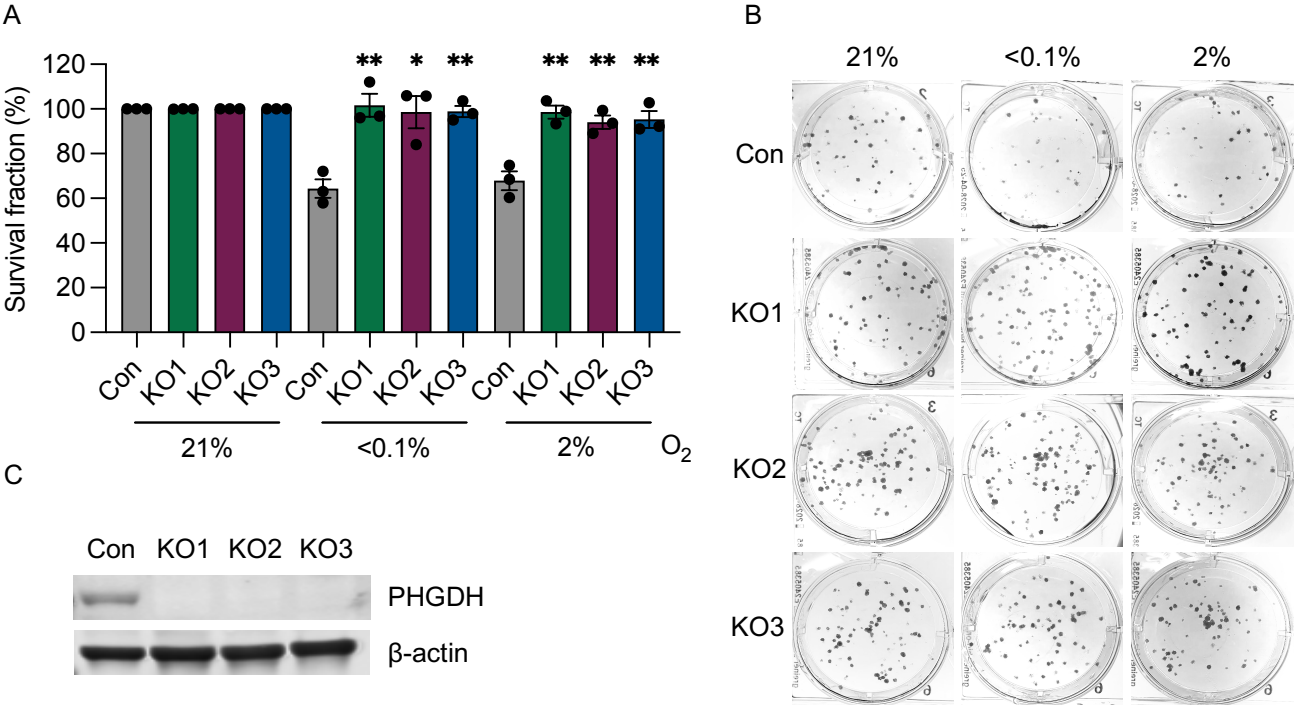

Figure 4.7 PHGDH KO cells survive better under hypoxia compared to Con cells. A. A549 (Con and PHGDH KO) grown in DMEM were exposed to hypoxia (<0.1 or 2% O_2) for 16 h. Cells were returned to normoxic conditions and colonies allowed to form. Colony survival is expressed as a percentage survival fraction relative to the 21% O_2 control. **B.** Representative, stained colony formation assay plates for parental control and PHGDH KO cells cultured in DMEM under normoxia and hypoxia (2% O_2 and <0.1% O_2). **C.** Loss of PHGDH was again confirmed by western blotting of the parental (Con) and PHGDH KO clones. β-actin as a loading control. Bars represent mean ± SEM, and individual dots represent independent biological replicates (n=3). For statistical analysis, a two-tailed Student's *t-test* was used. **p<0.05, **p<0.01.*

To assess the effect of extracellular serine levels on cell survival under hypoxia, the colony survival assay was repeated using HPLM and MEM. Similar to DMEM, parental cells exhibited reduced survival under hypoxia, whereas PHGDH KO cells showed no significant change in HPLM (**Figure 4.8A**). However, when extracellular serine was completely absent (MEM), both parental and KO cells showed a significant reduction in cell survival under hypoxia (**Figure 4.8B**). These findings suggest that under hypoxia, PHGDH-deficient cells adapt more effectively in DMEM and HPLM; however, this advantage is lost when cells are exposed to MEM.

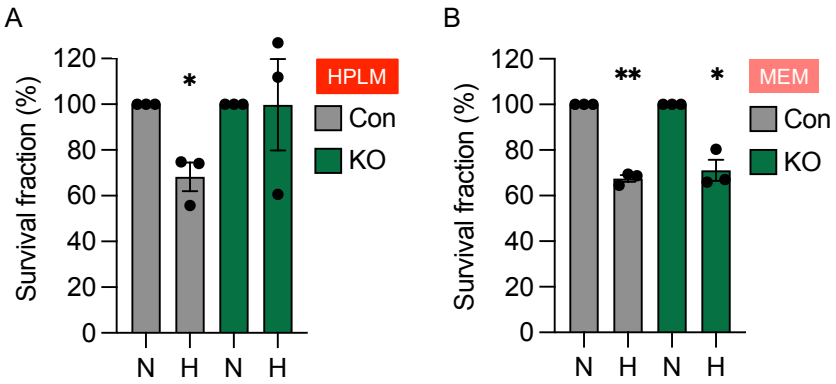

Figure 4.8 PHGDH KO cells survive better under hypoxia compared to Con cells in HPLM but not in MEM. A, B. A549 (Con and PHGDH KO) grown in HPLM (**A**) or MEM (**B**) were exposed to hypoxia (<0.1% O_2) for 16 h. Cells were returned to normoxic conditions, the media was changed to DMEM after 24 h, and colonies were allowed to form. Colony survival is expressed as a percentage survival fraction relative to the 21% O_2 control. Bars represent mean ± SEM, and individual dots represent independent biological replicates (n = 3). For statistical analysis, a two-tailed Student's *t-test* was used. **p<0.05, **p<0.01.* Absence of stars represents a non-significant difference.

To validate the PHGDH dependency of the observed improvement in survival under hypoxia, PHGDH expression was rescued in knockout cells, and the colony survival assay was repeated. PHGDH KO cells were transfected with a PHGDH expression construct to restore expression. The amount of plasmid transfected was optimised to achieve PHGDH expression comparable to endogenous levels in parental control cells. As a result, 0.3 µg was selected (**Figure 4.9**).

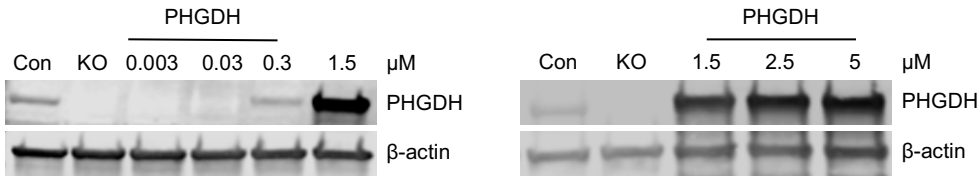

Figure 4.9 PHGDH rescue optimisation in KO cells. PHGDH KO A549 cells were transfected with the indicated amounts of PHGDH expression vector and lysed for western blotting. β-actin as a loading control.

Following the optimisation, PHGDH was rescued in KO cells to endogenously relevant levels and a colony survival assay was performed with cells exposed to normoxia and two different hypoxia levels (2% and <0.1% O_2). Cells with restored PHGDH expression showed reduced cell survival to levels comparable to those of parental control cells (**Figure 4.10**). Together, these data confirm the maintained cell survival in hypoxia to be PHGDH-dependent but independent of extracellular serine and glycine.

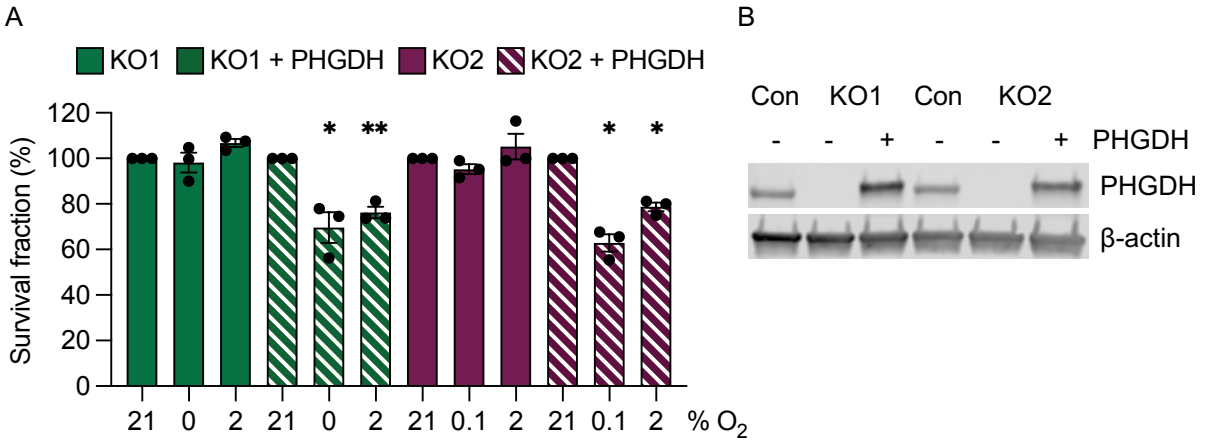

Figure 4.10 The effect of PHGDH overexpression in PHGDH KO cells in hypoxia. A. PHGDH KO1 and KO2 cells expressing an empty vector control or 0.3 μg PHGDH overexpression vector (KO1-2 + PHGDH) was cultured under normoxia and hypoxia (<0.1 or 2% O_2) for 16 h. Cells were returned to normoxic conditions and colonies allowed to form. **B.** Rescue of PHGDH was confirmed by western blotting of the parental (Con), PHGDH KO and KO1/2 + PHGDH cells. β-actin as a loading control. Bars represent mean ± SEM, and individual dots represent independent biological replicates (n = 3). For statistical analysis, a two-tailed Student's *t-test* was used. **p<0.05, **p<0.01.* Absence of stars represents a non-significant difference.

4.2.7 Loss of PHGDH does not reduce proliferation rates at <0.1% O_2

When analysing the colony survival assay performed in different oxygen levels, differences in colony diameter were apparent between parental control and PHGDH KO cells in hypoxia. To investigate whether this difference in colony size reflected an underlying difference in cell growth rates, a proliferation assay was performed. Cells were grown and counted over 7 days, and the fold change in cell number was quantified. Pre-treatment of parental controls with hypoxia (16 h) led to a significant reduction in proliferation rates in DMEM (**Figure 4.11A**). The same conditions did not cause any change in proliferation rates in PHGDH KO cells compared to the controls (**Figure 4.11B**).

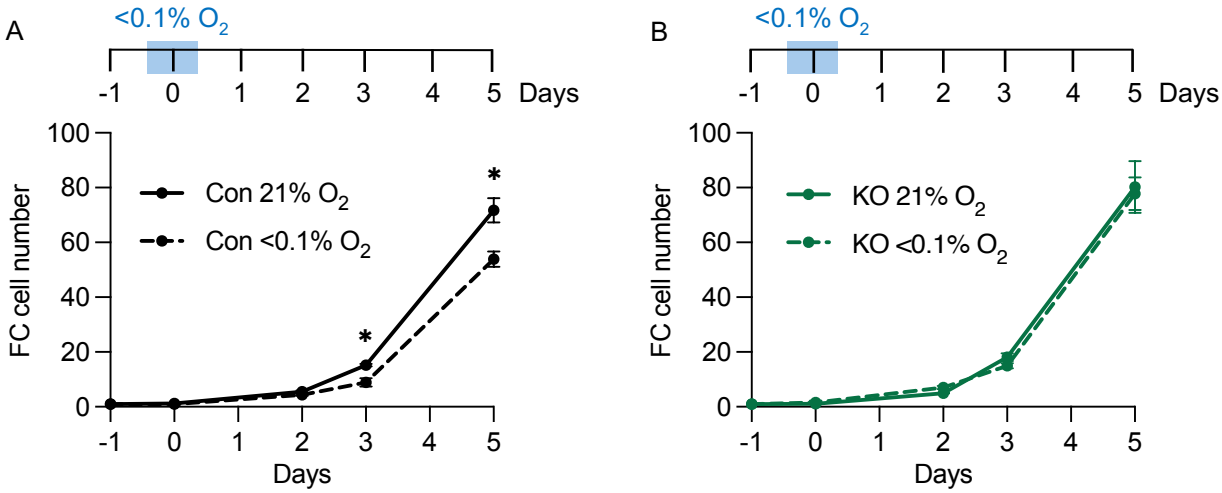

Figure 4.11 The effect of PHGDH KO on cell proliferation in hypoxia. Fold change in proliferation rates of parental con (**A**) and PHGDH KO (**B**) A549 cells grown in complete DMEM media with (dashed line) or without (solid line) 16 h exposure to <0.1% O_2. Bars represent mean ± SEM, and individual dots represent independent biological replicates (n = 3). For statistical analysis, a two-tailed Student's *t-test* was used. **p<0.05, **p<0.01.* Absence of stars represents a non-significant difference.

Because this experiment was performed in DMEM (i.e., under supraphysiological serine levels), the maintained growth rate in PHGDH KO cells cannot be attributable to serine limitation. These findings confirm better adaptation of PHGDH KO cells to hypoxic conditions.

4.2.8 PHGDH KO cells showed elevated levels of glycolysis

To elucidate the mechanisms underlying the improved survival of PHGDH knockout cells in hypoxia, we revisited our metabolomics dataset. As described, a substantial proportion of glycolytic metabolites were shown to be upregulated in PHDGH KO in baseline conditions under excess extracellular serine. Pyruvate and lactate, the end-point metabolites of glycolysis, were significantly increased in knockout cells compared to parental control (**Figure 4.12**).

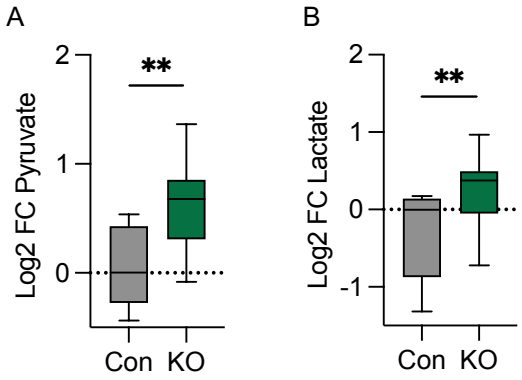

Figure 4.12 Intracellular pyruvate and lactate levels based on IC-MS metabolite analysis in PHGDH KO and parental control cells. A, B. Comparisons of the levels of Pyruvate (**A**), Lactate (**B**) between A549 and PHGDH KO cells under normoxia (21% O_2). ** *p < 0.01,* *** *p < 0.001*

Given the observed increase in intracellular lactate levels, we next performed extracellular flux analysis (glycolytic stress test) to measure export rates and assess differences in glycolytic activity between parental and KO cells. Extracellular acidification rate (ECAR: proxy for extracellular lactate) was found to be consistently higher in two PHGDH KO clones compared to the control cells (**Figure 4.13A**).

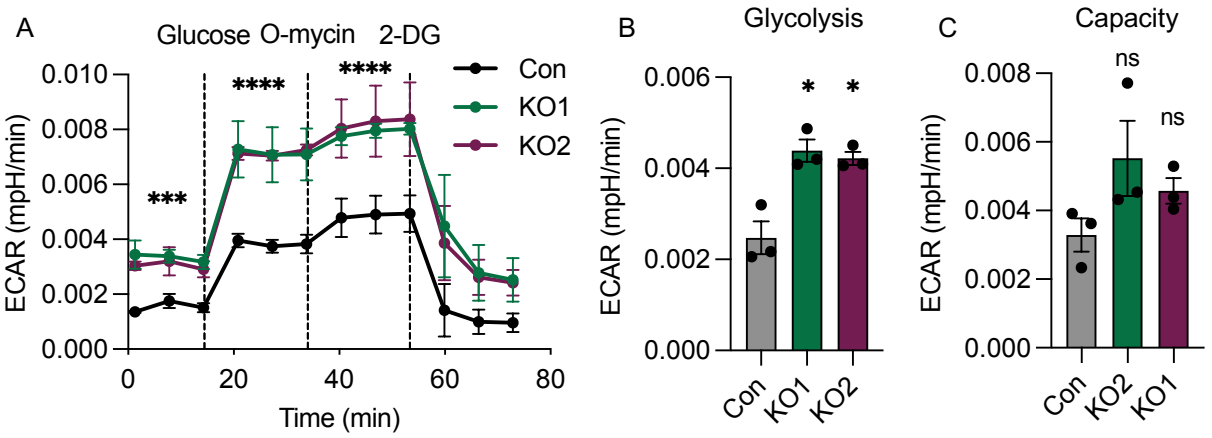

Figure 4.13 The effect of PHGDH KO on extracellular lactate and glycolysis levels. A. Glycolytic stress test was performed on parental control and PHGDH KO A549 cells by treating the cells with glucose (10 mM), oligomycin (O-mycin; 1 μM) and 2-deoxyglucose (2-DG; 50 mM). Vertical dashed lines represent the timepoint at which each of these stress reagents was added to the cells. Each datapoint represents a measurement cycle of approximately 6.5 min. **B.** Using data from part A, glycolysis levels were calculated based on the difference in ECAR levels following the injection of glucose. **C.** Using data from part A, glycolytic capacity was calculated based on the difference in ECAR levels following the injection of oligomycin (O-mycin). Bars represent mean ± SEM, and individual dots represent independent biological replicates (n = 3). One-way ANOVA was conducted for statistical analysis. **p<0.05, ***p<0.001, ****p<0.0001. ns* = statistically non-significant difference.

As part of the glycolytic stress test, cellular glycolysis was quantified based on the increase in ECAR following injection of saturating concentrations of glucose. Glycolysis rate was significantly higher in both PHGDH KO clones compared to the parental cells (**Figure 4.13B**). Maximum glycolytic capacity was determined following oligomycin injection, an ATP synthase inhibitor that suppresses oxidative phosphorylation, thereby revealing the maximal glycolytic activity the cells can achieve (I. Yoo et al., 2024).

The glycolytic stress test can also be used to determine the glycolytic capacity. The glycolytic capacity refers to the maximum level of glycolysis that can be achieved by cells following the inhibition of oxidative phosphorylation (OXPHOS) with oligomycin. Despite the increase, there

were no significant changes in glycolytic capacity between KO cells and controls (**Figure 4.13C**). The lack of further increase in glycolysis levels, with inhibited OXPHOS, suggests that cells rely on glycolysis even when the aerobic pathway of metabolism is not inhibited. Overall, we observed that, besides elevated intracellular lactate, PHGDH knockout cells display increased basal glycolysis and higher extracellular lactate levels.

4.2.9 Enhanced HIF-signalling in PHGDH KO cells

Previous studies have shown that elevated lactate can influence HIF-1α stability. Specifically, lactate has been reported to inhibit prolyl hydroxylase (PHD) activity and decrease HIF-1α turnover through lactate-dependent, chaperone-mediated autophagy under hypoxic conditions (De Saedeleer et al., 2012; Kshitiz et al., 2022). Hence, the elevated lactate observed earlier (section 4.2.6) could prime PHGDH KO cells to adapt better to hypoxic conditions due to improved HIF stability and signalling. To understand the effect of lactate, HIF-1α induction was first investigated at <0.1% O_2 using western blotting. HIF-1α accumulated more quickly in two KO clones compared to parental control cells, which indicates quicker induction of HIF-1 (**Figure 4.14**).

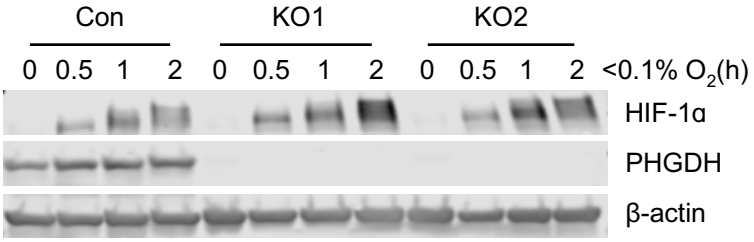

Figure 4.14 HIF-1α induction in parental and PHGDH KO cells. Cells were exposed to <0.1% O_2 for the time-course indicated. Cells were lysed, and western blotting was performed for HIF-1α and PHGDH. β-actin as a loading control.

To investigate HIF-1 activity, a hypoxia response element (HRE)-luciferase reporter was used to determine the impact of PHGDH loss. The reporter assay works by transfecting cells with a firefly luciferase (FLuc) construct that has 5 copies of the HRE from VEGF at the promoter site. Following exposure to hypoxia and subsequent expression of FLuc, luminescence is

measured as a proxy for HIF-1 activity (**Figure 4.15**). Constitutively expressed Renilla luciferase (RLuc) construct was co-transfected for signal normalisation.

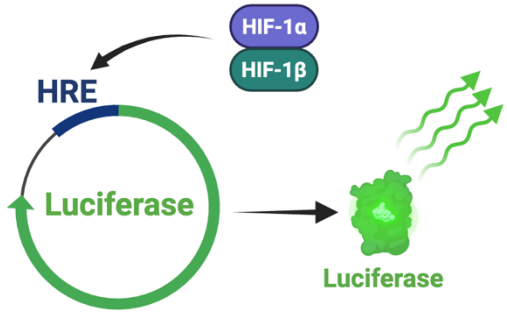

Figure 4.15 Schematic representation of HRE-Firefly luciferase (FLuc) reporter assay

This luciferase-based assay was used to determine whether PHGDH KO cells also increased HIF-1-activity in hypoxia (i.e. HRE binding and gene expression) in addition to quicker induction. PHGDH KO cells showed significantly increased HIF-1 activity. Although this observation was true for two different PHGDH KO clones, the induction kinetics were different. KO1 cells displayed significantly higher HRE-driven luciferase activity than control cells at all measured time points throughout the time course (**Figure 4.16A**).

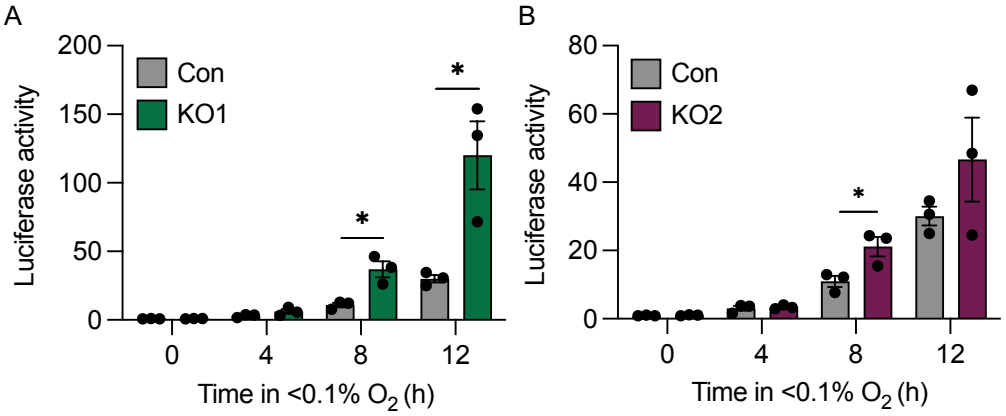

Figure 4.16 PHGDH loss induces HIF-signalling. A, B. Parental, PHGDH KO1 (**A**) and KO2 (**B**) A549 cells were exposed to hypoxia for the indicated times. HIF-activity was measured by measuring the expression levels of the HRE-Luciferase enzyme, normalised to Renilla. 0 h readings were used for normalisation. Bars represent mean ± SEM, with individual data points shown. One-way ANOVA was performed for statistical analysis. **p<0.05.* Absence of stars represents a non-significant difference.

In contrast, KO2 cells showed increased HIF activity at early time points (8 h); however, this difference was no longer significant at the final 12 h time point, when luciferase activity in control cells reached levels comparable to those observed in the knockout cells (**Figure**

4.16B). The differences in fold change induction in luciferase activity in different PHGDH KO clones (100-fold in KO1 and 40-fold in KO2) can be explained by potential differences in transfection efficiency.

The results of the HRE-luciferase assay were confirmed by measuring the mRNA induction levels of known HIF-target genes in parental and KO cells at <0.1% O_2. Expression levels of CAIX, GLUT1, LDHA and VEGF were measured following exposure to <0.1% O_2 using RT-qPCR. CAIX and GLUT1 mRNA levels were significantly upregulated in PHGDH KO compared to parental controls throughout the entire hypoxia time course (**Figure 4.17A, B**).

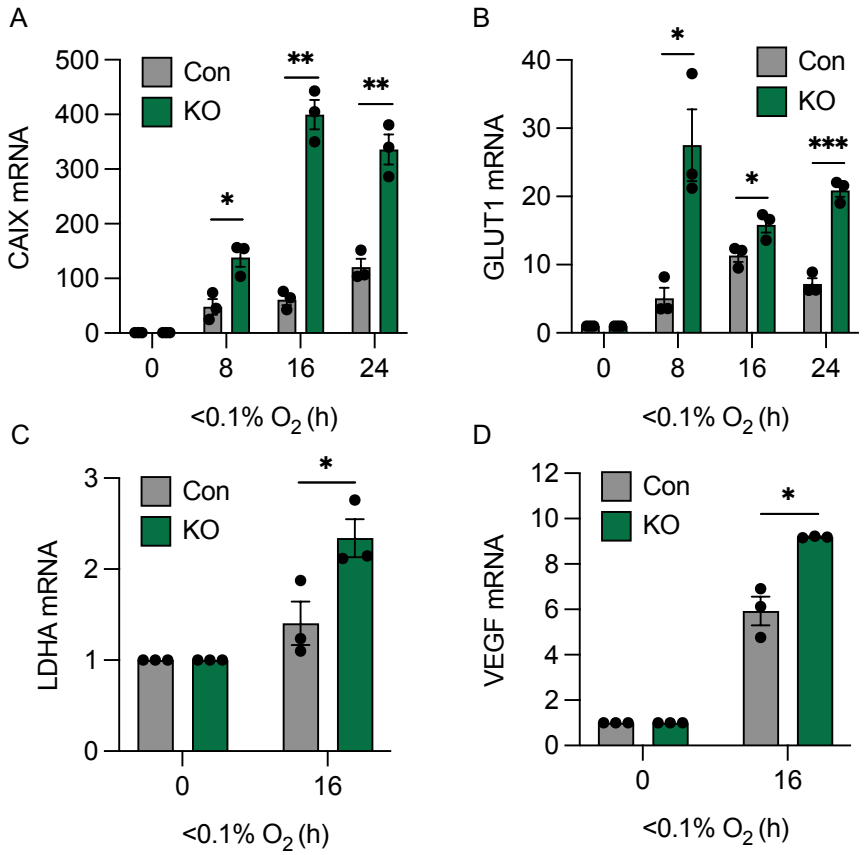

Figure 4.17 PHGDH KO leads to more significant induction of HIF-target genes. A-D. Con and PHGDH KO cells were exposed to <0.1% O_2 for the times indicated. mRNA levels of CAIX (**A**), GLUT1 (**B**), LDHA (**C**), and VEGF (**D**) were measured using RT-qPCR. Bars represent mean ± SEM, with individual data points shown. For statistical analysis, a two-tailed Student *t-test* was performed. **p<0.05, **p<0.01, ***p<0.001.*

Consistent with the other HIF-target genes, LDHA and VEGF mRNA levels showed significant upregulation at 16 h (**Figure 4.17C, D**). Together, these data show that, in addition to quicker induction, PHGDH knockout leads to higher levels of HIF-1-mediated gene expression. The

enhanced HIF-1 signalling in cells lacking PHGDH could account for the better adaptation of the KO cells to hypoxic conditions. Additionally, these observations were again made in the presence of excess extracellular serine (DMEM), meaning that despite the changes being PHGDH-dependent, they were independent of serine availability.

4.2.10 Loss of PHGDH affects macrophage polarisation in hypoxia

Hypoxia is a hallmark of the TME and has been associated with the induction of an immunosuppressive immune landscape through HIF-1 signalling (Ke et al., 2019). The increased HIF-1 signalling observed in KO cells prompted us to examine whether loss of PHGDH affects macrophage polarisation. First, to validate the immunosuppressive effect of hypoxia on macrophage polarisation, patient-derived PBMCs were exposed to normoxia and hypoxia (<0.1% O_2). Following the incubation, the percentage of M1 macrophages (% of CD80+ CD86+ cells in relation to CD11b+ cells) was then characterised using flow cytometry. As expected, the percentage of pro-inflammatory M1 macrophages dropped from 20% to less than 10% (**Figure 4.18**).

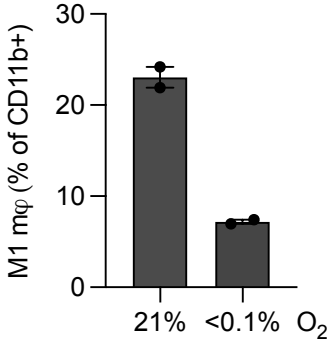

Figure 4.18 Macrophage polarisation following hypoxia exposure (<0.1% O_2). Patient-derived PBMCs were incubated at normoxia (21% O_2) and hypoxia (<0.1% O_2) for 16 h. The % of CD80+ and CD86+ double-positive cells (M1) was characterised in relation to the total macrophage pool (CD11b+) using flow cytometry analysis (lack of error bars as data is n=2).

To investigate the effect of PHGDH KO on the TME, culture media (DMEM) was conditioned on PHGDH control and KO cells at normoxic and hypoxic conditions. Following a 24 h conditioning, the media was transferred to PBMCs and incubated for another 24 h. Lastly, flow cytometry analysis was used to characterise the fraction of M1 macrophages. No statistically

significant differences were observed between the parental control and PHGDH KO cells in normoxia (**Figure 4.19**). However, the proportion of M1 macrophages in PHGDH KO cells was significantly lower (around 2-fold) compared to control cells when cultured with hypoxia-conditioned media.

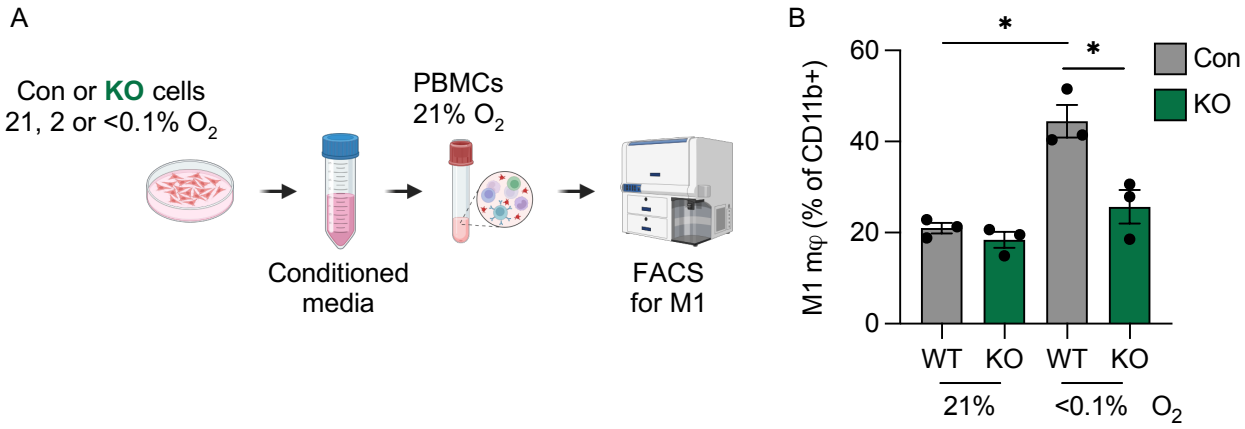

Figure 4.19 Macrophage polarisation following exposure to media conditioned with parental and PHGDH KO cells at 21% and <0.1% O_2. A. Schematic representation of the experimental setup. **B.** A549 parental control and PHGDH KO cells were incubated in normoxia (21% O_2) and hypoxia (<0.1% O_2) for 16 h. The conditioned media from the cancer cells were then transferred onto the PBMCs and incubated for 24 h. The effect of conditioned media on the M1 macrophage cluster was characterised in relation to the total macrophage pool (CD11b+) using flow cytometry analysis. Bars represent mean ± SEM, with individual data points shown. For statistical analysis, a two-tailed Student *t-test* was performed. **p<0.05*

Interestingly, in contrast to direct exposure to hypoxia (<0.1% O_2), exposure to media conditioned with hypoxic parental control cells led to an increase in the levels of M1 macrophages.

Overall, these findings show a PHGDH-dependent reduction in the pro-inflammatory macrophage levels in hypoxia but not in normoxia. This confirms our hypothesis of the establishment of an immunosuppressive TME in PHGDH KO cells, potentially due to enhanced HIF-1 signalling.

4.3 Discussion

Our principal aim was to determine whether PHGDH influences cellular radiosensitivity under different extracellular serine levels in normoxia and hypoxia. The only PHGDH-dependent radiosensitisation effect observed was when cells were completely deprived of extracellular serine supply (MEM), and this occurred both in normoxia and hypoxia. Our findings differ from previous reports proposing PHGDH as a potential target for radiosensitisation. In this context, the commonly used PHGDH inhibitor NCT-503 has been reported to influence radiosensitivity in hypoxia (Van de Gucht et al., 2022). However, several important differences distinguish our work. In contrast to the data shown here, pharmacological inhibition (i.e. not genetic loss as studied here) of PHGDH has been shown to increase the radiosensitivity of colorectal cancer cells in hypoxic conditions. It should be noted that the reported experimental conditions include non-physiological levels of extracellular serine (RPMI, 286 µM serine) (Moore et al., 1967). Therefore, it is plausible that off-target effects of the PHGDH inhibitor impacted radiosensitivity. However, NCT-503 has also been reported to have off-target effects by reducing glucose-derived citrate levels in a PHGDH-independent manner (Arlt et al., 2021). Hence, it is unclear what mechanism underpins the observed radiosensitivity. Our approach of CRISPR-Cas9 KO has its own limitations. Permanent loss of PHGDH allows cells to adapt and upregulate compensatory pathways. To address this potential limitation, transient knockdown of PHGDH using siRNA could be implemented. This would minimise long-term adaptive effects linked with the genetic targeting approach.

The only other report of PHGDH-dependent radiosensitisation focused on glioblastoma stem cells (X. Liu et al., 2025). However, there are differences between the cancer stem and differentiated cells, which could explain different stress and radiotherapy responses (Schneider et al., 2016).

PHGDH KO cells also showed signs of a more immunosuppressive TME, including a decrease in the M1 macrophage cluster compared to parental control cells. Interestingly, exposing PBMCs to media conditioned with parental control cells led to an increase in M1 macrophage polarisation. Although unexpected, this may be due to the release of tumour-derived soluble

factors into the media, which can drive M1 activation. Specifically, DAMPs released by necrotic cancer cells under hypoxia can cause a pro-inflammatory bias, contributing to increased M1 polarisation (Nakano et al., 2022).

Taken together with HIF-1 signalling induction in PHGDH KO cells and the signs of more immunosuppressive TME, our results suggest that the inhibition or targeting of PHGDH alone will not result in improving hypoxia-mediated radioresistance in lung cancer. Additionally, these results highlight the importance of considering access to nutrients when evaluating metabolic enzymes as targets combined with radiotherapy. This is consistent with evidence that dietary serine and glycine restriction can improve radiotherapy response in preclinical models (Falcone et al., 2022; Scott et al., 2025). Extracellular serine availability may therefore be an important variable to consider when designing radiosensitisation strategies targeting PHGDH. Moreover, it is also important to be cautious when devising radiosensitisation strategies from experiments conducted under non-physiological conditions.

Chapter 5: Investigating the nuclear function of PHGDH under hypoxia

5.1 Introduction

Previously, we established PHGDH as a hypoxia-inducible enzyme, which may function in both the cytoplasm and nucleus. Specifically, the effects of PHGDH loss, such as improved survival in hypoxia, were observed in the presence of excess serine. This suggests that PHGDH may play an important, non-serine-related role in regulating cell survival.

Several glycolytic enzymes have been shown to translocate to the nucleus, where they influence gene expression through histone modification and interaction with transcription factors involved in cancer cell proliferation (Gizak et al., 2019; J. Shen et al., 2020; W. Yang et al., 2012). PHGDH was recently found to have a non-canonical nuclear function. Upon glucose starvation, PHGDH was shown to translocate into the nucleus, where it inhibits PARP1 activity by acting as an NAD+ sink (C. Ma et al., 2021). Additionally, PHGDH has been described to have the capacity to interact with nucleic acids through its dinucleotide (NAD)-binding domain (C. M. Lee et al., 2024; Unterlass et al., 2017).

R-loops are three-stranded nucleic acid structures that are comprised of a DNA:RNA hybrid and a displaced ssDNA strand (Thomas et al., 1976). Aberrant accumulation of R-loops leads to genomic instability by blocking replication and leading to transcription-replication conflicts (TRCs) (Crossley et al., 2019). Moreover, R-loop levels were shown to be elevated under <0.1% O_2 (Ramachandran et al., 2021). Taken together, these findings led us to hypothesise that hypoxia (<0.1% O_2) may act as a stress analogous to glucose starvation, promoting the translocation of PHGDH to the nucleus. Once nuclear, PHGDH may associate with R-loop structures and contribute to the cellular response to hypoxia-induced genomic stress.

Specific aims:

- Identify evidence to support the hypothesis that PHGDH could be an R-loop binding protein
- Investigate PHGDH as an R-loop binding protein in hypoxia
- Determine the level of similarity between the normoxic and hypoxic R-loop interactome

5.2 Results

5.2.1 PHGDH potentially interacts with R-loops

Given its nuclear accumulation under hypoxic conditions (see Chapter 3) and the reported capacity to interact with nucleic acids via its NAD-binding domain, we hypothesised that PHGDH may have a role beyond the SSP (C. M. Lee et al., 2024; Unterlass et al., 2017). Supportively, PHGDH has recently been identified as an RNA-binding protein, with a dedicated binding domain distinct from its metabolic function (Cheng et al., 2025; T. S. Ma et al., 2023). Given that R-loops are known to accumulate under hypoxic conditions (<0.1% O_2), we examined published R-loop interactomes for the inclusion of PHGDH. Four available interactomes were used (Cristini et al., 2018; I. X. Wang et al., 2018; T. Wu et al., 2021; Yan et al., 2022). These studies isolated R-loops by using co-immunoprecipitation (co-IP) of DNA:RNA hybrids with the S9.6 antibody (Cristini et al., 2018; T. Wu et al., 2021), biotinylated hybrids (I. X. Wang et al., 2018), or proximity labelling (Yan et al., 2022), followed by identification of interacting proteins using liquid chromatography-mass spectrometry (LC-MS). Different cell lines were used across these studies (**Figure 5.1A**). When the interactomes were overlapped, PHGDH was identified in 3 out of 4 datasets, detected across three independent enrichment methods strongly supporting the hypothesis that PHGDH is a potential R-loop interacting protein (**Figure 5.1B**).

A

Interactome	Cell Line	Method	PHGDH
Cristini	HeLa	S9.6 co-IP	Yes
Wang	B-cells	Biotinylated hybrids	Yes
Wu	ESC	S9.6 co-IP	No
Yan	HEK293	Proximity labelling	Yes

B

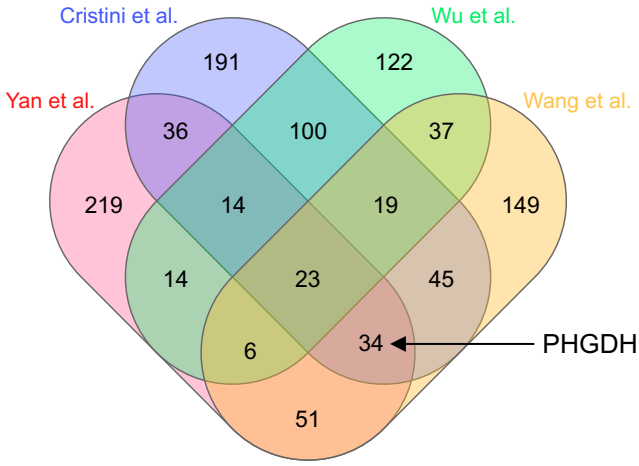

Figure 5.1 PHGDH was identified in three out of four published R-loop interactomes. A. Characteristics of the available interactomes, including the cell lines, method of R-loop pulldown and the presence of PHGDH. ESC - embryonic stem cells. **B.** Venn diagram representing the R-loop interactomes available in the literature (Cristini et al., 2018; I. X. Wang et al., 2018; T. Wu et al., 2021; Yan et al., 2022). Numbers represent the number of proteins common or unique to respective interactomes. The arrow represents the interactomes where PHGDH is found. The diagram was generated using the multiple list comparator on Molbiotools online software.

5.2.2 Optimisation of R-loop co-IP protocol with S9.6 antibody

Although PHGDH emerged as a potential R-loop-associated protein due to its presence in the majority of published R-loop interactomes, experimental validation was required. Notably, these interactomes were generated under normoxic conditions, highlighting the need to define the R-loop interactome under hypoxia. To characterise both normoxic and hypoxic R-loop interactomes, we used the S9.6 co-IP method established by Cristini et al., in FLO-1 oesophageal adenocarcinoma cells (Cristini et al., 2018) (**Figure 5.2**).

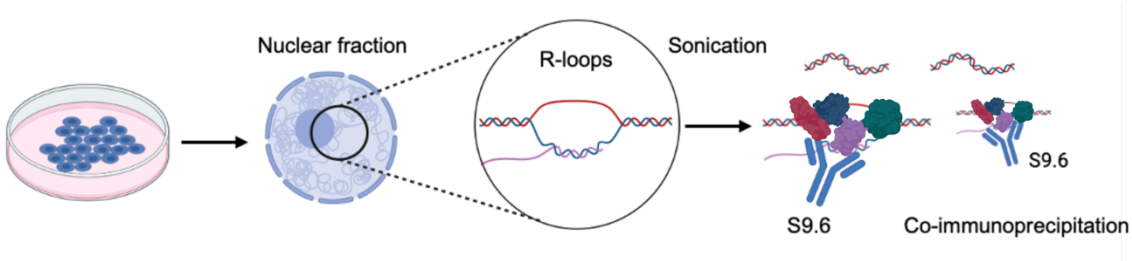

Figure 5.2 Schematic representation of S9.6 co-IP experimental workflow. For detailed experimental procedure, see Chapter 2.16: R-loop co-immunoprecipitation with S9.6 antibody.

FLO-1 was selected as it is a well-established oesophageal adenocarcinoma cell line. CIN is particularly prevalent in this cancer type, with 97% of cases belonging to the CIN subtype, representing one of the highest levels reported across all cancer types (Beernaert et al., 2026; Cancer Genome Atlas Research Network et al., 2017). This is notably higher than that observed in lung adenocarcinoma (40-60%) (Choi et al., 2009; Soca-Chafre et al., 2019). Critically, unresolved R-loops can impede replication fork progression, promoting DNA damage and structural chromosome aberrations, thereby potentially contributing to CIN (Crossley et al., 2019; Gan et al., 2011; Helmrich et al., 2011). Cells with dysregulated R-loop homeostasis, therefore, exhibit elevated genomic instability, highlighting high-CIN cancer contexts as particularly relevant systems for studying R-loop biology. Subsequently, FLO-1 was selected as a compelling model in which to study the functional role of R-loop-associated proteins.

The principal step optimised in this protocol was the nucleic acid sonication. This step was critical, as efficient pulldown of R-loop-binding proteins requires nucleic acids to be sheared

to 500-700 bp to preserve the integrity of the interactome (**Figure 5.3A**). Once an appropriate sonication time (4 min) was selected, the protocol was validated by performing co-IP westerns and blotting for known R-loop-interacting proteins. DHX9 and PARP1 were chosen due to their established role as R-loop binding proteins (P. Chakraborty et al., 2018; Laspata et al., 2023). These proteins were successfully detected in the S9.6 pull-down but not in the IgG isotype or no-antibody control conditions (**Figure 5.3B**). Additionally, nuclear proteins such as Lamin B1 and NPC, which do not have any known R-loop-interacting function, were not present in the S9.6 pulldown samples.

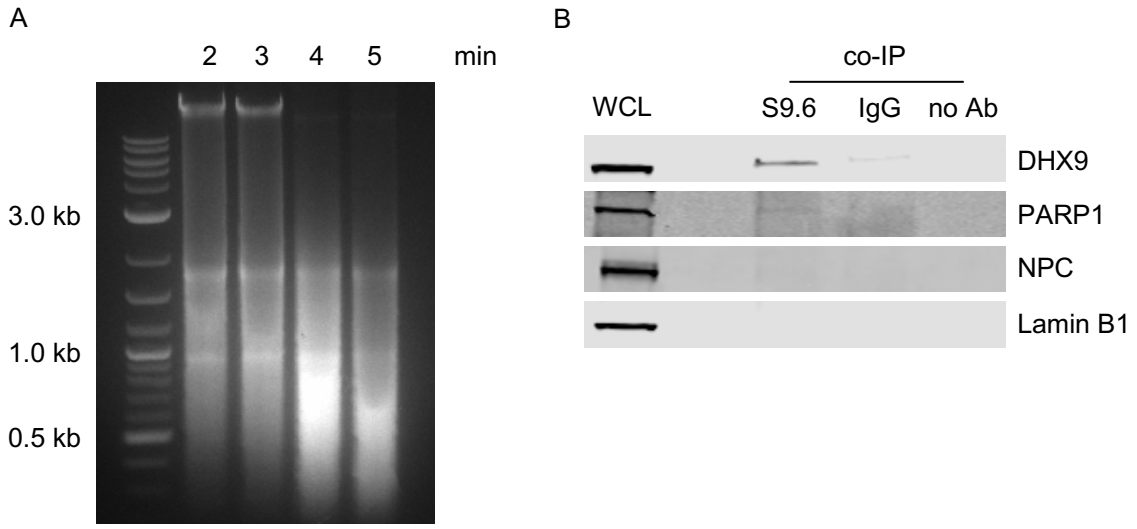

Figure 5.3 Optimisation of S9.6/R-loop co-IP method. A. Nuclear extracts from FLO-1 cells were sonicated for the times highlighted, followed by DNA gel electrophoresis. A DNA ladder was used to estimate fragment size. **B.** S9.6, IgG isotype control and no antibody co-IP samples were used for western blotting. DHX9 and PARP1 were used as positive controls for R-loop co-IP. NPC and Lamin B1 were used as negative controls for the pulldown. A whole cell lysate (WCL) control was included.

Despite the successful optimisation of the S9.6 co-IP western blot protocol, certain limitations also became apparent. When probing for control proteins such as DHX9 (positive control) or Lamin B1 (negative control), several non-specific bands were detected. These bands were present both on the S9.6 IP lanes as well as in no antibody controls (**Figure 5.4**). The most prominent bands were around 50 kDa. We suspected that these bands may be caused by the denatured heavy chains of the S9.6 IgG antibody (IgG HC). This hypothesis seemed plausible due to the appearance of additional bands around the 25 kDa mark, which corresponds to the molecular weight of the IgG light chain (IgG LC). Consistent with these observations, IgG LC

bands were absent in the no-antibody control lanes. However, the ~50 kDa bands were also present in the no antibody conditions. A potential source for these could be the protein A coating (pA) of the Dynabeads that were used for the IP, which have a molecular weight of around 45 kDa. The presence of these contaminants in the eluate and their molecular weight is a serious limitation for detecting PHGDH due to the similarity of their sizes (PHGDH molecular weight: 57 kDa).

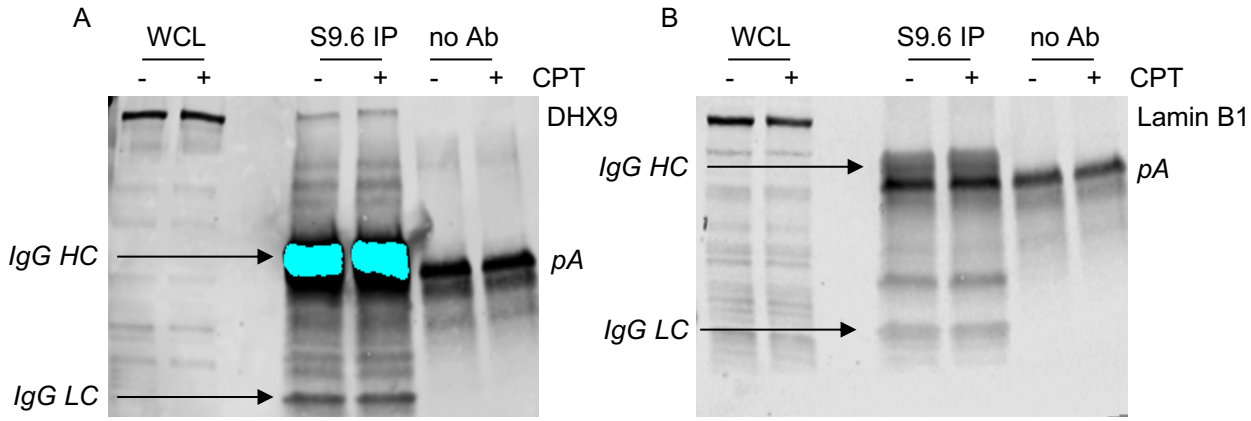

Figure 5.4 S9.6 heavy and light chains detected in S9.6 co-IP western blots. FLO-1 cells untreated (-) and treated (+) with camptothecin (CPT; 10 μM, 1 h) in normoxia were used for DNA:RNA pull-down using 5 μg of S9.6 antibody. 50 μg whole cell lysate (WCL) was used as a reference control. DHX9 and Lamin B1 were used as positive and negative controls for the S9.6 IP, respectively. No antibody controls were used as non-specific binding controls. IgG light chain (IgG LC) and IgG heavy chain (IgG HC) bands are highlighted.

Camptothecin (CPT), which increases R-loop levels by inhibiting DNA topoisomerase 1, was used to check whether the intensity or the number of bands changed with changing levels of R-loops (T. S. Ma et al., 2023). However, no apparent differences in band intensities were detected, confirming the potentially technical nature of the bands.

Furthermore, we confirmed the cause of these bands by using variable amounts of S9.6 antibody. As expected, when increasing the amount of S9.6 antibody from 3 to 10 μg, both IgG HC and LC band intensities increased accordingly (**Figure 5.5A**). DHX9 band intensity also appeared to increase, confirming the successful pulldown. To overcome this technical limitation, dimethyl pimelimidate (DMP)-based chemical crosslinking of the S9.6 antibody to protein A Dynabeads was used before the incubation with the co-IP samples. The goal of this experiment was to covalently attach the S9.6 antibody and protein A to the beads to reduce the contamination of the eluate. As a result, protein A and IgG LC levels were reduced in the crosslinked samples (**Figure 5.5B**). However, even in crosslinked samples, the IgG HC band was not fully eliminated, and the ~50 kDa band persisted after crosslinking. This residual signal remained a technical limitation, preventing us from determining conclusively whether PHGDH is present at R-loops using S9.6 co-IP.

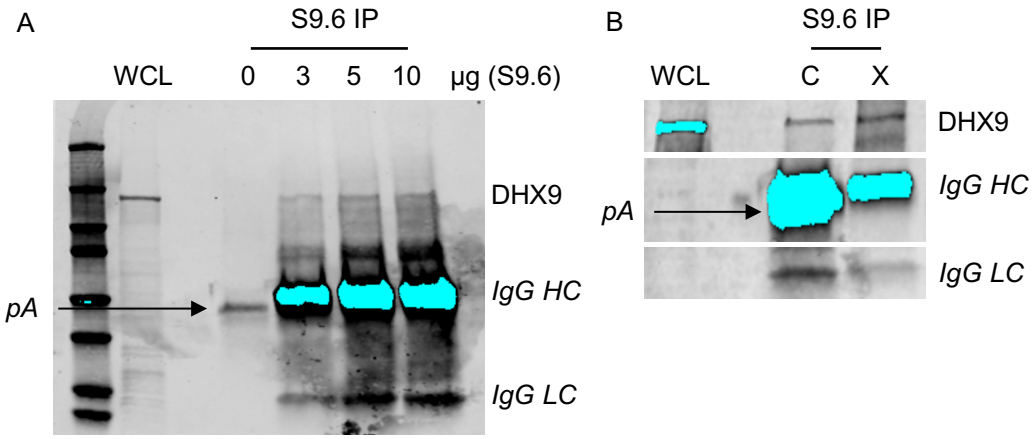

Figure 5.5 S9.6 heavy and light chains detected. A. S9.6 co-IP was performed using the S9.6 antibody with indicated amounts. No antibody control (0 μg) was used as a non-specific binding control. **B**. S9.6 co-IP was performed using Dynabeads with conjugated (C) or chemically crosslinked (X) S9.6 antibody. 50 μg whole cell lysate (WCL) was used as a reference control. DHX9 was used as a positive control for the S9.6 IP. IgG light chain (IgG LC) and IgG heavy chain (IgG HC) bands are highlighted.

5.2.3 LC-MS analysis revealed no detectable level of PHGDH enrichment in FLO-1 cells

Western blot analysis of S9.6 co-IP did not detect PHGDH due to interference from antibody-derived bands. As a result, immunoblotting was not a compatible method to assess PHGDH association with R-loops. To address this limitation, LC-MS was chosen as the analysis method following the S9.6 co-IP, to characterise the R-loop interactome both in normoxia and hypoxia (<0.1% O_2). An RNase H1 control was included in the experimental workflow as a negative control. RNase H1 resolves R-loops by selectively degrading the RNA strand in DNA:RNA hybrids (Nowotny et al., 2007). Samples with overexpressed RNase H1, designated for LC-MS analysis, were first checked for successful transfection using microscopy and western blotting (**Figure 5.6A**).

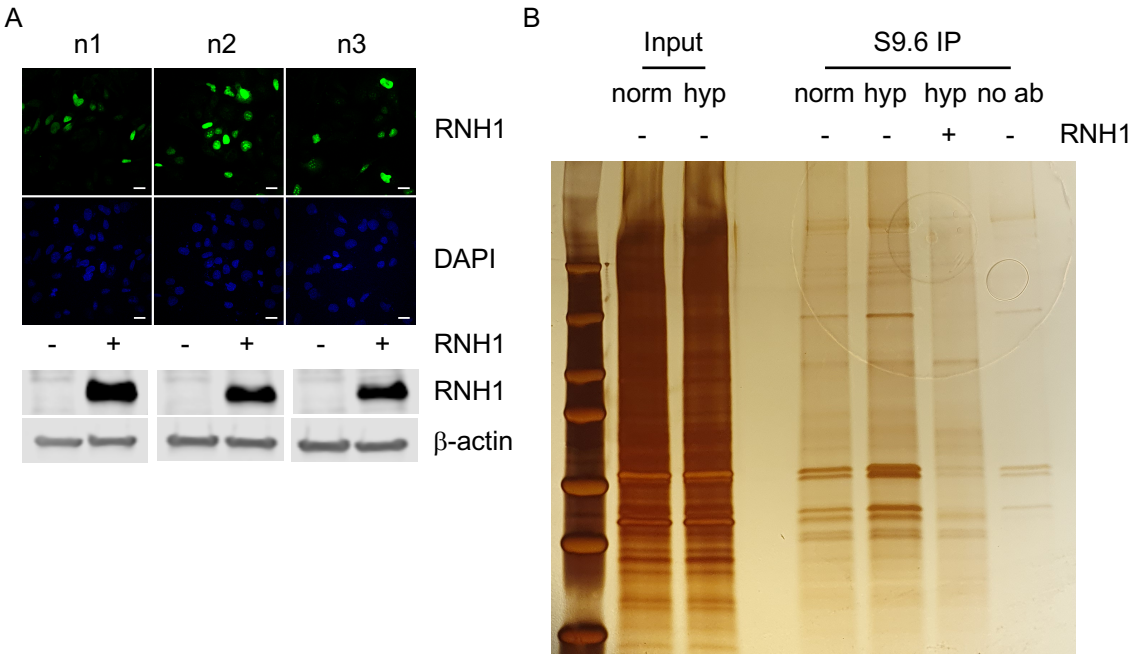

Figure 5.6 Validation of S9.6 co-IP samples for LC-MS analysis. A. Representative immunofluorescence images of FLO-1 cells transfected with GFP-tagged RNase H1 (RNH1) expression construct (+) or mock control (-) across three independent experiments (n1–n3). RNH1 is shown in green, and nuclei are counterstained with DAPI (blue). Scale bars represent 20 µm. Western blot analysis of RNH1 expression in corresponding samples confirms increased RNH1 levels upon transfection (+) compared to control (-). β-actin was used as a loading control. **B.** Representative silver-stained 4-20% polyacrylamide gel showing input lysates and S9.6 immunoprecipitated (IP) samples under normoxic (norm) and hypoxic (hyp; <0.1% O_2) conditions. Where indicated, RNase H1 (RNH1) transfected samples were added (+) before immunoprecipitation. A no antibody (no ab) control was included to assess non-specific binding.

Silver staining was performed for preliminary assessment of the R-loop interactome, both in normoxia and hypoxia (<0.1% O_2). As expected, the treatment with RNase H1 appeared to reduce the number of proteins pulled down with S9.6 (**Figure 5.6B**). The no-antibody control confirmed the absence of non-specific interacting partners. Overall protein signal intensity was increased in hypoxic samples relative to normoxia, consistent with our prediction based on a well-characterised increase in R-loop abundance at <0.1% O_2 (T. S. Ma et al., 2023).

Following the optimisation and validation of immunoprecipitated samples, LC-MS analysis was performed. Normalised protein intensity values were used for principal component analysis (PCA) to assess differences between experimental conditions (**Figure 5.7**).

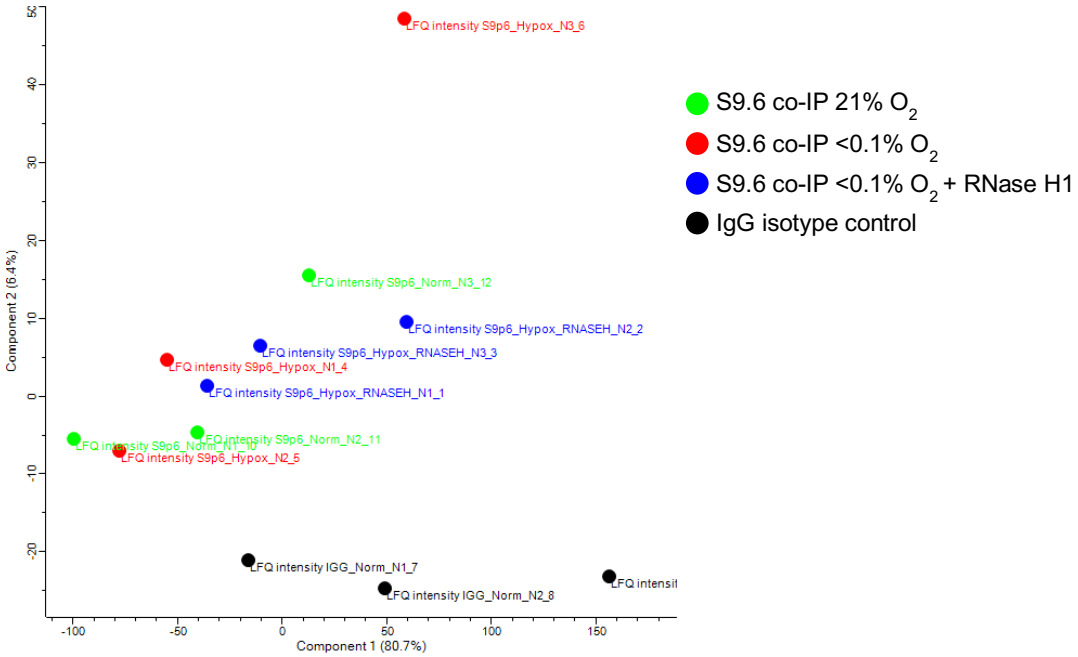

Figure 5.7 PCA of LC-MS results. Principal component analysis (PCA) of log2-transformed LFQ intensity values derived from S9.6 immunoprecipitated samples under normoxic (green), hypoxic (red) and RNase H1-treated hypoxic (blue) samples. The IgG control group is shown in black.

IgG control samples segregated distinctly along the principal component 1 (PC1) from S9.6 immunoprecipitated ones, confirming successful enrichment of R-loop-associated proteins. Normoxic and hypoxic S9.6 co-IP samples clustered together on the PCA plot, indicating potential similarities in these interactomes. The RNase H1-treated control also clustered with the normoxic and hypoxic samples, which was unexpected. This may reflect insufficient

RNase H1 expression to fully resolve R-loops, likely due to suboptimal transfection efficiency. As a result, differences at the global proteome level were not detected under these conditions. Notably, other studies that conducted LC-MS analysis of R-loop interactomes did not include RNase H1 controls.

To assess our S9.6 interactome, we compared it with previously published R-loop interactomes. The top 400 enriched proteins, ranked based on average label-free quantification (LFQ), were selected from the list of proteins pulled down with the S9.6 antibody. These proteins were then compared to the list of significantly enriched proteins from other available R-loop interactomes. Encouragingly, our S9.6 interactome shared more than half of the proteins with R-loop interactomes generated using the same S9.6 co-IP method. Specifically, 59% with Cristini et al and 54% with Wu et al (**Figure 5.8A, C**).

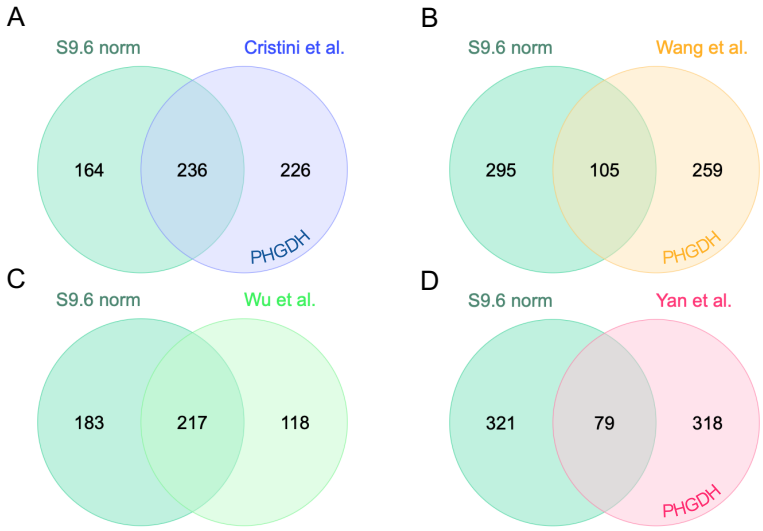

Figure 5.8 Overlapping S9.6 co-IP interactome with available R-loop interactomes. A-D. The list of top 400 proteins following S9.6 co-IP LC-MS analysis (normoxic) was overlapped with 4 available R-loop interactomes: Cristini et al. (**A**), Wang et al. (**B**), Wu et al. (**C**) and Yan et al. (**D**). Numbers represent the number of proteins common or unique to respective interactomes. The diagram was generated using the multiple list comparator on Molbiotools online software.

Interactomes acquired using different methods had a relatively lower number of proteins common with our dataset: 26% with Wang et al and 20% with Yan et al. (**Figure 5.8B, D**). Together, these results confirmed the validity of our interactome as well as highlighted method- and cell line-specific differences. R-loop binding proteins that were unique to various

interactomes can also be due to the differences in the cell lines used. Importantly, PHGDH was not identified in our S9.6 co-IP-based interactome.

To identify the proteins that interact with R-loops independent of the enrichment method or the cell line, all 5 interactomes were overlapped. As a result, 23 proteins were identified (**Figure 5.9**).

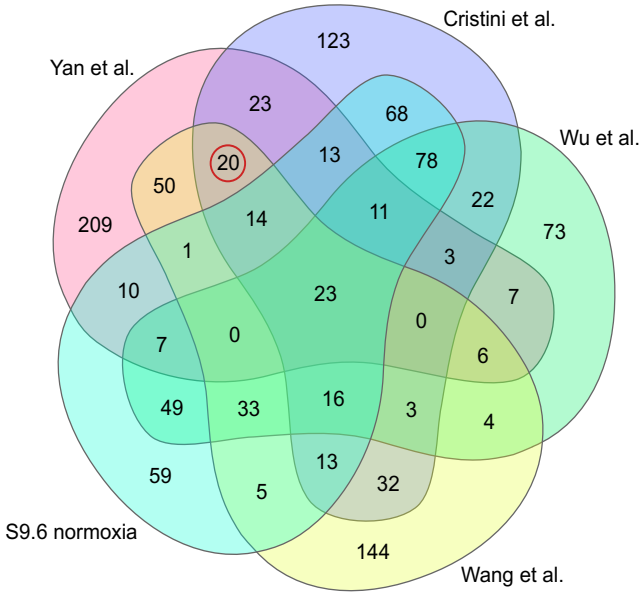

Figure 5.9 Overlap of proteins identified across all 5 interactomes. Venn diagram representing 4 published R-loop interactomes and S9.6 co-IP, LC-MS results in normoxia. The red circle highlights the intersecting interactomes containing PHGDH. Numbers represent the number of proteins common or unique to respective interactomes. The diagram was generated using the multiple list comparator on Molbiotools online software.

Among the 23 shared proteins, 9 (39.1%) have been experimentally validated to interact with R-loops (**Table 5.1**). Another 12 proteins (56.5%) were characterised as RNA-binding proteins. Only HSP90AB1 was not confirmed to interact with either R-loops or RNA; however, it has often been identified in other RNA-interactomes (Castello et al., 2012). Gene ontology analysis of the 23 shared proteins revealed significant enrichment for molecular functions related to RNA binding, RNA helicase activity, and ATP-dependent RNA processing, all of which are central to R-loop biology (**Table 5.2**). This enrichment further validates the biological relevance and specificity of our S9.6 co-IP and LC-MS approach. Specifically, more than 95% of proteins shared in all 5 interactomes have been shown to interact with either R-loops or RNA.

Table 5.1: List of targets identified in all R-loop interactomes. Proteins experimentally validated to interact with R-loops are highlighted in bold.

Identifier	Full Name	Validated R-loop or RNA interaction
CDC5L	Cell Division Cycle 5-Like Protein	RNA (Ajuh et al., 2001)
DDX17	DEAD-Box Helicase 17	**R-loop** (Boleslavska et al., 2022)
DDX18	DEAD-Box Helicase 18	**R-loop** (Lin et al., 2022)
DDX3X	DEAD-Box Helicase 3, X-Linked	**R-loop** (Xiong et al., 2024)
DDX5	DEAD-Box Helicase 5	**R-loop** (Z. Yu et al., 2020)
DHX15	DEAH-Box Helicase 15	**R-loop** (Ummethum et al., 2025)
DHX9	DEAH-Box Helicase 9	**R-loop** (Cristini et al., 2018)
HNRNPM	Heterogeneous Nuclear Ribonucleoprotein M	RNA (R. Zheng et al., 2024)
HSP90AB1	Heat Shock Protein 90 Alpha Family Class B Member 1	No validated interaction
ILF3	Interleukin Enhancer Binding Factor 3	**R-loop** (C. Wang et al., 2024)
MATR3	Matrin 3	**R-loop** (Islam et al., 2024)
MYBBP1A	MYB Binding Protein 1A	RNA (Hochstatter et al., 2012)
NAT10	N-Acetyltransferase 10	**R-loop** (K. Su et al., 2024)
NCL	Nucleolin	RNA (Fremerey et al., 2016)
NOP58	NOP58 Ribonucleoprotein	RNA (Lafontaine & Tollervey, 1999)
NPM1	Nucleophosmin 1	RNA (Y. Yu et al., 2025)
PABPC1	Poly(A) Binding Protein Cytoplasmic 1	RNA (Peng et al., 2017)
PDCD11	Programmed Cell Death 11	RNA (L. Ding et al., 2023)
PRPF8	Pre-mRNA Processing Factor 8	RNA (X. Li et al., 2013)
PTBP1	Polypyrimidine Tract Binding Protein 1	RNA (Ji et al., 2025)
TBL3	Transducin Beta-Like 3	RNA (Bao et al., 2024)
UTP14A	UTP14 Small Subunit Processome Component A	RNA (Hu et al., 2011)
WDR3	WD Repeat Domain 3	RNA (McMahon et al., 2010)

Table 5.2: Gene ontology analysis of proteins common in all interactomes.

GO molecular function	Reference list	Target number	Fold enrichment	FDR
RNA binding (GO:0003723)	1692	22	12.16	6.08E-21
Nucleic acid binding (GO:0003676)	4006	22	5.14	5.65E-13
RNA helicase activity (GO:0003724)	73	6	76.89	1.97E-07
ATP-dependent activity, acting on RNA (GO:0008186)	77	6	72.89	2.05E-07
mRNA binding (GO:0003729)	375	8	19.96	2.96E-06
Helicase activity (GO:0004386)	148	6	37.92	7.24E-06
Conformation isomerase activity (GO:0120545)	159	6	35.3	9.54E-06
Single-stranded RNA binding (GO:0003727)	85	5	55.03	1.70E-05
ATP hydrolysis activity (GO:0016887)	397	7	16.49	7.13E-05
Catalytic activity, acting on RNA (GO:0140098)	427	7	15.34	1.05E-04

We also looked into the differences between the normoxic and hypoxic interactome to examine whether oxygen level influences the R-loop interactome. PHGDH was also not found in the hypoxic R-loop interactome. After overlapping the top 400 hits showed around 88% of the interactors were shared across normoxia and hypoxia (Figure 5.10). However, 47 proteins were present only in the hypoxia interactome.

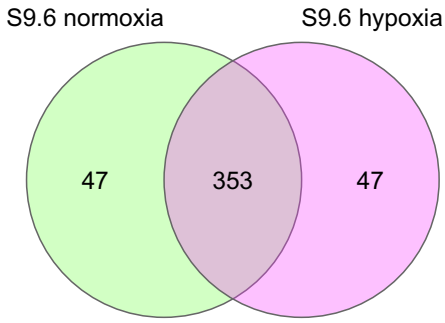

Figure 5.10 Overlap between normoxic and hypoxic R-loop interactomes. Venn diagram showing the overlap of proteins identified in S9.6 immunoprecipitates under normoxic and hypoxic (<0.1% O_2) conditions (top 400 proteins ranked by average LFQ intensity). A total of 353 proteins were shared between both conditions, while 47 proteins were uniquely detected in either normoxia or hypoxia.

Pathway enrichment analysis of these 47 proteins was then conducted. However, no enrichment in pathways directly associated with RNA or R-loop biology was observed (**Figure 5.11**). Following a literature search, only 3 of the 47 (6.4%) proteins have previously been linked to R-loops: PCBP1, LARP7 and IGF2BP3 (Devanathan et al., 2025; Karam et al., 2024; Ying et al., 2024).

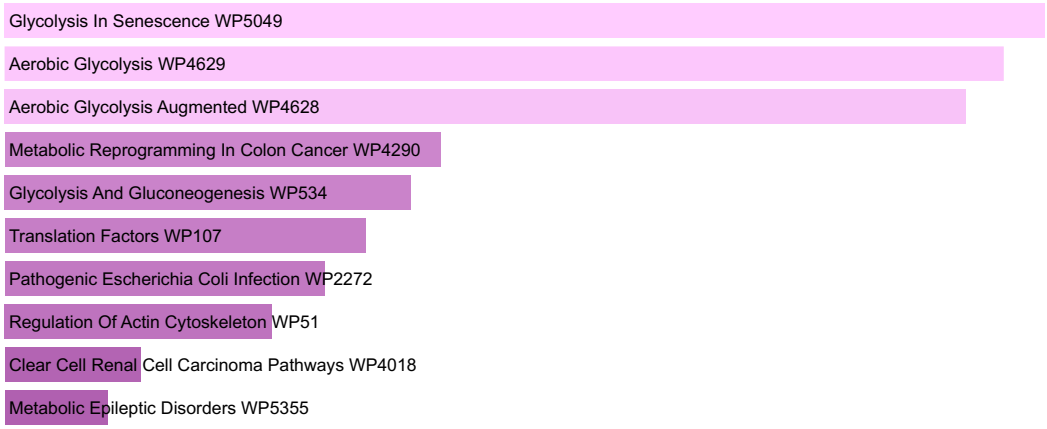

Figure 5.11 Pathway enrichment analysis of hypoxia-specific R-loop interactome. 47 proteins exclusively found in the hypoxic S9.6 co-IP interactome were checked for pathway enrichment in the WikiPathways (Human, 2024) database using the Enrichr online software.

The pathways identified from enrichment analysis of the 47 hypoxia-specific proteins are largely associated with abundant metabolic proteins. These are frequently observed as potential “contaminants” in affinity purification experiments (Mellacheruvu et al., 2013). To validate which of these can potentially be genuine R-loop-associated proteins, additional analysis is necessary.

5.2.4 Further investigation of the hypoxic interactome

In light of the enrichment patterns observed earlier, we re-analysed the complete proteomic dataset again using a more rigorous statistical approach that incorporated the RNase H1 control. Given RNase H1 samples clustered with other experimental conditions (**Figure 5.7**), it is important to note that PCA reflects global proteome variance, which can hide biologically meaningful differences at the individual protein level. Accordingly, evaluating RNase H1 effects on a protein-to-protein basis may provide clearer discrimination of genuine R-loop interactors. Therefore, a stringent FDR-based ANOVA filtering was performed, which did not identify broadly significant differences. Next, a p-value-based filtering approach was applied by post-hoc FDR correction, identifying approximately 50 proteins exhibiting differential trends. Hierarchical clustering of these proteins revealed distinct enrichment patterns (**Figure 5.12A**). This analysis revealed a cluster of proteins that are enriched in S9.6 hypoxic samples, absent in normoxia, and diminished in RNase H1-overexpressed samples (cluster highlighted in blue). These 18 proteins represent the hypoxia-specific interactome that is specifically bound to the DNA:RNA hybrids. Other clusters have also been identified that were susceptible to RNase H1 function. Specifically, 9 proteins were preferentially enriched under normoxic conditions alone (purple cluster), while 15 proteins were detected under both normoxic and hypoxic conditions (orange cluster). The hypoxia-specific, R-loop binding cluster was next overlapped with the published R-loop interactomes. All 18 genes had overlaps with at least one of the available enrichment datasets (**Figure 5.12B**). These findings together suggest that the hypoxic interactome does not differ from the one characterised under normoxic conditions.

A

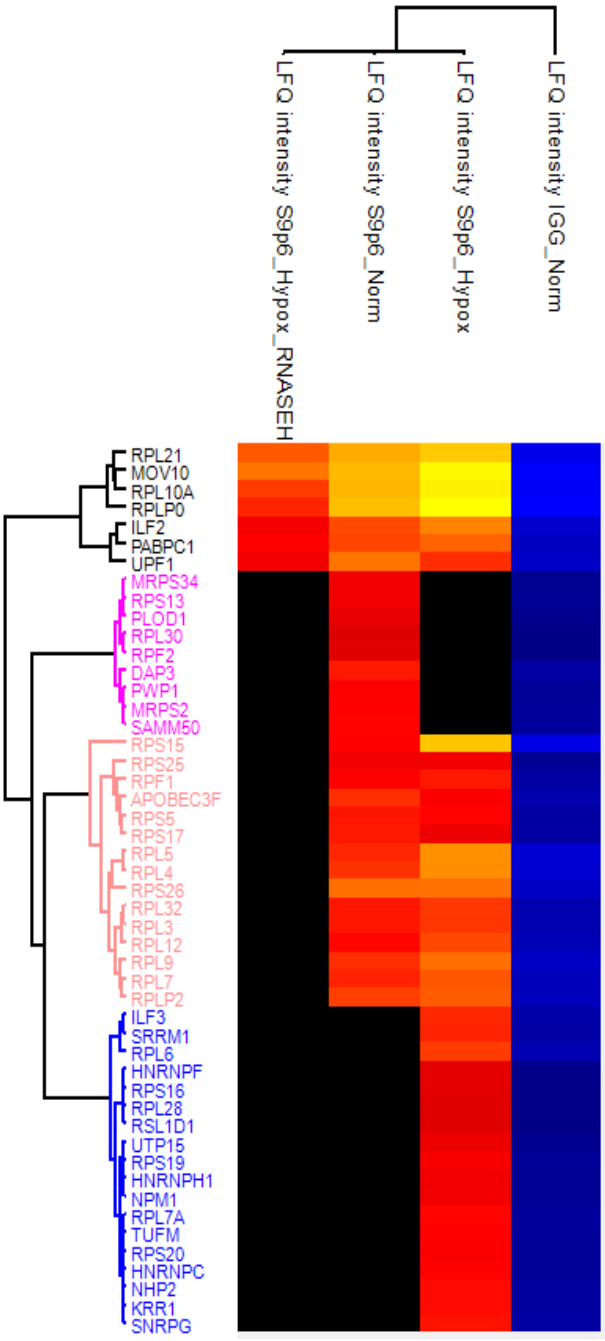

B

Gene name	Cristini *et al.*	Wang *et al.*	Wu *et al.*	Yan *et al.*
ILF3	+	+	+	+
SRRM1	+			
RPL6			+	
HNRNPF	+		+	
RPS16			+	
RPL28			+	
RSL1D1	+		+	
UTP15	+		+	
RPS19		+	+	
HNRNPH1	+	+		+
NPM1	+	+	+	+
RPL7A		+	+	
TUFM	+		+	+
RPS20			+	
HNRNPC	+		+	
NHP2	+		+	
KRR1	+			
SNRPG	+			

Figure 5.12 Hierarchical clustering of differentially enriched proteins in S9.6 pulldown samples. **A.** Heatmap showing relative LFQ intensity values of selected proteins identified in S9.6 pulldowns under normoxic, hypoxic (<0.1% O_2), and hypoxic with RNase H1 conditions, as well as IgG isotype control. Values are log2-transformed and scaled across samples (red = higher relative abundance; blue = lower). **B**. 18 hypoxia-specific R-loop interacting proteins overlapped with 4 published interactomes.

5.3 Discussion

R-loops accumulate under severe hypoxia (<0.1% O_2), driven by replication stress (Ramachandran et al., 2021). We aimed to determine whether the R-loop interactome also changes in hypoxia. Moreover, we also investigated whether PHGDH interacted with R-loops.

Bioinformatic analysis of available LC-MS-based R-loop interactomes showed that three out of four datasets contain PHGDH as a potential interacting protein. While PHGDH was reported in published R-loop interactomes, these datasets were acquired exclusively in normoxia, using different cell line models. To experimentally validate this, S9.6 co-IP was selected as the method of choice. Despite optimising and validating the protocol with known R-loop binding proteins such as DHX9 and PARP1, we could not detect PHGDH in the pulldown samples, due to antibody cross-reactivity between the S9.6 IgG heavy chain and PHGDH on western blots. It is worth noting that this reflects a technical constraint rather than confirmed absence of interaction. A targeted co-IP using light chain-specific secondary antibodies would be required to definitively address this question (Crossley et al., 2020; L. Zhang et al., 2013).

Our LC-MS analysis did not identify PHGDH in either the normoxic or hypoxic interactomes, despite its presence in 3 out of 4 available datasets. PHGDH is detected in approximately 60% of nuclear fraction-based affinity purification-MS datasets in the CRAPome database. This indicates a high background co-purification rate independent of functional association (Mellacheruvu et al., 2013). Hence, the nuclear role of PHGDH under hypoxia is likely not linked with direct regulation of R-loops. It is potentially exerting its established function as an NAD^+ sink, suppressing PARP1 activity, or continued serine synthesis within the nuclear compartment (C. Ma et al., 2021).

Further analysis confirmed overlap between our interactome and other available datasets, validating the reliability of our findings. Proteins shared among all five interactomes were experimentally confirmed to have an association with either R-loops (39.1%) or RNA (56.5%). The main finding of this chapter was the lack of identified differences in the R-loop interactomes in normoxia and hypoxia. Despite the known elevation of R-loops under <0.1%

O_2, the proteins associating with these structures seem largely unchanged. The 47 proteins found exclusively in the hypoxic interactome were not enriched for R-loop or RNA-binding functions, with only 3 previously linked to R-loop biology. These are unlikely to represent a specific hypoxic R-loop response. Instead, the existing normoxic interactors may be present at higher levels under hypoxia, without altering their composition. This is illustrated by the 18 proteins identified as hypoxia-enriched in our interactome, which, despite being present in published normoxic datasets, showed higher levels under hypoxic conditions.

Taken together, we did not find any evidence of hypoxia acting as a factor reshaping the R-loop interactome. Rather than mounting a distinct adaptive response, in hypoxia, cells appear to engage their existing interactome under conditions of increased R-loop burden. Whether parts of this machinery become rate-limiting under hypoxic stress and can be targeted therapeutically remains to be investigated.

Chapter 6: Final discussion

6.1 Discussion

Hypoxia is a prevalent characteristic of the TME and is associated with poor patient prognosis and resistance to radiotherapy, chemotherapy, and immunotherapy (Bigos et al., 2024; G. Chen et al., 2022; Ciepła & Smolarczyk, 2024; Hammond et al., 2014; Jing et al., 2019). Despite decades of efforts to exploit tumour hypoxia therapeutically, including the development of HAPs and hypoxic radiosensitisers, these approaches have failed to demonstrate meaningful clinical benefit. This leaves the selective targeting of hypoxic tumour regions an unresolved and pressing challenge.

Under hypoxic conditions (<0.1% O_2), cancer cells were shown to induce different stress responses, such as UPR and DDR. The activation of these pathways enables cells to adapt to the hostile TME, sustain proliferation, and evade death. However, these are not the only established mechanisms that are used by cancer cells to adapt to hypoxia. Metabolic reprogramming also represents a key adaptive response to hypoxia, whereby cancer cells shift from oxidative phosphorylation to glycolysis to maintain energy production (Warburg, 1925, 1956). This shift is primarily orchestrated by HIF-1, which transcriptionally upregulates key glycolytic enzymes and glucose transporters while suppressing mitochondrial oxidative metabolism.

De novo SSP is a vital pathway in cancer cells, supporting anabolic needs and maintaining redox balance under metabolic stress. PHGDH, the rate-limiting enzyme of the SSP, has recently attracted therapeutic interest in cancer, with its overexpression across various tumour types associated with increased proliferation, metastasis, and therapy resistance (C. M. Lee et al., 2024; McNamee et al., 2021). Although PHGDH has been studied in various cellular stress contexts, including serine deprivation, oxidative stress, and glutamine restriction, its role as a therapeutic target within the hypoxic TME remains largely unexplored. Our study aimed to fill this gap by examining the regulation of PHGDH under hypoxia and its potential as a target to enhance responses to radiotherapy.

We showed PHGDH was transcriptionally induced in <0.1% O_2 conditions. Both HIF1 and ATF4 transcription factors were found to be responsible for PHGDH induction at this level of hypoxia. Although seemingly redundant, such dual expression control is not uncommon, especially among genes relevant for survival under stress conditions. VEGF, REDD1 and BNIP3 are among the genes induced and regulated by both HIF-1 and ATF4 (Forsythe et al., 1996; K. Guo et al., 2001; J. Li et al., 2022; Oskolkova et al., 2008; D. Xu et al., 2020; Z. Zhang et al., 2024). Dual regulation of PHGDH may arise from the severe metabolic pressure imposed by radiobiological hypoxia, necessitating stronger induction at <0.1% O_2.

Despite being regulated by HIF-1, PHGDH was found to be induced at <0.1% O_2, but not 2%. The reason behind this unusual induction pattern was not fully resolved in this study. In addition to PHDs, FIH hydroxylates the CATD of HIF-1α, blocking p300/CBP recruitment and attenuating transcriptional output at milder hypoxia levels (Lando et al., 2002; Mahon et al., 2001). Because FIH has a lower oxygen Km than the PHDs, it remains active at 2% O_2 even when PHD-mediated HIF-1α degradation is partially suppressed, effectively limiting the transcriptional activity of HIF-1α. Full FIH inhibition at <0.1% O_2 may therefore be required for PHGDH induction. Whether PHGDH induction is suppressed by selective FIH reactivation or rescued in FIH-deficient cells at 2% O_2 would directly test this hypothesis.

Moreover, the observed discordance between PHGDH protein and mRNA induction kinetics, with protein accumulation preceding mRNA upregulation, suggests that post-translational stabilisation of PHGDH may contribute independently of transcription at <0.1% O_2. For instance, ubiquitination by various E3 ligases is among the PTMs that regulate the stability and half-life of PHGDH (C. Wang et al., 2020). The contributions of transcriptional vs post-translational mechanisms to PHGDH accumulation at <0.1% O_2 were not thoroughly investigated in this study. Chase assays with cycloheximide combined with proteasome inhibition under different levels of hypoxia would be needed to differentiate these effects. Cycloheximide treatment would enable us to determine whether PHGDH protein accumulation at <0.1% O_2 arises from increased stability or translation. The combined use of proteasome inhibitors would reveal whether the observed stabilisation is ubiquitin-proteasome dependent.

Together, these approaches would establish whether increased PHGDH levels in hypoxia arise from reduced proteasomal degradation and enhanced stability or from HIF-1/ATF4-mediated transcriptional induction. A potential mechanism that can be investigated involves p38 MAPK. Hypoxia and elevated ROS levels were shown to induce p38 signalling (Huelsemann et al., 2015; Sanchez et al., 2012; L. Xu et al., 2004). Simultaneously, under glucose starvation, PHGDH is directly phosphorylated by p38, which leads to its nuclear translocation (C. Ma et al., 2021). Given the increase in nuclear PHGDH under <0.1% O_2 conditions, a similar post-translational modification could occur in hypoxia. Importantly, p38 signalling has also been implicated to have a role in protein stability. p38 directly phosphorylates Snail, blocking the phosphorylation event required to prime Snail for ubiquitin-mediated degradation, thereby enhancing its stability (Ryu et al., 2019). If p38 was demonstrated to phosphorylate PHGDH under hypoxia, this could mask the residues required for subsequent ubiquitin-mediated degradation. This would reduce proteasomal turnover and account for early protein accumulation before transcriptional induction of PHGDH.

Loss of PHGDH was shown to result in elevated intra- and extracellular lactate levels andcells with PHGDH KO demonstrated quicker induction of HIF-1α. Together, these results indicate a potential link between PHGDH-dependent metabolic rewiring and HIF-1 activity. Specifically, loss of PHGDH redirects glucose-derived carbon moieties away from the SSP and towards glycolysis. This shift subsequently leads to elevated lactate production. Two possible pathways potentially explain the increased HIF-1 signalling in PHGDH KO cells. First, an increase in lactate levels can directly enhance HIF-1α stability. A recent study demonstrated that lactylation of HIF-1α at the Lys-12 residue promotes protein stability by impeding its recognition by PHD2 (C. Li et al., 2025). Secondly, increased lactate can increase HIF-1α stability indirectly. Elevated lactate can affect HIF-1α stability via conversion to pyruvate by LDH, enabling competition with αKG at PHD2 and inhibition of its activity. This, in its turn, would lead to reduced HIF-1α stability (Lu et al., 2002, 2005). Lactate has also been suggested to directly hinder αKG interaction with PHDs, implying a direct, pyruvate-independent effect on HIF stability (De Saedeleer et al., 2012). Competition with αKG by other non-glycolytic

metabolites has also been reported, highlighting the importance of this step in HIF induction during metabolic adaptation to hypoxia. The accumulation of fumarate and succinate, in FH- and SDH-deficient tumours, respectively, was shown to result in increased stabilisation of HIF-1α. These two metabolites, again, displace αKG, the lack of which leads to PHD inhibition and increased HIF-1α accumulation (Isaacs et al., 2005; Selak et al., 2005). PHGDH depletion in hypoxic tumours leads to improved cell adaptation, indicating a limitation for targeting PHGDH. Earlier, we demonstrated that PHGDH KO cells exhibited elevated lactate levels under hypoxia, consistent with redirected glycolytic flux following SSP abrogation. The subsequent HIF-1α amplification was also confirmed by increased upregulation of canonical transcriptional targets such as CAIX, GLUT1, LDHA, and VEGF in PHGDH KO cells, under hypoxia. This adaptation may confer a net survival advantage that counteracts any radiosensitisation achieved through SSP abrogation.

Due to the complexity of the signalling and regulation landscape, both upstream and downstream of HIF-1α, inhibiting single targets such as PHGDH may risk engagement of compensatory pathways. This principle has been illustrated by PKM2, a glycolytic enzyme whose ROS-induced inhibition paradoxically enhances the survival of lung cancer cells by diverting glucose into the PPP. This metabolic rewiring led to sustained NADPH production and GSH-mediated antioxidant defence (Anastasiou et al., 2011). Lung cancer cells expressing an oxidation-resistant PKM2 mutant showed significantly impaired proliferation and reduced tumour growth, an effect especially pronounced in hypoxia (1% O_2) with physiological glucose concentrations. Inhibition of a single metabolic node, therefore, activated a compensatory programme that enhanced rather than impaired cell survival under hypoxia, directly analogous to the HIF-1α-amplifying response observed following PHGDH abrogation. These observations imply that effective metabolic radiosensitisation requires combinatorial strategies disrupting the adaptive network at multiple points simultaneously. For PHGDH specifically, co-inhibiting SSP flux alongside HIF-1α with inhibitors such as PX-478 may induce radiosensitisation as well as prevent cancer cell adaptation to hypoxia (Welsh et al., 2004). Combined inhibition of PHGDH and HIF-1α would require rigorous evaluation under

physiological nutrient conditions, given our observations regarding the serine concentration-dependent radiosensitisation.

A key finding was that loss of PHGDH sensitised cells to radiation only under complete serine deprivation. No radiosensitisation occurred at physiological serine levels (HPLM: ~150 μM). Contrary to our findings, a study reported that inhibiting PHGDH with NCT-503 increased radiosensitivity in hypoxic colorectal cancer cells (Van de Gucht et al., 2022). This was observed in cells cultured in RPMI 1640, which contains 286 μM serine, roughly twice the physiological level (Moore et al., 1967; Wishart et al., 2012). The supraphysiological serine levels in RPMI can act as an external source of the amino acid. Moreover, NCT-503 has been shown to redirect glucose-derived carbon units in a PHGDH-independent manner, with off-target effects on the TCA cycle (Arlt et al., 2021). The rerouting of glucose-derived carbons towards oxidative metabolism due to NCT-503 treatment could result in the accumulation of ROS and impact radiosensitivity independently of blocking the SSP.

SHMT2, the enzyme converting serine to glycine, was also suggested to affect radiosensitivity through reductions in GSH and increased ROS (Sánchez-Castillo et al., 2024). This study also used complete RPMI 1640 media rich in serine, which makes the role of serine in radiosensitisation difficult to interpret. Sertraline is an approved SSRI, and its activity against SHMT2 is an off-target effect identified via drug repurposing rather than structure-based design (Geeraerts et al., 2021). Importantly, SSRIs like sertraline have been shown to disrupt mitochondrial membrane potential and decrease oxygen consumption at supraphysiological doses, independently of serotonergic pathways (Li et al., 2012). Similar mitochondrial effects, such as Complex I inhibition by metformin, have been linked to radiosensitisation, suggesting an alternative mechanism unrelated to serine-glycine synthesis (Koritzinsky, 2015). Consequently, the anti-cancer effects of sertraline may stem from mitochondrial disruption, serotonin receptor modulation, or other pleiotropic actions, rather than specific SHMT2 inhibition. Therefore, under these supraphysiological serine conditions, the mechanistic basis of radiosensitisation remains unclear, considering the off-target activities of both NCT-503 and sertraline. Moreover, as shown in Chapter 4, physiological serine levels can support GSH

biosynthesis, indicating that SSP disruption alone is unlikely to induce radiosensitisation in a clinical setting.

Extracellular serine availability is a critical factor that needs to be considered when investigating the effects of SSP abrogation. Standard culture media contain substantially higher serine concentrations than those observed in the circulation of cancer patients, with important implications for interpreting effects on radiosensitivity. It is also important to recognise that plasma metabolite concentrations do not always reflect the levels accessible to tumour cells, especially within poorly vascularised, hypoxic regions where nutrient availability can be markedly reduced. The quantification of metabolites in the TME of murine cancers demonstrated that various amino acids are present at concentrations significantly below matched plasma levels. Specifically, serine levels in tumour interstitial fluid dropped to an average of around 45-50 μM (Sullivan et al., 2019). Dietary restriction of serine, which has been shown to improve radiation response, was found to reduce the plasma serine levels from around 150 μM to 65 μM (Maddocks et al., 2017). Taken together, these observations suggest that serine availability in hypoxic lung tumours is likely reduced relative to physiological plasma levels. The sole use of HPLM and serine-deprived MEM limited our ability to investigate the potential effect of intermediate, sub-physiological serine concentrations on radiosensitivity. An immediate follow-up experiment would aim to determine the threshold extracellular serine concentration at which the radiosensitisation observed in MEM is lost in PHGDH KO cells under normoxia and hypoxia. If the critical serine concentration, especially under hypoxia, is comparable to that of the tumour interstitial fluid, then targeting PHGDH may have clinical relevance even without any dietary restrictions. If the threshold falls below tumour interstitial serine concentrations, dietary restriction of serine may be required in combination with PHGDH targeting to achieve radiosensitisation in a clinical setting. This is especially important, as dietary restriction of serine and glycine has already been shown to result in a better radiation response in mice (Falcone et al., 2022). Additionally, measuring GSH at each titration point would provide mechanistic validation, as GSH depletion precisely paralleled radiosensitisation across MEM and HPLM conditions.

The present study focused primarily on the A549 cell line as its main model, with H460 used in selected experiments. PHGDH has been implicated as a therapeutic target across multiple tumour types, including GBM and HNSCC (Locasale et al., 2011a; Possemato et al., 2011). Whether the hypoxia-dependent induction of PHGDH, the HIF-1α-amplifying response in PHGDH KO cells, and the serine concentration-dependent radiosensitisation are conserved across cell types remains untested. In the context of lung cancer, a broader cell line panel encompassing different histological subtypes and PHGDH expression levels would be necessary for assessing the ability to generalise these findings. Specifically, expression levels of extracellular serine transporters, such as ASC1/2, can be used as a criteria for cell line panel selection. This will indicate the cell line dependence on imported serine and its effect on radiosensitisation under serine-deprived conditions.

All experimental work was conducted in 2D cell culture, which does not fully recapitulate the oxygen gradients, nutrient diffusion limitations, or cell-to-cell interactions characteristic of tumours *in vivo*. To ameliorate this issue, 3D spheroid models that generate endogenous hypoxic cores and more faithfully model the TME metabolic heterogeneity can be used. The radiosensitisation findings should be interpreted with this caveat, as the relationship between extracellular serine concentration and SSP-dependent antioxidant defence may be substantially different in spatially complex tumour models. In addition to this, *in vivo* experiments can be designed to validate the key findings of Chapters 3 or 4. Data from xenograft models can help us understand how loss of PHGDH affects cell growth, metastasis formation, changes in radiosensitivity, as well as differences in HIF-signalling response *in vivo*. Importantly, PHGDH loss was modelled exclusively using CRISPR-Cas9 KO, representing chronic and irreversible gene abrogation. This differs from the acute, dose-dependent inhibition achievable with siRNA knockdown or small-molecule inhibitors such as NCT-503, BI-4924 and others. Even though the use of KO cells for extensive time periods was limited, the chronic absence of PHGDH may enable compensatory adaptations. These include upregulation of serine import via SLC1A5 or alternative 1C sources that would not develop under acute pharmacological inhibition. Whether the increased HIF-1 signalling and serine-

dependent radiosensitisation observed in PHGDH KO cells are recapitulated with acute inhibition remains unknown and requires further investigation. The use of small molecular inhibitors or siRNA knockdown will help to answer these questions.

The macrophage polarisation experiment used conditioned media from PHGDH KO and parental control cells, representing an indirect assessment of effects on macrophage phenotype. Conditioned media from PHGDH KO cells under hypoxia (<0.1% O_2) significantly reduced the fraction of M1 macrophages compared to parental control. This indicates a potential immunosuppressive effect exerted by PHGDH KO cells in the TME. However, the use of conditioned media does not account for direct tumour-immune cell contact, paracrine signalling operating at the cell surface, or the contributions of other immune populations present in the TME. Whether PHGDH loss affects $CD8^+$ T cell, NK, or other immune cell function and their immunosuppressive polarisation remains unknown. Given that serine supports effector T cell expansion, the immune effects of SSP inhibition in the hypoxic TME require further investigation using co-culture systems and syngeneic *in vivo* models (E. H. Ma et al., 2017).

Metabolomic profiling identified a reduction in purine nucleotides and an elevation in pyrimidine intermediates in PHGDH KO cells under normoxia. These changes were not investigated at <0.1% O_2. The SSP provides 1C units required for *de novo* purine biosynthesis via the folate cycle, and nucleotide imbalances can drive replication fork stalling and R-loop accumulation. This would link the metabolic findings to the genomic stress and test whether SSP loss under hypoxia affects nucleotide depletion and R-loop formation. As a first step towards uncovering this link, PHGDH Con and KO cells can be used to measure R-loop levels in hypoxia (<0.1% O_2). Additionally, manipulating extracellular serine levels would test whether cells preferentially rely on endogenous or exogenous serine to support 1C metabolism and nucleotide biosynthesis.

The R-loop co-IP strategy implemented in our study relied on the S9.6 antibody, which has recognised limitations in specificity, including cross-reactivity with dsRNA, particularly in ribosomal regions (Crossley et al., 2019; Hartono et al., 2018). The proximity of the IgG heavy

chain (~50 kDa) and protein A (~45 kDa) immunoprecipitation artefact bands to PHGDH (~57 kDa) further complicated definitive interpretation of co-IP immunoblots despite DMP crosslinking optimisation. Subsequently, a non-antibody-based method of R-loop-binding protein enrichment would circumvent the S9.6 co-IP artefacts imposed by IgG heavy chain and protein A bands. A potential alternative can be the use of electrophoretic mobility shift assays (EMSA), combining purified recombinant PHGDH protein and RNA:DNA hybrids (R-loops). The binding of PHGDH to the R-loop will slow the migration of the complex on a native gel, resulting in a shifted band that indicates direct interaction. The specificity of the interaction can be confirmed using WT RNase H1, which preferentially resolves R-loops by degrading the RNA moieties in RNA:DNA hybrids. This method has been used to demonstrate RPA interaction with R-loops (Mazina et al., 2020). Despite the inability to identify PHGDH in the S9.6 co-IP LC-MS dataset, a more targeted approach, like EMSA, will enable a definitive answer regarding the capacity of PHGDH to interact with R-loops. This is especially important given the ability of PHGDH to interact with RNA directly or through other RNA-interacting proteins. PHGDH has been shown to directly bind and stabilise PRKCD mRNA, and to interact with proteins such as eIF4A1 and eIF4E, which promote mRNA translation (Cheng et al., 2025; X. Ma et al., 2019).

If PHGDH is confirmed to interact with R-loops, its loss may be expected to impact R-loop processing and genome stability. In the absence of R-loop resolving factors, such as SETX and AQR, these structures are actively processed into DSBs by endonucleases XPG and XPF (Sollier et al., 2014). Recent work has shown that the targeting of R-loop stabilising factors and the subsequent aberrant R-loop processing by XPG/XPF endonucleases can result in the generation of cytosolic nucleic acid species (RNA:DNA hybrids). This then leads to the activation of innate immune signalling through the cGAS–STING pathway (Crossley et al., 2023). If interaction with R-loops is confirmed, targeting PHGDH may drive both cytoplasmic immune activation and accumulation of DSBs, which is particularly relevant in immune-evasive and radioresistant hypoxic tumours.

6.2 Concluding remarks

This thesis establishes PHGDH as a hypoxia-regulated metabolic enzyme while challenging its viability as a radiosensitisation target in lung cancer. Although induced under severe hypoxia via HIF-1 and ATF4, its loss is buffered by metabolic and transcriptional adaptations, with radiosensitisation emerging only under complete serine deprivation: a condition that is not typically representative of the TME.

Ultimately, this work underscores the importance of studying cancer metabolism under physiologically relevant conditions. Experimental context strongly influences metabolic dependencies, and future strategies should prioritise context-dependent, combinatorial approaches that reflect the adaptive nature of tumour cells.

Chapter 7: Appendix

Table 7.1: The composition of used culture media. All components, including those added before use, are indicated.

Component	DMEM (μM)	HPLM (μM)	MEM (μM)
Serine	400	150	0
Glycine	400	300	0
Cysteine	201	100	100
Glutamine	4000	550	0
Glutamate	0	80	0
Leucine	800	150	396
Threonine	798	140	400
Valine	800	220	393
Phenylalanine	400	80	194
Glucose	25000	25000	5500
Fructose	0	40	0
Folate	9	2	2
Formate	0	50	0
Uridine	0	3	0
Na-Pyruvate	0	50	0
Succinate	0	20	0
Malate	0	5	0
αKG	0	5	0
GSH	0	25	0
Supplements added to media before use			
Dialysed FBS (A3382001, Gibco)	9.1% (50 ml to 500 ml)	9.1% (50 ml to 500 ml)	9.1% (50 ml to 500 ml)
MEM Vitamins (11120052, Gibco)	0	0	0.91% (5 ml in 550 ml)
Glucose	0	0	Increase to 17000
Glutamine	0	0	2000

7.1 Papers published from this thesis

- **Petrosyan E**, Martin L, Legge I, Walsby-Tickle I, McCullagh J, Olcina M, Hammond E. 2026. PHGDH loss promotes hypoxia tolerance through glycolytic reprogramming and enhanced HIF-1 activity. **Cell Death Discovery [*in press*]**.
- Zhou C, Crusher J T, Friesen K, Twigger S A, **Petrosyan E**, Booker G, Samuel P, Parkes E E, Hammond E M. 2026. HIF-1-regulated TPM3 links hypoxia to motility and invasion beyond the hypoxic fraction in triple-negative breast cancer. **npj Breast Cancer**. https://doi.org/10.1038/s41523-026-00927-y

7.2 Conference presentations

- **Petrosyan E**, Hammond E. The role of PHGDH and *de novo* serine biosynthesis in targeting hypoxic tumours. Oral Presentation. BACR 65th Anniversary Meeting. Edinburgh, UK (2025).

Chapter 8: References

Aaltonen, L. A., Abascal, F., Abeshouse, A., Aburatani, H., Adams, D. J., Agrawal, N., Ahn, K. S., Ahn, S.-M., Aikata, H., Akbani, R., Akdemir, K. C., Al-Ahmadie, H., Al-Sedairy, S. T., Al-Shahrour, F., Alawi, M., Albert, M., Aldape, K., Alexandrov, L. B., Ally, A., … von Mering, C. (2020). Pan-cancer analysis of whole genomes. *Nature*, *578*(7793), 82–93. https://doi.org/10.1038/s41586-020-1969-6

Abou Khouzam, R., Zaarour, R. F., Brodaczewska, K., Azakir, B., Venkatesh, G. H., Thiery, J., Terry, S., & Chouaib, S. (2022). The Effect of Hypoxia and Hypoxia-Associated Pathways in the Regulation of Antitumor Response: Friends or Foes? *Frontiers in Immunology*, *13*. https://doi.org/10.3389/fimmu.2022.828875

Achuthankutty, D., Thakur, R. S., Haahr, P., Hoffmann, S., Drainas, A. P., Bizard, A. H., Weischenfeldt, J., Hickson, I. D., & Mailand, N. (2019). Regulation of ETAA1-mediated ATR activation couples DNA replication fidelity and genome stability. *Journal of Cell Biology*, *218*(12), 3943–3953. https://doi.org/10.1083/jcb.201905064

Aguilera, A., & García-Muse, T. (2012). R Loops: From Transcription Byproducts to Threats to Genome Stability. *Molecular Cell*, *46*(2), 115–124. https://doi.org/10.1016/j.molcel.2012.04.009

Airley, R. E., Loncaster, J., Raleigh, J. A., Harris, A. L., Davidson, S. E., Hunter, R. D., West, C. M. L., & Stratford, I. J. (2003). GLUT-1 and CAIX as intrinsic markers of hypoxia in carcinoma of the cervix: Relationship to pimonidazole binding. *International Journal of Cancer*, *104*(1), 85–91. https://doi.org/10.1002/ijc.10904

Ajuh, P., Sleeman, J., Chusainow, J., & Lamond, A. I. (2001). A Direct Interaction between the Carboxyl-terminal Region of CDC5L and the WD40 Domain of PLRG1 Is Essential for Pre-mRNA Splicing. *Journal of Biological Chemistry*, *276*(45), 42370–42381. https://doi.org/10.1074/jbc.M105453200

Amelio, I., Cutruzzolá, F., Antonov, A., Agostini, M., & Melino, G. (2014). Serine and glycine metabolism in cancer. *Trends in Biochemical Sciences*, *39*(4), 191–198. https://doi.org/10.1016/j.tibs.2014.02.004

Anastasiou, D., Poulogiannis, G., Asara, J. M., Boxer, M. B., Jiang, J., Shen, M., Bellinger, G., Sasaki, A. T., Locasale, J. W., Auld, D. S., Thomas, C. J., Vander Heiden, M. G., & Cantley, L. C. (2011). Inhibition of pyruvate kinase M2 by reactive oxygen species contributes to cellular antioxidant responses. *Science (New York, N.Y.)*, *334*(6060), 1278–1283. https://doi.org/10.1126/science.1211485

Anderson, N. M., & Simon, M. C. (2020). The tumor microenvironment. *Current Biology*, *30*(16), R921–R925. https://doi.org/10.1016/j.cub.2020.06.081

Appling, D. R. (1991). Compartmentation of folate-mediated one-carbon metabolism in eukaryotes. *The FASEB Journal*, *5*(12), 2645–2651. https://doi.org/10.1096/fasebj.5.12.1916088

Arany, Z., Huang, L. E., Eckner, R., Bhattacharya, S., Jiang, C., Goldberg, M. A., Bunn, H. F., & Livingston, D. M. (1996). An essential role for p300/CBP in the cellular response to hypoxia. *Proceedings of the National Academy of Sciences*, *93*(23), 12969–12973. https://doi.org/10.1073/pnas.93.23.12969

Arlt, B., Mastrobuoni, G., Wuenschel, J., Astrahantseff, K., Eggert, A., Kempa, S., & Deubzer, H. E. (2021). Inhibiting PHGDH with NCT-503 reroutes glucose-derived carbons into the TCA cycle, independently of its on-target effect. *Journal of Enzyme Inhibition and Medicinal Chemistry*, *36*(1), 1282–1289. https://doi.org/10.1080/14756366.2021.1935917

Arriza, J. L., Kavanaugh, M. P., Fairman, W. A., Wu, Y. N., Murdoch, G. H., North, R. A., & Amara, S. G. (1993). Cloning and expression of a human neutral amino acid transporter with structural similarity to the glutamate transporter gene family. *The Journal of Biological Chemistry*, *268*(21), 15329–15332.

Bader, S. B., Ma, T. S., Simpson, C. J., Liang, J., Maezono, S. E. B., Olcina, M. M., Buffa, F. M., & Hammond, E. M. (2021). Replication catastrophe induced by cyclic hypoxia leads to increased APOBEC3B activity. *Nucleic Acids Research*, *49*(13), 7492–7506. https://doi.org/10.1093/nar/gkab551

Bae, T., Hallis, S. P., & Kwak, M.-K. (2024). Hypoxia, oxidative stress, and the interplay of HIFs and NRF2 signaling in cancer. *Experimental & Molecular Medicine*, *56*(3), 501–514. https://doi.org/10.1038/s12276-024-01180-8

Baluk, P., Hashizume, H., & McDonald, D. M. (2005). Cellular abnormalities of blood vessels as targets in cancer. *Current Opinion in Genetics & Development*, *15*(1), 102–111. https://doi.org/10.1016/j.gde.2004.12.005

Bao, J., Su, B., Chen, Z., Sun, Z., Peng, J., & Zhao, S. (2024). A UTP3-dependent nucleolar translocation pathway facilitates pre-rRNA 5'ETS processing. *Nucleic Acids Research*, *52*(16), 9671–9694. https://doi.org/10.1093/nar/gkae631

Barlowe, C. K., & Appling, D. R. (1988). In vitro evidence for the involvement of mitochondrial folate metabolism in the supply of cytoplasmic one-carbon units. *BioFactors (Oxford, England)*, *1*(2), 171–176.

Beernaert, B., Jady-Clark, R. L., Shah, P., Ramon-Gil, E., Lawson, N. M., Brodtman, Z. D., Tagore, S., Stihler, F., Carter, A. S., Clarke, S., Liu, T., Zhu, W. M., Martin, J. E., Erdal, E., Easton, A., Campo, L., Browne, M., Ash, S., Raja, R. Q., … Parkes, E. E. (2026). Chromosomal instability shapes the tumor microenvironment of esophageal adenocarcinoma via a cGAS–chemokine–myeloid axis. *Science Advances*, *12*(11). https://doi.org/10.1126/sciadv.aeb1611

Behrooz, A., & Ismail-Beigi, F. (1997). Dual Control of glut1 Glucose Transporter Gene Expression by Hypoxia and by Inhibition of Oxidative Phosphorylation. *Journal of Biological Chemistry*, *272*(9), 5555–5562. https://doi.org/10.1074/jbc.272.9.5555

Bell, E. L., Klimova, T. A., Eisenbart, J., Schumacker, P. T., & Chandel, N. S. (2007). Mitochondrial Reactive Oxygen Species Trigger Hypoxia-Inducible Factor-Dependent Extension of the Replicative Life Span during Hypoxia. *Molecular and Cellular Biology*, *27*(16), 5737–5745. https://doi.org/10.1128/MCB.02265-06

Bellot, G., Garcia-Medina, R., Gounon, P., Chiche, J., Roux, D., Pouysségur, J., & Mazure, N. M. (2009). Hypoxia-Induced Autophagy Is Mediated through Hypoxia-Inducible Factor Induction of BNIP3 and BNIP3L via Their BH3 Domains. *Molecular and Cellular Biology*, *29*(10), 2570–2581. https://doi.org/10.1128/MCB.00166-09

Bencokova, Z., Kaufmann, M. R., Pires, I. M., Lecane, P. S., Giaccia, A. J., & Hammond, E. M. (2009). ATM Activation and Signaling under Hypoxic Conditions. *Molecular and Cellular Biology*, *29*(2), 526–537. https://doi.org/10.1128/MCB.01301-08

Bensaad, K., Favaro, E., Lewis, C. A., Peck, B., Lord, S., Collins, J. M., Pinnick, K. E., Wigfield, S., Buffa, F. M., Li, J.-L., Zhang, Q., Wakelam, M. J. O., Karpe, F., Schulze, A., & Harris, A. L. (2014). Fatty Acid Uptake and Lipid Storage Induced by HIF-1α Contribute to Cell Growth and Survival after Hypoxia-Reoxygenation. *Cell Reports*, *9*(1), 349–365. https://doi.org/10.1016/j.celrep.2014.08.056

Bensaad, K., Tsuruta, A., Selak, M. A., Vidal, M. N. C., Nakano, K., Bartrons, R., Gottlieb, E., & Vousden, K. H. (2006). TIGAR, a p53-Inducible Regulator of Glycolysis and Apoptosis. *Cell*, *126*(1), 107–120. https://doi.org/10.1016/j.cell.2006.05.036

Bersuker, K., Hendricks, J. M., Li, Z., Magtanong, L., Ford, B., Tang, P. H., Roberts, M. A., Tong, B., Maimone, T. J., Zoncu, R., Bassik, M. C., Nomura, D. K., Dixon, S. J., & Olzmann, J. A. (2019). The CoQ oxidoreductase FSP1 acts parallel to GPX4 to inhibit ferroptosis. *Nature*, *575*(7784), 688–692. https://doi.org/10.1038/s41586-019-1705-2

Bigos, K. JA., Quiles, C. G., Lunj, S., Smith, D. J., Krause, M., Troost, E. GC., West, C. M., Hoskin, P., & Choudhury, A. (2024). Tumour response to hypoxia: understanding the hypoxic tumour microenvironment to improve treatment outcome in solid tumours. *Frontiers in Oncology*, *14*. https://doi.org/10.3389/fonc.2024.1331355

Blancher, C., Moore, J. W., Talks, K. L., Houlbrook, S., & Harris, A. L. (2015). Relationship of Hypoxia-inducible Factor (HIF)-1 α α and HIF-2 α α Expression to Vascular Endothelial Growth Factor Induction and Hypoxia Survival in Human Breast Cancer Cell Lines. *Cancer Research*, *60*(24).

Boleslavska, B., Oravetzova, A., Shukla, K., Nascakova, Z., Ibini, O. N., Hasanova, Z., Andrs, M., Kanagaraj, R., Dobrovolna, J., & Janscak, P. (2022). DDX17 helicase promotes resolution of R-loop-mediated transcription–replication conflicts in human cells. *Nucleic Acids Research*, *50*(21), 12274–12290. https://doi.org/10.1093/nar/gkac1116

Bray, F., Laversanne, M., Sung, H., Ferlay, J., Siegel, R. L., Soerjomataram, I., & Jemal, A. (2024). Global cancer statistics 2022: GLOBOCAN estimates of incidence and mortality worldwide for 36 cancers in 185 countries. *CA: A Cancer Journal for Clinicians*, *74*(3), 229–263. https://doi.org/10.3322/caac.21834

Brizel, D. M., Scully, S. P., Harrelson, J. M., Layfield, L. J., Bean, J. M., Prosnitz, L. R., & Dewhirst, M. W. (1996). Tumor oxygenation predicts for the likelihood of distant metastases in human soft tissue sarcoma. *Cancer Research*, *56*(5), 941–943.

Bröer, S. (2022). Amino acid transporters as modulators of glucose homeostasis. *Trends in Endocrinology & Metabolism*, *33*(2), 120–135. https://doi.org/10.1016/j.tem.2021.11.004

Brunelle, J. K., Bell, E. L., Quesada, N. M., Vercauteren, K., Tiranti, V., Zeviani, M., Scarpulla, R. C., & Chandel, N. S. (2005). Oxygen sensing requires mitochondrial ROS but not oxidative phosphorylation. *Cell Metabolism*, *1*(6), 409–414. https://doi.org/10.1016/j.cmet.2005.05.002

Buffa, F. M., Harris, A. L., West, C. M., & Miller, C. J. (2010). Large meta-analysis of multiple cancers reveals a common, compact and highly prognostic hypoxia metagene. *British Journal of Cancer*, *102*(2), 428–435. https://doi.org/10.1038/sj.bjc.6605450

Cai, Z., Li, W., Hager, S., Wilson, J. L., Afjehi-Sadat, L., Heiss, E. H., Weichhart, T., Heffeter, P., & Weckwerth, W. (2024). Targeting PHGDH reverses the immunosuppressive phenotype of tumor-associated macrophages through α-ketoglutarate and mTORC1 signaling. *Cellular & Molecular Immunology*, *21*(5), 448–465. https://doi.org/10.1038/s41423-024-01134-0

Calon, A., Espinet, E., Palomo-Ponce, S., Tauriello, D. V. F., Iglesias, M., Céspedes, M. V., Sevillano, M., Nadal, C., Jung, P., Zhang, X. H.-F., Byrom, D., Riera, A., Rossell, D., Mangues, R., Massagué, J., Sancho, E., & Batlle, E. (2012). Dependency of Colorectal Cancer on a TGF-β-Driven Program in Stromal Cells for Metastasis Initiation. *Cancer Cell*, *22*(5), 571–584. https://doi.org/10.1016/j.ccr.2012.08.013

Cancer Genome Atlas Research Network, Analysis Working Group: Asan University, BC Cancer Agency, Brigham and Women's Hospital, Broad Institute, Brown University, Case Western Reserve University, Dana-Farber Cancer Institute, Duke University, Greater Poland Cancer Centre, Harvard

Medical School, Institute for Systems Biology, KU Leuven, Mayo Clinic, Memorial Sloan Kettering Cancer Center, National Cancer Institute, Nationwide Children's Hospital, Stanford University, University of Alabama, … Project Team: National Institutes of Health. (2017). Integrated genomic characterization of oesophageal carcinoma. *Nature*, *541*(7636), 169–175. https://doi.org/10.1038/nature20805

Cao, X.-Y., Li, X., Wang, F., Duan, Y., Wu, X., Lin, G.-Q., Geng, M., Huang, M., Tian, P., Tang, S., & Gao, D. (2024). Identification of benzo[b]thiophene-1,1-dioxide derivatives as novel PHGDH covalent inhibitors. *Bioorganic Chemistry*, *146*, 107330. https://doi.org/10.1016/j.bioorg.2024.107330

Cárdenas-Navia, L. I., Mace, D., Richardson, R. A., Wilson, D. F., Shan, S., & Dewhirst, M. W. (2008). The Pervasive Presence of Fluctuating Oxygenation in Tumors. *Cancer Research*, *68*(14), 5812–5819. https://doi.org/10.1158/0008-5472.CAN-07-6387

Carreau, A., Hafny-Rahbi, B. El, Matejuk, A., Grillon, C., & Kieda, C. (2011). Why is the partial oxygen pressure of human tissues a crucial parameter? Small molecules and hypoxia. *Journal of Cellular and Molecular Medicine*, *15*(6), 1239–1253. https://doi.org/10.1111/j.1582-4934.2011.01258.x

Castello, A., Fischer, B., Eichelbaum, K., Horos, R., Beckmann, B. M., Strein, C., Davey, N. E., Humphreys, D. T., Preiss, T., Steinmetz, L. M., Krijgsveld, J., & Hentze, M. W. (2012). Insights into RNA Biology from an Atlas of Mammalian mRNA-Binding Proteins. *Cell*, *149*(6), 1393–1406. https://doi.org/10.1016/j.cell.2012.04.031

Cerami, E., Gao, J., Dogrusoz, U., Gross, B. E., Sumer, S. O., Aksoy, B. A., Jacobsen, A., Byrne, C. J., Heuer, M. L., Larsson, E., Antipin, Y., Reva, B., Goldberg, A. P., Sander, C., & Schultz, N. (2012). The cBio Cancer Genomics Portal: An Open Platform for Exploring Multidimensional Cancer Genomics Data. *Cancer Discovery*, *2*(5), 401–404. https://doi.org/10.1158/2159-8290.CD-12-0095

Chakraborty, A. A., Laukka, T., Myllykoski, M., Ringel, A. E., Booker, M. A., Tolstorukov, M. Y., Meng, Y. J., Meier, S. R., Jennings, R. B., Creech, A. L., Herbert, Z. T., McBrayer, S. K., Olenchock, B. A., Jaffe, J. D., Haigis, M. C., Beroukhim, R., Signoretti, S., Koivunen, P., & Kaelin, W. G. (2019). Histone demethylase KDM6A directly senses oxygen to control chromatin and cell fate. *Science*, *363*(6432), 1217–1222. https://doi.org/10.1126/science.aaw1026

Chakraborty, P., Huang, J. T. J., & Hiom, K. (2018). DHX9 helicase promotes R-loop formation in cells with impaired RNA splicing. *Nature Communications*, *9*(1), 4346. https://doi.org/10.1038/s41467-018-06677-1

Chan, F.-F., Kwan, K. K.-L., Seoung, D.-H., Chin, D. W.-C., Ng, I. O.-L., Wong, C. C.-L., & Wong, C.-M. (2024). N6-Methyladenosine modification activates the serine synthesis pathway to mediate therapeutic resistance in liver cancer. *Molecular Therapy*, *32*(12), 4435–4447. https://doi.org/10.1016/j.ymthe.2024.10.025

Chandel, N. S., McClintock, D. S., Feliciano, C. E., Wood, T. M., Melendez, J. A., Rodriguez, A. M., & Schumacker, P. T. (2000). Reactive Oxygen Species Generated at Mitochondrial Complex III Stabilize Hypoxia-inducible Factor-1α during Hypoxia. *Journal of Biological Chemistry*, *275*(33), 25130–25138. https://doi.org/10.1074/jbc.M001914200

Chaneton, B., Hillmann, P., Zheng, L., Martin, A. C. L., Maddocks, O. D. K., Chokkathukalam, A., Coyle, J. E., Jankevics, A., Holding, F. P., Vousden, K. H., Frezza, C., O'Reilly, M., & Gottlieb, E. (2012). Serine is a natural ligand and allosteric activator of pyruvate kinase M2. *Nature*, *491*(7424), 458–462. https://doi.org/10.1038/nature11540

Chaplin, D. J., Olive, P. L., & Durand, R. E. (1987). Intermittent blood flow in a murine tumor: radiobiological effects. *Cancer Research*, *47*(2), 597–601.

Chen, C., Zhu, T., Liu, X., Zhu, D., Zhang, Y., Wu, S., Han, C., Zhang, H., Luo, J., & Kong, L. (2022). Identification of a novel PHGDH covalent inhibitor by chemical proteomics and phenotypic profiling. *Acta Pharmaceutica Sinica B*, *12*(1), 246–261. https://doi.org/10.1016/j.apsb.2021.06.008

Chen, G., Wu, K., Li, H., Xia, D., & He, T. (2022). Role of hypoxia in the tumor microenvironment and targeted therapy. *Frontiers in Oncology*, *12*. https://doi.org/10.3389/fonc.2022.961637

Chen, Z., Han, F., Du, Y., Shi, H., & Zhou, W. (2023). Hypoxic microenvironment in cancer: molecular mechanisms and therapeutic interventions. *Signal Transduction and Targeted Therapy*, *8*(1), 70. https://doi.org/10.1038/s41392-023-01332-8

Cheng, B., Peng, P., Chen, S., Liu, R., Li, X., Wang, K., Ma, J., Wang, K., Tang, N., & Huang, A. (2025). Phosphoglycerate dehydrogenase stabilizes protein kinase C delta type mRNA to promote hepatocellular carcinoma progression. *Signal Transduction and Targeted Therapy*, *10*(1), 236. https://doi.org/10.1038/s41392-025-02304-w

Chi, J.-T., Wang, Z., Nuyten, D. S. A., Rodriguez, E. H., Schaner, M. E., Salim, A., Wang, Y., Kristensen, G. B., Helland, Å., Børresen-Dale, A.-L., Giaccia, A., Longaker, M. T., Hastie, T., Yang, G. P., van de Vijver, M. J., & Brown, P. O. (2006). Gene Expression Programs in Response to Hypoxia: Cell Type Specificity and Prognostic Significance in Human Cancers. *PLoS Medicine*, *3*(3), e47. https://doi.org/10.1371/journal.pmed.0030047

Choi, C.-M., Seo, K. W., Jang, S. J., Oh, Y.-M., Shim, T.-S., Kim, W. S., Lee, D.-S., & Lee, S.-D. (2009). Chromosomal instability is a risk factor for poor prognosis of adenocarcinoma of the lung: Fluorescence in situ hybridization analysis of paraffin-embedded tissue from Korean patients. *Lung Cancer*, *64*(1), 66–70. https://doi.org/10.1016/j.lungcan.2008.07.016

Chouchani, E. T., Pell, V. R., Gaude, E., Aksentijević, D., Sundier, S. Y., Robb, E. L., Logan, A., Nadtochiy, S. M., Ord, E. N. J., Smith, A. C., Eyassu, F., Shirley, R., Hu, C.-H., Dare, A. J., James, A. M., Rogatti, S., Hartley, R. C., Eaton, S., Costa, A. S. H., … Murphy, M. P. (2014). Ischaemic accumulation of succinate controls reperfusion injury through mitochondrial ROS. *Nature*, *515*(7527), 431–435. https://doi.org/10.1038/nature13909

Ciepła, J., & Smolarczyk, R. (2024). Tumor hypoxia unveiled: insights into microenvironment, detection tools and emerging therapies. *Clinical and Experimental Medicine*, *24*(1), 235. https://doi.org/10.1007/s10238-024-01501-1

Comprehensive genomic characterization of squamous cell lung cancers. (2012). *Nature*, *489*(7417), 519–525. https://doi.org/10.1038/nature11404

Comprehensive molecular profiling of lung adenocarcinoma. (2014). *Nature*, *511*(7511), 543–550. https://doi.org/10.1038/nature13385

Conger, K. O., Chidley, C., Ozgurses, M. E., Zhao, H., Kim, Y., Semina, S. E., Burns, P., Rawat, V., Sheldon, R., Ben-Sahra, I., Frasor, J., Sorger, P. K., DeNicola, G. M., & Coloff, J. L. (2023). *ASCT2 is the primary serine transporter in cancer cells*. https://doi.org/10.1101/2023.10.09.561530

Coppé, J.-P., Patil, C. K., Rodier, F., Sun, Y., Muñoz, D. P., Goldstein, J., Nelson, P. S., Desprez, P.-Y., & Campisi, J. (2008). Senescence-Associated Secretory Phenotypes Reveal Cell-Nonautonomous Functions of Oncogenic RAS and the p53 Tumor Suppressor. *PLoS Biology*, *6*(12), e301. https://doi.org/10.1371/journal.pbio.0060301

Covello, K. L., Kehler, J., Yu, H., Gordan, J. D., Arsham, A. M., Hu, C.-J., Labosky, P. A., Simon, M. C., & Keith, B. (2006). HIF-2α regulates Oct-4: effects of hypoxia on stem cell function, embryonic development, and tumor growth. *Genes & Development*, *20*(5), 557–570. https://doi.org/10.1101/gad.1399906

Cristini, A., Groh, M., Kristiansen, M. S., & Gromak, N. (2018). RNA/DNA Hybrid Interactome Identifies DXH9 as a Molecular Player in Transcriptional Termination and R-Loop-Associated DNA Damage. *Cell Reports*, *23*(6), 1891–1905. https://doi.org/10.1016/j.celrep.2018.04.025

Crossley, M. P., Bocek, M., & Cimprich, K. A. (2019). R-Loops as Cellular Regulators and Genomic Threats. *Molecular Cell*, *73*(3), 398–411. https://doi.org/10.1016/j.molcel.2019.01.024

Crossley, M. P., Bocek, M. J., Hamperl, S., Swigut, T., & Cimprich, K. A. (2020). qDRIP: a method to quantitatively assess RNA–DNA hybrid formation genome-wide. *Nucleic Acids Research*, *48*(14), e84–e84. https://doi.org/10.1093/nar/gkaa500

Crossley, M. P., Song, C., Bocek, M. J., Choi, J.-H., Kousorous, J., Sathirachinda, A., Lin, C., Brickner, J. R., Bai, G., Lans, H., Vermeulen, W., Abu-Remaileh, M., & Cimprich, K. A. (2023). R-loop-derived cytoplasmic RNA–DNA hybrids activate an immune response. *Nature*, *613*(7942), 187–194. https://doi.org/10.1038/s41586-022-05545-9

Cybulski, R. L., & Fisher, R. R. (1976). Intramitochondrial localization and proposed metabolic significance of serine transhydroxymethylase. *Biochemistry*, *15*(15), 3183–3187. https://doi.org/10.1021/bi00660a004

Cybulski, R. L., & Fisher, R. R. (1977). Mitochondrial neutral amino acid transport: evidence for a carrier mediated mechanism. *Biochemistry*, *16*(23), 5116–5120. https://doi.org/10.1021/bi00642a026

Daidone, F., Florio, R., Rinaldo, S., Contestabile, R., di Salvo, M. L., Cutruzzolà, F., Bossa, F., & Paiardini, A. (2011). In silico and in vitro validation of serine hydroxymethyltransferase as a chemotherapeutic target of the antifolate drug pemetrexed. *European Journal of Medicinal Chemistry*, *46*(5), 1616–1621. https://doi.org/10.1016/j.ejmech.2011.02.009

Dalton, W. B. (2020). Parkin on serine: a Parkinson disease gene suppresses serine synthesis in cancer. *Journal of Clinical Investigation*, *130*(6), 2820–2822. https://doi.org/10.1172/JCI137411

Dayan, F., Roux, D., Brahimi-Horn, M. C., Pouyssegur, J., & Mazure, N. M. (2006). The Oxygen Sensor Factor-Inhibiting Hypoxia-Inducible Factor-1 Controls Expression of Distinct Genes through the Bifunctional Transcriptional Character of Hypoxia-Inducible Factor-1α. *Cancer Research*, *66*(7), 3688–3698. https://doi.org/10.1158/0008-5472.CAN-05-4564

de Bruijn, I., Kundra, R., Mastrogiacomo, B., Tran, T. N., Sikina, L., Mazor, T., Li, X., Ochoa, A., Zhao, G., Lai, B., Abeshouse, A., Baiceanu, D., Ciftci, E., Dogrusoz, U., Dufilie, A., Erkoc, Z., Garcia Lara, E., Fu, Z., Gross, B., … Schultz, N. (2023). Analysis and Visualization of Longitudinal Genomic and Clinical Data from the AACR Project GENIE Biopharma Collaborative in cBioPortal. *Cancer Research*, *83*(23), 3861–3867. https://doi.org/10.1158/0008-5472.CAN-23-0816

De Saedeleer, C. J., Copetti, T., Porporato, P. E., Verrax, J., Feron, O., & Sonveaux, P. (2012). Lactate Activates HIF-1 in Oxidative but Not in Warburg-Phenotype Human Tumor Cells. *PLoS ONE*, *7*(10), e46571. https://doi.org/10.1371/journal.pone.0046571

DeBerardinis, R. J., Mancuso, A., Daikhin, E., Nissim, I., Yudkoff, M., Wehrli, S., & Thompson, C. B. (2007). Beyond aerobic glycolysis: Transformed cells can engage in glutamine metabolism that exceeds the requirement for protein and nucleotide synthesis. *Proceedings of the National Academy of Sciences*, *104*(49), 19345–19350. https://doi.org/10.1073/pnas.0709747104

Deng, L., Yang, X., Zhang, J., Zhou, X., Ma, R., Wu, Z., & Chen, H. (2026). ΔNp63α drives serine synthesis to promote carboplatin resistance in NSCLC. *Cell Death & Disease*, *17*(1), 227. https://doi.org/10.1038/s41419-026-08497-4

DeNicola, G. M., Chen, P.-H., Mullarky, E., Sudderth, J. A., Hu, Z., Wu, D., Tang, H., Xie, Y., Asara, J. M., Huffman, K. E., Wistuba, I. I., Minna, J. D., DeBerardinis, R. J., & Cantley, L. C. (2015). NRF2

regulates serine biosynthesis in non–small cell lung cancer. *Nature Genetics*, *47*(12), 1475–1481. https://doi.org/10.1038/ng.3421

Devanathan, S. K., Li, Y.-R., Shelton, S. B., Nguyen, J., Tseng, W.-C., Shah, N. M., Mercado, M., Miller, K. M., & Xhemalçe, B. (2025). MePCE promotes homologous recombination through coordinating R-loop resolution at DNA double-stranded breaks. *Cell Reports*, *44*(6), 115740. https://doi.org/10.1016/j.celrep.2025.115740

Dewhirst, M. W., Braun, R. D., & Lanzen, J. L. (1998). Temporal changes in pO2 of R3230Ac tumors in fischer-344 rats. *International Journal of Radiation Oncology*Biology*Physics*, *42*(4), 723–726. https://doi.org/10.1016/S0360-3016(98)00304-6

Dey, S., Grant, G. A., & Sacchettini, J. C. (2005). Crystal Structure of Mycobacterium tuberculosis D-3-Phosphoglycerate Dehydrogenase. *Journal of Biological Chemistry*, *280*(15), 14892–14899. https://doi.org/10.1074/jbc.M414489200

Di Giovannantonio, M., Hartley, F., Elshenawy, B., Barberis, A., Hudson, D., Shafique, H. S., Allott, V. E. S., Harris, D. A., Lord, S. R., Haider, S., Harris, A. L., Buffa, F. M., & Harris, B. H. L. (2025). Defining hypoxia in cancer: A landmark evaluation of hypoxia gene expression signatures. *Cell Genomics*, *5*(2), 100764. https://doi.org/10.1016/j.xgen.2025.100764

Diebold, I., Petry, A., Hess, J., & Görlach, A. (2010). The NADPH oxidase subunit NOX4 is a new target gene of the hypoxia-inducible factor-1. *Molecular Biology of the Cell*, *21*(12), 2087–2096. https://doi.org/10.1091/mbc.e09-12-1003

Ding, J., Li, T., Wang, X., Zhao, E., Choi, J.-H., Yang, L., Zha, Y., Dong, Z., Huang, S., Asara, J. M., Cui, H., & Ding, H.-F. (2013). The Histone H3 Methyltransferase G9A Epigenetically Activates the Serine-Glycine Synthesis Pathway to Sustain Cancer Cell Survival and Proliferation. *Cell Metabolism*, *18*(6), 896–907. https://doi.org/10.1016/j.cmet.2013.11.004

Ding, L., Xu, Y., Xu, L., Zhao, C., Zhang, Z., Zhang, J., Liao, K., Chen, Y., Li, J., Mei, X., & Zhang, X. (2023). Programmed cell death 11 modulates but not entirely relies on p53-HDM2 loop to facilitate G2/M transition in colorectal cancer cells. *Oncogenesis*, *12*(1), 57. https://doi.org/10.1038/s41389-023-00501-2

Dings, J., Meixensberger, J., Jäger, A., & Roosen, K. (1998). Clinical Experience with 118 Brain Tissue Oxygen Partial Pressure Catheter Probes. *Neurosurgery*, *43*(5), 1082–1094. https://doi.org/10.1097/00006123-199811000-00045

Dreos, R., Ambrosini, G., Groux, R., Cavin Périer, R., & Bucher, P. (2017). The eukaryotic promoter database in its 30th year: focus on non-vertebrate organisms. *Nucleic Acids Research*, *45*(D1), D51–D55. https://doi.org/10.1093/nar/gkw1069

Dubois, L. J., Lieuwes, N. G., Janssen, M. H. M., Peeters, W. J. M., Windhorst, A. D., Walsh, J. C., Kolb, H. C., Öllers, M. C., Bussink, J., van Dongen, G. A. M. S., van der Kogel, A., & Lambin, P. (2011). Preclinical evaluation and validation of [^{18} F]HX4, a promising hypoxia marker for PET imaging. *Proceedings of the National Academy of Sciences*, *108*(35), 14620–14625. https://doi.org/10.1073/pnas.1102526108

Ducker, G. S., Chen, L., Morscher, R. J., Ghergurovich, J. M., Esposito, M., Teng, X., Kang, Y., & Rabinowitz, J. D. (2016). Reversal of Cytosolic One-Carbon Flux Compensates for Loss of the Mitochondrial Folate Pathway. *Cell Metabolism*, *23*(6), 1140–1153. https://doi.org/10.1016/j.cmet.2016.04.016

Dupuy, F., Tabariès, S., Andrzejewski, S., Dong, Z., Blagih, J., Annis, M. G., Omeroglu, A., Gao, D., Leung, S., Amir, E., Clemons, M., Aguilar-Mahecha, A., Basik, M., Vincent, E. E., St.-Pierre, J., Jones, R. G.,

& Siegel, P. M. (2015). PDK1-Dependent Metabolic Reprogramming Dictates Metastatic Potential in Breast Cancer. *Cell Metabolism*, *22*(4), 577–589. https://doi.org/10.1016/j.cmet.2015.08.007

Eales, K. L., Hollinshead, K. E. R., & Tennant, D. A. (2016). Hypoxia and metabolic adaptation of cancer cells. *Oncogenesis*, *5*(1), e190–e190. https://doi.org/10.1038/oncsis.2015.50

Ebert, B. L., Firth, J. D., & Ratcliffe, P. J. (1995). Hypoxia and Mitochondrial Inhibitors Regulate Expression of Glucose Transporter-1 via Distinct Cis-acting Sequences. *Journal of Biological Chemistry*, *270*(49), 29083–29089. https://doi.org/10.1074/jbc.270.49.29083

Ehmsen, J. T., Liu, Y., Wang, Y., Paladugu, N., Johnson, A. E., Rothstein, J. D., du Lac, S., Mattson, M. P., & Höke, A. (2016). The astrocytic transporter SLC7A10 (Asc-1) mediates glycinergic inhibition of spinal cord motor neurons. *Scientific Reports*, *6*(1), 35592. https://doi.org/10.1038/srep35592

Elhamamsy, A., Metge, B. J., Swain, C. A., Elbahoty, M. H., Hinshaw, D. C., Kammerud, S. C., Chen, D., Samant, R. S., & Shevde, L. A. (2025). Hypoxic stress incites HIF1α-driven ribosome biogenesis that can be exploited by targeting RNA Polymerase I. *Nature Communications*, *16*(1), 8018. https://doi.org/10.1038/s41467-025-63315-3

Epstein, A. C. R., Gleadle, J. M., McNeill, L. A., Hewitson, K. S., O'Rourke, J., Mole, D. R., Mukherji, M., Metzen, E., Wilson, M. I., Dhanda, A., Tian, Y.-M., Masson, N., Hamilton, D. L., Jaakkola, P., Barstead, R., Hodgkin, J., Maxwell, P. H., Pugh, C. W., Schofield, C. J., & Ratcliffe, P. J. (2001). C. elegans EGL-9 and Mammalian Homologs Define a Family of Dioxygenases that Regulate HIF by Prolyl Hydroxylation. *Cell*, *107*(1), 43–54. https://doi.org/10.1016/S0092-8674(01)00507-4

Estephan, H., Tailor, A., Parker, R., Kreamer, M., Papandreou, I., Campo, L., Easton, A., Moon, E. J., Denko, N. C., Ternette, N., Hammond, E. M., & Giaccia, A. J. (2025). Hypoxia promotes tumor immune evasion by suppressing MHC-I expression and antigen presentation. *The EMBO Journal*, *44*(3), 903–922. https://doi.org/10.1038/s44318-024-00319-7

Eustace, A., Mani, N., Span, P. N., Irlam, J. J., Taylor, J., Betts, G. N. J., Denley, H., Miller, C. J., Homer, J. J., Rojas, A. M., Hoskin, P. J., Buffa, F. M., Harris, A. L., Kaanders, J. H. A. M., & West, C. M. L. (2013). A 26-Gene Hypoxia Signature Predicts Benefit from Hypoxia-Modifying Therapy in Laryngeal Cancer but Not Bladder Cancer. *Clinical Cancer Research*, *19*(17), 4879–4888. https://doi.org/10.1158/1078-0432.CCR-13-0542

Falcone, M., Uribe, A. H., Papalazarou, V., Newman, A. C., Athineos, D., Stevenson, K., Sauvé, C.-E. G., Gao, Y., Kim, J. K., Del Latto, M., Kierstead, M., Wu, C., Smith, J. J., Romesser, P. B., Chalmers, A. J., Blyth, K., & Maddocks, O. D. K. (2022). Sensitisation of cancer cells to radiotherapy by serine and glycine starvation. *British Journal of Cancer*, *127*(10), 1773–1786. https://doi.org/10.1038/s41416-022-01965-6

Falk, S., Ward, R., & Bleehen, N. (1992). The influence of carbogen breathing on tumour tissue oxygenation in man evaluated by computerised p02 histography. *British Journal of Cancer*, *66*(5), 919–924. https://doi.org/10.1038/bjc.1992.386

Fan, J., Ye, J., Kamphorst, J. J., Shlomi, T., Thompson, C. B., & Rabinowitz, J. D. (2014). Quantitative flux analysis reveals folate-dependent NADPH production. *Nature*, *510*(7504), 298–302. https://doi.org/10.1038/nature13236

Fan, T. W. M., Bruntz, R. C., Yang, Y., Song, H., Chernyavskaya, Y., Deng, P., Zhang, Y., Shah, P. P., Beverly, L. J., Qi, Z., Mahan, A. L., Higashi, R. M., Dang, C. V., & Lane, A. N. (2019). De novo synthesis of serine and glycine fuels purine nucleotide biosynthesis in human lung cancer tissues. *Journal of Biological Chemistry*, *294*(36), 13464–13477. https://doi.org/10.1074/jbc.RA119.008743

Feng, M., Cui, H., Tu, W., Li, L., Gao, Y., Chen, L., Li, D., Chen, X., Xu, F., Zhou, C., & Cao, Y. (2022). An integrated pan-cancer analysis of PSAT1: A potential biomarker for survival and immunotherapy. *Frontiers in Genetics*, *13*. https://doi.org/10.3389/fgene.2022.975381

Finicle, B. T., Jayashankar, V., & Edinger, A. L. (2018). Nutrient scavenging in cancer. *Nature Reviews Cancer*, *18*(10), 619–633. https://doi.org/10.1038/s41568-018-0048-x

Firth, J. D., Ebert, B. L., Pugh, C. W., & Ratcliffe, P. J. (1994). Oxygen-regulated control elements in the phosphoglycerate kinase 1 and lactate dehydrogenase A genes: similarities with the erythropoietin 3' enhancer. *Proceedings of the National Academy of Sciences*, *91*(14), 6496–6500. https://doi.org/10.1073/pnas.91.14.6496

Forsythe, J. A., Jiang, B.-H., Iyer, N. V., Agani, F., Leung, S. W., Koos, R. D., & Semenza, G. L. (1996). Activation of Vascular Endothelial Growth Factor Gene Transcription by Hypoxia-Inducible Factor 1. *Molecular and Cellular Biology*, *16*(9), 4604–4613. https://doi.org/10.1128/MCB.16.9.4604

Foskolou, I. P., Jorgensen, C., Leszczynska, K. B., Olcina, M. M., Tarhonskaya, H., Haisma, B., D'Angiolella, V., Myers, W. K., Domene, C., Flashman, E., & Hammond, E. M. (2017). Ribonucleotide Reductase Requires Subunit Switching in Hypoxia to Maintain DNA Replication. *Molecular Cell*, *66*(2), 206-220.e9. https://doi.org/10.1016/j.molcel.2017.03.005

Frand, A. R., & Kaiser, C. A. (1998). The ERO1 Gene of Yeast Is Required for Oxidation of Protein Dithiols in the Endoplasmic Reticulum. *Molecular Cell*, *1*(2), 161–170. https://doi.org/10.1016/S1097-2765(00)80017-9

Franklin, C. C., Backos, D. S., Mohar, I., White, C. C., Forman, H. J., & Kavanagh, T. J. (2009). Structure, function, and post-translational regulation of the catalytic and modifier subunits of glutamate cysteine ligase. *Molecular Aspects of Medicine*, *30*(1–2), 86–98. https://doi.org/10.1016/j.mam.2008.08.009

Fremerey, J., Morozov, P., Meyer, C., Garzia, A., Teplova, M., Tuschl, T., & Borkhardt, A. (2016). Nucleolin Controls Ribosome Biogenesis through Its RNA-Binding Properties. *Blood*, *128*(22), 5056–5056. https://doi.org/10.1182/blood.V128.22.5056.5056

Fukasawa, Y., Segawa, H., Kim, J. Y., Chairoungdua, A., Kim, D. K., Matsuo, H., Cha, S. H., Endou, H., & Kanai, Y. (2000). Identification and Characterization of a Na+-independent Neutral Amino Acid Transporter That Associates with the 4F2 Heavy Chain and Exhibits Substrate Selectivity for Small Neutral d- and l-Amino Acids. *Journal of Biological Chemistry*, *275*(13), 9690–9698. https://doi.org/10.1074/jbc.275.13.9690

Galluzzi, L., Pietrocola, F., Bravo-San Pedro, J. M., Amaravadi, R. K., Baehrecke, E. H., Cecconi, F., Codogno, P., Debnath, J., Gewirtz, D. A., Karantza, V., Kimmelman, A., Kumar, S., Levine, B., Maiuri, M. C., Martin, S. J., Penninger, J., Piacentini, M., Rubinsztein, D. C., Simon, H., … Kroemer, G. (2015). Autophagy in malignant transformation and cancer progression. *The EMBO Journal*, *34*(7), 856–880. https://doi.org/10.15252/embj.201490784

Galon, J., Costes, A., Sanchez-Cabo, F., Kirilovsky, A., Mlecnik, B., Lagorce-Pagès, C., Tosolini, M., Camus, M., Berger, A., Wind, P., Zinzindohoué, F., Bruneval, P., Cugnenc, P.-H., Trajanoski, Z., Fridman, W.-H., & Pagès, F. (2006). Type, Density, and Location of Immune Cells Within Human Colorectal Tumors Predict Clinical Outcome. *Science*, *313*(5795), 1960–1964. https://doi.org/10.1126/science.1129139

Gan, W., Guan, Z., Liu, J., Gui, T., Shen, K., Manley, J. L., & Li, X. (2011). R-loop-mediated genomic instability is caused by impairment of replication fork progression. *Genes & Development*, *25*(19), 2041–2056. https://doi.org/10.1101/gad.17010011

Gao, D., Tang, S., Cen, Y., Yuan, L., Lan, X., Li, Q.-H., Lin, G.-Q., Huang, M., & Tian, P. (2023). Discovery of Novel Drug-like PHGDH Inhibitors to Disrupt Serine Biosynthesis for Cancer Therapy. *Journal of Medicinal Chemistry*, *66*(1), 285–305. https://doi.org/10.1021/acs.jmedchem.2c01202

Gao, J., Aksoy, B. A., Dogrusoz, U., Dresdner, G., Gross, B., Sumer, S. O., Sun, Y., Jacobsen, A., Sinha, R., Larsson, E., Cerami, E., Sander, C., & Schultz, N. (2013). Integrative Analysis of Complex Cancer Genomics and Clinical Profiles Using the cBioPortal. *Science Signaling*, *6*(269). https://doi.org/10.1126/scisignal.2004088

Gao, L., Mejías, R., Echevarría, M., & López-Barneo, J. (2004). Induction of the glucose-6-phosphate dehydrogenase gene expression by chronic hypoxia in PC12 cells. *FEBS Letters*, *569*(1–3), 256–260. https://doi.org/10.1016/j.febslet.2004.06.004

Geeraerts, S. L., Heylen, E., De Keersmaecker, K., & Kampen, K. R. (2021). The ins and outs of serine and glycine metabolism in cancer. *Nature Metabolism*, *3*(2), 131–141. https://doi.org/10.1038/s42255-020-00329-9

Gizak, A., Wiśniewski, J., Heron, P., Mamczur, P., Sygusch, J., & Rakus, D. (2019). Targeting a moonlighting function of aldolase induces apoptosis in cancer cells. *Cell Death & Disease*, *10*(10), 712. https://doi.org/10.1038/s41419-019-1968-4

Gnarra, J. R., Tory, K., Weng, Y., Schmidt, L., Wei, M. H., Li, H., Latif, F., Liu, S., Chen, F., Duh, F.-M., Lubensky, I., Duan, D. R., Florence, C., Pozzatti, R., Walther, M. M., Bander, N. H., Grossman, H. B., Brauch, H., Pomer, S., … Linehan, W. M. (1994). Mutations of the VHL tumour suppressor gene in renal carcinoma. *Nature Genetics*, *7*(1), 85–90. https://doi.org/10.1038/ng0594-85

Gordan, J. D., Bertout, J. A., Hu, C.-J., Diehl, J. A., & Simon, M. C. (2007). HIF-2α Promotes Hypoxic Cell Proliferation by Enhancing c-Myc Transcriptional Activity. *Cancer Cell*, *11*(4), 335–347. https://doi.org/10.1016/j.ccr.2007.02.006

Graeber, T. G., Osmanian, C., Jacks, T., Housman, D. E., Koch, C. J., Lowe, S. W., & Giaccia, A. J. (1996). Hypoxia-mediated selection of cells with diminished apoptotic potential in solid tumours. *Nature*, *379*(6560), 88–91. https://doi.org/10.1038/379088a0

Graham, K., & Unger, E. (2018). Overcoming tumor hypoxia as a barrier to radiotherapy, chemotherapy and immunotherapy in cancer treatment. *International Journal of Nanomedicine*, *Volume 13*, 6049–6058. https://doi.org/10.2147/IJN.S140462

Grant, G. A. (2006). The ACT Domain: A Small Molecule Binding Domain and Its Role as a Common Regulatory Element. *Journal of Biological Chemistry*, *281*(45), 33825–33829. https://doi.org/10.1074/jbc.R600024200

Grant, G. A., Xu, X. L., & Hu, Z. (2004). Quantitative Relationships of Site to Site Interaction in Escherichia coli d-3-Phosphoglycerate Dehydrogenase Revealed by Asymmetric Hybrid Tetramers. *Journal of Biological Chemistry*, *279*(14), 13452–13460. https://doi.org/10.1074/jbc.M313593200

Gray, L. H., Conger, A. D., Ebert, M., Hornsey, S., & Scott, O. C. A. (1953). The Concentration of Oxygen Dissolved in Tissues at the Time of Irradiation as a Factor in Radiotherapy. *The British Journal of Radiology*, *26*(312), 638–648. https://doi.org/10.1259/0007-1285-26-312-638

Gregory, J. F., Cuskelly, G. J., Shane, B., Toth, J. P., Baumgartner, T. G., & Stacpoole, P. W. (2000). Primed, constant infusion with [2H3]serine allows in vivo kinetic measurement of serine turnover, homocysteine remethylation, and transsulfuration processes in human one-carbon metabolism. *The American Journal of Clinical Nutrition*, *72*(6), 1535–1541. https://doi.org/10.1093/ajcn/72.6.1535

Grueso, M. J., Valero, R. M., Carmona, H. B., Ruiz, D. J., Peinado, J., McDonagh, B., Aguilar, R., Ruiz, J. A., & Peña, C. A. (2019). Peroxiredoxin 6 Down-Regulation Induces Metabolic Remodeling and Cell Cycle Arrest in HepG2 Cells. *Antioxidants*, *8*(11), 505. https://doi.org/10.3390/antiox8110505

Gumaa, K. A., Novello, F., & McLean, P. (1969). The pentose phosphate pathway of glucose metabolism. Hormonal and dietary control of the oxidative and non-oxidative reactions and related enzymes of the cycle in adipose tissue. *Biochemical Journal*, *114*(2), 253–264. https://doi.org/10.1042/bj1140253

Guo, J., Gu, X., Zheng, M., Zhang, Y., Chen, L., & Li, H. (2019). Azacoccone E inhibits cancer cell growth by targeting 3-phosphoglycerate dehydrogenase. *Bioorganic Chemistry*, *87*, 16–22. https://doi.org/10.1016/j.bioorg.2019.02.037

Guo, K., Searfoss, G., Krolikowski, D., Pagnoni, M., Franks, C., Clark, K., Yu, K. T., Jaye, M., & Ivashchenko, Y. (2001). Hypoxia induces the expression of the pro-apoptotic gene BNIP3. *Cell Death & Differentiation*, *8*(4), 367–376. https://doi.org/10.1038/sj.cdd.4400810

Guzy, R. D., Hoyos, B., Robin, E., Chen, H., Liu, L., Mansfield, K. D., Simon, M. C., Hammerling, U., & Schumacker, P. T. (2005). Mitochondrial complex III is required for hypoxia-induced ROS production and cellular oxygen sensing. *Cell Metabolism*, *1*(6), 401–408. https://doi.org/10.1016/j.cmet.2005.05.001

Hall, E. J. ., & Giaccia, A. J. . (2006). *Radiobiology for the radiologist* (6th edition). Lippincott Williams & Wilkins.

Hall, E. J. ., & Giaccia, A. J. . (2018). *Radiobiology for the radiologist* (8th ed.). Wolters Kluwer.

Hammond, E. M., Asselin, M.-C., Forster, D., O'Connor, J. P. B., Senra, J. M., & Williams, K. J. (2014). The Meaning, Measurement and Modification of Hypoxia in the Laboratory and the Clinic. *Clinical Oncology*, *26*(5), 277–288. https://doi.org/10.1016/j.clon.2014.02.002

Hammond, E. M., Denko, N. C., Dorie, M. J., Abraham, R. T., & Giaccia, A. J. (2002). Hypoxia Links ATR and p53 through Replication Arrest. *Molecular and Cellular Biology*, *22*(6), 1834–1843. https://doi.org/10.1128/MCB.22.6.1834-1843.2002

Hamperl, S., Bocek, M. J., Saldivar, J. C., Swigut, T., & Cimprich, K. A. (2017). Transcription-Replication Conflict Orientation Modulates R-Loop Levels and Activates Distinct DNA Damage Responses. *Cell*, *170*(4), 774-786.e19. https://doi.org/10.1016/j.cell.2017.07.043

Hanahan, D. (2022). Hallmarks of Cancer: New Dimensions. *Cancer Discovery*, *12*(1), 31–46. https://doi.org/10.1158/2159-8290.CD-21-1059

Hanahan, D. (2026). Hallmarks of cancer—Then and now, and beyond. *Cell*. https://doi.org/10.1016/j.cell.2025.12.049

Hanahan, D., & Weinberg, R. A. (2000). The Hallmarks of Cancer. *Cell*, *100*(1), 57–70. https://doi.org/10.1016/S0092-8674(00)81683-9

Hanahan, D., & Weinberg, R. A. (2011). Hallmarks of Cancer: The Next Generation. *Cell*, *144*(5), 646–674. https://doi.org/10.1016/j.cell.2011.02.013

Harding, H. P., Novoa, I., Zhang, Y., Zeng, H., Wek, R., Schapira, M., & Ron, D. (2000). Regulated Translation Initiation Controls Stress-Induced Gene Expression in Mammalian Cells. *Molecular Cell*, *6*(5), 1099–1108. https://doi.org/10.1016/S1097-2765(00)00108-8

Harris, B. H. L., Barberis, A., West, C. M. L., & Buffa, F. M. (2015). Gene Expression Signatures as Biomarkers of Tumour Hypoxia. *Clinical Oncology*, *27*(10), 547–560. https://doi.org/10.1016/j.clon.2015.07.004

Hartono, S. R., Malapert, A., Legros, P., Bernard, P., Chédin, F., & Vanoosthuyse, V. (2018). The Affinity of the S9.6 Antibody for Double-Stranded RNAs Impacts the Accurate Mapping of R-Loops in

Fission Yeast. *Journal of Molecular Biology*, *430*(3), 272–284. https://doi.org/10.1016/j.jmb.2017.12.016

Hayashi, M., Sakata, M., Takeda, T., Yamamoto, T., Okamoto, Y., Sawada, K., Kimura, A., Minekawa, R., Tahara, M., Tasaka, K., & Murata, Y. (2004). Induction of glucose transporter 1 expression through hypoxia-inducible factor 1α under hypoxic conditions in trophoblast-derived cells. *Journal of Endocrinology*, *183*(1), 145–154. https://doi.org/10.1677/joe.1.05599

Haze, K., Yoshida, H., Yanagi, H., Yura, T., & Mori, K. (1999). Mammalian Transcription Factor ATF6 Is Synthesized as a Transmembrane Protein and Activated by Proteolysis in Response to Endoplasmic Reticulum Stress. *Molecular Biology of the Cell*, *10*(11), 3787–3799. https://doi.org/10.1091/mbc.10.11.3787

Helmrich, A., Ballarino, M., & Tora, L. (2011). Collisions between Replication and Transcription Complexes Cause Common Fragile Site Instability at the Longest Human Genes. *Molecular Cell*, *44*(6), 966–977. https://doi.org/10.1016/j.molcel.2011.10.013

Hennequart, M., Labuschagne, C. F., Tajan, M., Pilley, S. E., Cheung, E. C., Legrave, N. M., Driscoll, P. C., & Vousden, K. H. (2021). The impact of physiological metabolite levels on serine uptake, synthesis and utilization in cancer cells. *Nature Communications*, *12*(1), 6176. https://doi.org/10.1038/s41467-021-26395-5

Higgins, G. S., & Hammond, E. M. (2022). Elucidating the role of transiently hypoxic tumour cells on radiation resistance. *British Journal of Cancer*, *126*(7), 971–972. https://doi.org/10.1038/s41416-022-01741-6

Hitosugi, T., Zhou, L., Elf, S., Fan, J., Kang, H.-B., Seo, J. H., Shan, C., Dai, Q., Zhang, L., Xie, J., Gu, T.-L., Jin, P., Alečković, M., LeRoy, G., Kang, Y., Sudderth, J. A., DeBerardinis, R. J., Luan, C.-H., Chen, G. Z., … Chen, J. (2012). Phosphoglycerate Mutase 1 Coordinates Glycolysis and Biosynthesis to Promote Tumor Growth. *Cancer Cell*, *22*(5), 585–600. https://doi.org/10.1016/j.ccr.2012.09.020

Hochstatter, J., Hölzel, M., Rohrmoser, M., Schermelleh, L., Leonhardt, H., Keough, R., Gonda, T. J., Imhof, A., Eick, D., Längst, G., & Németh, A. (2012). Myb-binding Protein 1a (Mybbp1a) Regulates Levels and Processing of Pre-ribosomal RNA. *Journal of Biological Chemistry*, *287*(29), 24365–24377. https://doi.org/10.1074/jbc.M111.303719

Hockel, M., Schlenger, K., Aral, B., Mitze, M., Schaffer, U., & Vaupel, P. (1996). Association between tumor hypoxia and malignant progression in advanced cancer of the uterine cervix. *Cancer Research*, *56*(19), 4509–4515.

Hollien, J., & Weissman, J. S. (2006). Decay of Endoplasmic Reticulum-Localized mRNAs During the Unfolded Protein Response. *Science*, *313*(5783), 104–107. https://doi.org/10.1126/science.1129631

Hu, L., Wang, J., Liu, Y., Zhang, Y., Zhang, L., Kong, R., Zheng, Z., Du, X., & Ke, Y. (2011). A Small Ribosomal Subunit (SSU) Processome Component, the Human U3 Protein 14A (hUTP14A) Binds p53 and Promotes p53 Degradation. *Journal of Biological Chemistry*, *286*(4), 3119–3128. https://doi.org/10.1074/jbc.M110.157842

Huang, D., Cai, H., & Huang, H. (2025). Serine metabolism in tumor progression and immunotherapy. *Discover Oncology*, *16*(1), 628. https://doi.org/10.1007/s12672-025-02358-w

Huang, Y., Fan, J., Li, Y., Fu, S., Chen, Y., & Wu, J. (2021). Imaging of Tumor Hypoxia With Radionuclide-Labeled Tracers for PET. *Frontiers in Oncology*, *11*. https://doi.org/10.3389/fonc.2021.731503

Huang, Z., Zhang, K., Jiang, Y., Wang, M., Li, M., Guo, Y., Gao, R., Li, N., Wang, C., Chen, J., Wang, J., Liu, N., Liu, X., Liu, S., Wei, M., Yang, C., & Yang, G. (2024). Molecular glue triggers degradation of

PHGDH by enhancing the interaction between DDB1 and PHGDH. *Acta Pharmaceutica Sinica B*, *14*(9), 4001–4013. https://doi.org/10.1016/j.apsb.2024.06.001

Huelsemann, M. F., Patz, M., Beckmann, L., Brinkmann, K., Otto, T., Fandrey, J., Becker, H. J., Theurich, S., von Bergwelt-Baildon, M., Pallasch, C. P., Zahedi, R. P., Kashkar, H., Reinhardt, H. C., Hallek, M., Wendtner, C. M., & Frenzel, L. P. (2015). Hypoxia-induced p38 MAPK activation reduces Mcl-1 expression and facilitates sensitivity towards BH3 mimetics in chronic lymphocytic leukemia. *Leukemia*, *29*(4), 981–984. https://doi.org/10.1038/leu.2014.320

Ichihara, A., & Greenberg, D. M. (1955). PATHWAY OF SERINE FORMATION FROM CARBOHYDRATE IN RAT LIVER. *Proceedings of the National Academy of Sciences*, *41*(9), 605–609. https://doi.org/10.1073/pnas.41.9.605

Inoue, A., & Fujimoto, D. (1969). Enzymatic deacetylation of histone. *Biochemical and Biophysical Research Communications*, *36*(1), 146–150. https://doi.org/10.1016/0006-291X(69)90661-5

Isaacs, J. S., Jung, Y. J., Mole, D. R., Lee, S., Torres-Cabala, C., Chung, Y.-L., Merino, M., Trepel, J., Zbar, B., Toro, J., Ratcliffe, P. J., Linehan, W. M., & Neckers, L. (2005). HIF overexpression correlates with biallelic loss of fumarate hydratase in renal cancer: Novel role of fumarate in regulation of HIF stability. *Cancer Cell*, *8*(2), 143–153. https://doi.org/10.1016/j.ccr.2005.06.017

Islam, Z., Polash, A., Suzawa, M., Chim, B., Kuhn, S., Sultana, S., Cutrona, N., Smith, P. T., Kabat, J., Ganesan, S., Foroushani, A., Hafner, M., & Muljo, S. A. (2024). MATRIN3 *deficiency triggers autoinflammation via cGAS-STING activation*. https://doi.org/10.1101/2024.04.01.587645

Itoh, K., Chiba, T., Takahashi, S., Ishii, T., Igarashi, K., Katoh, Y., Oyake, T., Hayashi, N., Satoh, K., Hatayama, I., Yamamoto, M., & Nabeshima, Y. (1997). An Nrf2/Small Maf Heterodimer Mediates the Induction of Phase II Detoxifying Enzyme Genes through Antioxidant Response Elements. *Biochemical and Biophysical Research Communications*, *236*(2), 313–322. https://doi.org/10.1006/bbrc.1997.6943

Ivan, M., Kondo, K., Yang, H., Kim, W., Valiando, J., Ohh, M., Salic, A., Asara, J. M., Lane, W. S., & Kaelin Jr., W. G. (2001). HIFα Targeted for VHL-Mediated Destruction by Proline Hydroxylation: Implications for O_2 Sensing. *Science*, *292*(5516), 464–468. https://doi.org/10.1126/science.1059817

Ji, C., Zhu, J., Hou, X., Zhou, C., Zhao, J., Zheng, X., & Tang, Y. (2025). PTBP1 and Cancer: From RNA Regulation to Therapeutic Potential. *Journal of Cellular and Molecular Medicine*, *29*(13). https://doi.org/10.1111/jcmm.70675

Jin, M., Lee, W. K., You, M.-H., Jang, A., Cheng, S., Kim, W. G., Jeon, M. J., & Lee, Y.-M. (2021). SHMT2 expression as a diagnostic and prognostic marker for thyroid cancer. *Endocrine Connections*, *10*(6), 630–636. https://doi.org/10.1530/EC-21-0135

Jin, Y., Jung, S.-N., Lim, M. A., Oh, C., Piao, Y., Kim, H. J., Nguyena, Q., Kang, Y. E., Chang, J. W., Won, H.-R., & Koo, B. S. (2022). SHMT2 Induces Stemness and Progression of Head and Neck Cancer. *International Journal of Molecular Sciences*, *23*(17), 9714. https://doi.org/10.3390/ijms23179714

Jing, X., Yang, F., Shao, C., Wei, K., Xie, M., Shen, H., & Shu, Y. (2019). Role of hypoxia in cancer therapy by regulating the tumor microenvironment. *Molecular Cancer*, *18*(1), 157. https://doi.org/10.1186/s12943-019-1089-9

Jonasch, E., Donskov, F., Iliopoulos, O., Rathmell, W. K., Narayan, V. K., Maughan, B. L., Oudard, S., Else, T., Maranchie, J. K., Welsh, S. J., Thamake, S., Park, E. K., Perini, R. F., Linehan, W. M., & Srinivasan, R. (2021). Belzutifan for Renal Cell Carcinoma in von Hippel–Lindau Disease. *New England Journal of Medicine*, *385*(22), 2036–2046. https://doi.org/10.1056/NEJMoa2103425

Kaanders, J. H. A. M., Wijffels, K. I. E. M., Marres, H. A. M., Ljungkvist, A. S. E., Pop, L. A. M., van den Hoogen, F. J. A., de Wilde, P. C. M., Bussink, J., Raleigh, J. A., & van der Kogel, A. J. (2002). Pimonidazole binding and tumor vascularity predict for treatment outcome in head and neck cancer. *Cancer Research*, *62*(23), 7066–7074.

Kaelin, W. G., & Ratcliffe, P. J. (2008). Oxygen Sensing by Metazoans: The Central Role of the HIF Hydroxylase Pathway. *Molecular Cell*, *30*(4), 393–402. https://doi.org/10.1016/j.molcel.2008.04.009

Kalhan, S. C., Gruca, L. L., Parimi, P. S., O'Brien, A., Dierker, L., & Burkett, E. (2003). Serine metabolism in human pregnancy. *American Journal of Physiology-Endocrinology and Metabolism*, *284*(4), E733–E740. https://doi.org/10.1152/ajpendo.00167.2002

Kalhan, S. C., Uppal, S. O., Moorman, J. L., Bennett, C., Gruca, L. L., Parimi, P. S., Dasarathy, S., Serre, D., & Hanson, R. W. (2011). Metabolic and Genomic Response to Dietary Isocaloric Protein Restriction in the Rat. *Journal of Biological Chemistry*, *286*(7), 5266–5277. https://doi.org/10.1074/jbc.M110.185991

Kamphorst, J. J., Chung, M. K., Fan, J., & Rabinowitz, J. D. (2014). Quantitative analysis of acetyl-CoA production in hypoxic cancer cells reveals substantial contribution from acetate. *Cancer & Metabolism*, *2*(1), 23. https://doi.org/10.1186/2049-3002-2-23

Kamphorst, J. J., Nofal, M., Commisso, C., Hackett, S. R., Lu, W., Grabocka, E., Vander Heiden, M. G., Miller, G., Drebin, J. A., Bar-Sagi, D., Thompson, C. B., & Rabinowitz, J. D. (2015). Human Pancreatic Cancer Tumors Are Nutrient Poor and Tumor Cells Actively Scavenge Extracellular Protein. *Cancer Research*, *75*(3), 544–553. https://doi.org/10.1158/0008-5472.CAN-14-2211

Kamura, T., Conrad, M. N., Yan, Q., Conaway, R. C., & Conaway, J. W. (1999). The Rbx1 subunit of SCF and VHL E3 ubiquitin ligase activates Rub1 modification of cullins Cdc53 and Cul2. *Genes & Development*, *13*(22), 2928–2933. https://doi.org/10.1101/gad.13.22.2928

Kamura, T., Koepp, D. M., Conrad, M. N., Skowyra, D., Moreland, R. J., Iliopoulos, O., Lane, W. S., Kaelin, W. G., Elledge, S. J., Conaway, R. C., Harper, J. W., & Conaway, J. W. (1999). Rbx1, a Component of the VHL Tumor Suppressor Complex and SCF Ubiquitin Ligase. *Science*, *284*(5414), 657–661. https://doi.org/10.1126/science.284.5414.657

Kanai, Y., Segawa, H., Miyamoto, K., Uchino, H., Takeda, E., & Endou, H. (1998). Expression Cloning and Characterization of a Transporter for Large Neutral Amino Acids Activated by the Heavy Chain of 4F2 Antigen (CD98). *Journal of Biological Chemistry*, *273*(37), 23629–23632. https://doi.org/10.1074/jbc.273.37.23629

Karam, J. A. Q., Fréreux, C., Mohanty, B. K., Dalton, A. C., Dincman, T. A., Palanisamy, V., Howley, B. V., & Howe, P. H. (2024). The RNA-binding protein PCBP1 modulates transcription by recruiting the G-quadruplex-specific helicase DHX9. *Journal of Biological Chemistry*, *300*(11), 107830. https://doi.org/10.1016/j.jbc.2024.107830

Ke, X., Chen, C., Song, Y., Cai, Q., Li, J., Tang, Y., Han, X., Qu, W., Chen, A., Wang, H., Xu, G., & Liu, D. (2019). Hypoxia modifies the polarization of macrophages and their inflammatory microenvironment, and inhibits malignant behavior in cancer cells. *Oncology Letters*. https://doi.org/10.3892/ol.2019.10956

Kim, J., Tchernyshyov, I., Semenza, G. L., & Dang, C. V. (2006). HIF-1-mediated expression of pyruvate dehydrogenase kinase: A metabolic switch required for cellular adaptation to hypoxia. *Cell Metabolism*, *3*(3), 177–185. https://doi.org/10.1016/j.cmet.2006.02.002

Koch, C. J. (2002). *Measurement of absolute oxygen levels in cells and tissues using oxygen sensors and 2-nitroimidazole EF5* (pp. 3–31). https://doi.org/10.1016/S0076-6879(02)52003-6

Koivunen, P., Hirsilä, M., Remes, A. M., Hassinen, I. E., Kivirikko, K. I., & Myllyharju, J. (2007). Inhibition of Hypoxia-inducible Factor (HIF) Hydroxylases by Citric Acid Cycle Intermediates. *Journal of Biological Chemistry*, *282*(7), 4524–4532. https://doi.org/10.1074/jbc.M610415200

Koritzinsky, M., Levitin, F., van den Beucken, T., Rumantir, R. A., Harding, N. J., Chu, K. C., Boutros, P. C., Braakman, I., & Wouters, B. G. (2013). Two phases of disulfide bond formation have differing requirements for oxygen. *Journal of Cell Biology*, *203*(4), 615–627. https://doi.org/10.1083/jcb.201307185

Kory, N., Wyant, G. A., Prakash, G., uit de Bos, J., Bottanelli, F., Pacold, M. E., Chan, S. H., Lewis, C. A., Wang, T., Keys, H. R., Guo, Y. E., & Sabatini, D. M. (2018). SFXN1 is a mitochondrial serine transporter required for one-carbon metabolism. *Science*, *362*(6416). https://doi.org/10.1126/science.aat9528

Koukourakis, M. I., Giatromanolaki, A., Sivridis, E., Bougioukas, G., Didilis, V., Gatter, K. C., & Harris, A. L. (2003). Lactate dehydrogenase-5 (LDH-5) overexpression in non-small-cell lung cancer tissues is linked to tumour hypoxia, angiogenic factor production and poor prognosis. *British Journal of Cancer*, *89*(5), 877–885. https://doi.org/10.1038/sj.bjc.6601205

Koumenis, C., Naczki, C., Koritzinsky, M., Rastani, S., Diehl, A., Sonenberg, N., Koromilas, A., & Wouters, B. G. (2002). Regulation of Protein Synthesis by Hypoxia via Activation of the Endoplasmic Reticulum Kinase PERK and Phosphorylation of the Translation Initiation Factor eIF2α. *Molecular and Cellular Biology*, *22*(21), 7405–7416. https://doi.org/10.1128/MCB.22.21.7405-7416.2002

Krupenko, N. I., Sharma, J., Pediaditakis, P., Helke, K. L., Hall, M. S., Du, X., Sumner, S., & Krupenko, S. A. (2020). Aldh1l2 knockout mouse metabolomics links the loss of the mitochondrial folate enzyme to deregulation of a lipid metabolism observed in rare human disorder. *Human Genomics*, *14*(1), 41. https://doi.org/10.1186/s40246-020-00291-3

Kshitiz, Afzal, J., Suhail, Y., Chang, H., Hubbi, M. E., Hamidzadeh, A., Goyal, R., Liu, Y., Sun, P., Nicoli, S., Dang, C. V., & Levchenko, A. (2022). Lactate-dependent chaperone-mediated autophagy induces oscillatory HIF-1α activity promoting proliferation of hypoxic cells. *Cell Systems*, *13*(12), 1048-1064.e7. https://doi.org/10.1016/j.cels.2022.11.003

Kyle, A. H., Huxham, L. A., Yeoman, D. M., & Minchinton, A. I. (2007). Limited Tissue Penetration of Taxanes: A Mechanism for Resistance in Solid Tumors. *Clinical Cancer Research*, *13*(9), 2804–2810. https://doi.org/10.1158/1078-0432.CCR-06-1941

Labuschagne, C. F., van den Broek, N. J. F., Mackay, G. M., Vousden, K. H., & Maddocks, O. D. K. (2014). Serine, but Not Glycine, Supports One-Carbon Metabolism and Proliferation of Cancer Cells. *Cell Reports*, *7*(4), 1248–1258. https://doi.org/10.1016/j.celrep.2014.04.045

Lafontaine, D. L. J., & Tollervey, D. (1999). Nop58p is a common component of the box C+D snoRNPs that is required for snoRNA stability. *RNA*, *5*(3), S135583829998192X. https://doi.org/10.1017/S135583829998192X

Lando, D., Peet, D. J., Whelan, D. A., Gorman, J. J., & Whitelaw, M. L. (2002). Asparagine Hydroxylation of the HIF Transactivation Domain: A Hypoxic Switch. *Science*, *295*(5556), 858–861. https://doi.org/10.1126/science.1068592

Lanzen, J., Braun, R. D., Klitzman, B., Brizel, D., Secomb, T. W., & Dewhirst, M. W. (2006). Direct Demonstration of Instabilities in Oxygen Concentrations within the Extravascular Compartment of an Experimental Tumor. *Cancer Research*, *66*(4), 2219–2223. https://doi.org/10.1158/0008-5472.CAN-03-2958

Laspata, N., Kaur, P., Mersaoui, S. Y., Muoio, D., Liu, Z. S., Bannister, M. H., Nguyen, H. D., Curry, C., Pascal, J. M., Poirier, G. G., Wang, H., Masson, J.-Y., & Fouquerel, E. (2023). PARP1 associates with

R-loops to promote their resolution and genome stability. *Nucleic Acids Research*, *51*(5), 2215–2237. https://doi.org/10.1093/nar/gkad066

Lee, A. S. (2005). The ER chaperone and signaling regulator GRP78/BiP as a monitor of endoplasmic reticulum stress. *Methods*, *35*(4), 373–381. https://doi.org/10.1016/j.ymeth.2004.10.010

Lee, C. M., Hwang, Y., Kim, M., Park, Y.-C., Kim, H., & Fang, S. (2024). PHGDH: a novel therapeutic target in cancer. *Experimental & Molecular Medicine*, *56*(7), 1513–1522. https://doi.org/10.1038/s12276-024-01268-1

Levental, K. R., Yu, H., Kass, L., Lakins, J. N., Egeblad, M., Erler, J. T., Fong, S. F. T., Csiszar, K., Giaccia, A., Weninger, W., Yamauchi, M., Gasser, D. L., & Weaver, V. M. (2009). Matrix Crosslinking Forces Tumor Progression by Enhancing Integrin Signaling. *Cell*, *139*(5), 891–906. https://doi.org/10.1016/j.cell.2009.10.027

Lewis, C. A., Parker, S. J., Fiske, B. P., McCloskey, D., Gui, D. Y., Green, C. R., Vokes, N. I., Feist, A. M., Vander Heiden, M. G., & Metallo, C. M. (2014). Tracing Compartmentalized NADPH Metabolism in the Cytosol and Mitochondria of Mammalian Cells. *Molecular Cell*, *55*(2), 253–263. https://doi.org/10.1016/j.molcel.2014.05.008

Li, C., Fu, C., Zhou, W., Li, H., Liu, Z., Wu, G., He, T., Shen, M., & Liu, H. (2025). Lactylation modification of HIF-1α enhances its stability by blocking VHL recognition. *Cell Communication and Signaling*, *23*(1), 364. https://doi.org/10.1186/s12964-025-02366-x

Li, J., Luo, X., Wei, M., Li, Z., Li, Y., Zhao, H., Miyagishi, M., Kasim, V., & Wu, S. (2023). YY2/PHGDH axis suppresses tumorigenesis by inhibiting tumor cell de novo serine biosynthesis. *Biomedicine & Pharmacotherapy*, *165*, 115006. https://doi.org/10.1016/j.biopha.2023.115006

Li, J., Quan, C., He, Y.-L., Cao, Y., Chen, Y., Wang, Y.-F., & Wu, L.-Y. (2022). Autophagy regulated by the HIF/REDD1/mTORC1 signaling is progressively increased during erythroid differentiation under hypoxia. *Frontiers in Cell and Developmental Biology*, *10*. https://doi.org/10.3389/fcell.2022.896893

Li, L., Li, Y., Timothy Sembiring Meliala, I., Kasim, V., & Wu, S. (2020). Biological roles of Yin Yang 2: Its implications in physiological and pathological events. *Journal of Cellular and Molecular Medicine*, *24*(22), 12886–12899. https://doi.org/10.1111/jcmm.15919

Li, X., Gracilla, D., Cai, L., Zhang, M., Yu, X., Chen, X., Zhang, J., Long, X., Ding, H.-F., & Yan, C. (2021). ATF3 promotes the serine synthesis pathway and tumor growth under dietary serine restriction. *Cell Reports*, *36*(12), 109706. https://doi.org/10.1016/j.celrep.2021.109706

Li, X., Zhang, W., Xu, T., Ramsey, J., Zhang, L., Hill, R., Hansen, K. C., Hesselberth, J. R., & Zhao, R. (2013). Comprehensive in vivo RNA-binding site analyses reveal a role of Prp8 in spliceosomal assembly. *Nucleic Acids Research*, *41*(6), 3805–3818. https://doi.org/10.1093/nar/gkt062

Liao, L., Ge, M., Zhan, Q., Huang, R., Ji, X., Liang, X., & Zhou, X. (2019). PSPH Mediates the Metastasis and Proliferation of Non-small Cell Lung Cancer through MAPK Signaling Pathways. *International Journal of Biological Sciences*, *15*(1), 183–194. https://doi.org/10.7150/ijbs.29203

Lin, W.-L., Chen, J.-K., Wen, X., He, W., Zarceno, G. A., Chen, Y., Chen, S., Paull, T. T., & Liu, H. (2022). DDX18 prevents R-loop-induced DNA damage and genome instability via PARP-1. *Cell Reports*, *40*(3), 111089. https://doi.org/10.1016/j.celrep.2022.111089

Liu, B., Jia, Y., Cao, Y., Wu, S., Jiang, H., Sun, X., Ma, J., Yin, X., Mao, A., & Shang, M. (2016). Overexpression of Phosphoserine Aminotransferase 1 (PSAT1) Predicts Poor Prognosis and Associates with Tumor Progression in Human Esophageal Squamous Cell Carcinoma. *Cellular Physiology and Biochemistry*, *39*(1), 395–406. https://doi.org/10.1159/000445633

Liu, C., Li, K., Sui, Y., Liu, H., Zhang, Y., Lu, Y., Lu, W., Chen, Y., Wang, G., Xu, S., Xiang, T., Cai, Y., & Huang, K. (2023). Different gene alterations in patients with non-small-cell lung cancer between the eastern and southern China. *Heliyon*, *9*(10), e20171. https://doi.org/10.1016/j.heliyon.2023.e20171

Liu, J., Guo, S., Li, Q., Yang, L., Xia, Z., Zhang, L., Huang, Z., & Zhang, N. (2013). Phosphoglycerate dehydrogenase induces glioma cells proliferation and invasion by stabilizing forkhead box M1. *Journal of Neuro-Oncology*, *111*(3), 245–255. https://doi.org/10.1007/s11060-012-1018-x

Liu, X., Liu, B., Wang, J., Liu, H., Wu, J., Qi, Y., Liu, Y., Zhu, H., Li, C., Yang, L., Song, J., Yao, G., Tian, W., Zhao, K., Han, L., Shu, K., Zhang, S., Man, J., You, C., … Li, R. (2025). PHGDH activation fuels glioblastoma progression and radioresistance via serine synthesis pathway. *Journal of Experimental & Clinical Cancer Research*, *44*(1), 99. https://doi.org/10.1186/s13046-025-03361-3

Liu, Y., Song, X., Wang, X., Wei, L., Liu, X., Yuan, S., & Lv, L. (2010). Effect of chronic intermittent hypoxia on biological behavior and hypoxia-associated gene expression in lung cancer cells. *Journal of Cellular Biochemistry*, *111*(3), 554–563. https://doi.org/10.1002/jcb.22739

Locasale, J. W., & Cantley, L. C. (2011). Genetic selection for enhanced serine metabolism in cancer development. *Cell Cycle*, *10*(22), 3812–3813. https://doi.org/10.4161/cc.10.22.18224

Locasale, J. W., Grassian, A. R., Melman, T., Lyssiotis, C. A., Mattaini, K. R., Bass, A. J., Heffron, G., Metallo, C. M., Muranen, T., Sharfi, H., Sasaki, A. T., Anastasiou, D., Mullarky, E., Vokes, N. I., Sasaki, M., Beroukhim, R., Stephanopoulos, G., Ligon, A. H., Meyerson, M., … Vander Heiden, M. G. (2011a). Phosphoglycerate dehydrogenase diverts glycolytic flux and contributes to oncogenesis. *Nature Genetics*, *43*(9), 869–874. https://doi.org/10.1038/ng.890

Locasale, J. W., Grassian, A. R., Melman, T., Lyssiotis, C. A., Mattaini, K. R., Bass, A. J., Heffron, G., Metallo, C. M., Muranen, T., Sharfi, H., Sasaki, A. T., Anastasiou, D., Mullarky, E., Vokes, N. I., Sasaki, M., Beroukhim, R., Stephanopoulos, G., Ligon, A. H., Meyerson, M., … Vander Heiden, M. G. (2011b). Phosphoglycerate dehydrogenase diverts glycolytic flux and contributes to oncogenesis. *Nature Genetics*, *43*(9), 869–874. https://doi.org/10.1038/ng.890

Lonergan, K. M., Iliopoulos, O., Ohh, M., Kamura, T., Conaway, R. C., Conaway, J. W., & Kaelin, W. G. (1998). Regulation of Hypoxia-Inducible mRNAs by the von Hippel-Lindau Tumor Suppressor Protein Requires Binding to Complexes Containing Elongins B/C and Cul2. *Molecular and Cellular Biology*, *18*(2), 732–741. https://doi.org/10.1128/MCB.18.2.732

Lu, H., Dalgard, C. L., Mohyeldin, A., McFate, T., Tait, A. S., & Verma, A. (2005). Reversible Inactivation of HIF-1 Prolyl Hydroxylases Allows Cell Metabolism to Control Basal HIF-1. *Journal of Biological Chemistry*, *280*(51), 41928–41939. https://doi.org/10.1074/jbc.M508718200

Lu, H., Forbes, R. A., & Verma, A. (2002). Hypoxia-inducible Factor 1 Activation by Aerobic Glycolysis Implicates the Warburg Effect in Carcinogenesis. *Journal of Biological Chemistry*, *277*(26), 23111–23115. https://doi.org/10.1074/jbc.M202487200

Ma, C., Zheng, K., Jiang, K., Zhao, Q., Sha, N., Wang, W., Yan, M., Chen, T., Zhao, Y., & Jiang, Y. (2021). The alternative activity of nuclear PHGDH contributes to tumour growth under nutrient stress. *Nature Metabolism*, *3*(10), 1357–1371. https://doi.org/10.1038/s42255-021-00456-x

Ma, E. H., Bantug, G., Griss, T., Condotta, S., Johnson, R. M., Samborska, B., Mainolfi, N., Suri, V., Guak, H., Balmer, M. L., Verway, M. J., Raissi, T. C., Tsui, H., Boukhaled, G., Henriques da Costa, S., Frezza, C., Krawczyk, C. M., Friedman, A., Manfredi, M., … Jones, R. G. (2017). Serine Is an Essential Metabolite for Effector T Cell Expansion. *Cell Metabolism*, *25*(2), 345–357. https://doi.org/10.1016/j.cmet.2016.12.011

Ma, T. S., Worth, K. R., Maher, C., Ng, N., Beghè, C., Gromak, N., Rose, A. M., & Hammond, E. M. (2023). Hypoxia-induced transcriptional stress is mediated by ROS-induced R-loops. *Nucleic Acids Research*. https://doi.org/10.1093/nar/gkad858

Ma, X., Li, B., Liu, J., Fu, Y., & Luo, Y. (2019). Phosphoglycerate dehydrogenase promotes pancreatic cancer development by interacting with eIF4A1 and eIF4E. *Journal of Experimental & Clinical Cancer Research*, *38*(1), 66. https://doi.org/10.1186/s13046-019-1053-y

Mackenzie, B., Schäfer, M. K.-H., Erickson, J. D., Hediger, M. A., Weihe, E., & Varoqui, H. (2003). Functional Properties and Cellular Distribution of the System A Glutamine Transporter SNAT1 Support Specialized Roles in Central Neurons. *Journal of Biological Chemistry*, *278*(26), 23720–23730. https://doi.org/10.1074/jbc.M212718200

Maddocks, O. D. K., Athineos, D., Cheung, E. C., Lee, P., Zhang, T., van den Broek, N. J. F., Mackay, G. M., Labuschagne, C. F., Gay, D., Kruiswijk, F., Blagih, J., Vincent, D. F., Campbell, K. J., Ceteci, F., Sansom, O. J., Blyth, K., & Vousden, K. H. (2017). Modulating the therapeutic response of tumours to dietary serine and glycine starvation. *Nature*, *544*(7650), 372–376. https://doi.org/10.1038/nature22056

Maddocks, O. D. K., Berkers, C. R., Mason, S. M., Zheng, L., Blyth, K., Gottlieb, E., & Vousden, K. H. (2013). Serine starvation induces stress and p53-dependent metabolic remodelling in cancer cells. *Nature*, *493*(7433), 542–546. https://doi.org/10.1038/nature11743

Maddocks, O. D. K., Labuschagne, C. F., Adams, P. D., & Vousden, K. H. (2016). Serine Metabolism Supports the Methionine Cycle and DNA/RNA Methylation through De Novo ATP Synthesis in Cancer Cells. *Molecular Cell*, *61*(2), 210–221. https://doi.org/10.1016/j.molcel.2015.12.014

Mahon, P. C., Hirota, K., & Semenza, G. L. (2001). FIH-1: a novel protein that interacts with HIF-1α and VHL to mediate repression of HIF-1 transcriptional activity. *Genes & Development*, *15*(20), 2675–2686. https://doi.org/10.1101/gad.924501

Maman, S., & Witz, I. P. (2018). A history of exploring cancer in context. *Nature Reviews Cancer*, *18*(6), 359–376. https://doi.org/10.1038/s41568-018-0006-7

Marí, M., Morales, A., Colell, A., García-Ruiz, C., & Fernández-Checa, J. C. (2009). Mitochondrial Glutathione, a Key Survival Antioxidant. *Antioxidants & Redox Signaling*, *11*(11), 2685–2700. https://doi.org/10.1089/ars.2009.2695

Marsin, A.-S., Bouzin, C., Bertrand, L., & Hue, L. (2002). The Stimulation of Glycolysis by Hypoxia in Activated Monocytes Is Mediated by AMP-activated Protein Kinase and Inducible 6-Phosphofructo-2-kinase. *Journal of Biological Chemistry*, *277*(34), 30778–30783. https://doi.org/10.1074/jbc.M205213200

Mathupala, S. P., Rempel, A., & Pedersen, P. L. (2001). Glucose Catabolism in Cancer Cells. *Journal of Biological Chemistry*, *276*(46), 43407–43412. https://doi.org/10.1074/jbc.M108181200

Mattaini, K. R., Sullivan, M. R., & Vander Heiden, M. G. (2016). The importance of serine metabolism in cancer. *Journal of Cell Biology*, *214*(3), 249–257. https://doi.org/10.1083/jcb.201604085

Maxwell, P. H., Wiesener, M. S., Chang, G.-W., Clifford, S. C., Vaux, E. C., Cockman, M. E., Wykoff, C. C., Pugh, C. W., Maher, E. R., & Ratcliffe, P. J. (1999). The tumour suppressor protein VHL targets hypoxia-inducible factors for oxygen-dependent proteolysis. *Nature*, *399*(6733), 271–275. https://doi.org/10.1038/20459

Maynard, M. A., Evans, A. J., Hosomi, T., Hara, S., Jewett, M. A. S., & Ohh, M. (2005). Human HIF-3α4 is a dominant-negative regulator of HIF-1 and is down-regulated in renal cell carcinoma. *The FASEB Journal*, *19*(11), 1396–1406. https://doi.org/10.1096/fj.05-3788com

Mazina, O. M., Somarowthu, S., Kadyrova, L. Y., Baranovskiy, A. G., Tahirov, T. H., Kadyrov, F. A., & Mazin, A. V. (2020). Replication protein A binds RNA and promotes R-loop formation. *Journal of Biological Chemistry*, *295*(41), 14203–14213. https://doi.org/10.1074/jbc.RA120.013812

McAleese, C. E., Choudhury, C., Butcher, N. J., & Minchin, R. F. (2021). Hypoxia-mediated drug resistance in breast cancers. *Cancer Letters*, *502*, 189–199. https://doi.org/10.1016/j.canlet.2020.11.045

McCabe, A., Martin, S., Rowe, S., Shah, J., Morgan, P. S., Borys, D., & Panek, R. (2024). Oxygen-enhanced MRI assessment of tumour hypoxia in head and neck cancer is feasible and well tolerated in the clinical setting. *European Radiology Experimental*, *8*(1), 27. https://doi.org/10.1186/s41747-024-00429-1

McKeown, S. R. (2014). Defining normoxia, physoxia and hypoxia in tumours—implications for treatment response. *The British Journal of Radiology*, *87*(1035), 20130676. https://doi.org/10.1259/bjr.20130676

McMahon, M., Ayllón, V., Panov, K. I., & O'Connor, R. (2010). Ribosomal 18 S RNA Processing by the IGF-I-responsive WDR3 Protein Is Integrated with p53 Function in Cancer Cell Proliferation. *Journal of Biological Chemistry*, *285*(24), 18309–18318. https://doi.org/10.1074/jbc.M110.108555

McNamee, M. J., Michod, D., & Niklison-Chirou, M. V. (2021). Can small molecular inhibitors that stop de novo serine synthesis be used in cancer treatment? *Cell Death Discovery*, *7*(1), 87. https://doi.org/10.1038/s41420-021-00474-4

Mellacheruvu, D., Wright, Z., Couzens, A. L., Lambert, J.-P., St-Denis, N. A., Li, T., Miteva, Y. V, Hauri, S., Sardiu, M. E., Low, T. Y., Halim, V. A., Bagshaw, R. D., Hubner, N. C., al-Hakim, A., Bouchard, A., Faubert, D., Fermin, D., Dunham, W. H., Goudreault, M., … Nesvizhskii, A. I. (2013). The CRAPome: a contaminant repository for affinity purification–mass spectrometry data. *Nature Methods*, *10*(8), 730–736. https://doi.org/10.1038/nmeth.2557

Mentch, S. J., Mehrmohamadi, M., Huang, L., Liu, X., Gupta, D., Mattocks, D., Gómez Padilla, P., Ables, G., Bamman, M. M., Thalacker-Mercer, A. E., Nichenametla, S. N., & Locasale, J. W. (2015). Histone Methylation Dynamics and Gene Regulation Occur through the Sensing of One-Carbon Metabolism. *Cell Metabolism*, *22*(5), 861–873. https://doi.org/10.1016/j.cmet.2015.08.024

Meredith, M. J., & Reed, D. J. (1982). Status of the mitochondrial pool of glutathione in the isolated hepatocyte. *Journal of Biological Chemistry*, *257*(7), 3747–3753. https://doi.org/10.1016/S0021-9258(18)34844-0

Metallo, C. M., Gameiro, P. A., Bell, E. L., Mattaini, K. R., Yang, J., Hiller, K., Jewell, C. M., Johnson, Z. R., Irvine, D. J., Guarente, L., Kelleher, J. K., Vander Heiden, M. G., Iliopoulos, O., & Stephanopoulos, G. (2012). Reductive glutamine metabolism by IDH1 mediates lipogenesis under hypoxia. *Nature*, *481*(7381), 380–384. https://doi.org/10.1038/nature10602

Mezghrani, A., Fassio, A., Benham, A., Simmen, T., Braakman, I., & Sitia, R. (2001). Manipulation of oxidative protein folding and PDI redox state in mammalian cells. *The EMBO Journal*, *20*(22), 6288–6296. https://doi.org/10.1093/emboj/20.22.6288

Michel, B., Sinha, A. K., & Leach, D. R. F. (2018). Replication Fork Breakage and Restart in Escherichia coli. *Microbiology and Molecular Biology Reviews*, *82*(3). https://doi.org/10.1128/MMBR.00013-18

Mills, G. C. (1957). Hemoglobin Catabolism: I. Glutathione Peroxidase, An Erythrocyte Enzyme Which Protects Hemoglobin From Oxidative Breakdown. *Journal of Biological Chemistry*, *229*(1), 189–197. https://doi.org/10.1016/S0021-9258(18)70608-X

Mims, J., Bansal, N., Bharadwaj, M. S., Chen, X., Molina, A. J., Tsang, A. W., & Furdui, C. M. (2015). Energy Metabolism in a Matched Model of Radiation Resistance for Head and Neck Squamous Cell Cancer. *Radiation Research*, *183*(3), 291–304. https://doi.org/10.1667/RR13828.1

Minakata, K., Takahashi, F., Nara, T., Hashimoto, M., Tajima, K., Murakami, A., Nurwidya, F., Yae, S., Koizumi, F., Moriyama, H., Seyama, K., Nishio, K., & Takahashi, K. (2012). Hypoxia induces gefitinib resistance in non-small-cell lung cancer with both mutant and wild-type epidermal growth factor receptors. *Cancer Science*, *103*(11), 1946–1954. https://doi.org/10.1111/j.1349-7006.2012.02408.x

Minchenko, A., Leshchinsky, I., Opentanova, I., Sang, N., Srinivas, V., Armstead, V., & Caro, J. (2002). Hypoxia-inducible Factor-1-mediated Expression of the 6-Phosphofructo-2-kinase/fructose-2,6-bisphosphatase-3 (PFKFB3) Gene. *Journal of Biological Chemistry*, *277*(8), 6183–6187. https://doi.org/10.1074/jbc.M110978200

Mistry, I. N., Thomas, M., Calder, E. D. D., Conway, S. J., & Hammond, E. M. (2017). Clinical Advances of Hypoxia-Activated Prodrugs in Combination With Radiation Therapy. *International Journal of Radiation Oncology*Biology*Physics*, *98*(5), 1183–1196. https://doi.org/10.1016/j.ijrobp.2017.03.024

Moore, G. E., Gerner, R. E., & Franklin, H. A. (1967). Culture of normal human leukocytes. *JAMA*, *199*(8), 519–524.

Mor, I., Cheung, E. C., & Vousden, K. H. (2011). Control of Glycolysis through Regulation of PFK1: Old Friends and Recent Additions. *Cold Spring Harbor Symposia on Quantitative Biology*, *76*(0), 211–216. https://doi.org/10.1101/sqb.2011.76.010868

Mullarky, E., Lucki, N. C., Beheshti Zavareh, R., Anglin, J. L., Gomes, A. P., Nicolay, B. N., Wong, J. C. Y., Christen, S., Takahashi, H., Singh, P. K., Blenis, J., Warren, J. D., Fendt, S.-M., Asara, J. M., DeNicola, G. M., Lyssiotis, C. A., Lairson, L. L., & Cantley, L. C. (2016). Identification of a small molecule inhibitor of 3-phosphoglycerate dehydrogenase to target serine biosynthesis in cancers. *Proceedings of the National Academy of Sciences*, *113*(7), 1778–1783. https://doi.org/10.1073/pnas.1521548113

Mullarky, E., Xu, J., Robin, A. D., Huggins, D. J., Jennings, A., Noguchi, N., Olland, A., Lakshminarasimhan, D., Miller, M., Tomita, D., Michino, M., Su, T., Zhang, G., Stamford, A. W., Meinke, P. T., Kargman, S., & Cantley, L. C. (2019). Inhibition of 3-phosphoglycerate dehydrogenase (PHGDH) by indole amides abrogates de novo serine synthesis in cancer cells. *Bioorganic & Medicinal Chemistry Letters*, *29*(17), 2503–2510. https://doi.org/10.1016/j.bmcl.2019.07.011

Mullen, A. R., Wheaton, W. W., Jin, E. S., Chen, P.-H., Sullivan, L. B., Cheng, T., Yang, Y., Linehan, W. M., Chandel, N. S., & DeBerardinis, R. J. (2012). Reductive carboxylation supports growth in tumour cells with defective mitochondria. *Nature*, *481*(7381), 385–388. https://doi.org/10.1038/nature10642

Munir, R., Lisec, J., Swinnen, J. V., & Zaidi, N. (2019). Lipid metabolism in cancer cells under metabolic stress. *British Journal of Cancer*, *120*(12), 1090–1098. https://doi.org/10.1038/s41416-019-0451-4

Murphy, M. P. (2009). How mitochondria produce reactive oxygen species. *Biochemical Journal*, *417*(1), 1–13. https://doi.org/10.1042/BJ20081386

Muthusamy, T., Cordes, T., Handzlik, M. K., You, L., Lim, E. W., Gengatharan, J., Pinto, A. F. M., Badur, M. G., Kolar, M. J., Wallace, M., Saghatelian, A., & Metallo, C. M. (2020). Serine restriction alters

sphingolipid diversity to constrain tumour growth. *Nature*, *586*(7831), 790–795. https://doi.org/10.1038/s41586-020-2609-x

Nakano, H., Murai, S., & Moriwaki, K. (2022). Regulation of the release of damage-associated molecular patterns from necroptotic cells. *Biochemical Journal*, *479*(5), 677–685. https://doi.org/10.1042/BCJ20210604

Noman, M. Z., Desantis, G., Janji, B., Hasmim, M., Karray, S., Dessen, P., Bronte, V., & Chouaib, S. (2014). PD-L1 is a novel direct target of HIF-1α, and its blockade under hypoxia enhanced MDSC-mediated T cell activation. *Journal of Experimental Medicine*, *211*(5), 781–790. https://doi.org/10.1084/jem.20131916

Nordlund, P., & Reichard, P. (2006). Ribonucleotide Reductases. *Annual Review of Biochemistry*, *75*(1), 681–706. https://doi.org/10.1146/annurev.biochem.75.103004.142443

Nordsmark, M., Bentzen, S. M., & Overgaard, J. (1994). Measurement of Human Tumour Oxygenation Status by a Polarographic Needle Electrode: An analysis of inter- and intratumour heterogeneity. *Acta Oncologica*, *33*(4), 383–389. https://doi.org/10.3109/02841869409098433

Nordsmark, M., & Overgaard, J. (2000). A confirmatory prognostic study on oxygenation status and loco-regional control in advanced head and neck squamous cell carcinoma treated by radiation therapy. *Radiotherapy and Oncology*, *57*(1), 39–43. https://doi.org/10.1016/S0167-8140(00)00223-1

Nowotny, M., Gaidamakov, S. A., Ghirlando, R., Cerritelli, S. M., Crouch, R. J., & Yang, W. (2007). Structure of Human RNase H1 Complexed with an RNA/DNA Hybrid: Insight into HIV Reverse Transcription. *Molecular Cell*, *28*(2), 264–276. https://doi.org/10.1016/j.molcel.2007.08.015

Obach, M., Navarro-Sabaté, À., Caro, J., Kong, X., Duran, J., Gómez, M., Perales, J. C., Ventura, F., Rosa, J. L., & Bartrons, R. (2004). 6-Phosphofructo-2-kinase (pfkfb3) Gene Promoter Contains Hypoxia-inducible Factor-1 Binding Sites Necessary for Transactivation in Response to Hypoxia. *Journal of Biological Chemistry*, *279*(51), 53562–53570. https://doi.org/10.1074/jbc.M406096200

Olcina, M., Lecane, P. S., & Hammond, E. M. (2010). Targeting Hypoxic Cells through the DNA Damage Response. *Clinical Cancer Research*, *16*(23), 5624–5629. https://doi.org/10.1158/1078-0432.CCR-10-0286

Olcina, M. M., Foskolou, I. P., Anbalagan, S., Senra, J. M., Pires, I. M., Jiang, Y., Ryan, A. J., & Hammond, E. M. (2013). Replication Stress and Chromatin Context Link ATM Activation to a Role in DNA Replication. *Molecular Cell*, *52*(5), 758–766. https://doi.org/10.1016/j.molcel.2013.10.019

Oppedisano, F., Pochini, L., Galluccio, M., Cavarelli, M., & Indiveri, C. (2004). Reconstitution into liposomes of the glutamine/amino acid transporter from renal cell plasma membrane: functional characterization, kinetics and activation by nucleotides. *Biochimica et Biophysica Acta (BBA) - Biomembranes*, *1667*(2), 122–131. https://doi.org/10.1016/j.bbamem.2004.09.007

Orimo, A., Gupta, P. B., Sgroi, D. C., Arenzana-Seisdedos, F., Delaunay, T., Naeem, R., Carey, V. J., Richardson, A. L., & Weinberg, R. A. (2005). Stromal Fibroblasts Present in Invasive Human Breast Carcinomas Promote Tumor Growth and Angiogenesis through Elevated SDF-1/CXCL12 Secretion. *Cell*, *121*(3), 335–348. https://doi.org/10.1016/j.cell.2005.02.034

Oskolkova, O. V., Afonyushkin, T., Leitner, A., von Schlieffen, E., Gargalovic, P. S., Lusis, A. J., Binder, B. R., & Bochkov, V. N. (2008). ATF4-dependent transcription is a key mechanism in VEGF up-regulation by oxidized phospholipids: critical role of oxidized sn-2 residues in activation of unfolded protein response. *Blood*, *112*(2), 330–339. https://doi.org/10.1182/blood-2007-09-112870

Ou, Y., Wang, S.-J., Jiang, L., Zheng, B., & Gu, W. (2015). p53 Protein-mediated Regulation of Phosphoglycerate Dehydrogenase (PHGDH) Is Crucial for the Apoptotic Response upon Serine Starvation. *Journal of Biological Chemistry*, *290*(1), 457–466. https://doi.org/10.1074/jbc.M114.616359

Ouyang, Y., Ou, Z., Zhong, W., Yang, J., Fu, S., Ouyang, N., Chen, J., Xu, L., Wu, D., Qian, J., Lin, Y., Lin, T., & Huang, J. (2023). *FGFR3* Alterations in Bladder Cancer Stimulate Serine Synthesis to Induce Immune-Inert Macrophages That Suppress T-cell Recruitment and Activation. *Cancer Research*, *83*(24), 4030–4046. https://doi.org/10.1158/0008-5472.CAN-23-1065

Pacold, M. E., Brimacombe, K. R., Chan, S. H., Rohde, J. M., Lewis, C. A., Swier, L. J. Y. M., Possemato, R., Chen, W. W., Sullivan, L. B., Fiske, B. P., Cho, S., Freinkman, E., Birsoy, K., Abu-Remaileh, M., Shaul, Y. D., Liu, C. M., Zhou, M., Koh, M. J., Chung, H., … Sabatini, D. M. (2016). A PHGDH inhibitor reveals coordination of serine synthesis and one-carbon unit fate. *Nature Chemical Biology*, *12*(6), 452–458. https://doi.org/10.1038/nchembio.2070

Paget, S. (1889). THE DISTRIBUTION OF SECONDARY GROWTHS IN CANCER OF THE BREAST. *The Lancet*, *133*(3421), 571–573. https://doi.org/10.1016/S0140-6736(00)49915-0

Papalazarou, V., Newman, A. C., Huerta-Uribe, A., Legrave, N. M., Falcone, M., Zhang, T., McGarry, L., Athineos, D., Shanks, E., Blyth, K., Vousden, K. H., & Maddocks, O. D. K. (2023). Phenotypic profiling of solute carriers characterizes serine transport in cancer. *Nature Metabolism*, *5*(12), 2148–2168. https://doi.org/10.1038/s42255-023-00936-2

Papandreou, I., Cairns, R. A., Fontana, L., Lim, A. L., & Denko, N. C. (2006). HIF-1 mediates adaptation to hypoxia by actively downregulating mitochondrial oxygen consumption. *Cell Metabolism*, *3*(3), 187–197. https://doi.org/10.1016/j.cmet.2006.01.012

Pauneto, C. del M. A., Riesenberg, B. P., Gandy, E. J., Kennedy, A. S., Clutton, G. T., Hem, J. W., Hurst, K. E., Hunt, E. G., Green, J. M., Miller, B. C., Angus, S. P., Johnson, G. L., Esther, R. J., Guerriero, J. L., Gao, P., Soto-Pantoja, D. R., Ferris, R. L., Modliszewski, J. L., Coleman, M. F., … Thaxton, J. E. (2025). Intra-tumoral hypoxia promotes CD8+ T cell dysfunction via chronic activation of integrated stress response transcription factor ATF4. *Immunity*, *58*(10), 2489-2504.e8. https://doi.org/10.1016/j.immuni.2025.09.003

Peng, Y., Yuan, J., Zhang, Z., & Chang, X. (2017). Cytoplasmic poly(A)-binding protein 1 (PABPC1) interacts with the RNA-binding protein hnRNPLL and thereby regulates immunoglobulin secretion in plasma cells. *Journal of Biological Chemistry*, *292*(29), 12285–12295. https://doi.org/10.1074/jbc.M117.794834

Petri, B. J., Piell, K. M., Wilt, A. E., Howser, A. D., Winkler, L., Whitworth, M. R., Valdes, B. L., Lehman, N. L., Clem, B. F., & Klinge, C. M. (2023). MicroRNA regulation of the serine synthesis pathway in endocrine-resistant breast cancer cells. *Endocrine-Related Cancer*, *30*(11). https://doi.org/10.1530/ERC-23-0148

Pires, I. M., Bencokova, Z., Milani, M., Folkes, L. K., Li, J.-L., Stratford, M. R., Harris, A. L., & Hammond, E. M. (2010). Effects of Acute versus Chronic Hypoxia on DNA Damage Responses and Genomic Instability. *Cancer Research*, *70*(3), 925–935. https://doi.org/10.1158/0008-5472.CAN-09-2715

Possemato, R., Marks, K. M., Shaul, Y. D., Pacold, M. E., Kim, D., Birsoy, K., Sethumadhavan, S., Woo, H.-K., Jang, H. G., Jha, A. K., Chen, W. W., Barrett, F. G., Stransky, N., Tsun, Z.-Y., Cowley, G. S., Barretina, J., Kalaany, N. Y., Hsu, P. P., Ottina, K., … Sabatini, D. M. (2011). Functional genomics reveal that the serine synthesis pathway is essential in breast cancer. *Nature*, *476*(7360), 346–350. https://doi.org/10.1038/nature10350

Quéré, I., Paul, V., Rouillac, C., Janbon, C., London, J., Demaille, J., Kamoun, P., Dufier, J.-L., Abitbol, M., & Chassé, J.-F. (1999). Spatial and Temporal Expression of the Cystathionine β-Synthase Gene During Early Human Development. *Biochemical and Biophysical Research Communications*, *254*(1), 127–137. https://doi.org/10.1006/bbrc.1998.9079

Racker, E. (1954). *Alternate Pathways of Glucose and Fructose Metabolism* (pp. 141–182). https://doi.org/10.1002/9780470122600.ch4

Racker, E. (1955). Glutathione Reductase From Bakers' Yeast And Beef Liver. *Journal of Biological Chemistry*, *217*(2), 855–865. https://doi.org/10.1016/S0021-9258(18)65950-2

Ramachandran, S., Ma, T. S., Griffin, J., Ng, N., Foskolou, I. P., Hwang, M.-S., Victori, P., Cheng, W.-C., Buffa, F. M., Leszczynska, K. B., El-Khamisy, S. F., Gromak, N., & Hammond, E. M. (2021). Hypoxia-induced SETX links replication stress with the unfolded protein response. *Nature Communications*, *12*(1), 3686. https://doi.org/10.1038/s41467-021-24066-z

Ravez, S., Corbet, C., Spillier, Q., Dutu, A., Robin, A. D., Mullarky, E., Cantley, L. C., Feron, O., & Frédérick, R. (2017). α-Ketothioamide Derivatives: A Promising Tool to Interrogate Phosphoglycerate Dehydrogenase (PHGDH). *Journal of Medicinal Chemistry*, *60*(4), 1591–1597. https://doi.org/10.1021/acs.jmedchem.6b01166

Rawat, V., Malvi, P., Della Manna, D., Yang, E. S., Bugide, S., Zhang, X., Gupta, R., & Wajapeyee, N. (2021). PSPH promotes melanoma growth and metastasis by metabolic deregulation-mediated transcriptional activation of NR4A1. *Oncogene*, *40*(13), 2448–2462. https://doi.org/10.1038/s41388-021-01683-y

Reczek, C. R., & Chandel, N. S. (2017). The Two Faces of Reactive Oxygen Species in Cancer. *Annual Review of Cancer Biology*, *1*(1), 79–98. https://doi.org/10.1146/annurev-cancerbio-041916-065808

Riddle, S. R., Ahmad, A., Ahmad, S., Deeb, S. S., Malkki, M., Schneider, B. K., Allen, C. B., & White, C. W. (2000). Hypoxia induces hexokinase II gene expression in human lung cell line A549. *American Journal of Physiology-Lung Cellular and Molecular Physiology*, *278*(2), L407–L416. https://doi.org/10.1152/ajplung.2000.278.2.L407

Robles-Oteíza, C., Hastings, K., Choi, J., Sirois, I., Ravi, A., Expósito, F., de Miguel, F., Knight, J. R., López-Giráldez, F., Choi, H., Socci, N. D., Merghoub, T., Awad, M., Getz, G., Gainor, J., Hellmann, M. D., Caron, É., Kaech, S. M., & Politi, K. (2025). Hypoxia is linked to acquired resistance to immune checkpoint inhibitors in lung cancer. *Journal of Experimental Medicine*, *222*(1). https://doi.org/10.1084/jem.20231106

Rohde, J. M., Brimacombe, K. R., Liu, L., Pacold, M. E., Yasgar, A., Cheff, D. M., Lee, T. D., Rai, G., Baljinnyam, B., Li, Z., Simeonov, A., Hall, M. D., Shen, M., Sabatini, D. M., & Boxer, M. B. (2018). Discovery and optimization of piperazine-1-thiourea-based human phosphoglycerate dehydrogenase inhibitors. *Bioorganic & Medicinal Chemistry*, *26*(8), 1727–1739. https://doi.org/10.1016/j.bmc.2018.02.016

Rosenberg, D., Artoul, S., Segal, A. C., Kolodney, G., Radzishevsky, I., Dikopoltsev, E., Foltyn, V. N., Inoue, R., Mori, H., Billard, J.-M., & Wolosker, H. (2013). Neuronal d-Serine and Glycine Release Via the Asc-1 Transporter Regulates NMDA Receptor-Dependent Synaptic Activity. *The Journal of Neuroscience*, *33*(8), 3533–3544. https://doi.org/10.1523/JNEUROSCI.3836-12.2013

Rossi, M., Altea-Manzano, P., Demicco, M., Doglioni, G., Bornes, L., Fukano, M., Vandekeere, A., Cuadros, A. M., Fernández-García, J., Riera-Domingo, C., Jauset, C., Planque, M., Alkan, H. F., Nittner, D., Zuo, D., Broadfield, L. A., Parik, S., Pane, A. A., Rizzollo, F., … Fendt, S.-M. (2022).

PHGDH heterogeneity potentiates cancer cell dissemination and metastasis. *Nature*, *605*(7911), 747–753. https://doi.org/10.1038/s41586-022-04758-2

Rubinstein, M. R., Wang, X., Liu, W., Hao, Y., Cai, G., & Han, Y. W. (2013). Fusobacterium nucleatum Promotes Colorectal Carcinogenesis by Modulating E-Cadherin/β-Catenin Signaling via its FadA Adhesin. *Cell Host & Microbe*, *14*(2), 195–206. https://doi.org/10.1016/j.chom.2013.07.012

Ryu, K.-J., Park, S.-M., Park, S.-H., Kim, I.-K., Han, H., Kim, H.-J., Kim, S.-H., Hong, K.-S., Kim, H., Kim, M., Yoon, S.-J., Asaithambi, K., Lee, K. H., Park, J.-Y., Hah, Y.-S., Cho, H. J., Yook, J. I., Yang, J. W., Ko, G.-H., … Yoo, J. (2019). p38 Stabilizes Snail by Suppressing DYRK2-Mediated Phosphorylation That Is Required for GSK3β-βTrCP–Induced Snail Degradation. *Cancer Research*, *79*(16), 4135–4148. https://doi.org/10.1158/0008-5472.CAN-19-0049

Rzymski, T., Milani, M., Pike, L., Buffa, F., Mellor, H. R., Winchester, L., Pires, I., Hammond, E., Ragoussis, I., & Harris, A. L. (2010). Regulation of autophagy by ATF4 in response to severe hypoxia. *Oncogene*, *29*(31), 4424–4435. https://doi.org/10.1038/onc.2010.191

Salberg, U. B., Skingen, V. E., Fjeldbo, C. S., Hompland, T., Ragnum, H. B., Vlatkovic, L., Hole, K. H., Seierstad, T., & Lyng, H. (2022). A prognostic hypoxia gene signature with low heterogeneity within the dominant tumour lesion in prostate cancer patients. *British Journal of Cancer*, *127*(2), 321–328. https://doi.org/10.1038/s41416-022-01782-x

Sanchez, A., Tripathy, D., Yin, X., Desobry, K., Martinez, J., Riley, J., Gay, D., Luo, J., & Grammas, P. (2012). p38 MAPK: A Mediator of Hypoxia-Induced Cerebrovascular Inflammation. *Journal of Alzheimer's Disease*, *32*(3), 587–597. https://doi.org/10.3233/JAD-2012-120829

Sánchez-Castillo, A., Heylen, E., Hounjet, J., Savelkouls, K. G., Lieuwes, N. G., Biemans, R., Dubois, L. J., Reynders, K., Rouschop, K. M., Vaes, R. D. W., De Keersmaecker, K., Lambrecht, M., Hendriks, L. E. L., De Ruysscher, D. K. M., Vooijs, M., & Kampen, K. R. (2024). Targeting serine/glycine metabolism improves radiotherapy response in non-small cell lung cancer. *British Journal of Cancer*, *130*(4), 568–584. https://doi.org/10.1038/s41416-023-02553-y

Saxena, S., & Zou, L. (2022). Hallmarks of DNA replication stress. *Molecular Cell*, *82*(12), 2298–2314. https://doi.org/10.1016/j.molcel.2022.05.004

Schneider, M., Ströbele, S., Nonnenmacher, L., Siegelin, M. D., Tepper, M., Stroh, S., Hasslacher, S., Enzenmüller, S., Strauss, G., Baumann, B., Karpel-Massler, G., Westhoff, M., Debatin, K., & Halatsch, M. (2016). A paired comparison between glioblastoma "stem cells" and differentiated cells. *International Journal of Cancer*, *138*(7), 1709–1718. https://doi.org/10.1002/ijc.29908

Schroedl, C., McClintock, D. S., Budinger, G. R. S., & Chandel, N. S. (2002). Hypoxic but not anoxic stabilization of HIF-1α requires mitochondrial reactive oxygen species. *American Journal of Physiology-Lung Cellular and Molecular Physiology*, *283*(5), L922–L931. https://doi.org/10.1152/ajplung.00014.2002

Schug, Z. T., Peck, B., Jones, D. T., Zhang, Q., Grosskurth, S., Alam, I. S., Goodwin, L. M., Smethurst, E., Mason, S., Blyth, K., McGarry, L., James, D., Shanks, E., Kalna, G., Saunders, R. E., Jiang, M., Howell, M., Lassailly, F., Thin, M. Z., … Gottlieb, E. (2015). Acetyl-CoA Synthetase 2 Promotes Acetate Utilization and Maintains Cancer Cell Growth under Metabolic Stress. *Cancer Cell*, *27*(1), 57–71. https://doi.org/10.1016/j.ccell.2014.12.002

Scott, A. J., Mittal, A., Meghdadi, B., O'Brien, A., Bailleul, J., Sravya, P., Achreja, A., Zhou, W., Xu, J., Lin, A., Wilder-Romans, K., Liang, N., Kothari, A. U., Korimerla, N., Edwards, D. M., Wu, Z., Feng, J., Su, S., Zhang, L., … Wahl, D. R. (2025). Rewiring of cortical glucose metabolism fuels human brain cancer growth. *Nature*, *646*(8084), 413–422. https://doi.org/10.1038/s41586-025-09460-7

Segawa, H., Fukasawa, Y., Miyamoto, K., Takeda, E., Endou, H., & Kanai, Y. (1999). Identification and Functional Characterization of a Na+-independent Neutral Amino Acid Transporter with Broad Substrate Selectivity. *Journal of Biological Chemistry*, *274*(28), 19745–19751. https://doi.org/10.1074/jbc.274.28.19745

Selak, M. A., Armour, S. M., MacKenzie, E. D., Boulahbel, H., Watson, D. G., Mansfield, K. D., Pan, Y., Simon, M. C., Thompson, C. B., & Gottlieb, E. (2005). Succinate links TCA cycle dysfunction to oncogenesis by inhibiting HIF-α prolyl hydroxylase. *Cancer Cell*, *7*(1), 77–85. https://doi.org/10.1016/j.ccr.2004.11.022

Semenza, G. L. (2012). Hypoxia-Inducible Factors in Physiology and Medicine. *Cell*, *148*(3), 399–408. https://doi.org/10.1016/j.cell.2012.01.021

Semenza, G. L., Jiang, B.-H., Leung, S. W., Passantino, R., Concordet, J.-P., Maire, P., & Giallongo, A. (1996). Hypoxia Response Elements in the Aldolase A, Enolase 1, and Lactate Dehydrogenase A Gene Promoters Contain Essential Binding Sites for Hypoxia-inducible Factor 1. *Journal of Biological Chemistry*, *271*(51), 32529–32537. https://doi.org/10.1074/jbc.271.51.32529

Semenza, G. L., Roth, P. H., Fang, H. M., & Wang, G. L. (1994). Transcriptional regulation of genes encoding glycolytic enzymes by hypoxia-inducible factor 1. *The Journal of Biological Chemistry*, *269*(38), 23757–23763.

Sen, B., Benoit, B., & Brand, M. D. (2024). Hypoxia decreases mitochondrial ROS production in cells. *Free Radical Biology and Medicine*, *224*, 1–8. https://doi.org/10.1016/j.freeradbiomed.2024.08.016

Shen, J., Jin, Z., Lv, H., Jin, K., Jonas, K., Zhu, C., & Chen, B. (2020). PFKP is highly expressed in lung cancer and regulates glucose metabolism. *Cellular Oncology*, *43*(4), 617–629. https://doi.org/10.1007/s13402-020-00508-6

Shen, L., Zhang, J., Zheng, Z., Yang, F., Liu, S., Wu, Y., Chen, Y., Xu, T., Mao, S., Yan, Y., Li, W., Zhang, W., & Yao, X. (2022). PHGDH Inhibits Ferroptosis and Promotes Malignant Progression by Upregulating SLC7A11 in Bladder Cancer. *International Journal of Biological Sciences*, *18*(14), 5459–5474. https://doi.org/10.7150/ijbs.74546

Shibata, T., Giaccia, A. J., & Brown, J. M. (2000). Development of a hypoxia-responsive vector for tumor-specific gene therapy. *Gene Therapy*, *7*(6), 493–498. https://doi.org/10.1038/sj.gt.3301124

Shu, M., Liu, Y., & Wang, J. (2025). Protein post-translational modifications in serine synthetic pathway: functions and molecular mechanisms. *Cell Communication and Signaling*, *23*(1), 311. https://doi.org/10.1186/s12964-025-02327-4

Shu, Y., Hao, Y., Feng, J., Liu, H., Li, S., Feng, J., Jiang, Z., Ye, L., Zhou, Y., Sun, Y., Zhou, Z., Wei, H., Gao, P., Zhang, H., & Sun, L. (2022). Non-canonical phosphoglycerate dehydrogenase activity promotes liver cancer growth via mitochondrial translation and respiratory metabolism. *The EMBO Journal*, *41*(23). https://doi.org/10.15252/embj.2022111550

Skourti-Stathaki, K., Proudfoot, N. J., & Gromak, N. (2011). Human Senataxin Resolves RNA/DNA Hybrids Formed at Transcriptional Pause Sites to Promote Xrn2-Dependent Termination. *Molecular Cell*, *42*(6), 794–805. https://doi.org/10.1016/j.molcel.2011.04.026

Smith, A. L., Andrews, K. L., Beckmann, H., Bellon, S. F., Beltran, P. J., Booker, S., Chen, H., Chung, Y.-A., D'Angelo, N. D., Dao, J., Dellamaggiore, K. R., Jaeckel, P., Kendall, R., Labitzke, K., Long, A. M., Materna-Reichelt, S., Mitchell, P., Norman, M. H., Powers, D., … Lipford, J. R. (2015). Discovery of 1 *H* -Pyrazol-3(2 *H*)-ones as Potent and Selective Inhibitors of Protein Kinase R-like Endoplasmic Reticulum Kinase (PERK). *Journal of Medicinal Chemistry*, *58*(3), 1426–1441. https://doi.org/10.1021/jm5017494

Soca-Chafre, G., Montiel-Dávalos, A., Rosa-Velázquez, I. A. D. La, Caro-Sánchez, C. H. S., Peña-Nieves, A., & Arrieta, O. (2019). Multiple Molecular Targets Associated with Genomic Instability in Lung Cancer. *International Journal of Genomics*, *2019*, 1–8. https://doi.org/10.1155/2019/9584504

Sollier, J., Stork, C. T., García-Rubio, M. L., Paulsen, R. D., Aguilera, A., & Cimprich, K. A. (2014). Transcription-Coupled Nucleotide Excision Repair Factors Promote R-Loop-Induced Genome Instability. *Molecular Cell*, *56*(6), 777–785. https://doi.org/10.1016/j.molcel.2014.10.020

Spears, C. P., Shahinian, A. H., Moran, R. G., Heidelberger, C., & Corbett, T. H. (1982). In vivo kinetics of thymidylate synthetase inhibition of 5-fluorouracil-sensitive and -resistant murine colon adenocarcinomas. *Cancer Research*, *42*(2), 450–456.

Spiegelberg, L., Houben, R., Niemans, R., de Ruysscher, D., Yaromina, A., Theys, J., Guise, C. P., Smaill, J. B., Patterson, A. V., Lambin, P., & Dubois, L. J. (2019). Hypoxia-activated prodrugs and (lack of) clinical progress: The need for hypoxia-based biomarker patient selection in phase III clinical trials. *Clinical and Translational Radiation Oncology*, *15*, 62–69. https://doi.org/10.1016/j.ctro.2019.01.005

Spillier, Q., Vertommen, D., Ravez, S., Marteau, R., Thémans, Q., Corbet, C., Feron, O., Wouters, J., & Frédérick, R. (2019). Anti-alcohol abuse drug disulfiram inhibits human PHGDH via disruption of its active tetrameric form through a specific cysteine oxidation. *Scientific Reports*, *9*(1), 4737. https://doi.org/10.1038/s41598-019-41187-0

Su, K., Zhao, Z., Wang, Y., Sun, S., Liu, X., Zhang, C., Jiang, Y., & Du, X. (2024). NAT10 resolves harmful nucleolar R-loops depending on its helicase domain and acetylation of DDX21. *Cell Communication and Signaling*, *22*(1), 490. https://doi.org/10.1186/s12964-024-01869-3

Su, P., Yang, Y., & Zheng, H. (2026). The “serine code” of metabolic reprogramming: multidimensional roles of the serine synthesis pathway in tumors and novel breakthroughs for targeted therapy. *Frontiers in Immunology*, *17*. https://doi.org/10.3389/fimmu.2026.1779543

Sullivan, M. R., Danai, L. V, Lewis, C. A., Chan, S. H., Gui, D. Y., Kunchok, T., Dennstedt, E. A., Vander Heiden, M. G., & Muir, A. (2019). Quantification of microenvironmental metabolites in murine cancers reveals determinants of tumor nutrient availability. *ELife*, *8*. https://doi.org/10.7554/eLife.44235

Sun, L., Song, L., Wan, Q., Wu, G., Li, X., Wang, Y., Wang, J., Liu, Z., Zhong, X., He, X., Shen, S., Pan, X., Li, A., Wang, Y., Gao, P., Tang, H., & Zhang, H. (2015). cMyc-mediated activation of serine biosynthesis pathway is critical for cancer progression under nutrient deprivation conditions. *Cell Research*, *25*(4), 429–444. https://doi.org/10.1038/cr.2015.33

Takeda, K., Ho, V. C., Takeda, H., Duan, L.-J., Nagy, A., & Fong, G.-H. (2006). Placental but Not Heart Defects Are Associated with Elevated Hypoxia-Inducible Factor α Levels in Mice Lacking Prolyl Hydroxylase Domain Protein 2. *Molecular and Cellular Biology*, *26*(22), 8336–8346. https://doi.org/10.1128/MCB.00425-06

Tan, Y., Zhou, X., Gong, Y., Gou, K., Luo, Y., Jia, D., Dai, L., Zhao, Y., & Sun, Q. (2022). Biophysical and biochemical properties of PHGDH revealed by studies on PHGDH inhibitors. *Cellular and Molecular Life Sciences*, *79*(1), 27. https://doi.org/10.1007/s00018-021-04022-2

Tannock, I. F. (1968). The relation between cell proliferation and the vascular system in a transplanted mouse mammary tumour. *British Journal of Cancer*, *22*(2), 258–273. https://doi.org/10.1038/bjc.1968.34

Tannock, I. F. (1998). Conventional cancer therapy: promise broken or promise delayed? *The Lancet*, *351*, SII9–SII16. https://doi.org/10.1016/S0140-6736(98)90327-0

Tarhonskaya, H., Hardy, A. P., Howe, E. A., Loik, N. D., Kramer, H. B., McCullagh, J. S. O., Schofield, C. J., & Flashman, E. (2015). Kinetic Investigations of the Role of Factor Inhibiting Hypoxia-inducible Factor (FIH) as an Oxygen Sensor. *Journal of Biological Chemistry*, *290*(32), 19726–19742. https://doi.org/10.1074/jbc.M115.653014

Thomas, M., White, R. L., & Davis, R. W. (1976). Hybridization of RNA to double-stranded DNA: formation of R-loops. *Proceedings of the National Academy of Sciences*, *73*(7), 2294–2298. https://doi.org/10.1073/pnas.73.7.2294

Thomlinson, R. H., & Gray, L. H. (1955). The Histological Structure of Some Human Lung Cancers and the Possible Implications for Radiotherapy. *British Journal of Cancer*, *9*(4), 539–549. https://doi.org/10.1038/bjc.1955.55

Thompson, G. A., & Meister, A. (1976). Hydrolysis and transfer reactions catalyzed by γ-glutamyl transpeptidase; Evidence for separate substrate sites and for high affinity of L-cystine. *Biochemical and Biophysical Research Communications*, *71*(1), 32–36. https://doi.org/10.1016/0006-291X(76)90245-X

Thomson, D. J., Slevin, N. J., Baines, H., Betts, G., Bolton, S., Evans, M., Garcez, K., Irlam, J., Lee, L., Melillo, N., Mistry, H., More, E., Nutting, C., Price, J. M., Schipani, S., Sen, M., Yang, H., West, C. M., Aynsley, E., … Wood, K. (2024). Randomized Phase 3 Trial of the Hypoxia Modifier Nimorazole Added to Radiation Therapy With Benefit Assessed in Hypoxic Head and Neck Cancers Determined Using a Gene Signature (NIMRAD). *International Journal of Radiation Oncology*Biology*Physics*, *119*(3), 771–782. https://doi.org/10.1016/j.ijrobp.2023.11.055

Tombari, C., Zannini, A., Bertolio, R., Pedretti, S., Audano, M., Triboli, L., Cancila, V., Vacca, D., Caputo, M., Donzelli, S., Segatto, I., Vodret, S., Piazza, S., Rustighi, A., Mantovani, F., Belletti, B., Baldassarre, G., Blandino, G., Tripodo, C., … Del Sal, G. (2023). Mutant p53 sustains serine-glycine synthesis and essential amino acids intake promoting breast cancer growth. *Nature Communications*, *14*(1), 6777. https://doi.org/10.1038/s41467-023-42458-1

Trujillo, M. N., Jennings, E. Q., Farrera, D. O., Kitamura, N., Anderson, C. C., Gehrke, S., Reisz, J. A., Johannsen, M., Roede, J. R., D'Alessandro, A., & Galligan, J. J. (2025). Glyoxalase 2 Coordinates de Novo Serine Metabolism. *ChemBioChem*, *26*(7). https://doi.org/10.1002/cbic.202401086

Tumeh, P. C., Harview, C. L., Yearley, J. H., Shintaku, I. P., Taylor, E. J. M., Robert, L., Chmielowski, B., Spasic, M., Henry, G., Ciobanu, V., West, A. N., Carmona, M., Kivork, C., Seja, E., Cherry, G., Gutierrez, A. J., Grogan, T. R., Mateus, C., Tomasic, G., … Ribas, A. (2014). PD-1 blockade induces responses by inhibiting adaptive immune resistance. *Nature*, *515*(7528), 568–571. https://doi.org/10.1038/nature13954

Twigger, S. A., Dominguez, B., Porto, V., Hacker, L., Chalmers, A. J., Breckenridge, R., Treder, M., Sedgwick, A. C., Dominguez, F., & Hammond, E. M. (2024). The activity of therapeutic molecular cluster Ag5 is dependent on oxygen level and HIF-1 mediated signalling. *Redox Biology*, *76*, 103326. https://doi.org/10.1016/j.redox.2024.103326

Ullah, M. S., Davies, A. J., & Halestrap, A. P. (2006). The Plasma Membrane Lactate Transporter MCT4, but Not MCT1, Is Up-regulated by Hypoxia through a HIF-1α-dependent Mechanism. *Journal of Biological Chemistry*, *281*(14), 9030–9037. https://doi.org/10.1074/jbc.M511397200

Ummethum, H., Murriello, A. C., Werner, M., Márquez-Gómez, E., König, A.-C., Kruse, E., Lalonde, M., Trauner, M., Chanou, A., Weiβ, M., Lee, C. S. K., Ettinger, A., Erhard, F., Hauck, S. M., & Hamperl, S. (2025). The CGG triplet repeat binding protein 1 counteracts R-loop induced transcription-replication stress. *EMBO Reports*, *26*(19), 4691–4722. https://doi.org/10.1038/s44319-025-00550-1

Unterlass, J. E., Wood, R. J., Baslé, A., Tucker, J., Cano, C., Noble, M. M. E., & Curtin, N. J. (2017). Structural insights into the enzymatic activity and potential substrate promiscuity of human 3-phosphoglycerate dehydrogenase (PHGDH). *Oncotarget*, *8*(61), 104478–104491. https://doi.org/10.18632/oncotarget.22327

Utsunomiya-Tate, N., Endou, H., & Kanai, Y. (1996). Cloning and Functional Characterization of a System ASC-like Na+-dependent Neutral Amino Acid Transporter. *Journal of Biological Chemistry*, *271*(25), 14883–14890. https://doi.org/10.1074/jbc.271.25.14883

Valkenburg, K. C., de Groot, A. E., & Pienta, K. J. (2018). Targeting the tumour stroma to improve cancer therapy. *Nature Reviews Clinical Oncology*, *15*(6), 366–381. https://doi.org/10.1038/s41571-018-0007-1

Van de Gucht, M., Dufait, I., Kerkhove, L., Corbet, C., de Mey, S., Jiang, H., Law, K. L., Gevaert, T., Feron, O., & De Ridder, M. (2022). Inhibition of Phosphoglycerate Dehydrogenase Radiosensitizes Human Colorectal Cancer Cells under Hypoxic Conditions. *Cancers*, *14*(20), 5060. https://doi.org/10.3390/cancers14205060

Varia, M. A., Calkins-Adams, D. P., Rinker, L. H., Kennedy, A. S., Novotny, D. B., Fowler, W. C., & Raleigh, J. A. (1998). Pimonidazole: A Novel Hypoxia Marker for Complementary Study of Tumor Hypoxia and Cell Proliferation in Cervical Carcinoma. *Gynecologic Oncology*, *71*(2), 270–277. https://doi.org/10.1006/gyno.1998.5163

Vassin, V. M., Anantha, R. W., Sokolova, E., Kanner, S., & Borowiec, J. A. (2009). Human RPA phosphorylation by ATR stimulates DNA synthesis and prevents ssDNA accumulation during DNA-replication stress. *Journal of Cell Science*, *122*(22), 4070–4080. https://doi.org/10.1242/jcs.053702

Vaupel, P., Kallinowski, F., & Okunieff, P. (1989). Blood flow, oxygen and nutrient supply, and metabolic microenvironment of human tumors: a review. *Cancer Research*, *49*(23), 6449–6465.

Vazquez, A., Tedeschi, P. M., & Bertino, J. R. (2013). Overexpression of the Mitochondrial Folate and Glycine–Serine Pathway: A New Determinant of Methotrexate Selectivity in Tumors. *Cancer Research*, *73*(2), 478–482. https://doi.org/10.1158/0008-5472.CAN-12-3709

Virchow, R. (1863). *Die krankhaften Geschwülste (translated: The Morbid Growths)* (Vol. 1). August Hirschwald.

Wadsworth, B. J., Lee, C.-M., & Bennewith, K. L. (2022). Transiently hypoxic tumour cell turnover and radiation sensitivity in human tumour xenografts. *British Journal of Cancer*, *126*(11), 1616–1626. https://doi.org/10.1038/s41416-021-01691-5

Wagschal, A., Rousset, E., Basavarajaiah, P., Contreras, X., Harwig, A., Laurent-Chabalier, S., Nakamura, M., Chen, X., Zhang, K., Meziane, O., Boyer, F., Parrinello, H., Berkhout, B., Terzian, C., Benkirane, M., & Kiernan, R. (2012). Microprocessor, Setx, Xrn2, and Rrp6 Co-operate to Induce Premature Termination of Transcription by RNAPII. *Cell*, *150*(6), 1147–1157. https://doi.org/10.1016/j.cell.2012.08.004

Walsh, J. C., Lebedev, A., Aten, E., Madsen, K., Marciano, L., & Kolb, H. C. (2014). The Clinical Importance of Assessing Tumor Hypoxia: Relationship of Tumor Hypoxia to Prognosis and Therapeutic Opportunities. *Antioxidants & Redox Signaling*, *21*(10), 1516–1554. https://doi.org/10.1089/ars.2013.5378

Wang, C., An, S., Zhao, L., Li, S., Huang, J., & Ren, W. (2025). Moonlighting functions of phosphoglycerate dehydrogenase in cancer. *Cell Reports*, *44*(7), 115940. https://doi.org/10.1016/j.celrep.2025.115940

Wang, C., Huang, Y., Yang, Y., Li, R., Li, Y., Qiu, H., Wu, J., Shi, G., Ma, W., & Songyang, Z. (2024). ILF3 safeguards telomeres from aberrant homologous recombination as a telomeric R-loop reader. *Protein & Cell*, *15*(7), 493–511. https://doi.org/10.1093/procel/pwad054

Wang, C., Wan, X., Yu, T., Huang, Z., Shen, C., Qi, Q., Xiang, S., Chen, X., Arbely, E., Ling, Z.-Q., Liu, C.-Y., & Yu, W. (2020). Acetylation Stabilizes Phosphoglycerate Dehydrogenase by Disrupting the Interaction of E3 Ligase RNF5 to Promote Breast Tumorigenesis. *Cell Reports*, *32*(6), 108021. https://doi.org/10.1016/j.celrep.2020.108021

Wang, G. L., Jiang, B. H., Rue, E. A., & Semenza, G. L. (1995). Hypoxia-inducible factor 1 is a basic-helix-loop-helix-PAS heterodimer regulated by cellular O2 tension. *Proceedings of the National Academy of Sciences*, *92*(12), 5510–5514. https://doi.org/10.1073/pnas.92.12.5510

Wang, I. X., Grunseich, C., Fox, J., Burdick, J., Zhu, Z., Ravazian, N., Hafner, M., & Cheung, V. G. (2018). Human proteins that interact with RNA/DNA hybrids. *Genome Research*, *28*(9), 1405–1414. https://doi.org/10.1101/gr.237362.118

Wang, J., Xie, G.-F., He, Y., Deng, L., Long, Y.-K., Yang, X.-H., Ma, J.-J., Gong, R., Cen, W.-J., Ye, Z.-L., Zeng, Y.-X., Wang, H.-Y., & Shao, J.-Y. (2019). Interfering Expression of Chimeric Transcript *SEPT7P2-PSPH* Promotes Cell Proliferation in Patients with Nasopharyngeal Carcinoma. *Journal of Oncology*, *2019*, 1–10. https://doi.org/10.1155/2019/1654724

Wang, J., Zhu, W., Han, J., Yang, X., Zhou, R., Lu, H., Yu, H., Yuan, W., Li, P., Tao, J., Lu, Q., Wei, J., & Yang, H. (2021). The role of the HIF-1α/ALYREF/PKM2 axis in glycolysis and tumorigenesis of bladder cancer. *Cancer Communications*, *41*(7), 560–575. https://doi.org/10.1002/cac2.12158

Wang, K., Luo, L., Fu, S., Wang, M., Wang, Z., Dong, L., Wu, X., Dai, L., Peng, Y., Shen, G., Chen, H.-N., Nice, E. C., Wei, X., & Huang, C. (2023). PHGDH arginine methylation by PRMT1 promotes serine synthesis and represents a therapeutic vulnerability in hepatocellular carcinoma. *Nature Communications*, *14*(1), 1011. https://doi.org/10.1038/s41467-023-36708-5

Wang, Q., Liberti, M. V., Liu, P., Deng, X., Liu, Y., Locasale, J. W., & Lai, L. (2017). Rational Design of Selective Allosteric Inhibitors of PHGDH and Serine Synthesis with Anti-tumor Activity. *Cell Chemical Biology*, *24*(1), 55–65. https://doi.org/10.1016/j.chembiol.2016.11.013

Wang, W., Wang, M., Du, T., Hou, Z., You, S., Zhang, S., Ji, M., Xue, N., & Chen, X. (2023). SHMT2 Promotes Gastric Cancer Development through Regulation of HIF1α/VEGF/STAT3 Signaling. *International Journal of Molecular Sciences*, *24*(8), 7150. https://doi.org/10.3390/ijms24087150

Wang, Y., Li, Z.-X., Wang, J.-G., Li, L.-H., Shen, W.-L., & Dang, X.-W. (2023). Deubiquitinating enzyme Josephin-2 stabilizes PHGDH to promote a cancer stem cell phenotype in hepatocellular carcinoma. *Genes & Genomics*, *45*(2), 215–224. https://doi.org/10.1007/s13258-022-01356-4

Warburg, O. (1925). über den Stoffwechsel der Carcinomzelle. *Klinische Wochenschrift*, *4*(12), 534–536. https://doi.org/10.1007/BF01726151

Warburg, O. (1956). On the Origin of Cancer Cells. *Science*, *123*(3191), 309–314. https://doi.org/10.1126/science.123.3191.309

Weinstabl, H., Treu, M., Rinnenthal, J., Zahn, S. K., Ettmayer, P., Bader, G., Dahmann, G., Kessler, D., Rumpel, K., Mischerikow, N., Savarese, F., Gerstberger, T., Mayer, M., Zoephel, A., Schnitzer, R., Sommergruber, W., Martinelli, P., Arnhof, H., Peric-Simov, B., … McConnell, D. B. (2019). Intracellular Trapping of the Selective Phosphoglycerate Dehydrogenase (PHGDH) Inhibitor **BI-4924** Disrupts Serine Biosynthesis. *Journal of Medicinal Chemistry*, *62*(17), 7976–7997. https://doi.org/10.1021/acs.jmedchem.9b00718

Welsh, S., Williams, R., Kirkpatrick, L., Paine-Murrieta, G., & Powis, G. (2004). Antitumor activity and pharmacodynamic properties of PX-478, an inhibitor of hypoxia-inducible factor-1alpha. *Molecular Cancer Therapeutics*, *3*(3), 233–244.

Wenger, R. H., Kvietikova, I., Rolfs, A., Camenisch, G., & Gassmann, M. (1998). Oxygen-regulated erythropoietin gene expression is dependent on a CpG methylation-free hypoxia-inducible factor-1 DNA-binding site. *European Journal of Biochemistry*, *253*(3), 771–777. https://doi.org/10.1046/j.1432-1327.1998.2530771.x

Winter, S. C., Buffa, F. M., Silva, P., Miller, C., Valentine, H. R., Turley, H., Shah, K. A., Cox, G. J., Corbridge, R. J., Homer, J. J., Musgrove, B., Slevin, N., Sloan, P., Price, P., West, C. M. L., & Harris, A. L. (2007). Relation of a Hypoxia Metagene Derived from Head and Neck Cancer to Prognosis of Multiple Cancers. *Cancer Research*, *67*(7), 3441–3449. https://doi.org/10.1158/0008-5472.CAN-06-3322

Wise, D. R., Ward, P. S., Shay, J. E. S., Cross, J. R., Gruber, J. J., Sachdeva, U. M., Platt, J. M., DeMatteo, R. G., Simon, M. C., & Thompson, C. B. (2011). Hypoxia promotes isocitrate dehydrogenase-dependent carboxylation of α-ketoglutarate to citrate to support cell growth and viability. *Proceedings of the National Academy of Sciences*, *108*(49), 19611–19616. https://doi.org/10.1073/pnas.1117773108

Wishart, D. S., Jewison, T., Guo, A. C., Wilson, M., Knox, C., Liu, Y., Djoumbou, Y., Mandal, R., Aziat, F., Dong, E., Bouatra, S., Sinelnikov, I., Arndt, D., Xia, J., Liu, P., Yallou, F., Bjorndahl, T., Perez-Pineiro, R., Eisner, R., … Scalbert, A. (2012). HMDB 3.0—The Human Metabolome Database in 2013. *Nucleic Acids Research*, *41*(D1), D801–D807. https://doi.org/10.1093/nar/gks1065

Wohlkoenig, C., Leithner, K., Deutsch, A., Hrzenjak, A., Olschewski, A., & Olschewski, H. (2011). Hypoxia-induced cisplatin resistance is reversible and growth rate independent in lung cancer cells. *Cancer Letters*, *308*(2), 134–143. https://doi.org/10.1016/j.canlet.2011.03.014

Wood, S. M., Wiesener, M. S., Yeates, K. M., Okada, N., Pugh, C. W., Maxwell, P. H., & Ratcliffe, P. J. (1998). Selection and Analysis of a Mutant Cell Line Defective in the Hypoxia-inducible Factor-1 α-Subunit (HIF-1α). *Journal of Biological Chemistry*, *273*(14), 8360–8368. https://doi.org/10.1074/jbc.273.14.8360

Wouters, B. G., & Brown, J. M. (1997). Cells at intermediate oxygen levels can be more important than the “hypoxic fraction” in determining tumor response to fractionated radiotherapy. *Radiation Research*, *147*(5), 541–550.

Wu, Q., Chen, X., Li, J., & Sun, S. (2020). Serine and Metabolism Regulation: A Novel Mechanism in Antitumor Immunity and Senescence. *Aging and Disease*, *11*(6), 1640. https://doi.org/10.14336/AD.2020.0314

Wu, T., Nance, J., Chu, F., & Fazzio, T. G. (2021). Characterization of R-Loop–Interacting Proteins in Embryonic Stem Cells Reveals Roles in rRNA Processing and Gene Expression. *Molecular & Cellular Proteomics*, *20*, 100142. https://doi.org/10.1016/j.mcpro.2021.100142

Wu, Y., Tang, L., Huang, H., Yu, Q., Hu, B., Wang, G., Ge, F., Yin, T., Li, S., & Yu, X. (2023). Phosphoglycerate dehydrogenase activates PKM2 to phosphorylate histone H3T11 and attenuate cellular senescence. *Nature Communications*, *14*(1), 1323. https://doi.org/10.1038/s41467-023-37094-8

Wu, Y.-Q., Zhang, C.-S., Xiong, J., Cai, D.-Q., Wang, C.-Z., Wang, Y., Liu, Y.-H., Wang, Y., Li, Y., Wu, J., Wu, J., Lan, B., Wang, X., Chen, S., Cao, X., Wei, X., Hu, H.-H., Guo, H., Yu, Y., … Lin, S.-C. (2023). Low glucose metabolite 3-phosphoglycerate switches PHGDH from serine synthesis to p53 activation to control cell fate. *Cell Research*, *33*(11), 835–850. https://doi.org/10.1038/s41422-023-00874-4

Xiong, J., Cheng, S., Cai, H., Qiu, Y.-R., & Zhao, W. L. (2024). DDX3X Mutation Endow R-Loop-Dependent Lymphomagenesis. *Blood*, *144*(Supplement 1), 5756–5756. https://doi.org/10.1182/blood-2024-206718

Xu, D., Dai, W., Kutzler, L., Lacko, H. A., Jefferson, L. S., Dennis, M. D., & Kimball, S. R. (2020). ATF4-Mediated Upregulation of REDD1 and Sestrin2 Suppresses mTORC1 Activity during Prolonged Leucine Deprivation. *The Journal of Nutrition*, *150*(5), 1022–1030. https://doi.org/10.1093/jn/nxz309

Xu, L., Pathak, P. S., & Fukumura, D. (2004). Hypoxia-Induced Activation of p38 Mitogen-Activated Protein Kinase and Phosphatidylinositol 3'-Kinase Signaling Pathways Contributes to Expression of Interleukin 8 in Human Ovarian Carcinoma Cells. *Clinical Cancer Research*, *10*(2), 701–707. https://doi.org/10.1158/1078-0432.CCR-0953-03

Xu, R., Jones, W., Wilcz-Villega, E., Costa, A. S., Rajeeve, V., Bentham, R. B., Bryson, K., Nagano, A., Yaman, B., Olendo Barasa, S., Wang, Y., Chelala, C., Cutillas, P., Szabadkai, G., Frezza, C., & Bianchi, K. (2020). The breast cancer oncogene IKKε coordinates mitochondrial function and serine metabolism. *EMBO Reports*, *21*(9). https://doi.org/10.15252/embr.201948260

Xu, Z., Li, X.-F., Zou, H., Sun, X., & Shen, B. (2017). 18F-Fluoromisonidazole in tumor hypoxia imaging. *Oncotarget*, *8*(55), 94969–94979. https://doi.org/10.18632/oncotarget.21662

Yan, Q., Wulfridge, P., Doherty, J., Fernandez-Luna, J. L., Real, P. J., Tang, H.-Y., & Sarma, K. (2022). Proximity labeling identifies a repertoire of site-specific R-loop modulators. *Nature Communications*, *13*(1), 53. https://doi.org/10.1038/s41467-021-27722-6

Yang, L., & West, C. M. (2018). Hypoxia gene expression signatures as predictive biomarkers for personalising radiotherapy. *The British Journal of Radiology*, *92*(1093). https://doi.org/10.1259/bjr.20180036

Yang, M., & Vousden, K. H. (2016). Serine and one-carbon metabolism in cancer. *Nature Reviews Cancer*, *16*(10), 650–662. https://doi.org/10.1038/nrc.2016.81

Yang, W., Xia, Y., Hawke, D., Li, X., Liang, J., Xing, D., Aldape, K., Hunter, T., Alfred Yung, W. K., & Lu, Z. (2012). PKM2 Phosphorylates Histone H3 and Promotes Gene Transcription and Tumorigenesis. *Cell*, *150*(4), 685–696. https://doi.org/10.1016/j.cell.2012.07.018

Yang, Y., Li, S., Yang, Y., Li, Q., Liu, Y., & Cao, J. (2024). ATF4/PHGDH mediates the effects of ER stress on cadmium-induced autophagy and glycolysis. *Toxicology*, *509*, 153976. https://doi.org/10.1016/j.tox.2024.153976

Ye, J., Fan, J., Venneti, S., Wan, Y.-W., Pawel, B. R., Zhang, J., Finley, L. W. S., Lu, C., Lindsten, T., Cross, J. R., Qing, G., Liu, Z., Simon, M. C., Rabinowitz, J. D., & Thompson, C. B. (2014). Serine Catabolism Regulates Mitochondrial Redox Control during Hypoxia. *Cancer Discovery*, *4*(12), 1406–1417. https://doi.org/10.1158/2159-8290.CD-14-0250

Ye, J., Mancuso, A., Tong, X., Ward, P. S., Fan, J., Rabinowitz, J. D., & Thompson, C. B. (2012). Pyruvate kinase M2 promotes de novo serine synthesis to sustain mTORC1 activity and cell proliferation. *Proceedings of the National Academy of Sciences*, *109*(18), 6904–6909. https://doi.org/10.1073/pnas.1204176109

Yin, K. (2015). Positive correlation between expression level of mitochondrial serine hydroxymethyltransferase and breast cancer grade. *OncoTargets and Therapy*, 1069. https://doi.org/10.2147/OTT.S82433

Ying, Y., Wu, Y., Zhang, F., Tang, Y., Yi, J., Ma, X., Li, J., Chen, D., Wang, X., Liu, X., Liu, B., Luo, J., Zheng, X., & Xie, L. (2024). Co-transcriptional R-loops-mediated epigenetic regulation drives growth

retardation and docetaxel chemosensitivity enhancement in advanced prostate cancer. *Molecular Cancer*, *23*(1), 79. https://doi.org/10.1186/s12943-024-01994-0

Yoo, H. C., Park, S. J., Nam, M., Kang, J., Kim, K., Yeo, J. H., Kim, J.-K., Heo, Y., Lee, H. S., Lee, M. Y., Lee, C. W., Kang, J. S., Kim, Y.-H., Lee, J., Choi, J., Hwang, G.-S., Bang, S., & Han, J. M. (2020). A Variant of SLC1A5 Is a Mitochondrial Glutamine Transporter for Metabolic Reprogramming in Cancer Cells. *Cell Metabolism*, *31*(2), 267-283.e12. https://doi.org/10.1016/j.cmet.2019.11.020

Yoo, I., Ahn, I., Lee, J., & Lee, N. (2024). Extracellular flux assay (Seahorse assay): Diverse applications in metabolic research across biological disciplines. *Molecules and Cells*, *47*(8), 100095. https://doi.org/10.1016/j.mocell.2024.100095

Yoshii, Y., Furukawa, T., Yoshii, H., Mori, T., Kiyono, Y., Waki, A., Kobayashi, M., Tsujikawa, T., Kudo, T., Okazawa, H., Yonekura, Y., & Fujibayashi, Y. (2009). Cytosolic acetyl-CoA synthetase affected tumor cell survival under hypoxia: the possible function in tumor acetyl-CoA/acetate metabolism. *Cancer Science*, *100*(5), 821–827. https://doi.org/10.1111/j.1349-7006.2009.01099.x

Young, R. M., Wang, S.-J., Gordan, J. D., Ji, X., Liebhaber, S. A., & Simon, M. C. (2008). Hypoxia-mediated Selective mRNA Translation by an Internal Ribosome Entry Site-independent Mechanism. *Journal of Biological Chemistry*, *283*(24), 16309–16319. https://doi.org/10.1074/jbc.M710079200

Yu, K., Chedin, F., Hsieh, C.-L., Wilson, T. E., & Lieber, M. R. (2003). R-loops at immunoglobulin class switch regions in the chromosomes of stimulated B cells. *Nature Immunology*, *4*(5), 442–451. https://doi.org/10.1038/ni919

Yu, T., Guo, F., Yu, Y., Sun, T., Ma, D., Han, J., Qian, Y., Kryczek, I., Sun, D., Nagarsheth, N., Chen, Y., Chen, H., Hong, J., Zou, W., & Fang, J.-Y. (2017). Fusobacterium nucleatum Promotes Chemoresistance to Colorectal Cancer by Modulating Autophagy. *Cell*, *170*(3), 548-563.e16. https://doi.org/10.1016/j.cell.2017.07.008

Yu, Y., Wang, Q., Wei, Y., Liu, J., Wang, G., Wang, Z., Shen, W., Han, L., Li, C., Lei, C.-Q., Xu, S., & Zhu, Q. (2025). Nucleophosmin 1 inhibits the replication of influenza A virus by competitively binding viral RNA with viral proteins. *Virologica Sinica*, *40*(3), 388–400. https://doi.org/10.1016/j.virs.2025.04.007

Yu, Z., Mersaoui, S. Y., Guitton-Sert, L., Coulombe, Y., Song, J., Masson, J.-Y., & Richard, S. (2020). DDX5 resolves R-loops at DNA double-strand breaks to promote DNA repair and avoid chromosomal deletions. *NAR Cancer*, *2*(3). https://doi.org/10.1093/narcan/zcaa028

Yuan, L., & Kaplowitz, N. (2009). Glutathione in liver diseases and hepatotoxicity. *Molecular Aspects of Medicine*, *30*(1–2), 29–41. https://doi.org/10.1016/j.mam.2008.08.003

Yun, H. J., Li, M., Guo, D., Jeon, S. M., Park, S. H., Lim, J. S., Lee, S. Bin, Liu, R., Du, L., Kim, S.-H., Shin, T. H., Eyun, S., Park, Y.-Y., Lu, Z., & Lee, J.-H. (2023). AMPK-HIF-1α signaling enhances glucose-derived de novo serine biosynthesis to promote glioblastoma growth. *Journal of Experimental & Clinical Cancer Research*, *42*(1), 340. https://doi.org/10.1186/s13046-023-02927-3

Zeman, M. K., & Cimprich, K. A. (2014). Causes and consequences of replication stress. *Nature Cell Biology*, *16*(1), 2–9. https://doi.org/10.1038/ncb2897

Zhang, D., Li, A. M., Hu, G., Huang, M., Yang, F., Zhang, L., Wellen, K. E., Xu, X., Conn, C. S., Zou, W., Kahn, M., Rhoades, S. D., Weljie, A. M., Fuchs, S. Y., Amankulor, N., Yoshor, D., Ye, J., Koumenis, C., Gong, Y., & Fan, Y. (2023). PHGDH-mediated endothelial metabolism drives glioblastoma resistance to chimeric antigen receptor T cell immunotherapy. *Cell Metabolism*, *35*(3), 517-534.e8. https://doi.org/10.1016/j.cmet.2023.01.010

Zhang, D., Tang, Z., Huang, H., Zhou, G., Cui, C., Weng, Y., Liu, W., Kim, S., Lee, S., Perez-Neut, M., Ding, J., Czyz, D., Hu, R., Ye, Z., He, M., Zheng, Y. G., Shuman, H. A., Dai, L., Ren, B., … Zhao, Y. (2019).

Metabolic regulation of gene expression by histone lactylation. *Nature*, *574*(7779), 575–580. https://doi.org/10.1038/s41586-019-1678-1

Zhang, L., Fok, J. J. L., Mirabella, F., Aronson, L. I., Fryer, R. A., Workman, P., Morgan, G. J., & Davies, F. E. (2013). Hsp70 inhibition induces myeloma cell death via the intracellular accumulation of immunoglobulin and the generation of proteotoxic stress. *Cancer Letters*, *339*(1), 49–59. https://doi.org/10.1016/j.canlet.2013.07.023

Zhang, W., Yin, C., Qi, L., Liu, Z., Xu, R., Tu, C., & Li, Z. (2025). RFWD3 Reprograms Nucleotide Metabolism Through PHGDH to Induce Chemoresistance In Osteosarcoma. *Advanced Science*, *12*(16). https://doi.org/10.1002/advs.202410937

Zhang, W., Zhang, M., Gao, C., Zhang, Y., Ge, Y., Guo, S., Guo, X., Zhou, Z., Liu, Q., Zhang, Y., Ma, C., Tao, F., & Xu, P. (2017). Coupling between <scp>d</scp> -3-phosphoglycerate dehydrogenase and <scp>d</scp> -2-hydroxyglutarate dehydrogenase drives bacterial <scp>l</scp> -serine synthesis. *Proceedings of the National Academy of Sciences*, *114*(36). https://doi.org/10.1073/pnas.1619034114

Zhang, X., Wang, S., Li, W., Wang, J., Gong, Y., Chen, Q., Cao, S., Pang, D., & Gao, S. (2024). PSAT1 Promotes Metastasis via p-AKT/SP1/ITGA2 Axis in Estrogen Receptor-Negative Breast Cancer Cell. *Biomolecules*, *14*(8), 990. https://doi.org/10.3390/biom14080990

Zhang, Z., Yang, D., Yan, X., Qiu, Q., Guo, J., & Qiu, L. (2024). KPNB1-ATF4 induces BNIP3-dependent mitophagy to drive odontoblastic differentiation in dental pulp stem cells. *Cellular & Molecular Biology Letters*, *29*(1), 145. https://doi.org/10.1186/s11658-024-00664-9

Zhao, E., Ding, J., Xia, Y., Liu, M., Ye, B., Choi, J.-H., Yan, C., Dong, Z., Huang, S., Zha, Y., Yang, L., Cui, H., & Ding, H.-F. (2016). KDM4C and ATF4 Cooperate in Transcriptional Control of Amino Acid Metabolism. *Cell Reports*, *14*(3), 506–519. https://doi.org/10.1016/j.celrep.2015.12.053

Zhao, J.-Y., Feng, K.-R., Wang, F., Zhang, J.-W., Cheng, J. F., Lin, G.-Q., Gao, D., & Tian, P. (2021). A retrospective overview of PHGDH and its inhibitors for regulating cancer metabolism. *European Journal of Medicinal Chemistry*, *217*, 113379. https://doi.org/10.1016/j.ejmech.2021.113379

Zhao, N., Cao, Y., Tao, R., Zhu, X., Li, R., Chen, Y., Tao, K., Li, L., Chen, H., & Ma, X. (2024). The circMYBL2-Encoded p185 Protein Suppresses Colorectal Cancer Progression by Inhibiting Serine Biosynthesis. *Cancer Research*, *84*(13), 2155–2168. https://doi.org/10.1158/0008-5472.CAN-23-2940

Zhao, Q., Li, Y., Tan, B., Fan, L., Yang, P., & Tian, Y. (2015). HIF-1α Induces Multidrug Resistance in Gastric Cancer Cells by Inducing MiR-27a. *PLOS ONE*, *10*(8), e0132746. https://doi.org/10.1371/journal.pone.0132746

Zheng, M., Guo, J., Xu, J., Yang, K., Tang, R., Gu, X., Li, H., & Chen, L. (2019). Ixocarpalactone A from dietary tomatillo inhibits pancreatic cancer growth by targeting PHGDH. *Food & Function*, *10*(6), 3386–3395. https://doi.org/10.1039/C9FO00394K

Zheng, R., Dunlap, M., Bobkov, G. O. M., Gonzalez-Figueroa, C., Patel, K. J., Lyu, J., Harvey, S. E., Chan, T. W., Quinones-Valdez, G., Choudhury, M., Le Roux, C. A., Bartels, M. D., Vuong, A., Flynn, R. A., Chang, H. Y., Van Nostrand, E. L., Xiao, X., & Cheng, C. (2024). hnRNPM protects against the dsRNA-mediated interferon response by repressing LINE-associated cryptic splicing. *Molecular Cell*, *84*(11), 2087-2103.e8. https://doi.org/10.1016/j.molcel.2024.05.004

Zhou, J., Xu, Y., Liu, J., Feng, L., Yu, J., & Chen, D. (2024). Global burden of lung cancer in 2022 and projections to 2050: Incidence and mortality estimates from GLOBOCAN. *Cancer Epidemiology*, *93*, 102693. https://doi.org/10.1016/j.canep.2024.102693

Zhou, Z., Ye, S., Chen, J., Dai, F., Chen, L., Ye, R., Zhang, J., Chen, G., Wang, Y., & Liu, Y. (2025). ATF4 promotes glutaminolysis and glycolysis in colorectal cancer by transcriptionally inducing SLC1A5. *Acta Biochimica et Biophysica Sinica*, *57*(7), 1093–1105. https://doi.org/10.3724/abbs.2024226

Zhu, H., Chua, M. L. K., Chitapanarux, I., Kaidar-Person, O., Mwaba, C., Alghamdi, M., Rodríguez Mignola, A., Amrogowicz, N., Yazici, G., Bourhaleb, Z., Mahmood, H., Faruque, G. M., Thiagarajan, M., Acharki, A., Ma, M., Harutyunyan, M., Sriplung, H., Chen, Y., Camacho, R., … Abdel-Wahab, M. (2024). Global radiotherapy demands and corresponding radiotherapy-professional workforce requirements in 2022 and predicted to 2050: a population-based study. *The Lancet Global Health*, *12*(12), e1945–e1953. https://doi.org/10.1016/S2214-109X(24)00355-3

Zhu, H., Yu, H., Zhou, H., Zhu, W., & Wang, X. (2023). Elevated Nuclear PHGDH Synergistically Functions with cMyc to Reshape the Immune Microenvironment of Liver Cancer. *Advanced Science*, *10*(17). https://doi.org/10.1002/advs.202205818

Zhu, J., Ma, J., Wang, X., Ma, T., Zhang, S., Wang, W., Zhou, X., & Shi, J. (2016). High Expression of PHGDH Predicts Poor Prognosis in Non–Small Cell Lung Cancer. *Translational Oncology*, *9*(6), 592–599. https://doi.org/10.1016/j.tranon.2016.08.003

Zou, L., & Elledge, S. J. (2003). Sensing DNA Damage Through ATRIP Recognition of RPA-ssDNA Complexes. *Science*, *300*(5625), 1542–1548. https://doi.org/10.1126/science.1083430

Cell Death Discovery

https://doi.org/10.1038/s41420-026-03194-9

Article in Press

PHGDH loss promotes hypoxia tolerance through glycolytic reprogramming and enhanced HIF-1 activity

Received: 9 February 2026

Revised: 19 May 2026

Accepted: 4 June 2026

Cite this article as: Petrosyan, E., Martin, L.A., Legge, I. *et al.* PHGDH loss promotes hypoxia tolerance through glycolytic reprogramming and enhanced HIF-1 activity. *Cell Death Discov.* (2026). https://doi.org/10.1038/s41420-026-03194-9

Eduard Petrosyan, Louise A. W. Martin, Isabelle Legge, John Walsby-Tickle, Adam C. Sedgwick, Mark A. Hill, James S. O. McCullagh, Monica M. Olcina & Ester M. Hammond

PHGDH loss promotes hypoxia tolerance through glycolytic reprogramming and enhanced HIF-1 activity

Eduard Petrosyan[1], Louise A. W. Martin[1], Isabelle Legge[2], John Walsby-Tickle[2], Adam C. Sedgwick[3], Mark A. Hill[1], James S. O. McCullagh[2], Monica M. Olcina[1], Ester M. Hammond[1]*

[1]Department of Oncology, The University of Oxford, Oxford, OX3 7DQ, UK [2]Chemistry Research Laboratory, Department of Chemistry, University of Oxford, Mansfield Road, Oxford, OX1 3TA, UK [3]Department of Chemistry, King's College London, London, SE1 1DB, UK

*Corresponding author **-** ester.hammond@oncology.ox.ac.uk

EMH – ORCID – 0000-0002-2335-3146

EP – ORCID – 0000-0002-8533-9331

Keywords - PHGDH, serine, radiosensitivity, hypoxia

Abstract

Radiotherapy is widely used in the treatment of lung cancer, however a number of intrinsic and extrinsic mechanisms of resistance exist, including hypoxia. Targeting metabolic pathways that support redox homeostasis has been proposed as a strategy to enhance radiosensitivity. The serine synthesis pathway enzyme, phosphoglycerate dehydrogenase (PHGDH) has been implicated in resistance to several anticancer therapies; however, its role in radiotherapy response is poorly defined. We show that PHGDH expression positively correlates with established hypoxia gene expression signatures in lung adenocarcinoma and squamous cell carcinoma patient datasets and is induced under hypoxia (<0.1% O_2) in lung cancer cell lines. Hypoxic induction of PHGDH appears mediated by both HIF-1 and PERK signalling, linking PHGDH regulation to hypoxia and the unfolded protein response. Using CRISPR-Cas9 PHGDH knockout models, we demonstrate that loss of PHGDH does not enhance radiosensitivity in normoxia or hypoxia when extracellular serine and glycine are available at physiological or supraphysiological concentrations. Radiosensitisation is observed only under complete serine/glycine deprivation. Unexpectedly, PHGDH loss confers increased tolerance to hypoxic stress, associated with elevated glycolytic flux, increased lactate production, accelerated HIF-1α stabilisation, and enhanced expression of hypoxia-inducible genes. Overall, these data indicate that targeting PHGDH alone is unlikely to impact radioresistance in lung cancer under physiologically relevant nutrient conditions and may instead promote metabolic adaptation to hypoxia. This highlights the importance of microenvironmental context when evaluating metabolic targets for combination with radiotherapy.

Introduction

Lung cancer is the leading cause of cancer-related deaths globally, accounting for 1.8 million deaths in 2022 [1]. A significant proportion of lung cancer patients receive radiotherapy with curative intent, although this is determined by factors including disease stage, patient fitness, comorbidities and access to facilities [2]. Hypoxia, or lack of oxygen, is a common hallmark of lung cancers, arising from an imbalance between elevated proliferation rates and insufficient vasculature. Importantly, hypoxia is a major cause of radioresistance, as oxygen is required to stabilise radiation-induced DNA damage [3]. Consequently, significant effort has been spent identifying agents that improve the efficacy of radiotherapy (radiosensitisers), with a particular focus on those agents that are effective in hypoxic conditions [4].

Serine and glycine synthesis pathways play an important role in the metabolic reprogramming of cancer cells and response to therapy. Serine and glycine are crucial for upregulation of cellular pathways that drive cell proliferation, including nucleotide synthesis through one-carbon metabolism. Serine is synthesised *de novo* through the serine synthesis pathway (SSP), which includes 3-phosphoglycerate dehydrogenase (PHGDH) as a rate-limiting step. PHGDH catalyses the conversion of 3-phosphoglycerate (3-PG), a glycolytic intermediate, into 3-phosphohydroxypyruvate (3-PHP). The subsequent two steps of the SSP are catalysed by enzymes phosphoserine aminotransferase 1 (PSAT1) and phosphoserine phosphatase (PSPH) [5,6]. Serine can then be converted into glycine through a reaction catalysed by serine hydroxymethyltransferase (SHMT1/2) enzymes [7]. Importantly, serine contributes to glutathione (GSH) production by serving as a precursor for glycine via these SHMT1/2-mediated reactions [8]. GSH is critical to antioxidant defence, and without sufficient levels, an increase in reactive oxygen species (ROS) occurs [9,10].

Evidence across multiple cancer types indicates that PHGDH promotes resistance to chemotherapy and targeted agents, whereas genetic or pharmacological inhibition enhances treatment sensitivity. For example, PHGDH upregulation has been demonstrated to contribute to

acquired resistance to erlotinib in EGFR-mutant lung adenocarcinoma cells [11]. Repression of PHGDH has been shown to sensitise triple-negative breast cancer cells to doxorubicin by increasing oxidative stress and apoptosis [12]. Most recently, high PHGDH expression was shown to promote 5-fluorouracil chemoresistance in colorectal cancer models by upregulating pro-survival Hedgehog signalling [13].

The role of PHGDH in radiotherapy response is less well-characterised. A recent study demonstrated that both knockdown and pharmacological inhibition of PHGDH increased the radiosensitivity of glioblastoma stem cells through ROS-mediated DNA damage [14]. Furthermore, inhibition of PHGDH has been shown to radiosensitise colorectal cancer cells in hypoxic (<0.1% O_2) conditions, again through disrupting the redox balance and elevating ROS levels [15]. Inhibition of the serine/glycine pathway has been more widely investigated. Notably, targeting SHMT with sertraline resulted in increased sensitivity to radiation in non-small cell lung cancer (NSCLC) and was attributed to decreased GSH and increased ROS [16]. Further support for targeting serine and glycine metabolism comes from evidence that dietary restriction of serine/glycine enhances radiosensitivity in breast, colorectal, and murine pancreatic cancer models [17].

PHGDH expression has not been characterised in hypoxic conditions, however it was shown to be a transcriptional target of Activating Transcription Factor 4 (ATF4) in response to serum starvation [18]. ATF4 plays a pivotal role in the unfolded protein response (UPR), which, in addition to being induced in response to starvation, is also active in the hypoxic conditions most associated with radiation resistance [19,20]. GSH levels increase in response to hypoxia, which also suggests a possible dependence on serine/glycine levels [10]. Together, these findings led us to hypothesise that targeting PHGDH could increase radiosensitivity and, most importantly, that this could combat hypoxia-mediated radiation resistance in lung cancer.

Materials and Methods

Cell culture

Cells were grown in DMEM supplemented with 10% FBS, in a standard humidified incubator at 37°C and 5% CO_2. Cell lines used for the study: A549 (human lung adenocarcinoma, ATCC), NCI-H460 (human large cell lung carcinoma, provided by Prof. Geoff Higgins, University of Oxford), RKO (human colorectal cancer cells, ATCC) and RKO$^{HIF1\alpha-/-}$ [21]. Additional media HPLM (A4899101, Gibco) and MEM (21090022, Gibco). PHGDH knockout clones were generated using a CRISPR-Cas9 ribonucleoprotein-based genome editing approach in accordance with Synthego's single-cell cloning workflow (guide sequences **Table S1**). Cells were regularly checked for mycoplasma (Mycoalert mycoplasma detection kit, Lonza).

Exposure to hypoxia

Cells were incubated in a Whitley A35 chamber (Don Whitley Scientific), Bactron II anaerobic chamber (Sheldon manufacturing) or Whitley H35 Hypoxystation (Don Whitley Scientific). For experiments conducted at <0.1% O_2 levels, cells were plated on glass dishes. Cells were harvested inside hypoxia chambers with equilibrated solutions.

Western blotting

Cells were lysed using UTB (9 M urea, 75 mM Tris-HCl, pH 7.5, 0.15 M β-mercaptoethanol) and sonicated briefly. Proteins were separated on a 4–20% polyacrylamide gel (Bio-Rad) and transferred onto a nitrocellulose membrane (Bio-Rad). Odyssey IR imaging technology (LI-COR Biosciences) was used. Primary antibodies: PHGDH (Novus Biologicals, NBP2-46389), HIF-1α (BD Biosciences, 610958), β-actin (Santa Cruz, AC-15), γH2AX (Sigma Aldrich, 05-636).

RT-qPCR

RNA was prepared using TRIzol (Invitrogen/Life Technologies). cDNA was reverse transcribed from total RNA using the Verso kit (Thermo Scientific). qPCR was performed using SYBR Green

PCR Master Mix kit (Applied Biosystems) in a 7500 FAST Real-Time PCR thermocycler with v2.0.5 software (Applied Biosystems). RNA fold change was calculated using a $2^{-\Delta\Delta Ct}$ method in relation to the 18S. The mean of three biological replicates ± SEM is shown. All primer sequences are available (**Table S2**).

HIF reporter assay

Cells were transiently transfected with 5x-HRE-luciferase [22] and pCMV-Renilla plasmids using Lipofectamine 2000 transfection reagent (Invitrogen Life Technologies). pCMV-Renilla was used for normalisation purposes. Firefly and Renilla luciferase activities were measured using the Dual Glo Luciferase assay (Promega).

Irradiation

Cells were irradiated using a Cs-137 irradiator (GSM: GSR D1; dose rate 1.7 Gy min^{-1} at room temperature). For irradiation in hypoxic conditions, cells were sealed in equilibrated air-tight boxes as previously described and transported to the source [23].

GSH measurements

A probe (FL-1) was used to measure the GSH levels in cells [10]. Cells were seeded (6000/well) in flat-bottomed 96-well plates. As a negative control, cells were treated with N-ethylmaleimide (NEM, 200 μM) for 6 h. FL-1 (10 μM) was then added to each well, and after 1 h, the fluorescence was measured (POLARstar plate reader, BMG LabTech).

Clonogenic survival assay

Cells were seeded at the appropriate density in 6-well plates. Each treatment condition was performed in triplicate. Colonies were allowed to grow in normal conditions for 10-14 days. Once the colonies had formed (>50 cells), the media was removed, and they were stained with crystal violet (0.5% w/v in 50% MeOH and 20% EtOH). Colonies were counted using a manual cell

counter (Stuart Scientific). The plating efficiency (PE = colonies counted/cells seeded) and the surviving fraction (SF = $PE_{IR\ dose}/PE_{0\ Gy}$) were calculated. A linear-quadratic equation was used for survival data fitting.

PHGDH overexpression

Knockout cells were transfected with pcDNA3.1+/C-(K)-DYK expression vector containing the wild-type (WT) PHGDH sequence (GeneScript Clone ID: OHu19607). Transfections were performed using Lipofectamine 2000 (Thermo Fisher Scientific).

Metabolomics analysis

Cells were fixed and collected in ice-cold methanol. The DNA concentration was normalised to the samples with the lowest concentration (expected range: 50-100 ng/µl). To remove the soluble proteins from the samples, the suspension was passed through a 10 kD molecular weight cut-off filter (Amicon Ultra, Millipore). Metabolomic analysis was carried out as previously described [24].

Real-time metabolic flux analysis

Real-time analysis of glycolytic stress was performed using the Agilent Seahorse XF analyser. Seahorse XF base medium supplemented with 2 mM Glutamine (GlutaMAX supplement, ThermoFisher Scientific) was used for the experiment. Additionally, the compounds for the glycolytic stress test were prepared: Glucose (10 mM), Oligomycin (1 µM) and 2-Deoxy-D-glucose (50 mM). Three measurement cycles were recorded following the addition of each compound (3 min mix and 3 min measure). Extracellular acidification rate (ECAR) readings were normalised to cell number. For normalisation, cells were fixed with 10% PFA and stained with Hoechst 33342 fluorescent dye (Thermo Fisher Scientific). Cells were counted following the measurement using

the Celigo imaging cytometer (Nexcelom). Glycolysis levels were calculated based on the changes in normalised ECAR values following the addition of glucose to the media.

Results

PHGDH is hypoxia-inducible

To investigate the potential relationship between expression of the SSP and hypoxia in lung cancer, we began by studying the expression of PHGDH, PSAT1 and PSPH in normal tissue versus tumour. In lung squamous cell carcinoma (LUSC), all three SSP genes showed significantly higher expression in tumour vs normal, whilst in lung adenocarcinoma (LUAD), only PSAT1 was significantly different (**Figure S1A, B**). Next, we looked for correlation between PHGDH/PSAT1/PSPH mRNA levels and established hypoxia gene expression signatures in the TCGA lung patient datasets [25,26]. PHGDH, PSAT1 and PSPH showed a positive correlation with two hypoxia signatures in LUSC and LUAD, suggesting that the SSP could be hypoxia-inducible in patients with lung cancer (**Figure S1C-F**) [27,28]. Given the druggable nature of PHGDH, we sought to confirm the relationship between expression and hypoxia *in vitro*. A549 cells were exposed to hypoxia, and RT-qPCR was carried out using the well-characterised HIF target gene, carbonic anhydrase IX (CAIX) as a positive control [29]. As expected, both PHGDH and CAIX levels were significantly increased in hypoxia (**Figure 1A, S2A**). Hypoxia-mediated induction of PHGDH was also determined in a second cell line, H460 (**Figure S2B, C**). PHGDH protein levels were found to increase earlier than the observed change in mRNA, reaching maximum levels after just 4 h in hypoxia (<0.1% O_2) (**Figure 1B, C**). Notably, no significant change in PHGDH protein was determined in H460 cells exposed to hypoxia, although we did note that they appeared to have higher baseline expression compared to A549 cells (**Figure S2D, E**).

The positive correlation between PHGDH expression and the hypoxia signatures suggested to us that PHGDH could be a target of the HIF transcription factors. To determine if PHGDH was regulated by HIF-1, PHGDH mRNA was measured in genetically matched cell lines RKO and RKO$^{HIF\text{-}1\alpha\text{-}/\text{-}}$ under normoxia and hypoxia (<0.1% O_2 and 2% O_2). PHGDH induction was again observed in hypoxia (<0.1% O_2), and was significantly reduced, but not entirely abrogated, in the absence of HIF-1α. Surprisingly, PHGDH was not induced in response to 2% O_2, where a robust induction of CAIX was observed (**Figure 1D, E**). To exclude the possibility that PHGDH was induced with different kinetics in 2% O_2, further analysis was carried out. However, no significant change in PHGDH expression was determined over the time period examined (0-24 h) (**Figure 1F**). Together, these data suggested that the induction of PHGDH in hypoxia is not entirely HIF-1 mediated and is dependent on the exact level of oxygen. PHGDH expression has been linked to the UPR, specifically via PERK-ATF4 signalling [30,31]. Given the established links between hypoxia and the UPR [32], we asked whether inhibiting PERK would influence PHGDH expression under hypoxic conditions. A549 cells were treated with PERKi (AMG PERK 44) and exposed to hypoxia, followed by RT-qPCR for PHGDH, CAIX and ATF4 (**Figure 1G-I**). Again, PHGDH was not induced in response to 2% O_2 but did increase in <0.1% O_2. Somewhat surprisingly, inhibition of PERK completely abrogated the induction of PHGDH and ATF4 in <0.1% O_2, whilst it did not affect CAIX expression. Together, these data suggest that PHGDH is regulated by both HIF-1 and the PERK-mediated UPR in hypoxic conditions, or that in this context PERK signalling controls HIF-1 activity. Interestingly, potential binding sites for both HIF-1 and ATF4 have been identified in the PHGDH promoter sequence (**Figure S2F, G**).

To test our hypothesis that targeting PHGDH could increase radiosensitivity, we generated CRISPR-Cas9 PHGDH knock-out (KO) cells. As expected, ion chromatography mass spectrometry (IC-MS) analysis of anionic metabolites in parental A549 and PHGDH KO cells revealed predicted changes in serine metabolism (**Figure 2A-C** and **S3A-C**) [24,33]. For example, a

significant reduction in O-Phosphoserine levels was observed in PHGDH KO cells, confirming the abrogation of the SSP (**Figure 2D**). Levels of NADH, the reduced form of the PHGDH co-factor NAD^+, were also significantly lower in the KO cells (**Figure 2E**). However, despite a complete loss of PHGDH and therefore SSP, there was no significant change in proliferation rate (**Figure S3D**). However, it is important to note that although PHGDH is essential for *de novo* serine synthesis, serine can also be imported from the media [34]. Standard tissue culture media contain supraphysiological levels of serine (DMEM - 420 μM vs 140-160 μM in human plasma) [35–37]. This readily available excess serine means that cells grown in DMEM are not dependent on the SSP. Therefore, we performed experiments using a range of media containing different serine concentrations: DMEM (420 μM serine), HPLM (150 μM serine) and MEM (~0 μM serine) (**Figure 2F** and **Table S3** for full description of the media). No PHGDH-dependent effect on proliferation rate was determined when cells were grown in HPLM; however, in MEM, cells lacking PHGDH grew significantly slower (**Figure 2G, H** and **S3E, F**). PHGDH expression was found to increase when A549 cells were grown in the media with either physiological levels of serine (HPLM) or no serine (MEM) (**Figure 2I, J** and **S3G, H**). To further verify the relationship between the expression of the SSP and exogenous serine levels, MEM was supplemented with increasing concentrations of serine. As previously, PHGDH levels increased in MEM, but this effect was lost as serine levels increased and was completely abrogated when the levels of serine found in DMEM (400 μM) were reached (**Figure 2K** and **S3I**).

Loss of PHGDH does not increase radiosensitivity

The cell lines (parental and KO1) were grown in the range of media (DMEM, HPLM and MEM) and irradiated (0-8 Gy) before allowing colonies to form. In agreement with a previous report, cells grown in MEM, i.e. the absence of serine/glycine, were significantly more sensitive to radiation than cells grown in DMEM or HPLM (**Figure S4A**) [17]. Loss of PHGDH did not have a significant

effect on radiosensitivity in DMEM or HPLM media (**Figure 3A, B**). However, when irradiated in MEM, the PHGDH KO cells (KO1 and KO2) showed significantly increased radiosensitivity (**Figure 3C, S4B**). Next, we asked how radiosensitivity in hypoxia was affected by the loss of PHGDH. As expected, cells irradiated in hypoxic conditions (<0.1% O_2) were more radioresistant than those treated in normoxia with oxygen enhancement ratios (OER) of 2-3.5 (**Figure S4C-E**). However, as determined in normoxia loss of PHGDH only led to enhanced radiosensitivity when grown in MEM in hypoxia (**Figure 3D-F**). To investigate further, we determined changes in GSH levels in each media type and found that a PHGDH-dependent difference in GSH was only significant when the cells were grown in MEM (**Figure 4A**). As expected, regardless of the media the cells were grown in, GSH levels increased in response to hypoxia indicating that even when grown in MEM, there are other cellular mechanisms to generate GSH. The hypoxia-mediated increase in GSH was not PHGDH dependent. As seen in normoxia, loss of PHGDH only reduced GSH in hypoxia, compared to the parental cells, when serine and glycine were also missing from the media, i.e. cells were grown in MEM (**Figure S5A**). Next, we investigated the levels of DNA damage, determined using γH2AX and found that PHGDH KO1 cells had both higher levels of γH2AX at baseline and post radiation (2 Gy) when grown in MEM but not DMEM or HPLM (**Figure 4B-G** and KO2 and KO3 **Figure S5B-D**). Overall, our data shows that loss of PHGDH only leads to significant radiosensitisation when cells are completely deprived of extracellular serine/glycine. This radiosensitisation effect is potentially due to reduced anti-oxidant capacity and higher levels of baseline DNA damage in the absence of PHGDH.

Loss of PHGDH leads to higher glycolytic rates and elevated levels of lactate

Whilst determining relative radiosensitivity, we noted that cells lacking PHGDH appeared to survive better in hypoxic conditions. To formally investigate, we exposed the PHGDH KO1 cells and parental control to hypoxia (<0.1 and 2% O_2) and carried out a colony survival assay. While

exposure to hypoxia led to a significant decrease in survival in the parental cell line, no change in survival was determined in the KO cells (**Figure 5A** and KO2 and KO3 **Figure S6A, B**). These data were further supported by demonstrating that exposure to hypoxia had a significant impact on proliferation rates when parental cells were returned to normal oxygen levels, whilst those lacking PHGDH were unaffected (**Figure S6C, D**). Next, we asked whether the resistance to hypoxia observed in PHGDH KO cells occurred in all media types. When grown in HPLM, cell survival under hypoxia was affected in PHGDH WT but not in KO1 cells (**Figure 5B** and KO2 and KO3 **Figure S6E**). Exposure to serine-free MEM led to reduced survival rates under hypoxia in both PHGDH Con and KO1 cells (**Figure 5C** and KO2 and KO3 **Figure S6F**). Together, these data suggest that loss of PHGDH could prime cells for survival in hypoxic conditions. Supportively, the metabolomic analysis showed elevated levels of pyruvate and intracellular lactate (**Figure 5D, E**). To further investigate the effect of PHGDH loss on changes in lactate and glycolysis, an extracellular flux glycolytic stress test was carried out. The extracellular acidification rate (ECAR), which can be used as a surrogate for extracellular lactate production, demonstrated a significantly higher rate in the PHGDH KO1 and KO2 cells (**Figure 5F**). Furthermore, following the glucose injection, PHGDH-deficient cells (KO1 and KO2) showed a larger increase in ECAR compared to parental controls, indicating a rapid elevation of glycolytic flux (**Figure 5G**). To confirm that the resistance to hypoxia observed in the KO cells was PHGDH dependent, a rescue experiment was carried out. Expression of physiological levels of PHGDH in the KO cells restored the sensitivity to hypoxia determined in the parental cell line (**Figure 5H, I** and KO2 **Figure S6G, H**).

Loss of PHGDH leads to increased HIF-1 activity

Increased lactate has been linked to HIF-1 stability [38–40]. Parental and KO A549 cells were exposed to hypoxia, and the speed with which HIF-1α accumulated was determined by western blotting. In response to hypoxia (<0.1% O_2), HIF-1α accumulated faster in the KO cells compared

to the parental control cells (**Figure 5J, S7A**). To investigate this further, a hypoxia response element (HRE)-luciferase reporter was used to demonstrate that loss of PHGDH led to increased HIF-1 activity under hypoxia in the KO cells (**Figure 5K** and KO2 **Figure S7B)**. This was further confirmed by determining the accumulation of known HIF target genes in response to hypoxia in both cell lines (parental and KO). The levels of CAIX, GLUT1, VEGF and LDHA were all found to be significantly higher in the KO1 cells exposed to hypoxia (<0.1% O_2) compared to the parental control (**Figure 5L, M** and **S7C-F**). Together, these data show that loss of PHGDH confers resistance to hypoxic stress, an effect that is reversible by PHGDH re-expression and is associated with enhanced HIF-1α accumulation and transcriptional activity under hypoxia.

Discussion

Here, we demonstrate that PHGDH loss does not increase radiosensitivity in cancer cells grown in physiologically relevant concentrations of extracellular serine/glycine. Increased radiosensitivity was observed when cells were irradiated in the complete absence of extracellular serine/glycine. Our data support the conclusion that increasing radiosensitivity through a PHGDH-dependent reduction of GSH levels is only achievable in the absence of extracellular serine/glycine.

Importantly, we found that loss of PHGDH increases tolerance to hypoxia in cells cultured in both DMEM and HPLM. Hypoxia is known to drive metabolic reprogramming, including an increased reliance on glycolysis. Elevated extracellular lactate levels have been associated with enhanced tumour invasion and metastasis, as well as impaired immune surveillance in lung, breast, and other cancer types [41–44]. Additionally, an increase in lactate has been shown to correlate with radioresistance, both *in vitro* and *in vivo* [39–4145]. Increased lactate levels have also been shown to stabilise HIF-1α through lactylation, which can block its recognition by the von Hippel–Lindau (VHL) complex [46]. We observed increased glycolysis and ECAR in cells lacking PHGDH, supportive of higher lactate levels, which could therefore contribute to increased HIF-

1α accumulation and HIF-1 activity. Moreover, enhanced induction of LDHA in PHGDH-deficient cells in hypoxia is likely to further increase glycolytic flux, thereby promoting lactate production and establishing a positive feedback loop [47]. Overall, these data show that PHGDH loss leads to increased glycolysis, effectively priming them to respond to hypoxic conditions.

Interestingly, we found that PHGDH was induced in a HIF-1-dependent manner in response to <0.1% O_2 but did not change in milder conditions (2% O_2), which are also associated with HIF-1 activity. A potential model to explain this expression pattern involves the oxygen-dependency of the hydroxylation pathways, which play key roles in HIF-1α stabilisation and activity. Specifically, inhibition of the prolyl hydroxylases (PHDs) occurs at relatively higher oxygen levels, allowing HIF-1α stabilisation, while Factor Inhibiting HIF (FIH) remains active, restricting recruitment of p300/CBP and limiting transcription [48]. As oxygen levels decrease further, FIH activity is progressively lost, permitting full HIF transcriptional activity and maximal expression of a subset of FIH-sensitive target genes [49]. Furthermore, certain chromatin remodelling proteins, such as KDM6A, are direct oxygen sensors and can change chromatin accessibility and affect HIF binding to the HREs in an oxygen-dependent manner [50]. To fully characterise the mechanism of PHGDH induction in response to hypoxia, chromatin immunoprecipitation of HIF-1 and potentially ATF4 would be required.

In contrast to the data shown here, pharmacological inhibition of PHGDH has also been shown to increase the radiosensitivity of colorectal cancer cells in hypoxic conditions [15]. However, it should be noted that the reported experimental conditions include non-physiological levels of extracellular serine (RPMI, 286 μM serine) [51]; therefore, it is unclear what mechanism underpins the observed increase in radiosensitivity. Moreover, the PHGDH inhibitor used, NCT-503, has been reported to have off-target effects by reducing glucose-derived citrate levels in a PHGDH-

independent manner [52]. Inherent biological differences between colorectal and lung cancer cells could also contribute to the differing observations. Similarly, the only other report on PHGDH-dependent radiosensitisation focused on glioblastoma stem cells, which exhibit a distinct metabolic landscape and therapy response [14].

Elevated PHGDH expression has been associated with poor patient outcomes in several studies [53–55]; however, recent evidence suggests a more complex role, as low or heterogeneous PHGDH expression has been linked to cancer cell dissemination and metastatic progression [56]. Taken together, these findings highlight a context-dependent role for PHGDH in tumour biology and suggest that inhibition of serine biosynthesis alone is unlikely to overcome hypoxia-mediated radioresistance in lung cancer. More broadly, this work underscores the importance of considering nutrient availability when evaluating metabolic targets for combination with radiotherapy and cautions against extrapolating radiosensitisation strategies from non-physiological culture conditions to the clinical setting.

Acknowledgements

We are grateful to Dr James Grist (University of Oxford) and Prof Daniel Tennant (University of Birmingham) for useful discussion of this work.

Funding

The authors acknowledge the support of an EPSRC Programme Grant (EP/S019901/1) awarded to EMH, and supported LAWM. EP is grateful for the support of an Oxford Clarendon fund scholarship.

Ethics approval and consent to participate

All patient data used in this study were publicly available, fully anonymised, and obtained from The Cancer Genome Atlas (TCGA). Hence, this study is exempt from institutional ethics review.

Conflict of interest

Authors declare no conflict of interest.

Author contributions

EP and EMH conceived the study. EP, LAWM performed experiments and analysed data. IL, JWT and JSOM performed the metabolomic experiments and analysed the data. ACS synthesised the GSH probe. MH assisted with the analysis of radiation colony survival data. EP and EMH wrote the manuscript with input from all authors. MO and EMH supervised the project and secured funding.

Data availability

The data supporting the results of this study will be made available by the corresponding author upon request. Supplementary information is available at the Cell Death and Discovery's website.

References

1 Zhou J, Xu Y, Liu J, Feng L, Yu J, Chen D. Global burden of lung cancer in 2022 and projections to 2050: Incidence and mortality estimates from GLOBOCAN. *Cancer Epidemiol* 2024; **93**: 102693.

2 Kagenaar E, Lugo-Palacios DG, Aggarwal A, Hutchings A, Han L, O'Neill S *et al.* Inequalities in the utilisation of curative-intent treatments for early-stage non-small cell lung cancer across urban and rural areas: A population-based study in England. *J Cancer Policy* 2025; **46**: 100662.

3 Worth KR, Papandreou I, Hammond EM. How the histological structure of some lung cancers shaped almost 70 years of radiobiology. *Br J Cancer* 2023; **128**: 407–412.

4 Skwarski M, Bowler E, Wilson JD, Higgins GS, Hammond EM. *Targeting tumor hypoxia*. 2020 doi:10.1007/978-3-030-49701-9_11.

5 Locasale JW, Grassian AR, Melman T, Lyssiotis CA, Mattaini KR, Bass AJ *et al.* Phosphoglycerate dehydrogenase diverts glycolytic flux and contributes to oncogenesis. *Nat Genet* 2011; **43**: 869–874.

6 Possemato R, Marks KM, Shaul YD, Pacold ME, Kim D, Birsoy K *et al.* Functional genomics reveal that the serine synthesis pathway is essential in breast cancer. *Nature* 2011; **476**: 346–350.

7 Pikman Y, Ocasio-Martinez N, Alexe G, Dimitrov B, Kitara S, Diehl FF *et al.* Targeting serine hydroxymethyltransferases 1 and 2 for T-cell acute lymphoblastic leukemia therapy. *Leukemia* 2022; **36**: 348–360.

8 Renwick SB, Snell K, Baumann U. The crystal structure of human cytosolic serine hydroxymethyltransferase: a target for cancer chemotherapy. *Structure* 1998; **6**: 1105–1116.

9 Hacker L, Sarsam E, Conway SJ, Hammond EM. A guide to reactive oxygen species in tumour hypoxia: measurement and therapeutic implications. *Mol Oncol* 2025; **19**: 3003–3022.

10 Twigger SA, Dominguez B, Porto V, Hacker L, Chalmers AJ, Breckenridge R *et al.* The activity of therapeutic molecular cluster Ag5 is dependent on oxygen level and HIF-1 mediated signalling. *Redox Biol* 2024; **76**: 103326.

11 Dong J-K, Lei H-M, Liang Q, Tang Y-B, Zhou Y, Wang Y *et al.* Overcoming erlotinib resistance in EGFR mutation-positive lung adenocarcinomas through repression of phosphoglycerate dehydrogenase. *Theranostics* 2018; **8**: 1808–1823.

12 Zhang X, Bai W. Repression of phosphoglycerate dehydrogenase sensitizes triple-negative breast cancer to doxorubicin. *Cancer Chemother Pharmacol* 2016; **78**: 655–659.

13 Mancini C, Lori G, Mattei G, Iozzo M, Desideri D, Cianchi F *et al.* PHGDH drives 5-FU chemoresistance in colorectal cancer through the Hedgehog signaling. *Journal of Experimental & Clinical Cancer Research* 2025; **44**: 198.

14 Liu X, Liu B, Wang J, Liu H, Wu J, Qi Y *et al.* PHGDH activation fuels glioblastoma progression and radioresistance via serine synthesis pathway. *Journal of Experimental & Clinical Cancer Research* 2025; **44**: 99.

15 Van de Gucht M, Dufait I, Kerkhove L, Corbet C, de Mey S, Jiang H *et al.* Inhibition of Phosphoglycerate Dehydrogenase Radiosensitizes Human Colorectal Cancer Cells under Hypoxic Conditions. *Cancers (Basel)* 2022; **14**: 5060.

16 Sánchez-Castillo A, Heylen E, Hounjet J, Savelkouls KG, Lieuwes NG, Biemans R *et al.* Targeting serine/glycine metabolism improves radiotherapy response in non-small cell lung cancer. *Br J Cancer* 2024; **130**: 568–584.

17 Falcone M, Uribe AH, Papalazarou V, Newman AC, Athineos D, Stevenson K *et al.* Sensitisation of cancer cells to radiotherapy by serine and glycine starvation. *Br J Cancer* 2022; **127**: 1773–1786.

18 Yang Y, Li S, Yang Y, Li Q, Liu Y, Cao J. ATF4/PHGDH mediates the effects of ER stress on cadmium-induced autophagy and glycolysis. *Toxicology* 2024; **509**: 153976.

19 Nagelkerke A, Bussink J, Van Der Kogel AJ, Sweep FCGJ, Span PN. The PERK/ATF4/LAMP3-arm of the unfolded protein response affects radioresistance by interfering with the DNA damage response. *Radiotherapy and Oncology* 2013; **108**: 415–421.

20 Rzymski T, Milani M, Pike L, Buffa F, Mellor HR, Winchester L *et al.* Regulation of autophagy by ATF4 in response to severe hypoxia. *Oncogene* 2010; **29**: 4424–4435.

21 Dang DT, Chen F, Gardner LB, Cummins JM, Rago C, Bunz F *et al.* Hypoxia-Inducible Factor-1α Promotes Nonhypoxia-Mediated Proliferation in Colon Cancer Cells and Xenografts. *Cancer Res* 2006; **66**: 1684–1693.

22 Shibata T, Giaccia AJ, Brown JM. Development of a hypoxia-responsive vector for tumor-specific gene therapy. *Gene Ther* 2000; **7**: 493–498.

23 Anbalagan S, Pires IM, Blick C, Hill MA, Ferguson DJP, Chan DA *et al.* Radiosensitization of renal cell carcinoma in vitro through the induction of autophagy. *Radiotherapy and Oncology* 2012; **103**: 388–393.

24 Williams R, Walsby-Tickle J, Hvinden IC, Legge I, Kacerova T, Lee KV *et al.* Metabolomics using anion-exchange chromatography mass spectrometry for the analysis of cells, tissues and biofluids. *Nat Protoc* 2025. doi:10.1038/s41596-025-01222-z.

25 Comprehensive genomic characterization of squamous cell lung cancers. *Nature* 2012; **489**: 519–525.

26 Comprehensive molecular profiling of lung adenocarcinoma. *Nature* 2014; **511**: 543–550.

27 Winter SC, Buffa FM, Silva P, Miller C, Valentine HR, Turley H *et al.* Relation of a Hypoxia Metagene Derived from Head and Neck Cancer to Prognosis of Multiple Cancers. *Cancer Res* 2007; **67**: 3441–3449.

28 Buffa FM, Harris AL, West CM, Miller CJ. Large meta-analysis of multiple cancers reveals a common, compact and highly prognostic hypoxia metagene. *Br J Cancer* 2010; **102**: 428–435.

29 Wykoff CC, Beasley N, Watson PH, Campo L, Chia SK, English R *et al.* Expression of the Hypoxia-Inducible and Tumor-Associated Carbonic Anhydrases in Ductal Carcinoma in Situ of the Breast. *Am J Pathol* 2001; **158**: 1011–1019.

30 Zhang D, Li AM, Hu G, Huang M, Yang F, Zhang L *et al.* PHGDH-mediated endothelial metabolism drives glioblastoma resistance to chimeric antigen receptor T cell immunotherapy. *Cell Metab* 2023; **35**: 517-534.e8.

31 Dai Z, Chen L, Pan K, Zhao X, Xu W, Du J *et al.* Multi-omics Analysis of the Role of PHGDH in Colon Cancer. *Technol Cancer Res Treat* 2023; **22**: 15330338221145994.

32 Bartoszewska S, Collawn JF. Unfolded protein response (UPR) integrated signaling networks determine cell fate during hypoxia. *Cell Mol Biol Lett* 2020; **25**: 18.

33 Walsby-Tickle J, Gannon J, Hvinden I, Bardella C, Abboud MI, Nazeer A *et al.* Anion-exchange chromatography mass spectrometry provides extensive coverage of primary metabolic pathways revealing altered metabolism in IDH1 mutant cells. *Commun Biol* 2020; **3**: 247.

34 Papalazarou V, Newman AC, Huerta-Uribe A, Legrave NM, Falcone M, Zhang T *et al.* Phenotypic profiling of solute carriers characterizes serine transport in cancer. *Nat Metab* 2023; **5**: 2148–2168.

35 Psychogios N, Hau DD, Peng J, Guo AC, Mandal R, Bouatra S *et al.* The Human Serum Metabolome. *PLoS One* 2011; **6**: e16957.

36 Hennequart M, Labuschagne CF, Tajan M, Pilley SE, Cheung EC, Legrave NM *et al.* The impact of physiological metabolite levels on serine uptake, synthesis and utilization in cancer cells. *Nat Commun* 2021; **12**: 6176.

37 Dulbecco R, Freeman G. Plaque production by the polyoma virus. *Virology* 1959; **8**: 396–397.

38 De Saedeleer CJ, Copetti T, Porporato PE, Verrax J, Feron O, Sonveaux P. Lactate activates HIF-1 in oxidative but not in Warburg-phenotype human tumor cells. *PLoS One* 2012; **7**: e46571.

39 Gao J, Liu R, Huang K, Li Z, Sheng X, Chakraborty K *et al.* Dynamic investigation of hypoxia-induced L-lactylation. *Proceedings of the National Academy of Sciences* 2025; **122**. doi:10.1073/pnas.2404899122.

40 Kshitiz, Afzal J, Suhail Y, Chang H, Hubbi ME, Hamidzadeh A *et al.* Lactate-dependent chaperone-mediated autophagy induces oscillatory HIF-1α activity promoting proliferation of hypoxic cells. *Cell Syst* 2022; **13**: 1048-1064.e7.

41 Xie H, Hanai J, Ren J-G, Kats L, Burgess K, Bhargava P *et al.* Targeting Lactate Dehydrogenase-A Inhibits Tumorigenesis and Tumor Progression in Mouse Models of Lung Cancer and Impacts Tumor-Initiating Cells. *Cell Metab* 2014; **19**: 795–809.

42 Brand A, Singer K, Koehl GE, Kolitzus M, Schoenhammer G, Thiel A *et al.* LDHA-Associated Lactic Acid Production Blunts Tumor Immunosurveillance by T and NK Cells. *Cell Metab* 2016; **24**: 657–671.

43 Faubert B, Li KY, Cai L, Hensley CT, Kim J, Zacharias LG *et al.* Lactate Metabolism in Human Lung Tumors. *Cell* 2017; **171**: 358-371.e9.

44 Brizel DM, Schroeder T, Scher RL, Walenta S, Clough RW, Dewhirst MW *et al.* Elevated tumor lactate concentrations predict for an increased risk of metastases in head-and-neck cancer. *International Journal of Radiation Oncology*Biology*Physics* 2001; **51**: 349–353.

45 Doherty M, Feng J, Wang T, Yin C, Byrne NM, Chambers S *et al.* Metabolic Radiosensitization by Targeting Lactate Metabolism with Microfluidic Liposomal Nanocarriers. *ACS Biomater Sci Eng* 2026. doi:10.1021/acsbiomaterials.5c02175.

46 Li C, Fu C, Zhou W, Li H, Liu Z, Wu G *et al.* Lactylation modification of HIF-1α enhances its stability by blocking VHL recognition. *Cell Communication and Signaling* 2025; **23**: 364.

47 Semenza GL, Jiang B-H, Leung SW, Passantino R, Concordet J-P, Maire P *et al.* Hypoxia Response Elements in the Aldolase A, Enolase 1, and Lactate Dehydrogenase A Gene Promoters Contain Essential Binding Sites for Hypoxia-inducible Factor 1. *Journal of Biological Chemistry* 1996; **271**: 32529–32537.

48 Tarhonskaya H, Hardy AP, Howe EA, Loik ND, Kramer HB, McCullagh JSO *et al.* Kinetic Investigations of the Role of Factor Inhibiting Hypoxia-inducible Factor (FIH) as an Oxygen Sensor. *Journal of Biological Chemistry* 2015; **290**: 19726–19742.

49 Dayan F, Roux D, Brahimi-Horn MC, Pouyssegur J, Mazure NM. The Oxygen Sensor Factor-Inhibiting Hypoxia-Inducible Factor-1 Controls Expression of Distinct Genes through the Bifunctional Transcriptional Character of Hypoxia-Inducible Factor-1α. *Cancer Res* 2006; **66**: 3688–3698.

50 Chakraborty AA, Laukka T, Myllykoski M, Ringel AE, Booker MA, Tolstorukov MY *et al.* Histone demethylase KDM6A directly senses oxygen to control chromatin and cell fate. *Science (1979)* 2019; **363**: 1217–1222.

51 Moore GE, Gerner RE, Franklin HA. Culture of normal human leukocytes. *JAMA* 1967; **199**: 519–24.

52 Arlt B, Mastrobuoni G, Wuenschel J, Astrahantseff K, Eggert A, Kempa S *et al.* Inhibiting PHGDH with NCT-503 reroutes glucose-derived carbons into the TCA cycle, independently of its on-target effect. *J Enzyme Inhib Med Chem* 2021; **36**: 1282–1289.
53 Metcalf S, Petri BJ, Kruer T, Green B, Dougherty S, Wittliff JL *et al.* Serine synthesis influences tamoxifen response in ER+ human breast carcinoma. *Endocr Relat Cancer* 2021; **28**: 27–37.
54 Itoyama R, Yasuda-Yoshihara N, Kitamura F, Yasuda T, Bu L, Yonemura A *et al.* Metabolic shift to serine biosynthesis through 3-PG accumulation and PHGDH induction promotes tumor growth in pancreatic cancer. *Cancer Lett* 2021; **523**: 29–42.
55 Jia XQ, Zhang S, Zhu HJ, Wang W, Zhu JH, Wang XD *et al.* Increased Expression of PHGDH and Prognostic Significance in Colorectal Cancer. *Transl Oncol* 2016; **9**: 191–196.
56 Rossi M, Altea-Manzano P, Demicco M, Doglioni G, Bornes L, Fukano M *et al.* PHGDH heterogeneity potentiates cancer cell dissemination and metastasis. *Nature* 2022; **605**: 747–753.
57 Wishart DS, Jewison T, Guo AC, Wilson M, Knox C, Liu Y *et al.* HMDB 3.0—The Human Metabolome Database in 2013. *Nucleic Acids Res* 2012; **41**: D801–D807.

Figure legends

Figure 1. Hypoxia-mediated induction of PHGDH is dependent on HIF-1 and the UPR

A. A549 cells were treated with <0.1% O_2 for 0-24 h, and RT-qPCR for PHGDH was carried out. The levels of CAIX in the same samples are shown in Figure S2A. **B**. A549 cells were exposed to <0.1% O_2 for the times indicated, followed by western blotting for PHGDH, HIF-1α and β-actin as a loading control. **C**. Quantification of changes in PHGDH from western blots generated in part B. Band intensities were normalised to β-actin loading control. **D, E**. HIF-1α wild-type and knock-out RKO cells were exposed to 21, 2, or <0.1% O_2 for 16 h and PHGDH (D) and CAIX (E) expression levels were determined using RT-qPCR. **F.** A549 cells were treated with <2% O_2 for 0-24 h, and RT-qPCR for PHGDH was carried out. **G-I**. A549 cells were exposed to 21, 2 or <0.1% O_2 for 16 h with or without AMG PERK 44 (20 μM). RT-qPCR for PHGDH (G), ATF4 (H) and CAIX (I) was carried out**.** Data represent the mean of three replicates, and error bars indicate the SEM. For statistical analysis, a two-tailed Student *t-test* was performed. **p<0.05, **p<0.01, ***p<0.001, ns*=non-significant

Figure 2. PHGDH-dependent control of metabolic state and proliferation

A. IC-MS metabolomics heatmap showing z-scored relative metabolite abundances in parental control (Con) and PHGDH KO1 A549 cells grown in normoxia (21% O_2), with metabolites hierarchically clustered and samples grouped by condition. **B**. Validation of PHGDH knock-out in three A549 CRISPR-Cas9 clones (KO1, KO2, KO3). A549 cells were used as a parental control (Con). **C**. Schematic representation of the *de novo* serine synthesis pathway (SSP). **D, E.** Comparisons of the levels of O-Phosphoserine (D), NADH (E) between A549 and PHGDH KO1 cells under normoxia (21% O_2). **F**. The levels of serine (μM) in each of the media used compared to normal plasma [57]. **G**. Proliferation of parental and PHGDH KO1 cells was measured over 7 days of growth in HPLM. Fold change relative to the first day post-seeding was calculated. **H**. Proliferation of parental and PHGDH KO1 cells was measured over 7 days of growth in MEM. Fold change relative to the first day post-seeding was calculated. **I**. Quantification of PHGDH protein expression in parental A549 cells cultured in HPLM for the indicated times. Band intensity values were normalised to β-actin loading control and are relative to the 0 h condition. A representative western blot is shown in Figure S3G. **J.** Quantification of PHGDH protein expression in parental A549 cells cultured in MEM for the indicated times. Band intensity values were normalised to β-actin loading control and are relative to the 0 h condition. A representative western blot is shown in Figure S3H. **K.** Quantification of PHGDH protein levels in parental A549 cells cultured in DMEM (D), MEM (M), or MEM supplemented with increasing concentrations of serine (50-400 μM). Band intensity values were normalised to β-actin loading control and expressed relative to the DMEM condition. A representative western blot is shown in Figure S3I. Data represent the mean of three replicates, and error bars indicate the SEM. For statistical analysis of western blot data, a two-tailed unpaired Student *t-test* was performed. For proliferation data, a two-tailed paired Student *t-test* was used. *$p<0.05$, **$p<0.01$, ***$p<0.001$.

Figure 3. The effect of PHGDH KO on radiosensitivity in normoxia and hypoxia

A-C. A549 (parental and PHGDH KO1) cells were irradiated (0-8 Gy) in normoxia (21% O_2) followed by a colony survival assay. Prior to and during irradiation, cells were either grown in DMEM (A), HPLM (B) or MEM (C). 24 h after irradiation, all media were replaced with fresh DMEM. A schematic of the experimental setup is indicated. **D-F**. A549 (parental and PHGDH KO1) cells were irradiated (0-8 Gy) in hypoxia (<0.1% O_2) followed by a colony survival assay. Prior to and during irradiation cells were either grown in DMEM (D), HPLM (E) or MEM (F). 16 h before irradiation, cells were transferred to hypoxia (<0.1% O_2) and were irradiated in hypoxic conditions. Cells were returned to normoxia shortly after irradiation. 24 h after irradiation, all media was replaced with fresh DMEM. A schematic of the experimental set-up is indicated. Data represent the mean of three replicates, and error bars indicate the SEM. For statistical analysis, survival curves were fitted using a linear–quadratic model and compared by an extra-sum-of-squares F test. ****p<0.001, ****p<0.0001*.

Figure 4. Loss of PHGDH in the absence of extracellular serine results in decreased GSH levels and increased DNA damage.

A. Parental control and PHGDH KO1 A549 cells were grown in DMEM, HPLM and MEM for 16 h, under normoxia. Fold change in GSH levels was calculated in relation to baseline levels in cells cultured in DMEM. A549 cells were also treated with N-ethylmaleimide (NEM) (200 μM, 6 h) in each media type to reduce GSH, as a negative control. **B-G.** A549 (parental and PHGDH KO1) cells were grown in the media indicated DMEM (B), HPLM (C) and MEM (D) for 24 h followed by irradiation (2 Gy). Western blotting and quantification of changes in γH2AX relative to β-actin was carried out. Fold change relative to non-irradiated control cells (0 Gy, Con) is shown. Representative western blots are shown in (E-G). Data represent the mean of three replicates,

and error bars indicate the SEM. For statistical analysis, a two-tailed Student's *t-test* was performed. *$p<0.05$, **$p<0.01$, ***$p<0.001$.

Figure 5. Loss of PHGDH leads to improved survival in hypoxic conditions

A. A549 (Con and PHGDH KO1) grown in DMEM were exposed to hypoxia (<0.1 or 2% O_2) for 16 h. Cells were returned to normoxic conditions and colonies allowed to form. Colony survival is shown as a per cent survival fraction relative to the 21% O_2 control. **B.** Parental and PHGDH KO1 A549 cells were grown in HPLM media for 45 h. After 5 h in HPLM, cells were exposed to hypoxia (0.1% O_2) for 16 h. Following the hypoxia exposure, cells were kept in HPLM for an additional 24 h and then returned to DMEM and grown under normoxia to allow colony formation. **C.** Parental and PHGDH KO1 A549 cells were grown in MEM media for 45 h. After 5 h in MEM, cells were exposed to hypoxia (0.1% O_2) for 16 h. Following the hypoxia exposure, cells were kept in MEM for an additional 24 h and then returned to DMEM and grown under normoxia to allow colony formation. **D, E.** Comparisons of the levels of pyruvate (D), lactate (E) between A549 and PHGDH KO1 cells under normoxia (21% O_2). **F.** Glycolytic stress test on parental (Con) and PHGDH KO1 and KO2 A549 cells. **G.** Using the data from part F**,** glycolysis levels were calculated based on the extracellular acidification rates (ECAR) in parental (Con) and KO1 and KO2 cell lines. **H**. PHGDH KO1 cells expressing an empty vector control or PHGDH overexpression vector (KO1 + PHGDH) were cultured in DMEM, under normoxia and hypoxia (<0.1 or 2% O_2) for 16 h. Cells were returned to normoxic conditions and colonies allowed to form. **I**. Representative western blot showing the expression of PHGDH in parental control, PHGDH KO1 and PHGDH overexpressing cells. β-actin was used as a loading control. **J.** Quantification of HIF-1α protein levels in parental control (Con) and PHGDH KO clones (KO1 and KO2) following exposure to hypoxia (<0.1% O_2) for the indicated times. Band intensity values were normalised to β-actin and expressed as fold change relative to normoxic Con cells (0 h, Con). A representative western blot is shown in Figure

S7A. **K.** A549 cells and PHGDH KO1 cells were transfected with an HRE-Luciferase reporter and then exposed to hypoxia (<0.1% O_2) for 0-12 hours. Relative luciferase levels are shown. **L, M.** A549 and PHGDH KO1 cells were exposed to hypoxia (<0.1% O_2) for the times indicated, followed by qPCR for CAIX (L), GLUT1 (M). Data represent the mean of three replicates, and error bars show the standard error of the mean (SEM). An ordinary one-way ANOVA test was performed for statistical analysis of the extracellular flux analysis data. Elsewhere, a two-tailed Student *t-test* was performed. *$p<0.05$, **$p<0.01$, ***$p<0.001$.

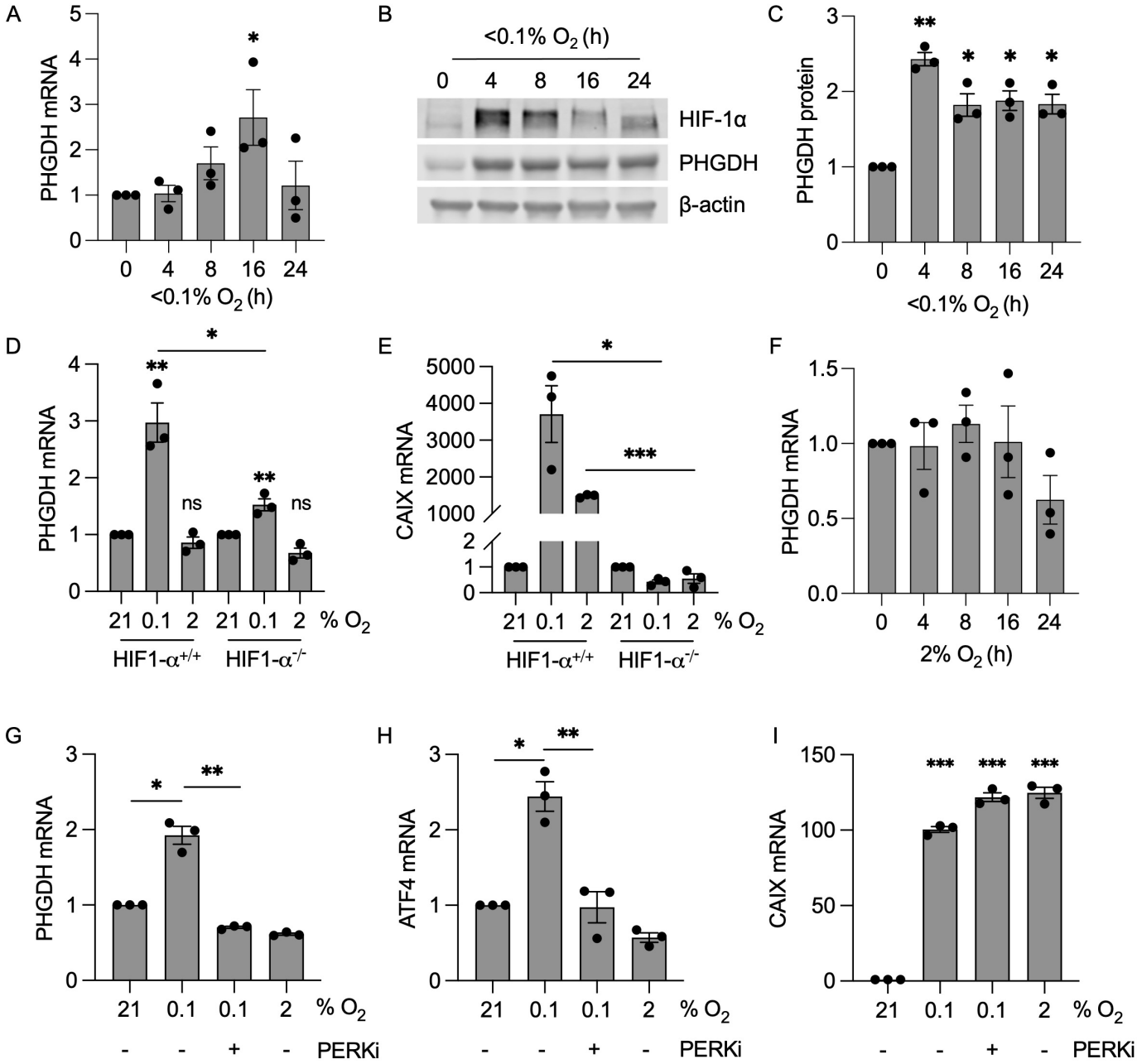
A
PHGDH mRNA
<0.1% O2 (h)
B
<0.1% O2 (h)
0 4 8 16 24
HIF-1α
PHGDH
β-actin
C
PHGDH protein
<0.1% O2 (h)
D
PHGDH mRNA
ns
21 0.1 2 21 0.1 2 % O2
HIF1-α+/+ HIF1-α-/-
E
CAIX mRNA
21 0.1 2 21 0.1 2 % O2
HIF1-α+/+ HIF1-α-/-
F
PHGDH mRNA
2% O2 (h)
G
PHGDH mRNA
21 0.1 0.1 2 % O2
- - + - PERKi
H
ATF4 mRNA
21 0.1 0.1 2 % O2
- - + - PERKi
I
CAIX mRNA
21 0.1 0.1 2 % O2
- - + - PERKi

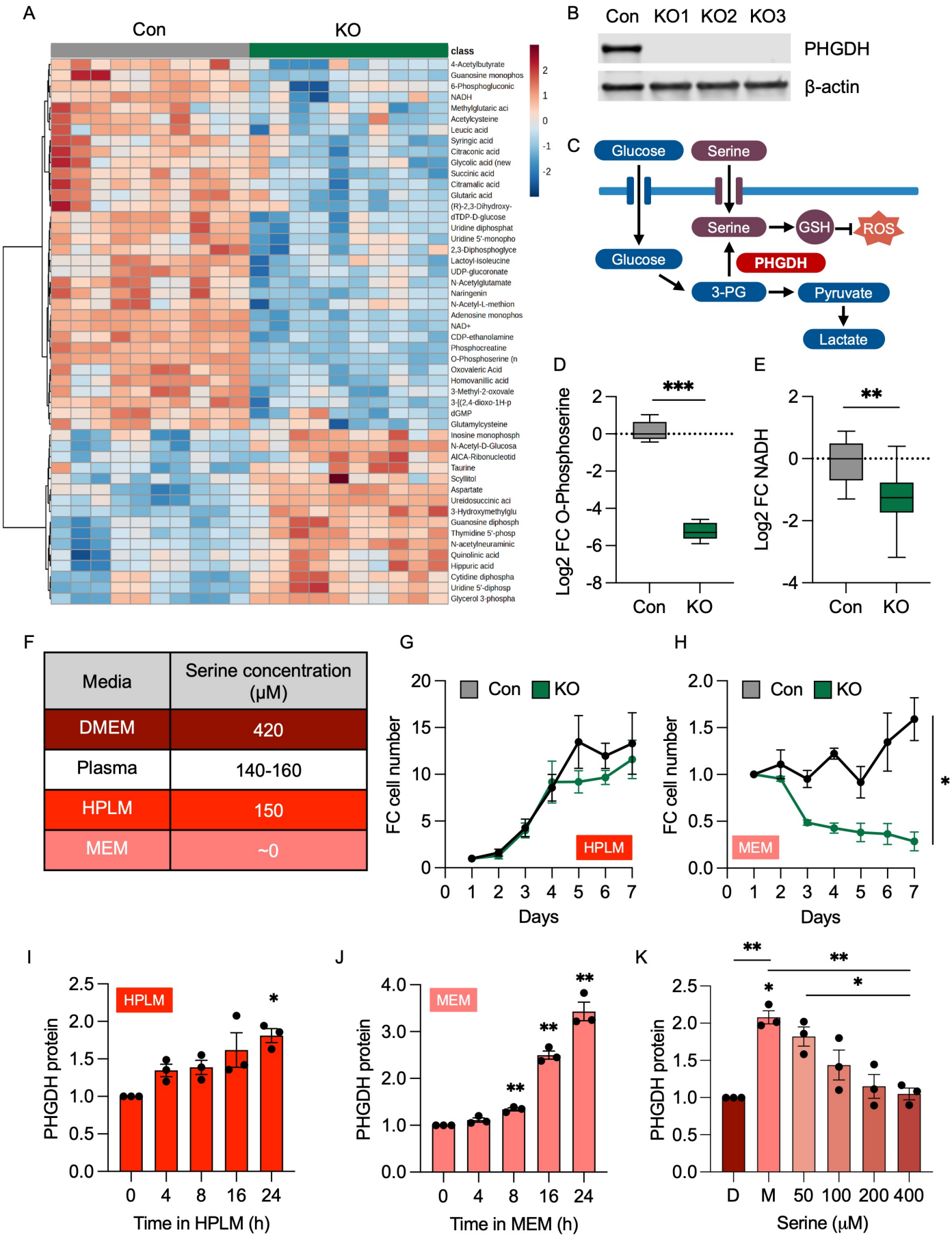

F

Media	Serine concentration (μM)
DMEM	420
Plasma	140-160
HPLM	150
MEM	~0

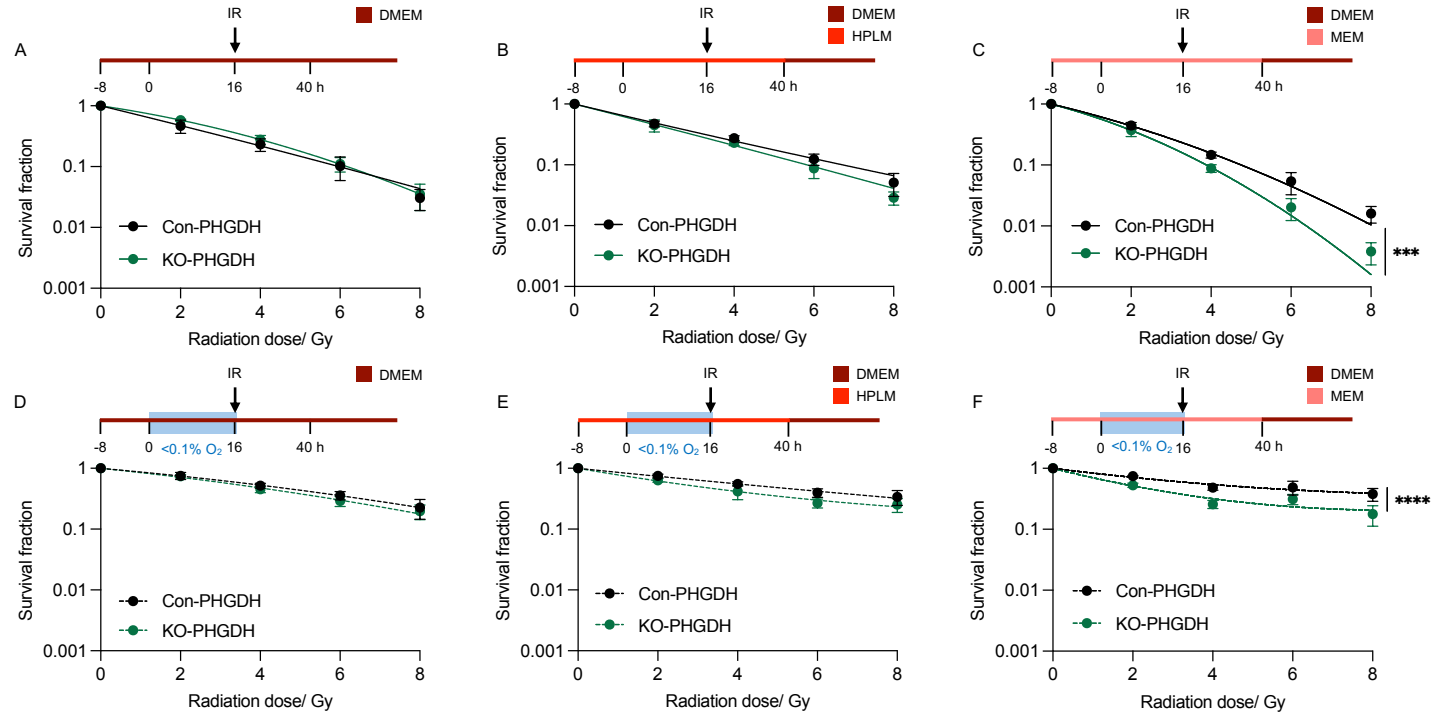
A
IR
DMEM
-8
0
16
40 h
Survival fraction
1
0.1
0.01
0.001
Con-PHGDH
KO-PHGDH
0
2
4
6
8
Radiation dose/ Gy
B
IR
DMEM
HPLM
-8
0
16
40 h
Survival fraction
Con-PHGDH
KO-PHGDH
Radiation dose/ Gy
C
IR
DMEM
MEM
-8
0
16
40 h
Survival fraction
Con-PHGDH
KO-PHGDH
***
Radiation dose/ Gy
D
IR
DMEM
-8
0
<0.1% O2
16
40 h
Survival fraction
Con-PHGDH
KO-PHGDH
Radiation dose/ Gy
E
IR
DMEM
HPLM
-8
0
<0.1% O2
16
40 h
Survival fraction
Con-PHGDH
KO-PHGDH
Radiation dose/ Gy
F
IR
DMEM
MEM
-8
0
<0.1% O2
16
40 h
Survival fraction
Con-PHGDH
KO-PHGDH
****
Radiation dose/ Gy

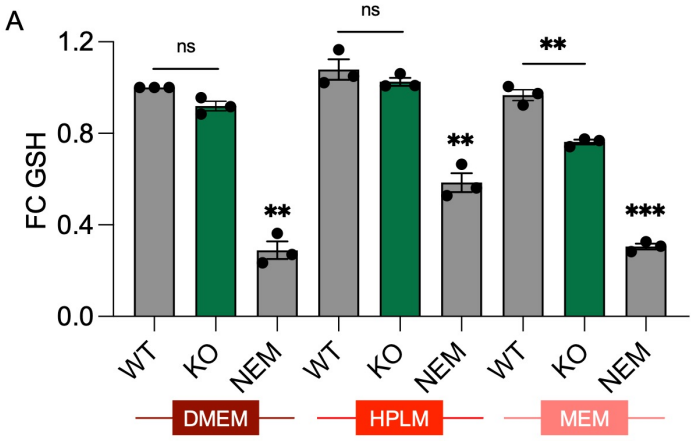
A
FC GSH
1.2
0.8
0.4
0.0
ns
ns
**
**
**
***
WT
KO
NEM
WT
KO
NEM
WT
KO
NEM
DMEM
HPLM
MEM

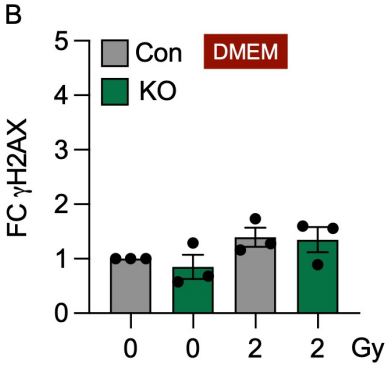
B
FC γH2AX
Con
KO
DMEM
0
0
2
2
Gy

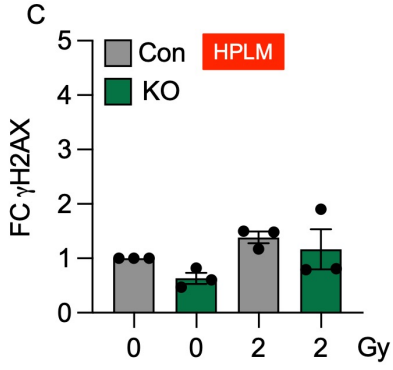
C
FC γH2AX
Con
KO
HPLM
0
0
2
2
Gy

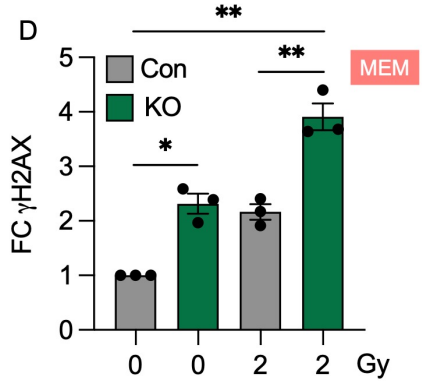
D
FC γH2AX
Con
KO
MEM
**
**
*
0
0
2
2
Gy

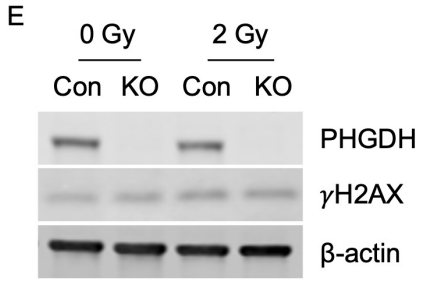
E
0 Gy
2 Gy
Con
KO
Con
KO
PHGDH
γH2AX
β-actin

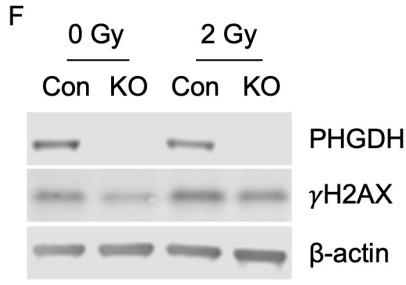
F
0 Gy
2 Gy
Con
KO
Con
KO
PHGDH
γH2AX
β-actin

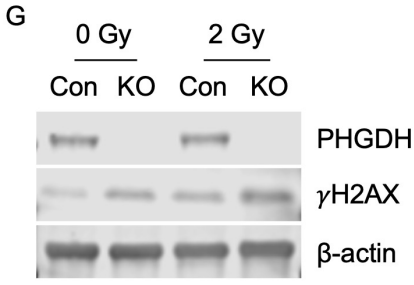
G
0 Gy
2 Gy
Con
KO
Con
KO
PHGDH
γH2AX
β-actin

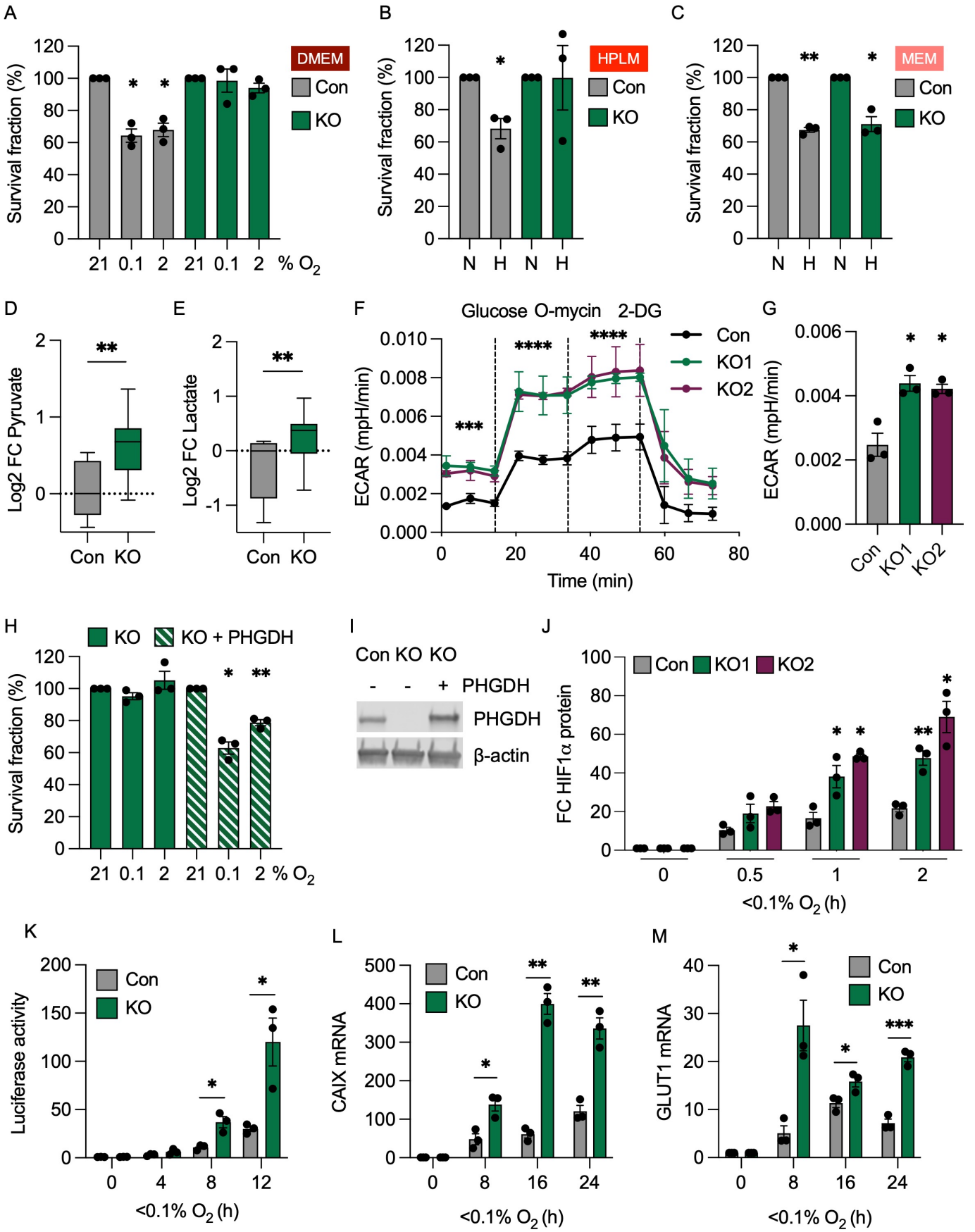
A
Survival fraction (%)
DMEM
Con
KO
21 0.1 2 21 0.1 2 % O2
B
HPLM
N H N H
C
MEM
D
Log2 FC Pyruvate
Con KO
E
Log2 FC Lactate
F
Glucose O-mycin 2-DG
ECAR (mpH/min)
Con
KO1
KO2
Time (min)
G
H
KO
KO + PHGDH
I
Con KO KO
- - + PHGDH
PHGDH
β-actin
J
FC HIF1α protein
<0.1% O2 (h)
K
Luciferase activity
L
CAIX mRNA
M
GLUT1 mRNA

npj | breast cancer

Article

Published in partnership with the Breast Cancer Research Foundation

https://doi.org/10.1038/s41523-026-00927-y

HIF-1–regulated TPM3 links hypoxia to motility and invasion beyond the hypoxic fraction in triple-negative breast cancer

Chumin Zhou[1], Jack T. Crusher[1], Kate Friesen[1], Sophie A. Twigger[1], Eduard Petrosyan[1], Graham Booker[1], Priya Samuel[2], Eileen E. Parkes[1] & Ester M. Hammond[1] ✉

Hypoxia is a defining feature of triple-negative breast cancer (TNBC), driving invasion, metastasis, and therapy resistance. Understanding the molecular effectors of hypoxia is essential to identify new therapeutic targets. Here, we investigated tropomyosin 3 (TPM3), an actin-binding protein that regulates filament stability. TPM3 is significantly upregulated in breast cancer, including in TNBC, where elevated levels correlate with poor overall survival. Using validated hypoxia signatures and TNBC cell models, we show that TPM3 is induced in physiologically relevant hypoxic conditions in a HIF-1–dependent manner. Both mRNA and protein levels of TPM3 increased in response to hypoxia, and TPM3 colocalised with F-actin, supporting cytoskeletal organisation. Functional assays demonstrated that depletion or inhibition of TPM3 impaired cell morphology, motility, and invasion in hypoxic TNBC cells, while not affecting viability. Notably, TPM3 inhibition synergised with Paclitaxel and Doxorubicin, enhancing therapeutic efficacy. In addition, TPM3 was incorporated into extracellular vesicles (EVs), with hypoxia increasing EV-mediated transfer of TPM3 to normoxic cells and promoting their motility. These findings establish TPM3 as a hypoxia-inducible, HIF-1–regulated effector of cytoskeletal dynamics and intercellular communication, underscoring its potential as a therapeutic target to limit TNBC aggressiveness and improve treatment outcomes.

Hypoxia (conditions of insufficient oxygen) is a hallmark of the tumour microenvironment (TME) in solid cancers, arising as a consequence of rapid tumour growth and inadequate or inefficient vasculature. Hypoxia is associated with therapy resistance and poor patient prognosis[1]. The adverse prognostic impact of hypoxia has been particularly well documented in breast cancer and is even more pronounced in triple-negative breast cancer (TNBC), the most aggressive subtype which lacks targeted treatment options[2,3]. Patients who succumb to TNBC do so because of metastatic disease and while a relationship between hypoxia and increased metastasis is well-known, the underpinning mechanisms are less clear. Emerging evidence suggests that hypoxia-driven changes in gene expression, activation of hypoxia-inducible factors (HIFs), epithelial-to-mesenchymal transition (EMT), metabolic reprogramming, and remodelling of the TME may all contribute to enhanced metastatic dissemination[4,5]. The identification of hypoxic tumour markers which predict poor patient outcome is therefore critical to identify novel therapeutic strategies.

TPM3 (Tropomyosin 3) encodes a member of the tropomyosin family of actin-binding proteins which stabilise actin filaments and regulate the cytoskeleton. TPM3 plays important roles in maintaining cell structure, intracellular transport, and muscle contraction[6,7]. While TPM3 function has been predominantly characterised in muscle cells/myopathies, dysregulation or gene fusions involving TPM3 have been implicated in various cancers[7–13]. The mRNA for TPM3 has been described in microvesicles generated by platelets and it has been suggested that TPM3 could be delivered to breast cancer cells and promote metastasis[14]. Interestingly, the hypoxia-inducible Right Open Reading Frame Kinase 3 (RIOK3) was found to interact with TPM3 leading to the hypothesis that this interaction could support RIOK3-dependent migration and invasion in hypoxia[15]. Together, these studies led us to investigate a role for TPM3 in the biological response to hypoxia.

Here, we found that TPM3 is a target of the HIF-1 transcription factor in a broad range of hypoxic conditions and controls the motility and invasion capacity of hypoxic TNBC cells. Most importantly, we identify TPM3 as an extracellular vesicle (EV) cargo protein which can increase the motility of normoxic cells. Together, these data suggest that the hypoxia-mediated induction of TPM3 contributes to the metastatic potential of both the hypoxic and oxygenated tumour fractions of TNBC.

[1]Department of Oncology, University of Oxford, Oxford, UK. [2]School of Biological & Medical Sciences, Oxford Brookes University, Headington, Oxford, UK. ✉e-mail: ester.hammond@oncology.ox.ac.uk

Results

TPM3 is hypoxia-inducible in conditions relevant to TNBC

TPM3 expression was found to be significantly higher in breast cancer (BRCA) tissue, compared to normal breast tissue (Fig. 1A and Fig. S1A). Furthermore, TPM3 expression was found to be significantly higher in TNBC compared to normal tissue (Fig. 1B and Fig. S1B). Next, we asked how TPM3 expression correlated with TNBC patient survival and found that high TPM3 is associated with a poorer overall survival rate in TNBC (Fig. 1C). To further explore a relationship between TPM3 and hypoxia, we used two validated hypoxia signatures and found a significant correlation in patient samples, demonstrating that TPM3 expression is increased in more hypoxic TNBC (Fig. 1D and S1C)[16,17].

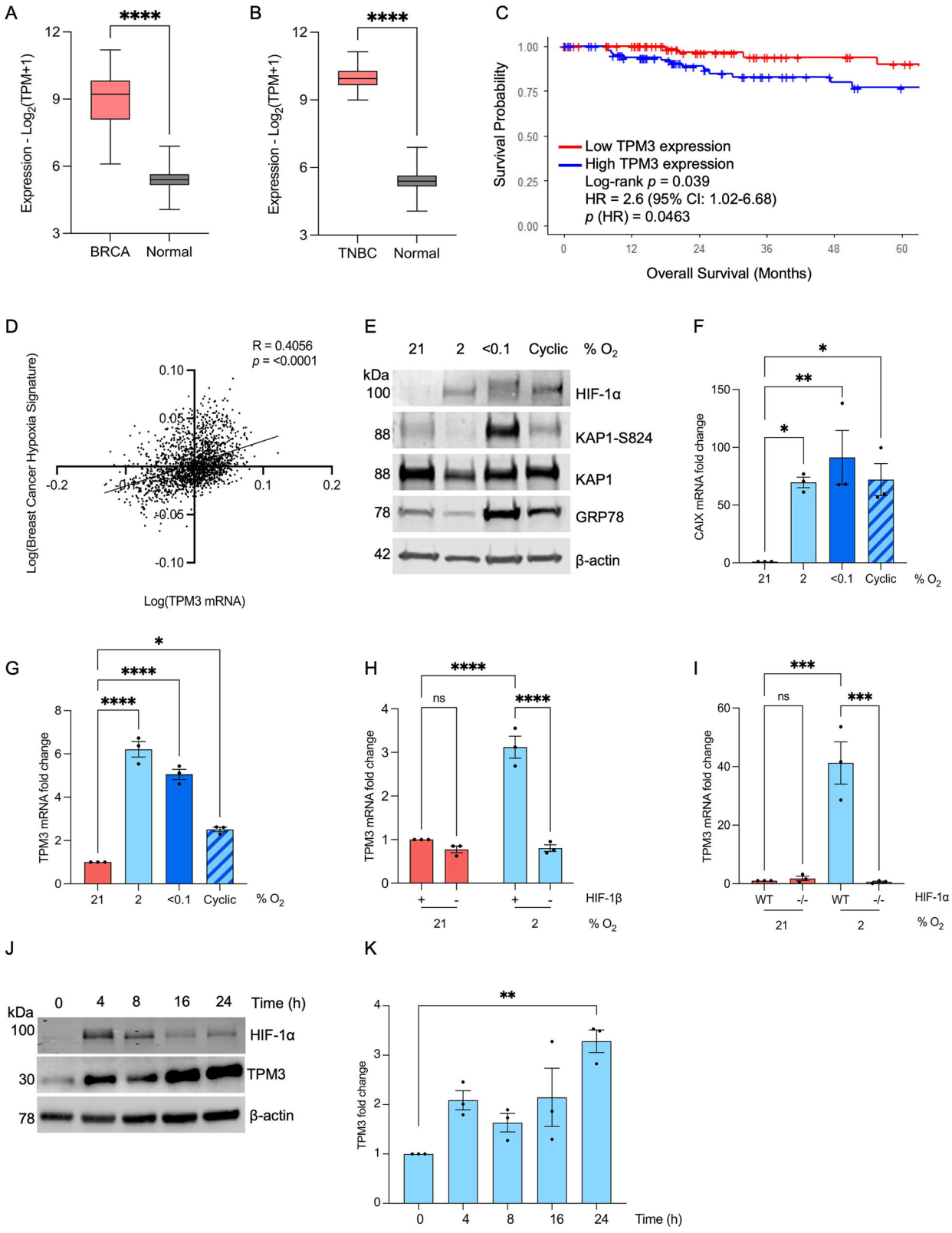

Fig. 1 | TPM3 is induced in hypoxia in a HIF-1-dependent manner. A TPM3 mRNA levels in BRCA and normal breast tissue generated using TPM3 mRNA expression from TCGA-BRCA. num(BRCA) = 1082; num(Normal)=514. **B** TPM3 mRNA levels in TNBC and normal breast tissue generated using TPM3 mRNA from Genotype-Tissue Expression (GTEx). num(TNBC) = 171; num(Normal)=514. **C** Kaplan-Meier curve of overall survival in TNBC patients with high or low TPM3 expression, generated using TCGA-BRCA (dichotomised at the median). Statistical significance was assessed by log-rank test. **D** Correlation between the Buffa hypoxia signature and TPM3 mRNA expression from Metabric dataset. Statistical analysis was determined using simple linear regression test and Pearson correlation. **E** MDA-MB-231 cells were exposed to a range of hypoxic conditions for 16 h followed by western blotting for the proteins indicated, β-actin was used as a loading control. **F** MDA-MB-231 cells were exposed to a range of hypoxic conditions for 16 h followed by RT-qPCR to determine CAIX mRNA level. Statistical testing was done using a paired *t*-test. **G**. MDA-MB-231 cells were exposed to a range of hypoxic conditions for 16 h followed by RT-qPCR for TPM3. Statistical testing was done using a paired *t*-test. **H** MDA-MB-231 cells were treated with siRNA to HIF-1β followed by exposure to 21% or 2% O_2 for 16 h. TPM3 mRNA level was determined and shown relative to the normoxic control. Statistical testing was done by two-way ANOVA with Šídák's multiple comparisons test. **I** RKO and RKO$^{HIF\text{-}1\alpha\text{-}/\text{-}}$ cells were exposed to hypoxia (2% O_2) for 16 h followed by RT-qPCR for TPM3. Statistical testing was done by two-way ANOVA with Tukey's multiple comparisons test. **J** MDA-MB-231 cells were exposed to 2% O_2 for the times shown followed by western blotting for the proteins indicated. **K** Quantification of TPM3 levels in cells treated as in part J. Statistical testing was done by paired *t*-test. Data shown from three separate experiments ($n = 3$) are displayed with mean ± standard error of the mean (SEM) unless specified otherwise. Statistical testing was carried out as indicated. $^*p < 0.05$, $^{**}p < 0.01$, $^{***}p < 0.001$, $^{****}p < 0.0001$ and ns $p > 0.05$.

Tumour hypoxia exists as a gradient of oxygen tensions within a tumour and also includes transitions between levels, known as cyclic or intermittent hypoxia[18]. It is important to consider a range of hypoxic conditions when investigating hypoxia-mediated biology as the biological response can differ[19]. Here, we considered 2% O_2, <0.1% O_2 and cyclic conditions (transitions between 2 and <0.1% O_2). As expected, HIF-1α was stabilised in all of the hypoxic conditions, however evidence of the DNA damage response was limited to <0.1% O_2 and the unfolded protein response to <0.1% O_2 and cyclic conditions (Fig. 1E)[20]. TNBC cell lines (MDA-MB-231 and MDA-MB-453) were exposed to the hypoxic conditions (2, <0.1% O_2 and cyclic) and changes in TPM3 mRNA determined. As expected, the well-validated HIF target, CAIX was induced in response to hypoxia (Fig. 1F)[21]. A significant increase in TPM3 mRNA was observed in all the hypoxic conditions tested in both cell lines demonstrating that TPM3 is hypoxia inducible in a broad range of hypoxic conditions relevant to TNBC (Fig. 1G and S1D).

This hypoxia-mediated induction in all three conditions and correlation with hypoxia signatures suggested the possibility that TPM3 was regulated by one of the hypoxia inducible factors (HIFs). In support of this, a hypoxia responsive element (HRE) was identified upstream of the TPM3 coding sequence (Fig. S1E). To investigate possible HIF dependence, we treated MDA-MB-231 cells with siRNA to HIF-1β to prevent both HIF-1 and HIF-2 mediated signalling and determined the impact on TPM3 expression. Loss of HIF-1β abrogated the induction of TPM3 and CAIX in hypoxia (Fig. 1H and S1F–H). To determine if TPM3 induction in hypoxia was mediated by HIF-1 or HIF-2, we used the matched colorectal cell lines RKO and RKO$^{HIF\text{-}1\alpha\text{-}/\text{-}}$ and found that TPM3 induction in hypoxia was abrogated by loss of HIF-1α (Fig. 1I and S1I–K). Notably, these data do not rule out the possibility that HIF-2 could also regulate TPM3 expression at specific oxygen levels or times. Together, these data confirm that TPM3 is hypoxia-inducible in all the cell lines investigated and suggests that this occurs in a HIF-1-dependent manner.

MDA-MB-231 and MDA-MB-453 cells were then exposed to hypoxia (2% O_2) and western blotting carried out for TPM3. TPM3 protein was found to increase in response to hypoxia in both cell lines (MDA-MB-231 Fig. 1J, K and MDA-MB-453 S2A, B). Hypoxia-mediated induction of TPM3 was further confirmed in response to <0.1% O_2, cyclic conditions and a third TNBC cell line (BT-549) (Figure S2C-E).

TPM3 promotes motility and invasion in hypoxia

Next, we validated that TPM3 colocalised with F-actin (detected using phalloidin)[22]. TPM3 appeared predominantly cytoplasmic with an apparent filamentous structure. Notably, a punctate signal near to the nucleus was also observed however this was unaffected by siRNA mediated knockdown of TPM3 and was therefore considered non-specific staining (Fig. S2F, G). A clear colocalisation of TPM3 and F-actin was observed which did not change in response to hypoxia (Fig. 2A, B). Next, we analysed cell morphology with and without siTPM3 knockdown and observed an increase in elongated trailing edges following loss of TPM3, suggesting a loss of actin filament structure and a reduced ability to contract the trailing edge during migration. To confirm, we measured the circularity of cells and found a significant reduction in cell circularity when TPM3 was depleted, in both normoxic and hypoxic (2% O_2) conditions (Fig. 2C). As loss of TPM3 appeared to impair the ability of MDA-MB-231 cells to recoil their trailing edge, we hypothesised that TPM3 may also influence the leading edge, where F-actin stabilisation in lamellipodia and focal adhesions is essential for generating the mechanical force required for trailing edge recoil[23]. Loss of TPM3 significantly reduced the intensity of phalloidin staining at the leading edge under both hypoxic (2% O_2) and normoxic conditions (Fig. 2D). Depletion of TPM3 had no effect on the width of the leading edge under normoxia but had a significant effect under hypoxia, further supporting a role for TPM3 in stabilising F-actin and cell motility (Fig. 2E, F). Together, our data suggest the hypothesis that TPM3, through its role in stabilising actin filaments, could promote the motility of hypoxic cells and therefore drive metastatic progression in aggressive TNBC.

To test the role of TPM3 in hypoxia-mediated motility, we carried out wound healing assays in MDA-MB-231 cells with siRNA-mediated depletion of TPM3. Before investigating motility, we verified that cell cycle distribution and viability were not altered in the hypoxic conditions used (Fig. S3A–C). Furthermore, we demonstrated that loss of TPM3 had no significant effect on clonogenic survival of cells in any of the hypoxic conditions tested (Fig. S3D-E). Depletion of TPM3 was found to significantly slow down wound closure in hypoxic conditions but had no impact in normoxia (Fig. 3A–C and S4A, B). A small molecule inhibitor of TPM3 has been described (ATM-3507) which we also used to test the role of TPM3 in hypoxia-mediated motility[24]. Again, we first verified that ATM-3507 did not significantly impact viability in both normoxic and hypoxic conditions at the dose reported to inhibit TPM3 activity (Fig. S4C)[12]. Cells exposed to ATM-3507 were significantly less motile in hypoxic conditions (Fig. 3D, E and S4D, E). Both motility and the ability to invade play important roles in metastatic potential, therefore we investigated the contribution of TPM3 to hypoxia-mediated invasion[25]. As expected, hypoxic cells showed a greater invasion capacity compared to the normoxic however, this was significantly reduced when TPM3 was depleted (Fig. 3F–H and S4F, G). In conclusion, TPM3 has an important role in cell migration and invasion in hypoxic TNBC cells.

Combination of TPM3 inhibition with TNBC standard of care

The standard of care for TNBC patients includes Carboplatin, Doxorubicin, Paclitaxel and radiotherapy. Inhibition of TPM3 has been shown to combine effectively with Paclitaxel and Doxorubicin in normoxia, resulting in the reduction of cell viability in neuroblastoma and ovarian cancer cell lines[12,26]. Here, we investigated the efficacy of combining TPM3 inhibition or siRNA-mediated loss with the standard of care for TNBC in physiologically relevant conditions. MDA-MB-231 cells were exposed to hypoxia (2% O_2) and a range of doses of ATM-3507 with Carboplatin, Doxorubicin or Paclitaxel followed by an assay for viability. The Highest Single Agent (HSA) model was used to investigate potential synergy and revealed a reduction of cell viability across increasing concentrations of ATM-3507, Carboplatin,

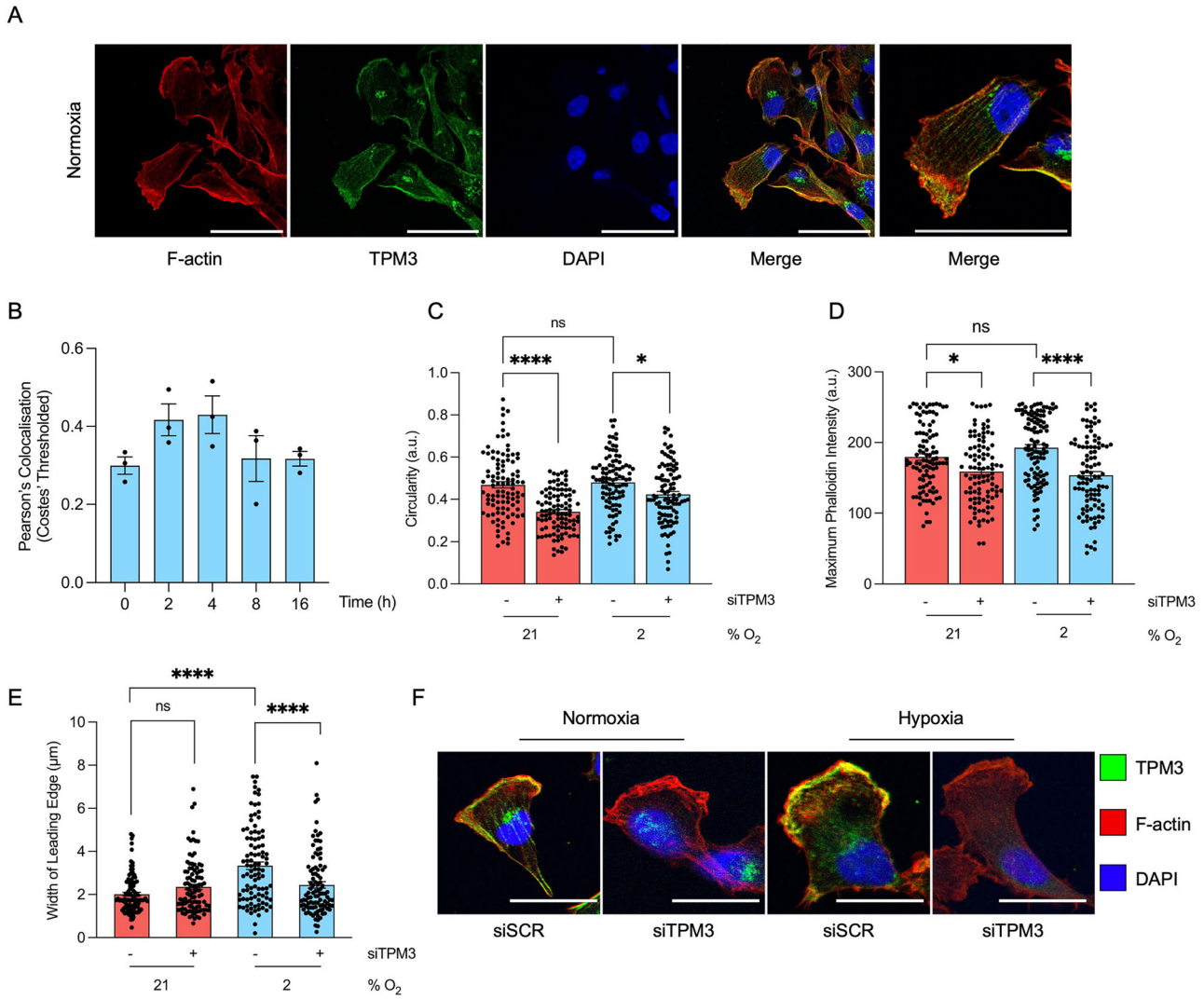

Fig. 2 | TPM3 affects F-actin organisation at the leading edge under hypoxia. **A** Representative images of immunofluorescence of MDA-MB-231 cells. Cells were stained for F-actin (phalloidin; red), TPM3 (green) and DAPI (blue). Scale bar is 50 µm. **B** MDA-MB-231 cells were exposed to hypoxia (2% O_2) for the times indicated followed by staining for TPM3 and F-actin. Quantification of colocalisation of TPM3 and F-actin was carried out using Costes' thresholded Pearson's coefficient. **C** MDA-MB-231 cells were treated with a scramble siRNA or siTPM3 and then exposed to 21% or 2% O_2 for 16 h. Cells were then stained for TPM3, F-actin and DAPI. Quantification of cell circularity (a.u.) was determined and shown. Data collected from ≥100 cells per condition. Statistical testing was done by one-way ANOVA with Tukey's multiple comparisons test. **D** Cells were treated as in part A. Quantification of maximum phalloidin intensity at the leading edge was determined. Data collected from ≥100 cells per condition. Statistical testing was done by one-way ANOVA with Tukey's multiple comparisons test. **E** Cells treated as in part A. Quantification of the leading-edge width is shown. Data collected from ≥100 cells per condition. Statistical testing was done by one-way ANOVA with Tukey's multiple comparisons test. **F** Representative immunofluorescence microscopy images showing TPM3 (green), F-actin (phalloidin; red), and DAPI (blue) at the leading edge of MDA-MB-231 cells, transfected with scramble control (siSCR) or TPM3 siRNA in 21% or 2% O_2. Scale bar is 50 µm. Data shown from three separate experiments ($n = 3$) are displayed with mean ± standard error of the mean (SEM) unless specified otherwise. $^*p < 0.05$, $^{****}p < 0.0001$ and ns $p > 0.05$.

Doxorubicin and Paclitaxel (Figure S5A–C). In addition, strong synergy (score >10) was observed with ATM-3507 combined with Doxorubicin or Paclitaxel, no antagonistic or additivity regions were indicated (Fig. 4A, B, C). To determine any effect on radiosensitivity, MDA-MB-231 cells were treated with siTPM3 followed by irradiation in hypoxia (2% O_2). Loss of TPM3 had no impact on radiosensitivity in normoxia or hypoxia (Fig. 4D and S5D). In addition, inhibition of TPM3 in normoxia or hypoxia (2% O_2) did not significantly impact radiosensitivity (Fig. S5E). Together, these data suggest that inhibition of TPM3 could be combined with standard of care for TNBC to potentially reduce metastatic spread and improve patient prognosis.

Hypoxia-induced TPM3 influences motility in normoxic cells

The hypoxic TME is known to impact neighbouring oxygenated cancer cells although a role for TPM3 in this has not been described[27]. MDA-MB-231 cells were treated with siRNA TPM3, exposed to normoxia or hypoxia (2% O_2) and conditioned media collected and transferred to normoxic cells followed by a wound healing assay (Fig. 5A, B). Conditioned media from hypoxic cells (donor cells) when added to normoxic cells (recipient cells) significantly increased the wound healing rate of the normoxic cells. However, when the conditioned media from TPM3 depleted donor cells was added to recipient cells no increase in the motility of the normoxic recipients was observed (Fig. 5C, D). This finding suggests that TPM3 contributes to factors present in the conditioned media or regulates the export of proteins and/or EVs from hypoxic cells, thereby influencing the migratory behaviour of normoxic recipient cells.

To investigate further, we again generated conditioned media from normoxic and hypoxic (2% O_2) cells and added it to wounded normoxic recipient cells (Fig. 5E). However, this time we also included the dynamin inhibitor, Dynasore, to prevent EV uptake in the recipient cells (Fig.

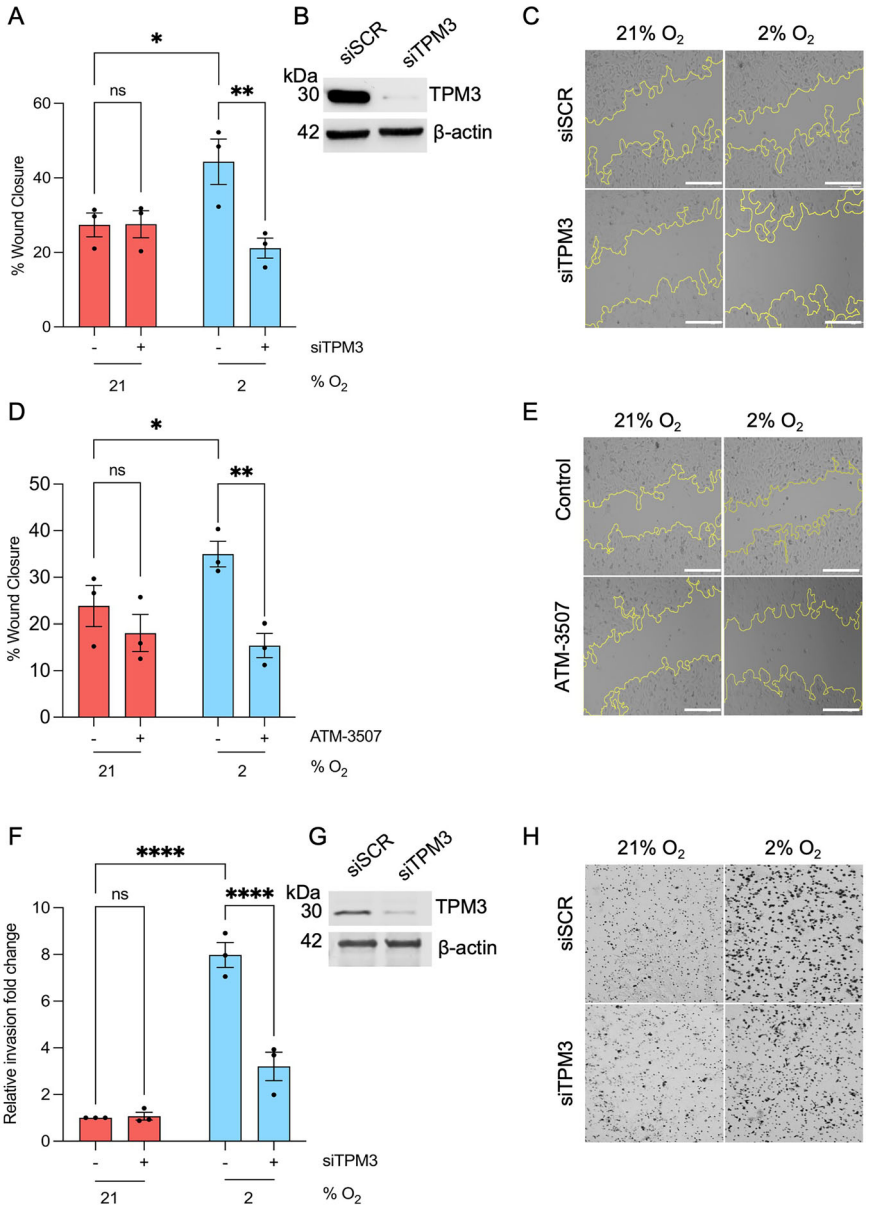

Fig. 3 | Hypoxia-mediated migration and invasion are TPM3 dependent. A MDA-MB-231 cells were treated with siTPM3 or a scramble siRNA followed by exposure to 21% or 2% O_2 for 8 h. The % of wound closure is shown in each condition. Statistical testing was done by two-way ANOVA with Šídák's multiple comparison test. **B** Knockdown of TPM3 in cells part A was validated by western blotting, β-actin was used as a loading control. **C** Representative images of wound healing assay in part A. Scale bars are 200 µm. **D** MDA-MB-231 cells were treated with ATM-3507 (6 µM) for 1 h prior to and during exposure to 21% or 2% O_2 for 8 h. The % of wound closure is shown in each condition. Statistical testing was done using a two-way ANOVA with Šídák's multiple comparison test. **E** Representative images of wound healing assay in part D. Scale bars are 200 µm. **F** MDA-MB-231 cells were treated with siTPM3 or a scramble siRNA (siSCR) followed by exposure to 21% or 2% O_2 for 16 h. The invasion fold change relative to normoxic control is shown in each condition. Statistical testing was done by two-way ANOVA with Šídák's multiple comparison test. **G** Knockdown of TPM3 in cells used in part F was validated by western blotting, β-actin was used as a loading control. **H** Representative images of invasion assay in part F. Data from three separate experiments ($n = 3$) are displayed with mean ± standard error of the mean (SEM) unless specified otherwise. $^{*}p < 0.05$, $^{**}p < 0.01$, $^{****}p < 0.0001$ and ns $p > 0.05$.

5F). As previously, we saw a significant increase in wound healing with the addition of hypoxic conditioned media. However, when Dynasore was added a significant reduction in wound closure rate was observed (Fig. 5F, G and S6A). This suggests EV uptake from the hypoxic conditioned media is critical to the impact on recipient cell motility in normoxia. To account for the known off-target effect of Dynasore in reducing basal motility, data were normalised to control cells treated with Dynasore alone[28]. Importantly, we confirmed that Dynasore did not affect TPM3 expression validating that the reduction of wound healing in hypoxic conditioned media following Dynasore treatment was not due to TPM3 suppression in the migrating cells (Fig. S6B). These data again confirm that hypoxia-induced TPM3 contributes to a conditioned media which has the capacity to increase the motility of normoxic cells and implicates EV transfer as the underlying mechanism. Therefore, we isolated and purified EVs to confirm if they were responsible for the impact on normoxic cell motility.

First, we verified using transmission electron microscopy (TEM) that EV production could be seen in MDA-MB-231 cells in hypoxic conditions. Late endosomes and EVs were observed in normoxia and hypoxia with an apparent increase in vesicle release in hypoxia (2% O_2) (Fig. 6A). A clear increase in the abundance of mitochondria following 2% O_2 exposure was also observed and has been reported previously[29]. To investigate the apparent increase in EVs detected by TEM, we isolated EVs from the conditioned media of normoxic and hypoxic (2% O_2) MDA-MB-231 cells and quantified them using nanoparticle tracking analysis (NTA). The total concentration of EVs increased significantly in hypoxia (2% O_2), while the size distribution was similar in normoxic and hypoxic conditions (Fig. 6B–D). Next, to determine if EVs released by hypoxic cells impacted recipient cell migration, MDA-MB-231 cells were again exposed to hypoxia (2% O_2) and TPM3 induction confirmed (Fig. 6E). EVs were then isolated and added to wounded normoxic recipient cells to determine impact on wound healing rate (Fig. 6F). EVs isolated from hypoxic cells increased the motility of normoxic cells and this was abrogated in the presence of Dynasore (Fig. 6G and S6C).

TPM3 is an EV cargo protein

These data led us to the non-mutually exclusive conclusions that TPM3 could play a role in EV production in hypoxic cells or that TPM3 could be transferred as cargo through EVs to recipient cells. MDA-MB-231 cells were treated with scramble siRNA or siTPM3 and exposed to hypoxia (2% O_2)

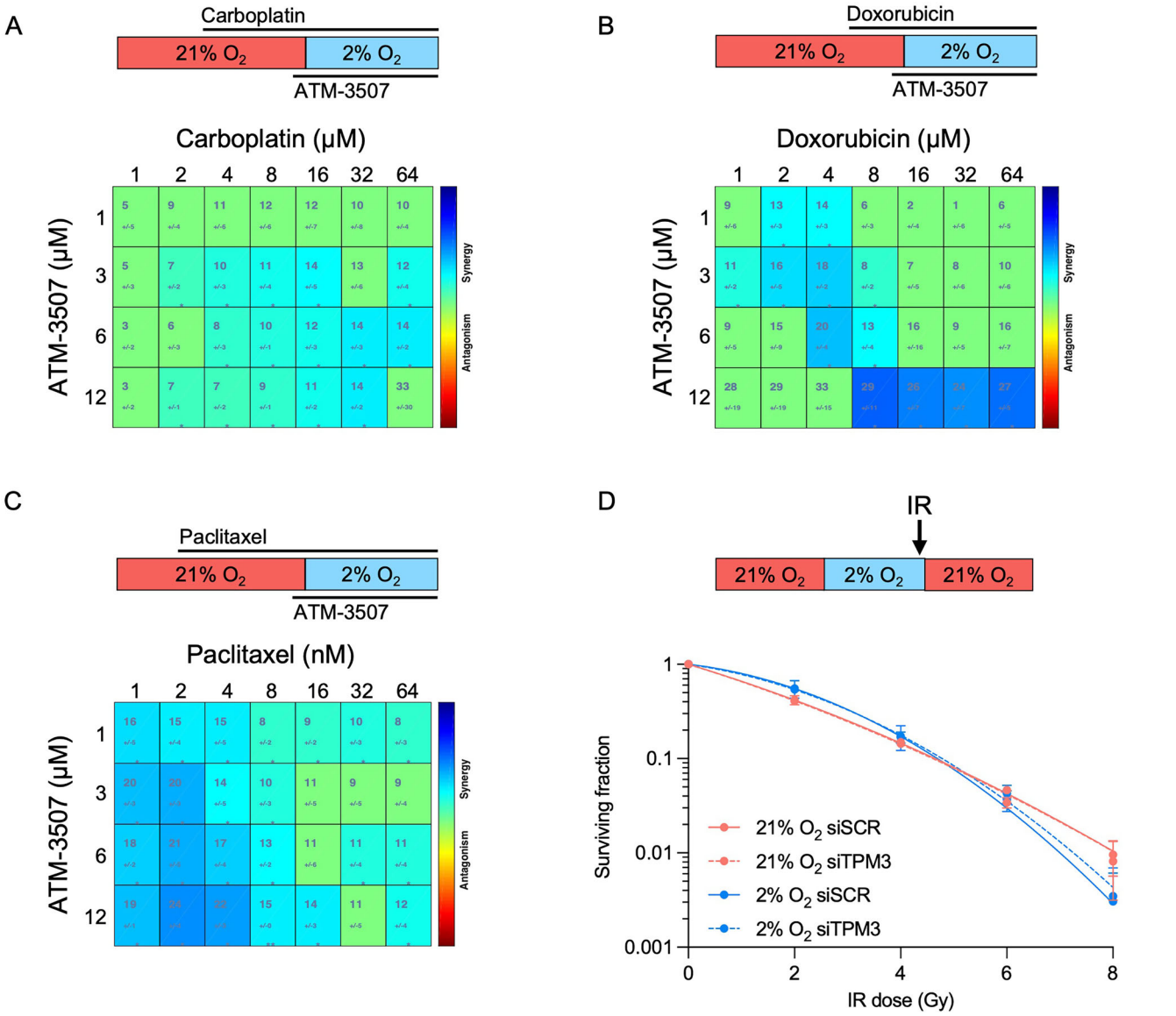

Fig. 4 | Inhibition of TPM3 combines effectively with standard of care for TNBC. **A** MDA-MB-231 cells were treated with Carboplatin (1–64 μM) for 48 h and ATM-3507 (1.5-12 μM) for 17 h. For the 16 h before an MTT assay was carried out the cells were in hypoxia (2% O_2). **B** MDA-MB-231 cells were treated with Doxorubicin (1–64 μM) for 24 h and ATM-3507 (1.5-12 μM) for 17 h. For the 16 h before an MTT assay was carried out the cells were in hypoxia (2% O_2). **C** MDA-MB-231 cells were treated with Paclitaxel (1–64 nM) for 72 h and ATM-3507 (1.5–12 μM) for 17 h. For the 16 h before an MTT assay was carried out the cells were in hypoxia (2% O_2). In A, B and C Highest Single Agent (HSA) synergy score was assessed by an interactive platform Combenefit, scores > 0 represent synergism (blue) and scores < 0 represent antagonism (red). Dose-response matrices with drug concentrations on axes and combination effects as a heatmap overlay are shown. Statistical testing was carried out using the built-in analysis algorithm[39]. **D** MDA-MB-231 cells were treated with siTPM3 or a scramble siRNA (siSCR) followed by exposure to 21% or 2% O_2 for 16 h prior to irradiation using the doses indicated. Cells in hypoxia were irradiated in hypoxic conditions (shown schematically). After irradiation, all cells were returned to 21% O_2 and a colony survival assay carried out. Data from three separate experiments ($n = 3$) are displayed with mean ± standard error of the mean (SEM).

followed by EV isolation and NTA. Again, EV production was increased in hypoxic conditions but loss of TPM3 did not significantly change EV production or size distribution in normoxia or hypoxia (Fig. 7A, B, C). Next, we again isolated EVs from normoxic and hypoxic cells and used NTA to ensure equal loading for western blotting. ALIX is a well-characterised EV protein and was used as a control[30]. Blotting for the mitochondrial protein PRDX3 and Golgi-associated GM130 was also included to demonstrate the purity of the EVs[31]. As expected, western blotting of whole cell lysates showed that ALIX, PRDX3 and GM130 were expressed equally in normoxic and hypoxic cells while TPM3 was induced in hypoxia (Fig. 7D). TPM3 was found to be included in normoxic EVs and the levels increased in EVs generated from hypoxic cells therefore validating TPM3 as an EV cargo protein (Fig. 7E, F).

Discussion

In this study, we demonstrate that TPM3 is a hypoxia-inducible gene in TNBC, and that this occurs in a HIF-1-dependent manner. Under hypoxic conditions, TPM3 supports actin filament stability, maintaining cell shape and enabling efficient migration and invasion. Loss of TPM3 disrupted F-actin organisation at both the leading and trailing edges, reduced cell circularity, and impaired motility. Importantly, TPM3 is also incorporated into EVs released by hypoxic cells, which enhance motility in normoxic recipient cells. Together, these findings demonstrate that hypoxia-induced TPM3 enhances migration capacity across the tumour, extending its impact beyond the hypoxic fraction (Fig. 7G). Our findings support that targeting TPM3 during treatment of TNBC could reduce metastatic burden, by reducing the migratory potential and invasiveness of residual hypoxic and

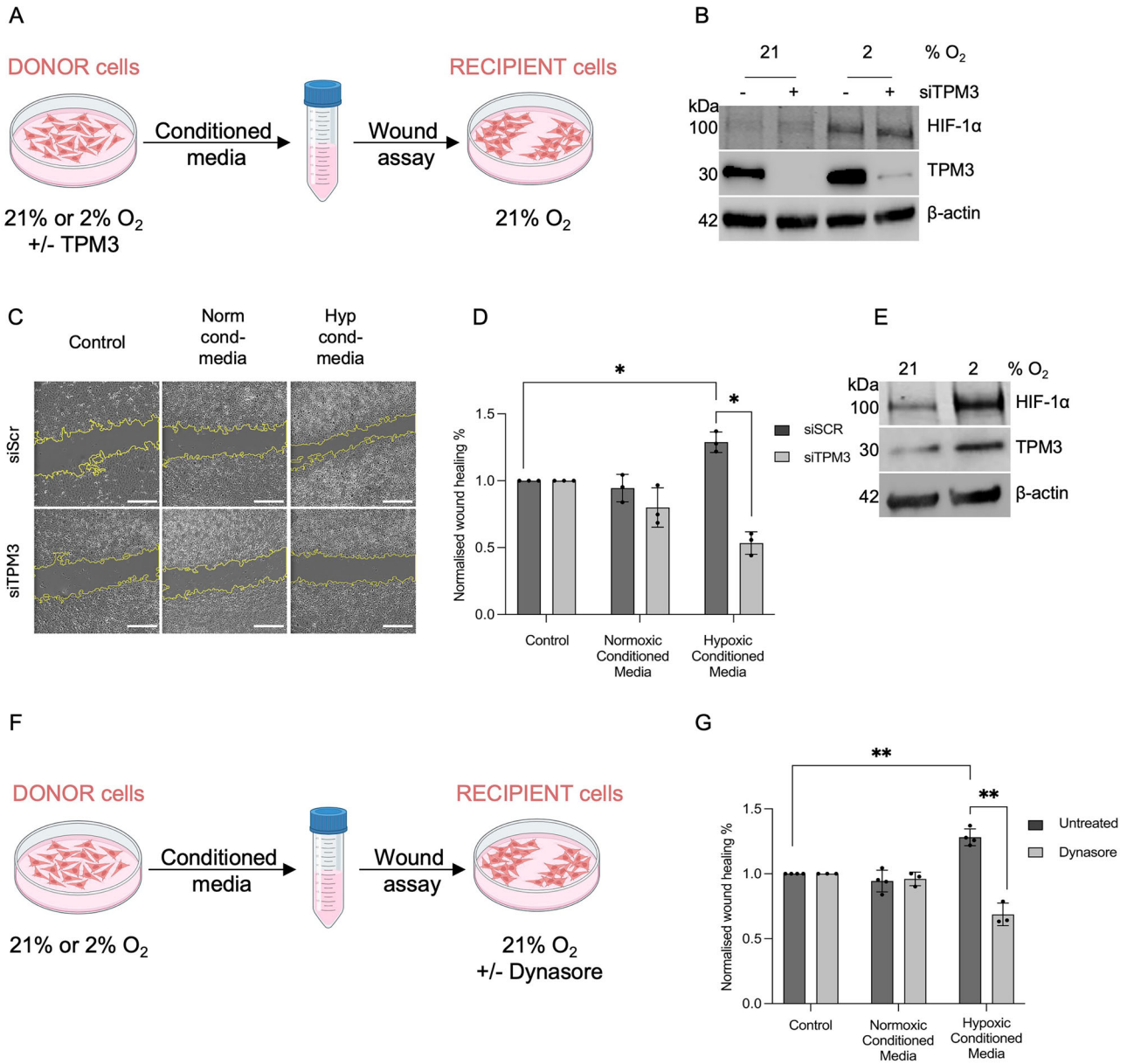

Fig. 5 | Conditioned media from hypoxic cells increase migration in normoxic cells in a TPM3-dependent manner. A Schematic representation of the wound assay used to determine the impact of TPM3 loss in donor cells on recipient cell migration. **B** MDA-MB-231 (donor) cells were treated with siTPM3 or a scramble siRNA and exposed to 21% or 2% O_2 for 16 h, followed by western blotting to validate TPM3 knockdown and HIF-1α stabilisation. **C** Representative images of wound healing assay from cells treated as in part D. Scale bars, 500 µm. **D** MDA-MB-231 donor cells were treated with siTPM3 or a scramble siRNA (siSCR) followed by exposure to 21% or 2% O_2 for 16 h Conditioned media was then collected and applied to wounded MDA-MB-231 recipient cells in 21% O_2 for 16 h. Quantification of normalised wound healing % is shown as fold change relative to control media. Statistical testing was done by paired *t*-test. **E** MDA-MB-231 donor cells were exposed to 21% and 2% O_2 for 16 h, followed by western blotting to indicated proteins. **F** Schematic representation of the wound healing assay used to determine the impact of Dynasore. **G** MDA-MB-231 donor cells were exposed to 21% or 2% O_2 for 16 h. Conditioned media was then collected and added to wounded MDA-MB-231 normoxic recipient cells +/- Dynasore (50 µM) for 16 h. Quantification of normalised wound healing % is shown as fold change relative to control media. Statistical testing was done by paired *t*-test. Data from three separate experiments ($n = 3$) are displayed with mean ± standard error of the mean (SEM). $^{*}p < 0.05$, $^{**}p < 0.01$.

normoxic cancer cells. Importantly, TPM3 is druggable and appeared well-tolerated in vivo as evidenced by preclinical studies with ATM-3507 and its precursor TR100[12,26,32].

Whilst our data demonstrate that TPM3 expression in hypoxia is controlled by HIF-1 it should be noted that this does not conclusively demonstrate a direct role for HIF-1 or rule out a role for HIF-2 in some contexts. Interestingly, a previous study identified a HIF-1α binding peak 20–30 kb upstream of the TPM3 transcription start site in hypoxic colorectal cancer cell lines (HCT116 and RK0) which overlapped with H3K27ac suggesting a possible distal hypoxia-responsive regulatory element[33]. Notably, the previously reported proteomic analysis which determined a direct interaction between TPM3 and RIOK3 suggests that in addition to the mechanism of hypoxia-induction described here, TPM3 could also be phosphorylated and potentially stabilised by RIOK3 in hypoxia[15].

A previous report has shown that TPM3 mRNA is included in EVs generated by platelet cells therefore raising the question of whether this also occurs in TNBC cells and increases in hypoxia[14]. Our study is the first to experimentally validate TPM3 as an EV cargo protein. Notably, this is

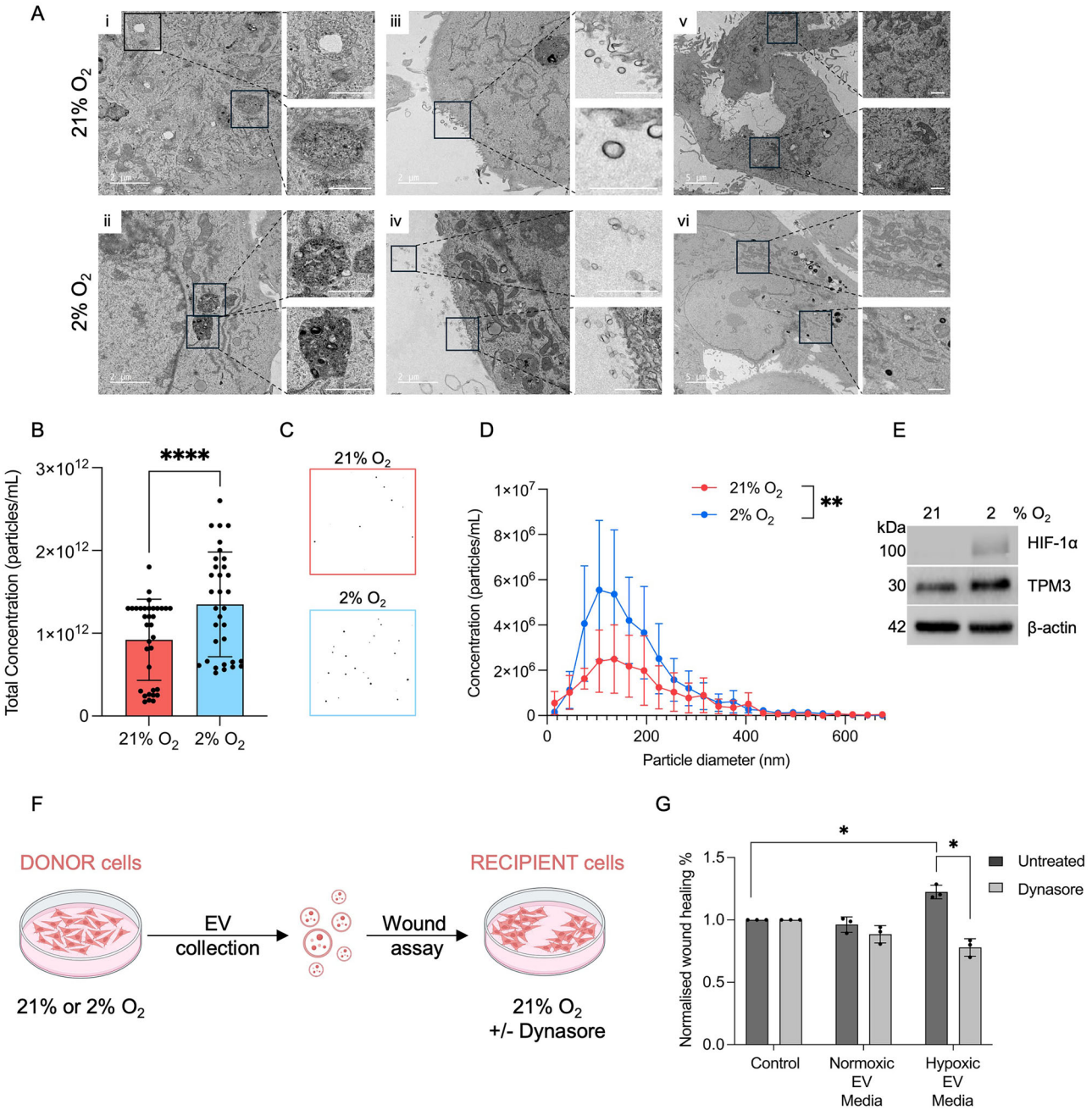

Fig. 6 | EVs generated by hypoxic cells increase migration of normoxic cells. **A** MDA-MB-231 cells in 21% O_2 and 2% O_2 (12 h) were processed and imaged by TEM. Images of late endosomes (enlarged in i, ii), EVs (enlarged in iii, iv) and mitochondria (enlarged in v, vi) are shown. Scale bars are indicated on each image. **B** MDA-MB-231 cells were exposed to 21% or 2% O_2 for 24 h followed by EV isolation. Nanoparticle tracking analysis (NTA) was then carried out to determine the total concentration of EVs. Statistical testing was done by paired *t*-test. **C** Representative images of NTA from part B. **D** Particle diameter was determined for the EVs isolated in part B using NTA. **E** MDA-MB-231 cells were exposed to 21% or 2% O_2 for 24 h, followed by western blotting of whole cell lysates for the indicated proteins. **F** Schematic representation of the wound healing assay to determine the impact of addition of EVs from normoxic or hypoxic cells on normoxic recipient cells. **G** MDA-MB-231 donor cells were exposed to 21% or 2% O_2 for 24 h. Conditioned media was then collected and EVs isolated. EVs were then resuspended in FBS free normoxic culture media and added to MDA-MB-231 normoxic recipient cells +/- Dynasore (50 μM) for 16 h. Quantification of normalised wound healing % is shown as fold change relative to control media. Statistical testing was done by paired *t*-test. Data from three separate experiments ($n = 3$) are displayed with mean ± standard error of the mean (SEM). *$p < 0.05$, **$p < 0.01$, and ****$p < 0.0001$.

supported by previous proteomic datasets that also detected TPM3 in EV preparations, although these studies were not focused on TPM3 and did not pursue validation or functional investigation[34,35]. Although we have identified TPM3 as an EV cargo protein we are not able to conclusively conclude that the TPM3 in hypoxic-EVs is responsible for the phenotype observed in normoxic recipient cells. It is also possible that hypoxia-induced TPM3 influences EV content more broadly and the effect observed here is indirect. It is important to note that hypoxic EVs have been described to contain many proteins and micro RNAs which impact invasion, migration, proliferation, angiogenesis and immunomodulation[36].

In conclusion, our study identifies TPM3 as a novel, HIF-1–regulated effector that links hypoxia to cytoskeletal remodelling, motility, and intercellular communication in TNBC. By demonstrating its incorporation into EVs and its functional contribution to both hypoxic and normoxic cell

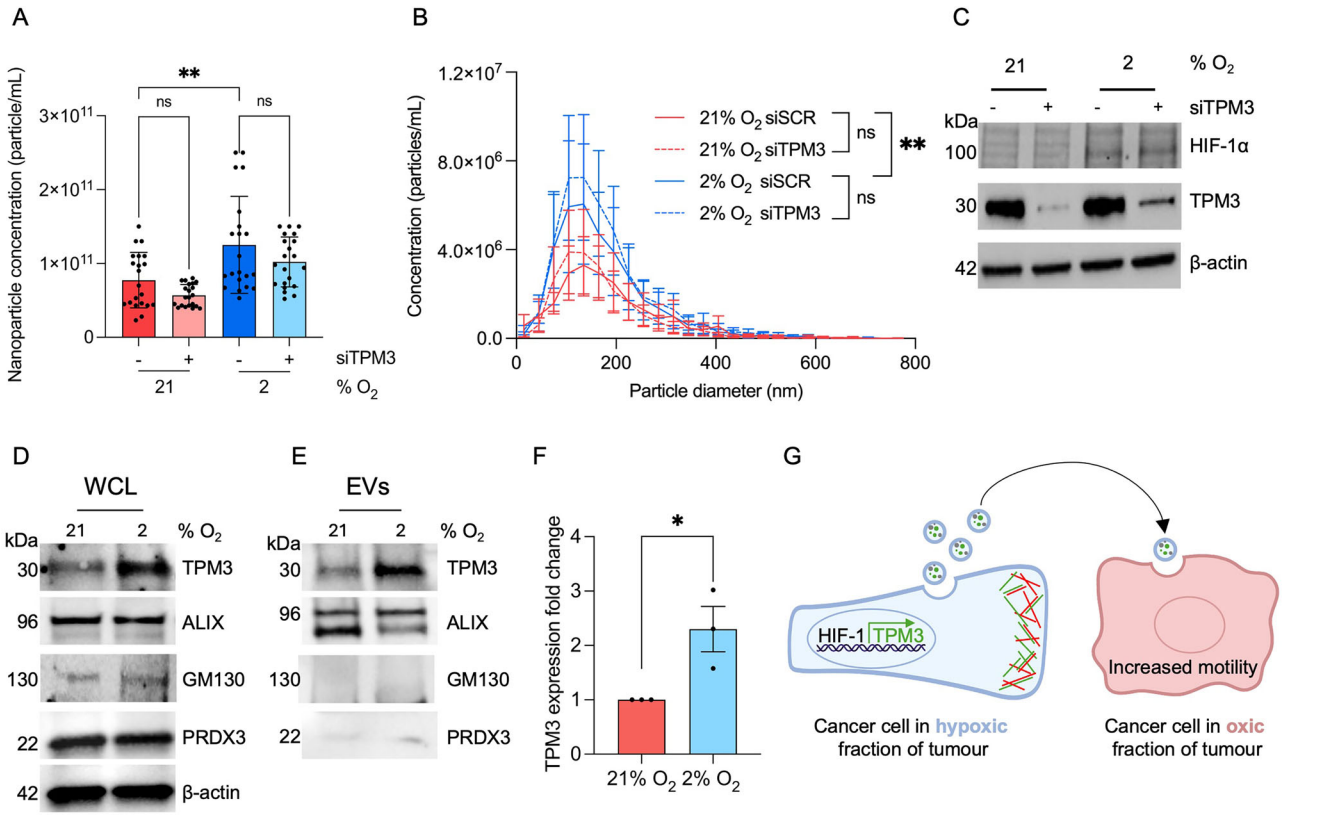

Fig. 7 | TPM3 is an EV cargo protein. A MDA-MB-231 cells were treated with siTPM3 or a scramble siRNA and exposed to 21% or 2% O_2 for 24 h. EVs were isolated, followed by nanoparticle tracking analysis (NTA). The total concentration of EVs from each condition is shown. Statistical testing was done by paired *t*-test. **B** Particle diameter distribution of the EVs isolated in part A. Statistical testing was done using a paired *t*-test. **C** Western blotting of lysates from cells in part A to verify TPM3 knockdown and HIF-1α stabilisation. **D** MDA-MB-231 cells cultured under normoxic (21% O_2) or hypoxic (2% O_2) conditions for 24 h followed by western blotting of whole cell lysates (WCL) as indicated. **E** Western blotting of purified EVs isolated from cells in part D followed by NTA quantification to ensure equal loading. ALIX was used as an EV marker and PRDX3/GM130 used to validate EV purity. **F** Quantification of TPM3 protein expression in EVs from part E. TPM3 band intensity was normalised to ALIX (loading control) and expressed relative to 21% O_2. **G** A summary schematic. TPM3 is induced in a broad range of physiologically relevant hypoxic conditions in a HIF-1 dependent manner. The accumulation of TPM3 (shown in green) contributes to F-actin (shown in red) stabilisation at the leading edge and increased cell motility/invasion. EVs produced by the hypoxic cells contain TPM3, in addition to many other proteins, and when transferred to cells in normoxia (oxic) conditions also increases their motility. $^*p < 0.05$, $^{**}p < 0.01$, and ns $p > 0.05$.

behaviour, we highlight TPM3 as a mediator that bridges the heterogeneity of the tumour microenvironment. Together, these findings position TPM3 as both a biomarker of hypoxic adaptation and a promising therapeutic target to constrain TNBC aggressiveness and improve patient outcomes.

Methods

Cell lines and reagents

MDA-MB-231 (TNBC, provided by Dr Amanda Coutts, University of Oxford), MDA-MB-453 (TNBC, provided by Dr Isabel Pires, University of Manchester) and BT-549 (TNBC, provided by Prof. Katherine Vallis, University of Oxford). Colorectal RKO and RKO$^{HIF\text{-}1\alpha\text{-}/\text{-}}$ cancer cells were grown in DMEM[37]. Cell culture media was supplemented with 10% FBS and cells were maintained in an incubator set at 37°C and 5% CO_2. All cell lines were verified mycoplasma free using a MycoAlert™ mycoplasma detection kit (Lonza). Inhibitors/drugs used were ATM-3507 (Sigma-Aldrich, 1861449-70-8), Dynasore (Med Chem Express, 304448-55-3). For siRNA-mediated knockdowns, MDA-MB-231 cells were transfected with siRNA to a final concentration of 50 nM using Lipofectamine RNAiMAX (Invitrogen) following the manufacturer's protocols. siRNA sequences are provided in **Table SI**.

Hypoxia

A Bactron II anaerobic chamber (Shel Labs) was used for hypoxic treatment at <0.1% O_2. A Whitley M35 Workstation (Don Whitley Scientific) was used for 2% O_2 or cyclic hypoxia. Cycling conditions were <0.1% O_2 for 2 h followed by 2% O_2 for 2 h as described previously[19]. For all experiments except MTT assays, cells were seeded on glass dishes and harvested inside the chambers with equilibrated reagents.

Western blotting

Samples were lysed in UTB (9 M Urea and 75 mM Tris-HCl pH 7.5 supplemented with 0.15 M β-mercaptoethanol prior to use). EV samples were lysed in 1× RIPA lysis buffer (Millipore, 20-188) supplemented with protease inhibitor cocktail (Roche, 11873580001). After a brief sonication, proteins were separated on a 4–20% polyacrylamide gel (Bio-Rad) and transferred onto a nitrocellulose membrane (Bio-Rad). Primary antibodies used were: TPM3 (Abcam, ab113692), β-actin (Santa Cruz, sc-69879), HIF-1α (BD Biosciences, 610958), GRP78 (BD Biosciences, 610979), KAP1 (Bethyl, A300-274A), KAP1-S824 (Bethyl, A300-767A), ALIX (Abcam, ab275377), PRDX3 (Abcam, ab73349), GM130 (Abcam, ab52649). Secondary antibodies: IRDye 680RD goat anti-mouse IgG (LI-COR, 926-68070), IRDye 800CW Goat anti-rabbit IgG (LI-COR, 926-32211), Goat anti-mouse IgG HRP (Invitrogen, 31430), Goat anti-rabbit IgG HRP (Invitrogen, 31460). Images were acquired by chemiluminescence using Odyssey Infrared Imaging (LI-COR Biosciences) or ChemiDoc XRS+ Gel Imaging System (Bio-Rad).

RT-qPCR

Trizol (Invitrogen) was used to isolate RNA, and the Verso enzyme kit (Thermo Fisher Scientific) to reverse transcribe RNA. SYBR Green PCR

Master Mix kit (Applied Biosystems) was used, and the reaction was carried out on a StepOne Real-Time PCR System (Thermo Fisher Scientific) with v2.0.5 software (Applied Biosystems). RNA fold change was measured using a $2^{-\Delta\Delta Ct}$ method relative to the 18S endogenous control gene. Data shown are the mean of three biological replicates ± SEM. All primers sequences are available in supplementary Table S2.

Immunofluorescence

Cells were seeded onto autoclaved cover slips (Menzel-Glaser). Cells were fixed in 4% (w/v) paraformaldehyde in PBS. Samples were permeabilised in 0.1% PBS-Triton X-100 and blocked with 5% (w/v) BSA (Thermo Fisher) in PBS. A LSM710 confocal microscope (Carl Zeiss Microscopy Ltd) was used for imaging. Antibodies/reagents used: TPM3 (Abcam, ab113692), β-actin (Santa Cruz, sc-69879), Alexa Fluor 488-conjugated goat anti-mouse (Invitrogen, A32723), Alexa Fluor Plus 647 Phalloidin (Invitrogen, A30107).

3-(4,5-dimethylthiazol-2-yl)-2,5-diphenyl-2H-tetrazolium bromide (MTT) assay

Cells were seeded in flat bottomed 96-well plates. Each experiment was carried out in triplicate. MTT reagent (5 mg/mL, Invitrogen) was added to cells in the dark for 3 hours (37 °C, 5% CO_2). After MTT containing culture media was removed, DMSO was added to cells and incubated in the dark for 15 min (37 °C). The plate was then read using a POLARstar Omega plate reader (BMG Labtech) (absorbance 570 nm). Cell viability was measured relative to the untreated control.

Flow cytometry

Cells were fixed in ice-cold 70% ethanol. Propidium Iodide (Sigma Aldrich) and RNaseA (NEB) were added to samples for 15 min incubation (37 °C). Samples were run on a CytoFLEX flow cytometer (Beckman Coulter Life Science) and results were analysed with FloJo software.

Wound healing assay

Cells were seeded and grown to 95–100% confluency before treatment. At least five parallel wounds were made by scratching the cell monolayer with a 20 μL pipette tip. After rinsing in PBS, the cells were incubated in 0.5% FBS containing culture media. EVOS M5000 (Thermo Fisher) was used to image the wounds immediately after scratching and over time. The area of each wound was measured by ImageJ (National Institutes of Health). The wound closure % was calculated using the following formula where A is the area of the wound:

$$\text{Wound Closure}\,\% = \left(\frac{A_{t=0} - A_{t=Dt}}{A_{t=0}}\right) \times 100\% \quad (1)$$

Invasion assay

Cells were seeded in an 8 μm pore size BioCoat™ Matrigel Invasion Chamber (Corning). Trypsinised cells (5×10^5) were added to the upper chambers of a 24-well plate in DMEM containing 0.1% FBS. After treatment, the motile cells at the bottom of the filter were stained with crystal violet (0.5% w/v in 50% MeOH and 20% EtOH). The number of cells which had invaded was measured by counting the stained cells using EVOS M5000 (Thermo Fisher).

Colony survival assay

Cells were seeded at the appropriate density for siRNA transfection/drug treatment under normoxia or hypoxia for the indicated periods, each experiment was carried out in triplicate. Colonies were allowed to grow for 8–10 days in a standard humidified incubator at 37 °C and 5% CO_2. Once the colonies formed (≥50 cells), crystal violet (0.5% w/v in 50% MeOH and 20% EtOH) was used for staining. Colonies were counted using an automated colony counter GelCount™ (Oxford Optronix) with GelCount (version 1.2) software, or a manual cell counter (Stuart Scientific). The survival fraction was calculated by number of colonies counted/number of cells seeded × PE, where PE is the plating efficiency of the untreated control (number of colonies counted/number of cells seeded). Colonies with radiation treatment in hypoxic conditions were carried out as previously described[38].

Transmission electron microscopy (TEM)

Cells were seeded onto glass coverslips and cultured until approximately 70% confluency was reached. Following treatment, cells were fixed in 2.5% glutaraldehyde and 4% PFA in 0.1 M PIPES buffer (pH 7.2) followed by washes in 0.1 M PIPES buffer, incubated in 50 mM glycine/PIPES for 15 min, washed once in 0.1 M PIPES, embedded in low-melting-point agarose, chilled, trimmed into 1–2 mm blocks, and returned to buffer. Samples were then treated with 1% osmium tetroxide and 1.5% potassium ferrocyanide in 0.1 M PIPES buffer for 1 h at 4 °C. Samples were washed in Milli-Q water and incubated overnight in 0.5% uranyl acetate at 4 °C in the dark, followed by washes in Milli-Q water. Dehydration was performed on ice using a graded ethanol series (30%, 50%, 70%, 80%, 90%, 95%, and 3 × 100%) at room temperature. Samples were infiltrated with Taab low-viscosity epoxy resin via ethanol:resin series (3:1 for 1 hour, 1:1 for 1.5 hours, and 1:3 for 1 h), then 100% resin at room temperature overnight. Resin was refreshed twice the next day, with centrifugation (12,000 rpm, 3 min) between changes. Agarose-embedded blocks were transferred to Beem capsules containing fresh resin and polymerised at 60 °C for a minimum of 24 h. Ultrathin sections (~90 nm) were prepared using a Diatome diamond knife on a Leica UC7 ultramicrotome, mounted onto 200 mesh copper grids, and post-stained using Reynolds' lead citrate for 5 min at room temperature, followed by washes in Milli-Q water. Sections were imaged using a JEOL 1400 transmission electron microscope equipped with a Gatan Rio CMOS detector.

EV isolation and purification

After treatment, culture media (FBS-free DMEM) was collected and transferred to a 50 mL Falcon tube for EV isolation. EV-containing media was centrifuged at 111.8 × *g* for 5 min at 4 °C (Jouan CR4i Centrifuge, Thermo Electron Corporation). Supernatant was collected, transferred to a new Falcon tube, and centrifuged at 1006.2 × *g* for 10 min at 4 °C. Supernatant was collected, transferred to a new Falcon tube and centrifuged at 1788.8 × *g* for 30 min at 4 °C. The supernatant was transferred to an ultracentrifuge tube (Ultra-Clear centrifuge tubes, Beckman Coulter). Ultracentrifugation was conducted in a pre-cooled SW 32.1 Ti Swinging-Bucket rotor in an Optima XPN-80 Ultracentrifuge (Beckman Coulter) at 87,945 × *g* for 140 min at 4°C. Following ultracentrifugation, the media was removed, and the pellet resuspended in cold, sterile PBS. Samples were ultracentrifuged again at 87,945 × *g* for 140 min at 4 °C. Supernatant was carefully aspirated leaving the purified EVs, which were resuspended in sterile PBS or fresh 10% FBS supplemented DMEM for subsequent experiments.

Nanoparticle tracking analysis (NTA)

Isolated EVs were resuspended in equal volumes of 1 × PBS across all conditions. EV number and size distribution were assessed using ZetaView® (Particlemetrix) according to the manufacturer's instructions. Stock EV samples were diluted in 1 × PBS to working concentrations ranging from 1:10,000 to 1:100,000 and loaded into the flow cell. Measurements were recorded as videos from 8–11 separate positions across the flow cell. EV number and size were estimated from this using the ZetaView analysis software.

Statistical analysis

A two-tailed, paired Student's *t*-test was used for the comparison of two means and a two-way analysis of variance (ANOVA) with Tukey's multiple comparisons or Šídák's multiple comparison test were used for the comparison of more than two means.

Data availability

All data supporting the findings of this study are available within the paper and its Supplementary Information or by request to the corresponding author.

Received: 1 October 2025; Accepted: 1 March 2026;
Published online: 14 March 2026

References

1. Liao, C., Liu, X., Zhang, C. & Zhang, Q. Tumor hypoxia: From basic knowledge to therapeutic implications. *Semin. Cancer Biol.* **88**, 172–186 (2023).
2. Tutzauer, J. et al. Breast cancer hypoxia in relation to prognosis and benefit from radiotherapy after breast-conserving surgery in a large, randomised trial with long-term follow-up. *Br. J. Cancer* **126**, 1145–1156 (2022).
3. Comprehensive molecular portraits of human breast tumours. *Nature* **490**, 61–70 (2012).
4. Chen, Z., Han, F., Du, Y., Shi, H. & Zhou, W. Hypoxic microenvironment in cancer: molecular mechanisms and therapeutic interventions. *Signal Transduct. Target. Ther.* **8**, 70 (2023).
5. Schito, L. & Rey-Keim, S. Hypoxia signaling and metastatic progression. *Semin. Cancer Biol.* **97**, 42–49 (2023).
6. Gunning, P. W., Hardeman, E. C., Lappalainen, P. & Mulvihill, D. P. Tropomyosin – master regulator of actin filament function in the cytoskeleton. *J. Cell Sci*. https://doi.org/10.1242/jcs.172502 (2015).
7. Zhao, Y.-C. et al. TPM3: a novel prognostic biomarker of cervical cancer that correlates with immune infiltration and promotes malignant behavior in vivo and in vitro. *Am. J. Cancer Res.* **13**, 3123–3139 (2023).
8. Yang, J. et al. ALK-TPM3 rearrangement in adult renal cell carcinoma: a case report and literature review. *Diagn. Pathol.* **14**, 112 (2019).
9. Tian, Z., Zhao, J. & Wang, Y. The prognostic value of TPM1–4 in hepatocellular carcinoma. *Cancer Med* **11**, 433–446 (2022).
10. Zhu, Y. et al. Dual drive coexistence of *EML4-ALK* and *TPM3-ROS1* fusion in advanced lung adenocarcinoma. *Thorac. Cancer* **9**, 324–327 (2018).
11. Lam, C. Y. et al. Identification and Characterization of Tropomyosin 3 Associated with Granulin-Epithelin Precursor in Human Hepatocellular Carcinoma. *PLoS One* **7**, e40324 (2012).
12. Currier, M. A. et al. Identification of Cancer-Targeted Tropomyosin Inhibitors and Their Synergy with Microtubule Drugs. *Mol. Cancer Ther.* **16**, 1555–1565 (2017).
13. Chen, S. et al. TPM3 mediates epithelial-mesenchymal transition in esophageal cancer via MMP2/MMP9. *Ann. Transl. Med.* **9**, 1338 (2021).
14. Yao, B. et al. Delivery of platelet *TPM3* mRNA into breast cancer cells via microvesicles enhances metastasis. *FEBS Open Bio* **9**, 2159–2169 (2019).
15. Singleton, D. C. et al. Hypoxic regulation of RIOK3 is a major mechanism for cancer cell invasion and metastasis. *Oncogene* **34**, 4713–4722 (2015).
16. Ye, I. C. et al. Molecular Portrait of Hypoxia in Breast Cancer: A Prognostic Signature and Novel HIF-Regulated Genes. *Molecular Cancer Research* **16**, 1889–1901 (2018).
17. Buffa, F. M., Harris, A. L., West, C. M. & Miller, C. J. Large meta-analysis of multiple cancers reveals a common, compact and highly prognostic hypoxia metagene. *Br. J. Cancer* **102**, 428–435 (2010).
18. Bader, S. B., Dewhirst, M. W. & Hammond, E. M. Review cyclic hypoxia: An update on its characteristics, methods to measure it and biological implications in cancer. *Cancers (Basel)* **13**, 23 (2021).
19. Bader, S. B. et al. Replication catastrophe induced by cyclic hypoxia leads to increased APOBEC3B activity. *Nucleic Acids Res*. https://doi.org/10.1093/nar/gkab551 (2021).
20. Ma, T. S. et al. Hypoxia-induced transcriptional stress is mediated by ROS-induced R-loops. *Nucleic Acids Res* **51**, 11584–11599 (2023).
21. Ledaki, I. et al. Carbonic anhydrase IX induction defines a heterogeneous cancer cell response to hypoxia and mediates stem cell-like properties and sensitivity to HDAC inhibition. *Oncotarget* **6**, 19413–19427 (2015).
22. Kumari, R. et al. Focal adhesions contain three specialized actin nanoscale layers. *Nat. Commun.* **15**, 2547 (2024).
23. Nagano, M., Hoshino, D., Koshikawa, N., Akizawa, T. & Seiki, M. Turnover of Focal Adhesions and Cancer Cell Migration. *Int. J. Cell Biol.* **2012**, 310616 (2012).
24. Janco, M. et al. Molecular integration of the anti-tropomyosin compound ATM-3507 into the coiled coil overlap region of the cancer-associated Tpm3. *1. Sci. Rep.* **9**, 11262 (2019).
25. Li, Y. et al. Invasion and metastasis in cancer: molecular insights and therapeutic targets. *Signal Transduct. Target. Ther.* **10**, 57 (2025).
26. Xu, X. et al. Targeting the actin/tropomyosin cytoskeleton in epithelial ovarian cancer reveals multiple mechanisms of synergy with anti-microtubule agents. *Br. J. Cancer* **125**, 265–276 (2021).
27. Meng, S.-S. et al. LincRNA-p21 promotes mesenchymal stem cell migration capacity and survival through hypoxic preconditioning. *Stem Cell Res. Ther.* **9**, 280 (2018).
28. Zang, J. L. et al. CCSer2 gates dynein activity at the cell periphery. *J. Cell Biol.* **224**, e202406153 (2025).
29. Roy, S. et al. Hypoxic tumor microenvironment: Implications for cancer therapy. *Exp. Biol. Med.* **245**, 1073 (2020).
30. Willms, E. et al. Cells release subpopulations of exosomes with distinct molecular and biological properties. *Sci. Rep.* **6**, 22519 (2016).
31. Gomes, F., Turano, H., Haddad, L. A. & Netto, L. E. S. Human mitochondrial peroxiredoxin Prdx3 is dually localized in the intermembrane space and matrix subcompartments. *Redox Biol* **78**, 103436 (2024).
32. Kee, A. J. et al. On-target action of anti-tropomyosin drugs regulates glucose metabolism. *Sci. Rep.* **8**, 4604 (2018).
33. Andrysik, Z., Bender, H., Galbraith, M. D. & Espinosa, J. M. Multi-omics analysis reveals contextual tumor suppressive and oncogenic gene modules within the acute hypoxic response. *Nat. Commun.* **12**, 1375 (2021).
34. Zhang, Q. et al. Supermeres are functional extracellular nanoparticles replete with disease biomarkers and therapeutic targets. *Nat. Cell Biol.* **23**, 1240–1254 (2021).
35. Hurwitz, S. N. et al. Proteomic profiling of NCI-60 extracellular vesicles uncovers common protein cargo and cancer type-specific biomarkers. *Oncotarget* **7**, 86999–87015 (2016).
36. Bister, N. et al. Hypoxia and extracellular vesicles: A review on methods, vesicular cargo and functions. *J. Extracell. Vesicles* **10**, e12002 (2020).
37. Dang, D. T. et al. Hypoxia-Inducible Factor-1α Promotes Nonhypoxia-Mediated Proliferation in Colon Cancer Cells and Xenografts. *Cancer Res* **66**, 1684–1693 (2006).
38. Pires, I. M. Targeting radiation-resistant hypoxic tumour cells through ATR inhibition. *Br. J. Cancer* **107**, 291–299 (2012).
39. Di Veroli, G. Y. et al. Combenefit: an interactive platform for the analysis and visualization of drug combinations. *Bioinformatics* **32**, 2866–2868 (2016).

Acknowledgements

We are grateful to Raman Dhaliwal and Dr Charlotte Melia at the Sir William Dunn School of Pathology Electron Microscopy Facility. C.Z. was supported by Breast Cancer Now (2022FebPR1492 awarded to EMH and EEP). S.A.T. and E.M.H. thank the EPSRC for the support of programme grant EP/S019901/1. G.B. was supported by a UNIQ+ Research Internship (University of Oxford). E.P. was supported by a Clarendon scholarship (University of Oxford).

Author contributions

C.Z., J.T.C., K.F., P.S., S.T., E.P., G.B., E.E.P. and E.M.H. were responsible for collecting, analysing, and interpreting data. E.M.H. and C.Z. drafted the manuscript. E.M.H. was responsible for study conceptualisation and study oversight. J.T.C., C.Z. and E.M.H. were responsible for figure creation. All authors critically reviewed the manuscript and approved the final version.

Competing interests

The authors declare no competing interests.

Additional information

Supplementary information The online version contains supplementary material available at https://doi.org/10.1038/s41523-026-00927-y.

Correspondence and requests for materials should be addressed to Ester M. Hammond.